

University of Warwick institutional repository: <http://go.warwick.ac.uk/wrap>

**A Thesis Submitted for the Degree of PhD at the University of Warwick**

<http://go.warwick.ac.uk/wrap/58244>

This thesis is made available online and is protected by original copyright.

Please scroll down to view the document itself.

Please refer to the repository record for this item for information to help you to cite it. Our policy information is available from the repository home page.

## Library Declaration and Deposit Agreement

### 1. STUDENT DETAILS

*Please complete the following:*

Full name: .....

University ID number: .....

### 2. THESIS DEPOSIT

2.1 I understand that under my registration at the University, I am required to deposit my thesis with the University in BOTH hard copy and in digital format. The digital version should normally be saved as a single pdf file.

2.2 The hard copy will be housed in the University Library. The digital version will be deposited in the University's Institutional Repository (WRAP). Unless otherwise indicated (see 2.3 below) this will be made openly accessible on the Internet and will be supplied to the British Library to be made available online via its Electronic Theses Online Service (EThOS) service.

[At present, theses submitted for a Master's degree by Research (MA, MSc, LLM, MS or MMedSci) are not being deposited in WRAP and not being made available via EThOS. This may change in future.]

2.3 In exceptional circumstances, the Chair of the Board of Graduate Studies may grant permission for an embargo to be placed on public access to the hard copy thesis for a limited period. It is also possible to apply separately for an embargo on the digital version. (Further information is available in the *Guide to Examinations for Higher Degrees by Research*.)

2.4 *If you are depositing a thesis for a Master's degree by Research, please complete section (a) below. For all other research degrees, please complete both sections (a) and (b) below:*

#### (a) Hard Copy

I hereby deposit a hard copy of my thesis in the University Library to be made publicly available to readers (please delete as appropriate) EITHER immediately OR after an embargo period of ..... months/years as agreed by the Chair of the Board of Graduate Studies.

I agree that my thesis may be photocopied.

YES / NO (*Please delete as appropriate*)

#### (b) Digital Copy

I hereby deposit a digital copy of my thesis to be held in WRAP and made available via EThOS.

Please choose one of the following options:

EITHER My thesis can be made publicly available online. YES / NO (*Please delete as appropriate*)

OR My thesis can be made publicly available only after.....[date] (*Please give date*)

YES / NO (*Please delete as appropriate*)

OR My full thesis cannot be made publicly available online but I am submitting a separately identified additional, abridged version that can be made available online.

YES / NO (*Please delete as appropriate*)

OR My thesis cannot be made publicly available online.

YES / NO (*Please delete as appropriate*)

### 3. GRANTING OF NON-EXCLUSIVE RIGHTS

Whether I deposit my Work personally or through an assistant or other agent, I agree to the following:

Rights granted to the University of Warwick and the British Library and the user of the thesis through this agreement are non-exclusive. I retain all rights in the thesis in its present version or future versions. I agree that the institutional repository administrators and the British Library or their agents may, without changing content, digitise and migrate the thesis to any medium or format for the purpose of future preservation and accessibility.

### 4. DECLARATIONS

(a) I DECLARE THAT:

- I am the author and owner of the copyright in the thesis and/or I have the authority of the authors and owners of the copyright in the thesis to make this agreement. Reproduction of any part of this thesis for teaching or in academic or other forms of publication is subject to the normal limitations on the use of copyrighted materials and to the proper and full acknowledgement of its source.
- The digital version of the thesis I am supplying is the same version as the final, hard-bound copy submitted in completion of my degree, once any minor corrections have been completed.
- I have exercised reasonable care to ensure that the thesis is original, and does not to the best of my knowledge break any UK law or other Intellectual Property Right, or contain any confidential material.
- I understand that, through the medium of the Internet, files will be available to automated agents, and may be searched and copied by, for example, text mining and plagiarism detection software.

(b) IF I HAVE AGREED (in Section 2 above) TO MAKE MY THESIS PUBLICLY AVAILABLE DIGITALLY, I ALSO DECLARE THAT:

- I grant the University of Warwick and the British Library a licence to make available on the Internet the thesis in digitised format through the Institutional Repository and through the British Library via the EThOS service.
- If my thesis does include any substantial subsidiary material owned by third-party copyright holders, I have sought and obtained permission to include it in any version of my thesis available in digital format and that this permission encompasses the rights that I have granted to the University of Warwick and to the British Library.

### 5. LEGAL INFRINGEMENTS

I understand that neither the University of Warwick nor the British Library have any obligation to take legal action on behalf of myself, or other rights holders, in the event of infringement of intellectual property rights, breach of contract or of any other right, in the thesis.

---

*Please sign this agreement and return it to the Graduate School Office when you submit your thesis.*

Student's signature: ..... Date: .....

# **Tetrazine–Norbornene Cycloadditions in Macromolecular Synthesis and Functionalisation**

**Claire Hansell**

*submitted for the degree of Doctor of Philosophy*

Department of Chemistry

THE UNIVERSITY OF  
**WARWICK**

The logo of the University of Warwick, featuring a stylized 'W' that incorporates a curved line resembling a bridge or a path.

2013



# Table of Contents

<b>List of Figures, Schemes and Tables .....</b>	<b>v</b>
<b>Figures .....</b>	<b>v</b>
<b>Schemes.....</b>	<b>xi</b>
<b>Tables .....</b>	<b>xii</b>
<b>Acknowledgements .....</b>	<b>xv</b>
<b>Declaration of authorship .....</b>	<b>xvi</b>
<b>List of publications .....</b>	<b>xvii</b>
<b>Summary of thesis .....</b>	<b>xix</b>
<b>Abbreviations .....</b>	<b>xx</b>

## Chapter 1. Introduction

<b>1.1. Abstract.....</b>	<b>1</b>
<b>1.2. Polymers .....</b>	<b>2</b>
<b>1.3. Controlled Radical Polymerisation .....</b>	<b>5</b>
1.3.1. Atom Transfer Radical Polymerisation .....	5
1.3.2. Nitroxide Mediated Polymerisation .....	7
1.3.3. Reversible Addition Fragmentation chain Transfer Polymerisation .....	8
<b>1.4. Post-polymerisation modification .....</b>	<b>11</b>
<b>1.5. ‘Click’ Reactions.....</b>	<b>12</b>
1.5.1. Copper catalysed azide–alkyne (CuAAC) .....	15
1.5.2. Dipolar cycloadditions .....	16
1.5.3. Thiol-based reactions .....	19

1.5.4. Oxime ligation.....	23
1.5.5. Activated esters.....	24
1.5.6. Staudinger Ligation .....	25
1.5.7. Diels-Alder/hetero-Diels-Alder .....	27
1.5.8. Inverse Diels-Alder reaction .....	29
<b>1.6. Tetrazine DA<sub>inv</sub> applications .....</b>	<b>34</b>
<b>1.7. Tetrazine synthesis .....</b>	<b>38</b>
<b>1.8. Conclusions.....</b>	<b>40</b>
<b>1.9. References .....</b>	<b>41</b>

## Chapter 2. Tetrazine–norbornene reaction in polymer functionalisation and polymer–polymer coupling

<b>2.1. Abstract.....</b>	<b>57</b>
<b>2.2. Background .....</b>	<b>58</b>
<b>2.3. Results and discussion .....</b>	<b>62</b>
2.3.1. Small molecule studies.....	62
2.3.2. Functionalised polymer synthesis .....	69
2.3.3. End group modification.....	75
2.3.4. Polymer–polymer coupling .....	82
2.3.5. Polymer–polymer coupling in water .....	93
2.3.6. Polymer–polymer coupling of poly(ester)s .....	94
<b>2.4. Conclusions.....</b>	<b>100</b>
<b>2.5. Experimental.....</b>	<b>101</b>
2.5.1. Materials and methods .....	101
2.5.2. Syntheses.....	103
2.5.3. Small molecule kinetics .....	106
2.5.4. General polymer functionalisation and polymer–polymer coupling .....	107

<b>2.6. Appendix: Supplementary Data .....</b>	<b>107</b>
<b>2.7. References .....</b>	<b>112</b>

### **Chapter 3. Micelle functionalisation using the tetrazine-norbornene reaction**

<b>3.1. Abstract.....</b>	<b>116</b>
<b>3.2. Background .....</b>	<b>117</b>
<b>3.3. Results and discussion .....</b>	<b>121</b>
3.3.1. Small molecule model reactions.....	122
3.3.2. Polymer synthesis and characterisation.....	125
3.3.3. Micelle synthesis and characterisation.....	138
3.3.4. Micelle functionalisation .....	141
3.3.5. Characterisation of functionalised micelles .....	146
<b>3.4. Conclusions .....</b>	<b>157</b>
<b>3.5. Experimental.....</b>	<b>158</b>
3.5.1. Materials and methods .....	158
3.5.2. Competition reactions.....	161
3.5.3. Syntheses.....	161
3.5.4. Micelle reactions.....	167
<b>3.6. References .....</b>	<b>170</b>

### **Chapter 4. Nanoparticle formation using single chain collapse of norbornene-functionalised polymers**

<b>4.1. Abstract.....</b>	<b>176</b>
<b>4.2. Background .....</b>	<b>177</b>
<b>4.3. Results and discussion .....</b>	<b>185</b>

4.3.1. Crosslinker Synthesis .....	185
4.3.2. SCPN Synthesis .....	189
4.3.3. Control experiments .....	191
4.3.4. SCPN Characterisation .....	195
4.3.5. Characterisation summary .....	212
<b>4.4. Conclusions .....</b>	<b>214</b>
<b>4.5. Experimental .....</b>	<b>215</b>
4.5.1. Materials and methods .....	215
4.5.2. Syntheses .....	218
<b>4.6. References .....</b>	<b>223</b>

## **Chapter 5. Expanding the scope of tetrazine cycloadditions using alkene polymers**

<b>5.1. Abstract .....</b>	<b>229</b>
<b>5.2. Background .....</b>	<b>230</b>
<b>5.3. Results and discussion .....</b>	<b>232</b>
5.3.1. Preliminary rate screening .....	232
5.3.2. Polymer synthesis .....	234
5.3.3. Functional tetrazine synthesis .....	243
5.3.4. Polymer functionalisation .....	250
<b>5.4. Conclusions .....</b>	<b>255</b>
<b>5.5. Experimental .....</b>	<b>256</b>
5.5.1. Materials and methods .....	256
5.5.2. Syntheses .....	257
5.5.3. General polymerisation procedure .....	262
5.5.4. General polymer functionalisation procedure .....	263

5.6. References .....	264
Conclusions and further work .....	267

## List of Figures, Schemes and Tables

### Figures

<b>Figure 1.1</b> Some of the many architectures accessible by contemporary polymerisation techniques .....	2
<b>Figure 1.2</b> Evolution of molecular weight with conversion for chain-growth, step-growth and living polymerisations .....	3
<b>Figure 1.3</b> Some NMP-mediating species .....	8
<b>Figure 1.4</b> Types of RAFT chain transfer agent (CTA) .....	9
<b>Figure 1.5</b> Number of results returned by the CAS database for the search term 'click' – cumulative hits to year end .....	13
<b>Figure 1.6</b> Polymer-specific click criteria – blue are Sharpless' original criteria, green are ones particularly important or specific to polymer click reactions .....	14
<b>Figure 1.7</b> Alkynes used in strain-promoted azide–alkyne (SPAAC) reactions.....	17
<b>Figure 1.8</b> PEG–protein ligation using the Staudinger ligation .....	26
<b>Figure 1.9</b> Frontier molecular orbital diagrams for normal and inverse electron demand Diels-Alder reactions.....	30
<b>Figure 1.10</b> Aza-dienes commonly used in DA <sub>inv</sub> –rDA reactions.....	31
<b>Figure 1.11</b> Reactivity of tetrazines in aqueous buffer solutions .....	33
<b>Figure 1.12</b> Reactivity of various cyclic dienophiles .....	33
<b>Figure 1.13</b> Cyclooctene/octyne reactivity rates with dipyriddy tetrazine in methanol	34
<b>Figure 1.14</b> Cellular imaging using Tz–Nb DA <sub>inv</sub> .....	35

<b>Figure 1.15</b> Tetrazine- and norbornene-functionalised unnatural amino acids genetically encoded for in vivo labelling using complementary norbornene- or tetrazine-functionalised fluorescent tags.....	36
<b>Figure 2.1</b> Diblock copolymer formation using the CuAAC reaction to ligate PEG and PMMA homopolymers .....	59
<b>Figure 2.2</b> Example SEC traces for polymer–polymer coupling by light-induced RAFT-HDA methodology .....	61
<b>Figure 2.3</b> $^1\text{H}$ NMR spectrum of conjugation product 2.02 .....	64
<b>Figure 2.4</b> HRMS for small molecule product 2.02.....	65
<b>Figure 2.5</b> Section of the $^1\text{H}$ NMR spectra of the reaction mixture forming 2.01 and 2.02 over time, with signals arising from the starting materials highlighted. ....	66
<b>Figure 2.6</b> Kinetics of the equimolar small molecule reaction at 0.06 M monitored by $^1\text{H}$ NMR spectroscopy.....	67
<b>Figure 2.7</b> UV/vis absorbance at 546 nm against time for the reaction of Nb–TTC with Tz(pyr) <sub>2</sub> , varying equivalents of Nb–TTC at constant [Tz] and concentration of both Nb–TTC and Tz in equimolar amounts .....	68
<b>Figure 2.8</b> $^1\text{H}$ NMR spectrum of PEG–Tz .....	73
<b>Figure 2.9</b> Partial $^1\text{H}$ NMR spectrum of PS–Nb pre- and post-reaction with 1 equivalent Tz(pyr) <sub>2</sub> .....	75
<b>Figure 2.10</b> Section of $^1\text{H}$ NMR spectra showing near identical tetrazine functionalisation peaks for polymers 2.03–2.05.....	76
<b>Figure 2.11</b> Section of UV/vis spectra for reaction of PS 2.03 with Tz(pyr) <sub>2</sub> .....	77
<b>Figure 2.12</b> UV/vis absorbance at 546 nm against time for the reaction of polymers 2.03–2.05 with Tz(pyr) <sub>2</sub> .....	78
<b>Figure 2.13</b> $^1\text{H}$ NMR spectrum of polymer 2.10 functionalised with norbornene dimethanol in water.....	79

<b>Figure 2.14</b> MALDI spectra of PEG–NH <sub>2</sub> and functionalised PEG–Tz.....	80
<b>Figure 2.15</b> SEC traces for polymer end-functionalisation: PS–Nb functionalised with dipyridyl tetrazine, PNIPAM–Nb functionalised with dipyridyl tetrazine, PEG–Tz functionalised with norbornene dimethanol. ....	81
<b>Figure 2.16</b> UV/vis absorbance at 546 nm for the coupling of PS–Nb 2.03 and PEG–Tz 2.10 in CH <sub>2</sub> Cl <sub>2</sub> and a 1:1 DMSO/CH <sub>2</sub> Cl <sub>2</sub> mixture .....	83
<b>Figure 2.17</b> Photographs of dried polymers 2.03, 2.10 and 2.13 showing the colour change arising from the Tz–Nb reaction.....	84
<b>Figure 2.18</b> Evolution of the PS- <i>b</i> -PEG conjugation SEC traces with time, and SEC traces of unpurified diblock PS- <i>b</i> -PEG and the constituent homopolymers .....	84
<b>Figure 2.19</b> Number distributions of polymers 2.03, 2.10 and 2.13 derived from the <i>wlogM</i> distribution .....	87
<b>Figure 2.20</b> LC–SEC chromatogram under non-critical conditions .....	89
<b>Figure 2.21</b> DOSY NMR spectrum of crude 2.13 .....	91
<b>Figure 2.22</b> <sup>1</sup> H NMR spectrum of purified PS- <i>b</i> -PEG 2.13.....	92
<b>Figure 2.23</b> SEC traces for polymers 2.05, 2.10 and the resulting diblock PEG- <i>b</i> - PNIPAM .....	93
<b>Figure 2.24</b> SEC traces of the crude reaction mixtures formed between Nb- terminated poly(esters) and PEG–Tz 2.10 .....	97
<b>Figure 2.25</b> SEC traces by RI detection and UV detection at 320 nm for the conjugation of PVL–Nb and PVL–Tz .....	98
<b>Figure 2.26</b> LC chromatograms (UV detection at 310 nm) of reaction mixture (Scheme 2.1) after 1 hour and 2 hours.....	108
<b>Figure 2.27</b> <sup>1</sup> H-NMR spectrum of PS–Nb (DP 55) prepared by RAFT .....	109
<b>Figure 2.28</b> <sup>1</sup> H-NMR spectrum of PNIPAM–Nb (DP 140) prepared by RAFT .....	109
<b>Figure 2.29</b> <sup>1</sup> H NMR spectrum of PCL–Nb prepared by ROP .....	110

<b>Figure 2.30</b> $^1\text{H}$ NMR spectrum of PVL–Nb prepared by ROP .....	110
<b>Figure 2.31</b> $^1\text{H}$ NMR spectrum of PVL–Tz prepared by ROP .....	111
<b>Figure 3.1</b> Self-assembly of a polymer amphiphile to form a micellar structure ....	118
<b>Figure 3.2</b> Alternative routes to functional micelles .....	119
<b>Figure 3.3</b> Examples of micelle functionalisation using the Diels-Alder and thiol-ene reactions .....	121
<b>Figure 3.4</b> Examples of functional micelles that exploit the CuAAC reaction to functionalise the micelle surface, shell, core-shell interface and core .	121
<b>Figure 3.5</b> $^1\text{H}$ NMR spectrum of selective reaction of tetrazine with norbornene over propargyl chloride .....	124
<b>Figure 3.6</b> $^1\text{H}$ NMR spectrum of selective reaction of propargyl alcohol with azidoacetic acid over norbornene dimethanol .....	125
<b>Figure 3.7</b> $^1\text{H}$ and $^{13}\text{C}$ NMR spectra for Nb–St monomer, peaks for <i>endo</i> isomer assigned .....	127
<b>Figure 3.8</b> Kinetic plot of $[\text{M}]:[\text{CTA}]:[\text{AIBN}] = 100:1:0.1$ for 100% St, 100% Nb–St and 50 mol% Nb–St:St .....	129
<b>Figure 3.9</b> Assigned $^1\text{H}$ NMR spectrum of polymer 3.01 .....	130
<b>Figure 3.10</b> Evolution of SEC traces and $M_w/M_n$ with time of THPA chain extension from poly(St-co-Nb–St) .....	132
<b>Figure 3.11</b> Assigned $^1\text{H}$ and $^{13}\text{C}$ spectra in $\text{CDCl}_3$ for PA–TMS monomer .....	134
<b>Figure 3.12</b> $^1\text{H}$ NMR spectra ( $\text{CDCl}_3$ ) of polymers 3.01, 3.02 and 3.03 .....	135
<b>Figure 3.13</b> FT-IR spectra of polymers; segment showing alkyne C–H stretch expanded .....	136
<b>Figure 3.14</b> SEC traces of polymers .....	138
<b>Figure 3.15</b> DLS traces and correlogram for the core-shell functionalised micelles	140
<b>Figure 3.16</b> TEM images of micelles unstained on GO and stained with uranyl acetate .....	140



<b>Figure 3.17</b> Histogram of particle diameters measured from TEM imaging on GO141	
<b>Figure 3.18</b> UV/vis absorbance at 546 nm for functionalisation of micelles with dipyridyl tetrazine, and first derivative of the smoothed curve used to determine reaction completion.....	143
<b>Figure 3.19</b> $^1\text{H}$ and $^{13}\text{C}$ NMR spectra of coumarin- $\text{N}_3$ .....	145
<b>Figure 3.20</b> DLS traces and correlograms for micelles .....	147
<b>Figure 3.21</b> Representative TEM images and size histograms of micelles .....	149
<b>Figure 3.22</b> Photograph of micelle solutions under a long wave UV lamp .....	150
<b>Figure 3.23</b> Fluorescence spectra of micelles and free coumarin- $\text{N}_3$ .....	151
<b>Figure 3.24</b> Section of 2D SEC-UV/vis spectrum for polymer 3.03 .....	154
<b>Figure 3.25</b> Section of 2D SEC-UV/vis spectrum for freeze-dried micelles .....	154
<b>Figure 3.26</b> Section of $^1\text{H}$ NMR spectra for polymers isolated by freeze-drying micelles.....	156
<b>Figure 3.27</b> FT-IR spectra of parent polymer and freeze-dried micelles .....	157
<b>Figure 4.1</b> Self-crosslinking of polymer chains to form defined single polymer chain nanoparticles (SCPNS).....	179
<b>Figure 4.2</b> Crosslinking reactions employed for the irreversible formation of SCPNS .....	181
<b>Figure 4.3</b> H-bonding motifs used for the formation of SCPNS .....	183
<b>Figure 4.4</b> $^1\text{H}$ and $^{13}\text{C}$ NMR spectra of unexpected product 4.01.....	186
<b>Figure 4.5</b> $^1\text{H}$ and $^{13}\text{C}$ NMR spectra of Tz-Tz crosslinker 4.02 .....	188
<b>Figure 4.6</b> SEC traces for linear polymer 4.03, and after heating at 80 °C for 24 hours in DMF .....	191
<b>Figure 4.7</b> Single chain folding with only one or two covalent links per chain38...	192
<b>Figure 4.8</b> $^1\text{H}$ NMR spectra of linear polymer 4.03, control polymer 4.15 .....	194
<b>Figure 4.9</b> SEC traces for linear polymer 4.03, 4.03 heated for 24 h, and model substituted polymer 4.15.....	195

<b>Figure 4.10</b> $^1\text{H}$ NMR spectrum of linear polymer and SCPN 4.03 .....	196
<b>Figure 4.11</b> SEC traces for linear and SCPN 4.03 .....	197
<b>Figure 4.12</b> SEC traces for linear and SCPN 4.12 .....	198
<b>Figure 4.13</b> $D_h$ values at different temperatures calculated using the automatic cumulant fit, and by re-fitting the data.....	201
<b>Figure 4.15</b> SANS data for linear and SCPN 4.03 .....	202
<b>Figure 4.16</b> Kratky plot and Porod plot from SANS data .....	203
<b>Figure 4.17</b> Guinier plot for linear, SCPN 4.03 and control polymer 4.15 .....	205
<b>Figure 4.18</b> Zimm plots for control polymer 4.15 and SCPN 4.03 .....	207
<b>Figure 4.19</b> AFM Z height images for linear precursor 4.03 and control polymer 4.15 .....	209
<b>Figure 4.20</b> Amplitude and phase AFM images of SCPN 4.03 .....	210
<b>Figure 4.21</b> Z height image and line section of two SCPNs .....	210
<b>Figure 4.23</b> Representative TEM images on GO of SCPNs 4.03 .....	211
<b>Figure 4.24</b> Plot profile of one particle in the TEM images, taken from a line scan across the image .....	211
<b>Figure 4.25</b> Histogram of particle $D$ for SCPN 4.03 imaged by TEM on GO .....	212
<b>Figure 5.1</b> Pendant alkene-containing polymers found in the literature .....	231
<b>Figure 5.2</b> Evolution of SEC traces with time for copolymerisation of 5.01 with $t\text{BuA}$ at different concentrations in 1,4-dioxane .....	236
<b>Figure 5.3</b> SEC traces for polymers 5.02–5.08 .....	238
<b>Figure 5.4</b> $^1\text{H}$ NMR spectrum ( $\text{CDCl}_3$ ) of $t\text{BuA}$ copolymer 5.02 .....	239
<b>Figure 5.5</b> $^1\text{H}$ NMR spectrum ( $\text{CDCl}_3$ ) of MA copolymer 5.06 .....	240
<b>Figure 5.6</b> $^1\text{H}$ NMR spectrum ( $\text{CDCl}_3$ ) of IBA copolymer 5.07 .....	240
<b>Figure 5.7</b> $^1\text{H}$ NMR spectrum ( $\text{CDCl}_3$ ) of TEGA copolymer 5.08 .....	241
<b>Figure 5.8</b> $^1\text{H}$ NMR spectrum ( $\text{D}_2\text{O}$ ) of AA copolymer 5.09 .....	242

<b>Figure 5.9</b> Illustration of potential route to fully hydrophobic and amphiphilic graft copolymers .....	244
<b>Figure 5.10</b> $^1\text{H}$ and $^{13}\text{C}$ NMR ( $\text{CDCl}_3$ ) spectra of biotin-Tz .....	245
<b>Figure 5.11</b> $^1\text{H}$ and $^{13}\text{C}$ NMR ( $\text{CDCl}_3$ ) spectra of BODIPY-Tz .....	246
<b>Figure 5.12</b> $^1\text{H}$ NMR spectrum ( $\text{CDCl}_3$ ) of PVL-Tz .....	248
<b>Figure 5.13</b> MALDI mass spectrum and a portion of the predicted and actual mass values of PVL-Tz.....	248
<b>Figure 5.14</b> SEC trace and SEC-UV/vis traces for PVL-Tz .....	249

## Schemes

<b>Scheme 1.1</b> General ATRP mechanism.....	6
<b>Scheme 1.2</b> Equilibrium step in NMP process where the stable nitroxide radical released is TEMPO.....	7
<b>Scheme 1.3</b> Basic RAFT mechanism consisting of conventional free radical initiation, propagation and termination, overlaid with equilibrium steps.	10
<b>Scheme 1.4</b> Comparison between thermal and copper-catalysed azide-alkyne 1,3-cycloadditions .....	15
<b>Scheme 1.5</b> Nitrile oxide-alkyne 1,3 dipolar cycloaddition .....	18
<b>Scheme 1.6</b> Nitrile imine-mediated tetrazole-ene cycloaddition reaction .....	18
<b>Scheme 1.7</b> Thiol-ene/yne and thiol Michael addition click reactions.....	19
<b>Scheme 1.8</b> Thiol-based click reactions: thiol-bromoester, thiol-isocyanate, thiol-pentafluorostyrene, thiol-maleimide, thiol-bromomaleimide and thiol-epoxide .....	21
<b>Scheme 1.9</b> Oxime bond formation from aldehyde and aminoxy functionalities ...	23
<b>Scheme 1.10</b> Reaction of PFP styrenic and methacrylic esters selectively with two different amines in a sequential manner.....	24

<b>Scheme 1.11</b> Staudinger elimination, Staudinger-Bertozzi ligation .....	25
<b>Scheme 1.12</b> DA reaction between butadiene and ethylene to form cyclohexene .	27
<b>Scheme 1.13</b> Reversible formation by DA/rDA reactions of 3-armed stars using a trifunctional furan core and maleimide-terminated polymers .....	28
<b>Scheme 1.14</b> General reaction between a symmetrical 1,2,4,5-tetrazine and alkene — multiple regioisomers are formed if asymmetric reagents are used .....	32
<b>Scheme 1.15</b> Tetrazine-based polymers for optoelectronics: metal-conjugated, incorporated along the backbone and as a pendent functionality.....	37
<b>Scheme 1.16</b> Pinner synthesis of aromatic-substituted tetrazine, dimerisation of ethyl diazoacetate to form dicarboxy tetrazine .....	38
<b>Scheme 2.1</b> Reaction between norbornene-functionalised RAFT agent and dipyridyl 1-2-4-5-tetrazine .....	63
<b>Scheme 2.2</b> General RAFT synthesis of Nb-terminated PS and PNIPAM .....	70
<b>Scheme 2.3</b> Synthesis by ROP of Nb-terminated PVL and PCL.....	70
<b>Scheme 2.4</b> Synthesis of Tz–COOH in three steps. ....	71
<b>Scheme 2.5</b> Synthesis of tetrazine-terminated PEG .....	72
<b>Scheme 2.6</b> Synthesis of PVL–Tz by acid-catalysed ROP .....	73
<b>Scheme 2.7</b> Polymer–polymer coupling between PS–Nb and PEG–Tz .....	82
<b>Scheme 2.8</b> Attempted couplings of Nb-terminated poly(ester)s and PEG–Tz.....	94
<b>Scheme 3.1</b> Competition reaction between tetrazine, norbornene and propargyl chloride .....	123
<b>Scheme 3.2</b> Competition reaction between water-soluble 2-azidoacetic acid, propargyl alcohol and norbornene <i>endo</i> -, <i>endo</i> - dimethanol .....	125
<b>Scheme 3.3</b> Nb–St monomer synthesis .....	126
<b>Scheme 3.4</b> Copolymerisation of Nb–St and St .....	128
<b>Scheme 3.5</b> Synthesis of trimethyl silane-protected propargyl acrylate .....	133

<b>Scheme 3.6</b> Synthetic approach to polymers 3.01, 3.02, and 3.03 .....	137
<b>Scheme 3.7</b> Formation of micelles from polymer 3.03 .....	139
<b>Scheme 3.8</b> Approach to functionalisation of micelles .....	142
<b>Scheme 3.9</b> Synthesis of pro-fluorescent coumarin- $N_3$ .....	144
<b>Scheme 4.1</b> Attempted synthesis of a bifunctional tetrazine crosslinker, and the unexpected product resulting.....	185
<b>Scheme 4.2</b> Synthesis of bifunctional tetrazine crosslinker 4.02.....	187
<b>Scheme 4.3</b> Formation of substituted, uncrosslinked polymer 4.15 .....	193
<b>Scheme 5.1</b> Synthesis of pendent alkene-containing monomer 5.01 .....	234
<b>Scheme 5.2</b> General RAFT copolymerisation of 5.01 and acrylate monomers.....	235
<b>Scheme 5.3</b> Acid-catalysed deprotection of <i>t</i> BuA copolymer .....	242
<b>Scheme 5.4</b> Synthesis of tetrazine-functionalised biotin and fluorescent BODIPY dye 5.11 .....	244
<b>Scheme 5.5</b> Synthesis of PVL-Tz by acid-catalysed ROP .....	247

## Tables

<b>Table 2.1</b> Polymers synthesised and used in this chapter.....	74
<b>Table 2.2</b> Molecular weights and dispersities of homopolymers and crude diblock	86
<b>Table 2.3</b> Relative integrals from number distributions in Figure 2.19 and calculated fraction of homo- and block copolymer chains .....	88
<b>Table 2.4</b> Volume fractions of peaks detected in LC-SEC chromatogram .....	90
<b>Table 2.5</b> Integration values of Tz peak for each LC chromatogram .....	108
<b>Table 3.1</b> $D_h$ of micelles measured by DLS and $D_{av}$ of micelles measured by TEM (imaging on GO) .....	148
<b>Table 3.2</b> Approximate copper concentrations in micelle solutions obtained by ICP- MS .....	152

<b>Table 3.3</b> Properties of polymers obtained from freeze-dried micelles, obtained by SEC .....	153
<b>Table 4.1</b> Apparent $M_n$ , $M_w$ and $M_w/M_n$ values by SEC for equivalent linear polymers and SCPNs .....	190
<b>Table 4.2</b> $M_w$ values by SLS for SCPN 4.03 and control polymer 4.15 .....	208
<b>Table 4.3</b> SCPN 4.03 sizes by various analytical techniques .....	213
<b>Table 5.1</b> Relative reaction rates of alkenes with dipyrityl tetrazine .....	233
<b>Table 5.2</b> Copolymerisations of monomer 5.01 with various acrylate monomers .	238
<b>Table 5.3</b> Conversion of alkene in polymer 5.02 after 24 h reaction with $Tz(pyr)_2$ in varying solvents with increasing polarity.....	251
<b>Table 5.4</b> Conversion of alkene functionalities in the Lewis acid-catalysed reaction of polymer 5.02 with $Tz(pyr)_2$ .....	253

## **Acknowledgements**

First and foremost my thanks go to my supervisor, Rachel O'Reilly, who has supported me all the way from my first forays into synthetic chemistry during an undergraduate summer project up until now. I am grateful to the Warwick Postgraduate Research Scholarship fund for providing me with PhD funding, and to Rachel for shuffling the accounts when that ran out.

To all the members of the O'Reilly group, past and present – thanks for the good times in and out of the lab, especially the class of 2009: Tom, Annie and Joe, and of course the O'Reilly group Triathlon Team. Special thanks also go to Shirley Ye, an MChem student who helped out a lot with the work in Chapter 5.

Thank you also to Professor Filip Du Prez, Pieter Espeel and Milan Stamenovic at the University of Gent, for their kind hospitality during the summer I spent working in their labs and subsequent fruitful collaboration.

To my long-suffering parents – thank you for the support, financial and otherwise, over my many years of higher education; I promise I'll get a job now... And Olly, my best friend and partner in (strictly metaphorical) crime, thank you more than I can ever say, for more than you'll ever know.

## **Declaration of authorship**

This thesis is submitted to the University of Warwick in support of my application for the degree of Doctor of Philosophy. It has been composed by myself and has not been submitted in any previous application for any degree. The work presented (including data generated and data analysis) was carried out by the author except in the case of Chapter 2, which was carried out in collaboration with Milan Stamenovic and Pieter Espeel from Professor Filip Du Prez's group at Ghent University, Belgium, and Ian Barker and Dr Andrew Dove at the University of Warwick. Any materials synthesised or data analysis carried out by persons other than the author are clearly labelled in the text of that chapter.



## List of publications

- RAFT techniques for the synthesis of functional materials. O'Reilly, R. K.; Skey, J.; Hansell, C. F. *Abstracts of Papers, 235th ACS National Meeting*, New Orleans, **2008**, POLY-060
- Mild and facile synthesis of multi-functional RAFT chain transfer agents. O'Reilly, R. K.; Hansell, C.F. *Polymers (Basel)* **2009**, 1, 3-15
- Stabilization of amino acid derived diblock copolymer micelles through favourable D:L side chain interactions. Skey, J.; Hansell, C. F.; O'Reilly, R.K. *Macromolecules* **2010**, 43, 1309-1318
- Tetrazine-norbornene click reactions to functionalize degradable polymers derived from lactide. Barker, I. A.; Hall, D. J.; Hansell, C. F.; Du Prez, F. E.; O'Reilly, R. K.; Dove, A. P. *Macromol. Rapid Comm.* **2011**, 32, 1362-1366
- Additive-free clicking for polymer functionalization and coupling by tetrazine-norbornene chemistry. Hansell, C. F.; Espeel, P.; Stamenovic, M. M.; Barker, I. A.; Dove, A. P.; Du Prez, F. E.; O'Reilly, R. K. *J. Am. Chem. Soc.* **2011**, 133, 13828-13831 (**Chapter 2**)
- Norbornenyl based chain transfer agents enabling the preparation of functional polymers via RAFT and post-polymerization modification. Espeel, P.; Stamenovic, M. M.; Hansell, C. F.; O'Reilly, R. K.; Du Prez, F.

E. *Abstracts of Papers, 242nd ACS National Meeting & Exposition, Denver, 2011*, POLY-544

- Tetrazine-norbornene click chemistry: polymer coupling and functionalization. Hansell, C. F.; Espeel, P.; Stamenovic, M. M.; Barker, I. A.; Dove, A. P.; Du Prez, F. E.; O'Reilly, R. K. *Abstracts of Papers, 243rd ACS National Meeting & Exposition, San Diego, 2012*, PMSE-445
- A 'mix-and-click' approach to double core-shell micelle functionalization. Hansell, C.F. & O'Reilly, R.K. *ACS Macro Lett.* **2012**, 1, 896-891  
(Chapter 3)
- pH-Switchable polymer nanostructures for controlled release. Doncom, K.E.B.; Hansell, C.F.; Theato, P.; O'Reilly, R. K. *Polym. Chem.* **2012**, 3, 3007-3015
- Synthesis of responsive polymers by RAFT polymerization, and their self-assembly into morphology switching nanostructures. Doncom, K.E.B.; Hansell, C.F.; O'Reilly, R. K.; Theato, P. *Abstracts of Papers, 245th ACS National Meeting & Exposition, New Orleans, 2013*, PMSE-539
- One-pot synthesis of responsive sulfobetaine nanoparticles by RAFT polymerisation: the effect of branching on the UCST cloud point. Willcock, H.; Lu, A; Hansell, C.F.; Chapman, E.; Collins, I.R.; O'Reilly, R.K. *Polym. Chem.* **2013**, submitted

## Summary of thesis

This thesis explores the use of the tetrazine–norbornene inverse electron demand Diels-Alder cycloaddition reaction in polymer and materials science.

Chapter 1 gives an introduction to the main concepts and techniques used throughout the thesis.

Chapter 2 applies the tetrazine–norbornene reaction to polymer end-functionalisation and polymer–polymer coupling, in both organic media and water, and establishes the methods (UV/vis and  $^1\text{H}$  NMR spectroscopies) for monitoring the coupling reaction.

Chapter 3 applies the reaction to the modification of a self-assembled polymer micelle and demonstrates its use in tandem with the copper-catalysed azide–alkyne click reaction. The synthesis of an amphiphile bearing both norbornene and alkyne groups is described, the amphiphile is self-assembled and a one-pot dual functionalisation of both the core and shell carried out.

Chapter 4 describes the formation and analysis by a variety of methods of sub-20 nm sized polystyrene nanoparticles through the single chain collapse of a norbornene-decorated polymer, ligated with a bisfunctional tetrazine.

Chapter 5 discusses attempts to further expand the use of the reaction of tetrazines to polymers bearing pendent alkene groups. The synthesis and characterisation of such polymers is detailed, and attempts to functionalise with a variety of tetrazines described.

## Abbreviations

$\delta$  – chemical shift

$\lambda$  – wavelength

$\nu$  – wavenumber

AFM – Atomic Force Microscopy

AIBN – Azobisisobutyronitrile

ARGET – Activators ReGenerated by Electron Transfer

ATNRC – Atom Transfer Nitroxide Radical Coupling

ATRP – Atom Transfer Radical Polymerisation

BCB – Benzocyclobutene

BODIPY – boron-dipyrromethene

b.p. – boiling point

CAS – Chemical Abstracts Service

COSY – Correlation Spectroscopy

CRP – Controlled Radical Polymerisation

CTA – Chain Transfer Agent

CuAAC – Copper-catalysed Azide-Alkyne Cycloaddition

d – doublet

DA – Diels-Alder

DA<sub>inv</sub> – inverse electron demand Diels-Alder

DDMAT – 2-(dodecylthiocarbonothioylthio)-2-methylpropionic acid

$D_h$  – Hydrodynamic diameter

DLS – Dynamic Light Scattering

DMAP – 4-(Dimethylamino)pyridine

DNA – Deoxyribonucleic acid

DMF – *N,N*-Dimethylformamide

DMSO – Dimethyl Sulfoxide

dn – ‘down’ (in  $^{13}\text{C}$ -ATP NMR spectrum)

DOSY – Diffusion Ordered Spectroscopy

DP – Degree of Polymerisation

DPP – Diphenyl phosphate

EDCI – *N*-(3-Dimethylaminopropyl)-*N'*-ethylcarbodiimide hydrochloride

eq. – equivalents

ESI – Electrospray Ionisation

FT-IR – Fourier Transform InfraRed

GO – Graphene Oxide

GTP – Group Transfer Polymerisation

HBTU – *O*-(Benzotriazol-1-yl)-*N,N,N',N'*-tetramethyluronium

hexafluorophosphate

HDA – Hetero Diels-Alder

HMBC – Heteronuclear Multiple-Bond Correlation Spectroscopy

HOMO – Highest Occupied Molecular Orbital

HPLC – High Pressure Liquid Chromatography

HRMS – High Resolution Mass Spectrometry

HSQC – Heteronuclear Single-Quantum Correlation Spectroscopy

IBA – isobornyl acrylate

ICAR – Initiators for Continuous Activator Regeneration

ICP-MS – Inductively-Coupled Plasma Mass Spectrometry

IUPAC – International Union of Pure and Applied Chemistry

*J* – coupling constant

LC – Liquid Chromatography

LCST – Lower Critical Solution Temperature

LUMO – Lowest Unoccupied Molecular Orbital

m – multiplet

MA – methyl acrylate

MADIX – Macromolecular Design by Interchange of Xanthates

MALDI – Matrix-Assisted Laser Desorption Ionisation

MOF – Metal-Organic Framework

mol% – mole percent

$M_n$  – number-average molecular weight

$M_w$  – weight-average molecular weight

$M_w/M_n$  – dispersity index

Nb – norbornene

NHS – *N*-hydroxysuccinimide

NITEC – Nitrile Imine-mediated Tetrazole Alkene Cycloaddition

NMP – Nitroxide-Mediated Polymerisation

NMR – Nuclear Magnetic Resonance

PAA – poly(acrylic acid)

PEG – poly(ethylene glycol)

PCL – poly( $\epsilon$ -caprolactone)

PFP – pentafluorophenyl

PFS – pentafluorostyrene

PLA – polylactide

PMMA – poly(methyl methacrylate)

PNIPAM – poly(*N*-isopropylacrylamide)

PS – polystyrene

PTFE – polytetrafluoroethylene

PVL – poly( $\delta$ -valerolactone)

q – quartet

quin – quintet

RAFT – Reversible Addition-Fragmentation chain Transfer

rDA – retro Diels-Alder

RDRP – Reversible-Deactivation Radical Polymerisation

$R_f$  – Retardation factor

$R_g$  – Radius of gyration

$R_h$  – Hydrodynamic radius

RI – Refractive Index

ROP – Ring Opening Polymerisation

ROMP – Ring Opening Metathesis Polymerisation

s – singlet



SANS – Small Angle Neutron Scattering

SCORE – Speedy COmponent Resolution

SCPN – Single Chain Polymer Nanoparticle

SEC – Size Exclusion Chromatography

SLD – Scattering Length Density

SLS – Static Light Scattering

SPAAC – Strain Promoted Azide Alkyne Cycloaddition

St – styrene

t – triplet

*t*BuA – *tert*-butyl acrylate

TEA – triethylamine

TEGA – triethylene glycol acrylate

TEM – Transmission Electron Microscopy

TEMPO – 2,2,6,6-Tetramethylpiperidin-1-yl)oxyl

$T_g$  – Glass transition temperature

THF – Tetrahydrofuran

THPA – Tetrahydropyranyl acrylate

THPTA – tris(hydroxypropyl)triazolylmethyl-amine

ToF – Time of Flight

TTC – trithiocarbonate

Tz – tetrazine

u – ‘up’ (in  $^{13}\text{C}$ -ATP NMR spectrum)

UV/vis – ultraviolet/visible

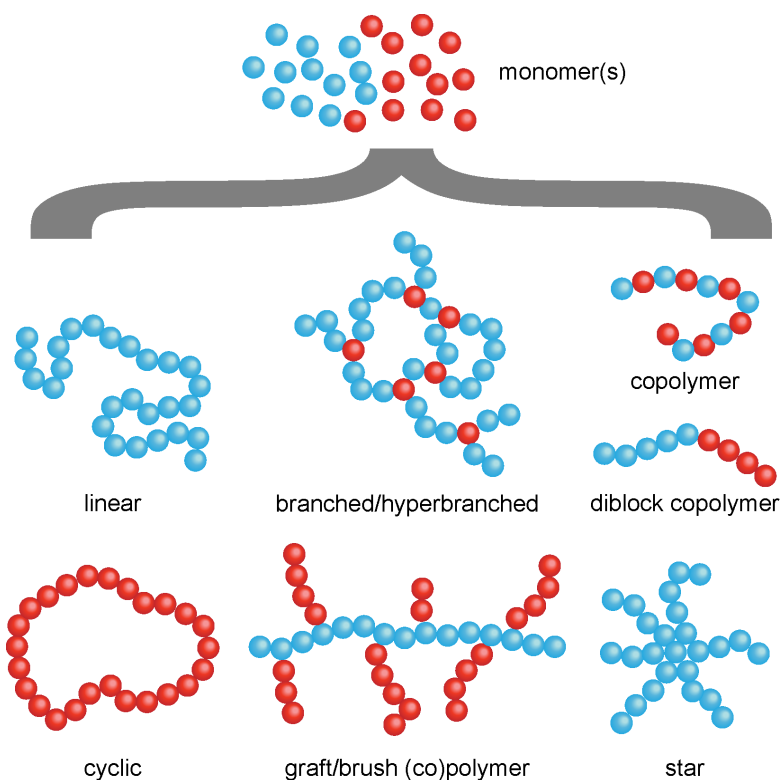
# **Chapter 1. Introduction**

## **1.1. Abstract**

In this chapter an introduction and background to the main themes of this thesis is laid out. The synthesis of polymers by controlled radical methods is described, followed by a variety of 'click' methods for post polymerisation modification. The Diels-Alder with inverse electron demand is introduced as a potential click methodology, specifically between tetrazines and strained alkenes, and the background to this reaction followed by examples of its use in other chemical fields. A brief overview of approaches to the synthesis of functional tetrazines is also described.

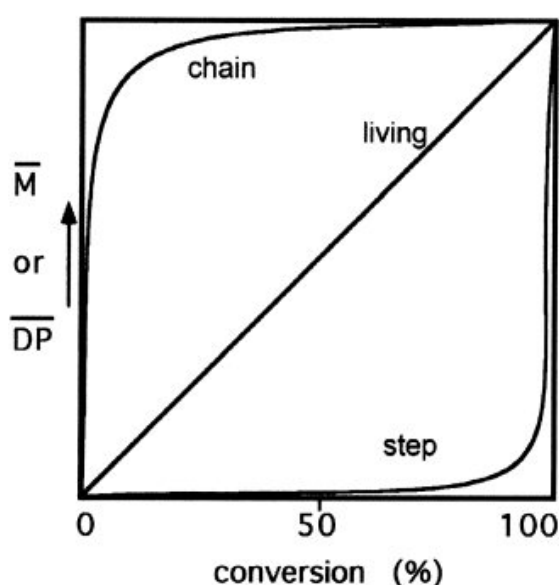
## 1.2. Polymers

Since the birth of polymer chemistry in the early 20<sup>th</sup> century, with the seminal discoveries and theories of Baekeland, Staudinger,<sup>1</sup> Stockmayer,<sup>2</sup> Carothers and Flory,<sup>3</sup> macromolecular and polymeric materials have become indispensable to modern life. The first synthetic polymers, such as Bakelite and Nylon, were created for their bulk properties with little attention paid to finer control of molecular weight or architecture – or indeed the ability to affect such variables. However, since those first steps towards a ‘plastic world’, synthetic and analytical techniques have developed apace such that now almost any molecular weight, structure, topology of polymer (Figure 1.1), or functionality contained therein, is accessible.



**Figure 1.1 Some of the many architectures accessible by contemporary polymerisation techniques**

A great deal of this progress has been due to the development of “living” and “pseudo-living” polymerisation techniques. The difference in the manner of polymer formation between traditional chain-growth and step-growth polymerisations and living polymerisation processes are seen in Figure 1.2. Intuitively it can be seen that living polymerisations afford finer control over molecular weights due to the linear molecular weight evolution with conversion.



**Figure 1.2 Evolution of molecular weight with conversion for chain-growth, step-growth and living polymerisations<sup>4</sup>**

A living polymerisation is one from which chain termination and chain transfer are absent,<sup>5</sup> and the experimental criteria which can be used to determine whether a polymerisation is living or not are:<sup>6</sup>

- The polymerisation proceeds until all of the monomer has been consumed, and further addition of monomer results in continued polymerisation
- The number average molecular weight ( $M_n$ ), or number average degree of polymerisation (DP) correlates linearly with conversion
- The number of active propagating sites, and therefore polymer molecules, is constant and independent of conversion
- Molecular weight can be controlled by the monomer to initiator ratio
- Narrow molecular weight distribution polymers are produced
- Block copolymers can be prepared by sequential addition of monomers
- Chain-end functionalised polymers are produced in quantitative yield

The first living polymerisation system was the anionic polymerisation of styrene using sodium naphthalene as an initiator;<sup>7</sup> however this and other living ionic polymerisations suffer from very poor functional group tolerance, and a need for extremely stringent reaction conditions and prohibitively high solvent and reagent purity. As such, alternative polymerisations have been developed that still give good control over polymer molecular weight parameters, but are much easier to set up and tolerant to both functional groups in the monomer and slight impurities; these include Ring-Opening Polymerisation (ROP),<sup>8</sup> Ring-Opening Metathesis Polymerisation (ROMP),<sup>9</sup> Group Transfer Polymerisation (GTP)<sup>10</sup> and Controlled Radical Polymerisation (CRP).

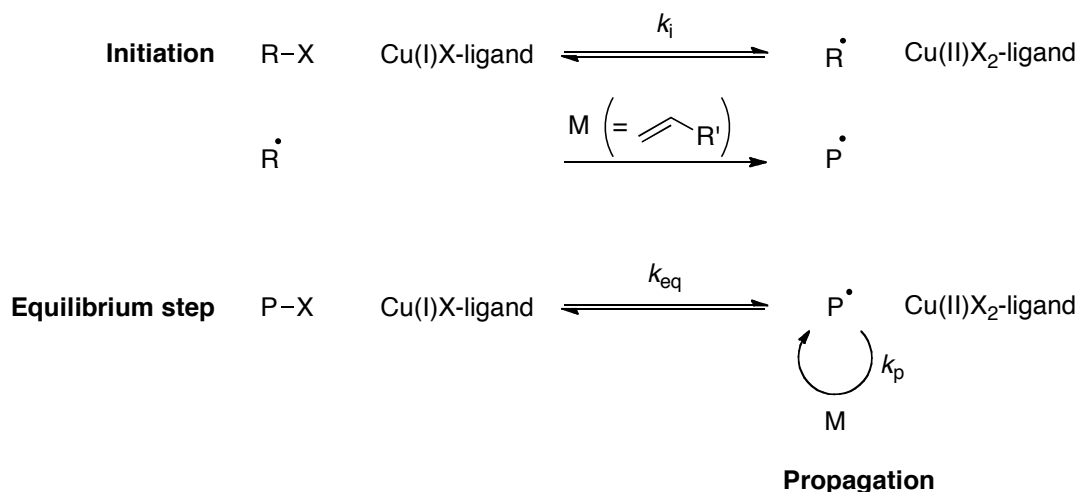
### 1.3. Controlled Radical Polymerisation

Free radical polymerisation of vinyl monomers provides access to a wide range of functionality inherent to the monomers, but control of molecular weight and dispersity is encumbered by the large amount of radical–radical termination present, which increases with increasing radical concentration. An important development towards the synthesis of functional polymers was the development of “pseudo-living” radical polymerisations, which aim to reduce the concentration of radicals used in the polymerisation and therefore also reduce termination events to confer some living character on the polymerisation. Strictly speaking, the term (pseudo-)living radical polymerisation is strongly discouraged by IUPAC,<sup>11</sup> with “reversible-deactivation radical polymerisation” (RDRP) or “controlled radical polymerisation” (CRP) preferred; for the remainder of this thesis CRP shall be the term used for these types of polymerisations. Of the CRP techniques, there are three main protagonists: ATRP, NMP and RAFT/MADIX, all are based on the “iniferter” concept of Otsu *et. al.*,<sup>12</sup> whereby a single species is used to mediate *initiation*, chain *transfer* and *termination* within a polymerisation system.

#### 1.3.1. Atom Transfer Radical Polymerisation

ATRP was first reported almost simultaneously by Sawamoto<sup>13</sup> and Matyjaszewski<sup>14</sup> in 1995. The principle on which termination is minimised and therefore control is gained is the reversible capping or “degenerative transfer” of the growing polymer chain end with a halide leaving group. This

takes advantage of the so-called ‘persistent radical effect’,<sup>15</sup> whereby released radical species are stable (in this case the halide radical, which coordinates to a Cu–ligand complex) and can build up in the system without causing deleterious termination, disproportionation or unwanted propagation events. In contrast, the active polymer chain end reacts with any monomer present to propagate the chain, before being reversibly capped by the halide radical again. The process is mediated by the Cu(I)–ligand species, the composition of which determines the equilibrium constant ( $k_{eq}$  in Scheme 1.1) between the dormant species and the propagating chain end, and therefore is the determinant of control over the polymerisation. To minimise radical termination events,  $k_{eq}$  needs to favour the dormant polymer chain capped by halide X. This drastically lowers the concentration of radicals in the system and therefore reduces the likelihood of radical coupling or disproportionation events.



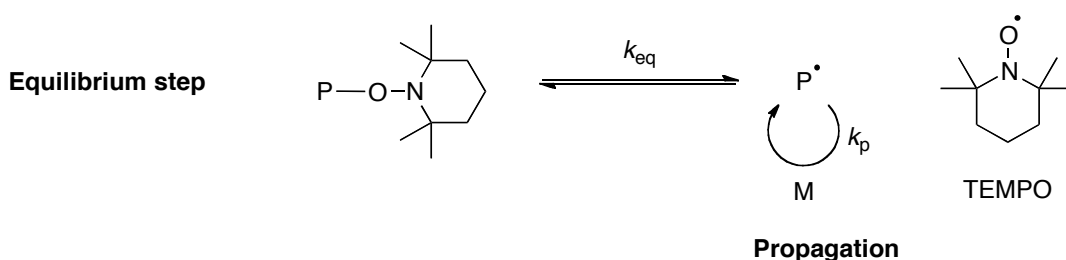
**Scheme 1.1 General ATRP mechanism**



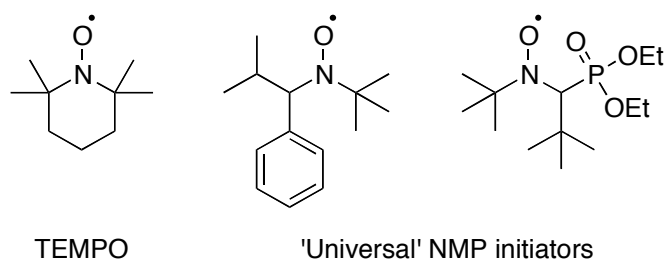
The chief drawback of ATRP is the requirement for relatively large amounts of copper which must be subsequently removed; however, several variants on the standard ATRP system have been developed, for example Activators ReGenerated by Electron Transfer (ARGET)-ATRP<sup>16</sup> and Initiators for Continuous Activator Regeneration (ICAR)-ATRP,<sup>17</sup> which can reduce the amount of copper required down to ppm levels.

### 1.3.2. Nitroxide Mediated Polymerisation

Nitroxide-Mediated Polymerisation (NMP)<sup>18</sup> was the first of the CRP techniques to be developed.<sup>19</sup> It works on the same principle as ATRP, that of an equilibrium between dormant capped polymer chains and active radical chain ends; in the case of NMP this equilibrium is provided by an alkoxyamine initiator which releases a persistent free nitroxide radical during the equilibrium process (Scheme 1.2). The first generation of these was based on 2,2,6,6-tetramethylpiperidin-1-yl)oxyl (TEMPO), but that gave only moderate control in a limited number of (mainly styrenic) cases.



**Scheme 1.2 Equilibrium step in NMP process where the stable nitroxide radical released is TEMPO**



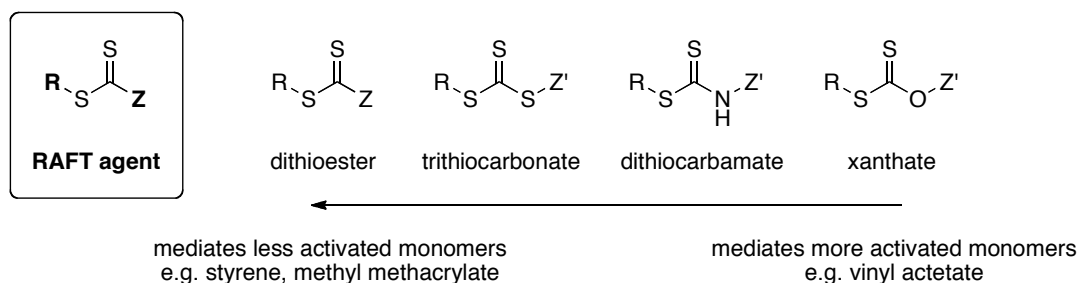
**Figure 1.3 Some NMP-mediating species<sup>20</sup>**

There have since been reported many NMP initiators to expand the scope and versatility of NMP to a greater variety of monomer families, including so-called 'universal initiators'<sup>20</sup> (Figure 1.3), however the technique tends to be overlooked in favour of ATRP and RAFT, possibly due to the high temperatures (typically > 100 °C) generally required, and the limited success in polymerising methacrylates.<sup>21</sup>

### **1.3.3. Reversible Addition Fragmentation chain Transfer Polymerisation**

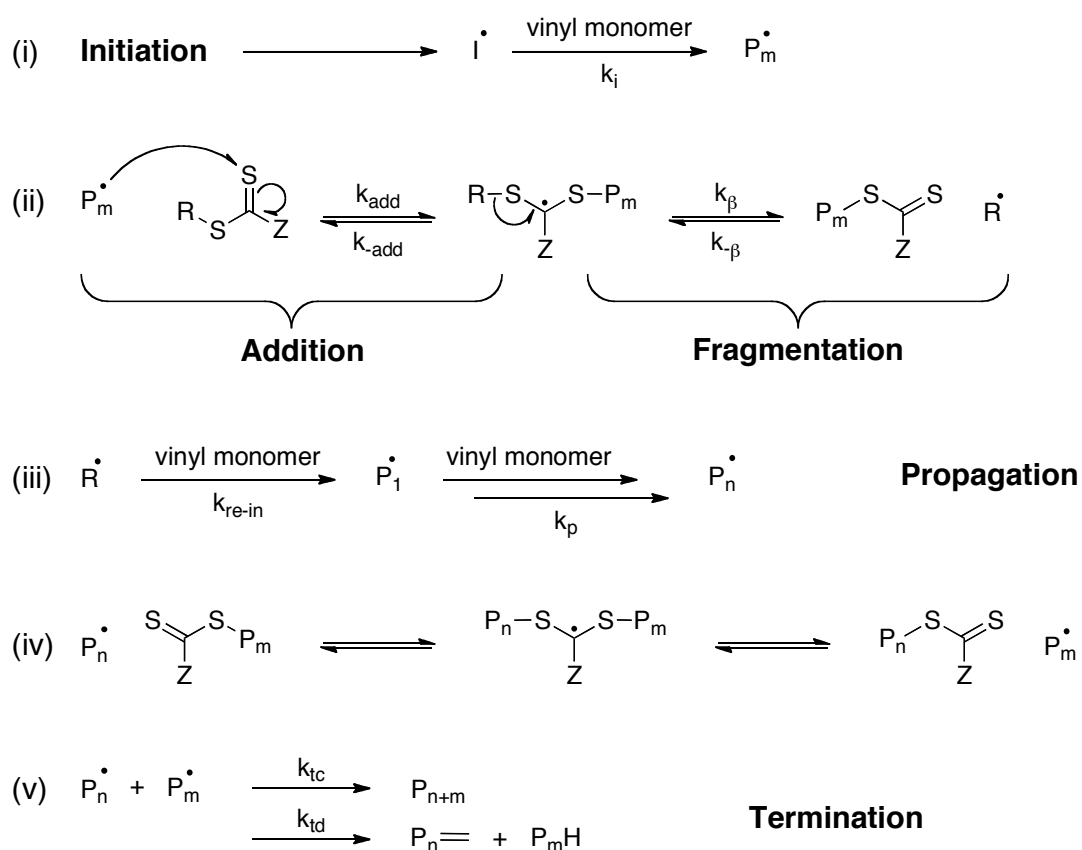
RAFT polymerisation was developed almost simultaneously in Australia<sup>22</sup> and France, where it was called Macromolecular Design by Interchange of Xanthates (MADIX).<sup>23</sup> However, as MADIX is more properly a subtype of RAFT — they both have the same reaction mechanism but MADIX is limited to xanthate mediation whereas RAFT is mediated by more general thioester-type chain transfer agents (CTAs) (Figure 1.4) — RAFT is the term most used to describe these polymerisations. It differs from both ATRP and NMP in that control is not achieved by an equilibrium between a dormant and active chain end, but rather an equilibrium between all polymer

chains, such that the thioester group rapidly ‘shuffles’ between chains, thus giving all chains an equal opportunity to propagate and conferring control upon the system.



**Figure 1.4 Types of RAFT chain transfer agent (CTA)**

Whilst there is some debate over missing reaction steps and/or potential side reactions in the early stages of the reaction,<sup>24</sup> the generally accepted basic RAFT mechanism<sup>25</sup> is shown in Scheme 1.3, and consists of a free radical polymerisation (initiation, propagation and termination) overlaid with two important equilibrium processes – the pre-equilibrium (ii) and main equilibrium (iv). Initiation is by an external free radical source, often the thermal decomposition of diazo compounds such as azobisisobutyronitrile (AIBN); the oligomeric radicals produced react with the RAFT agent (the pre-equilibrium step ii), and in an ideal RAFT polymerisation all CTAs are consumed in this way before propagation commences.<sup>26</sup> Propagation occurs in the normal free radical way, but the main equilibrium (step iv) means that growing radicals rapidly exchange with thioester-capped chains so that all chains grow at a similar rate, and termination steps, although present, are minimised.



**Scheme 1.3 Basic RAFT mechanism consisting of conventional free radical**  
**(i) initiation (iii) propagation and (v) termination, overlaid with equilibrium**  
**steps (ii) and (iv)**

The R and Z groups have a significant effect on the polymerisation: the former governs the pre-equilibrium in that it should be stable enough for fragmentation to be favoured, yet it also needs to be unstable enough to be a good (re)initiator in step iii. The Z group affects the stability of the thiocarbonylthio double bond and therefore the stability of the adduct radical in the main equilibrium; monomers that have corresponding unstable radicals (such as vinyl acetate) are best controlled by CTAs with a stabilising Z group to favour the adduct radical and therefore set up the

rapid main equilibrium required to control the system. Likewise, monomers with relatively stable radicals (e.g. styrene) require destabilising Z groups such as phenyl groups.

Because of the wide variation in R and Z groups that is possible, and the relative ease of synthesis of the CTAs,<sup>27</sup> RAFT is a versatile method for the polymerisation of vinyl monomers, and has experienced an explosion in popularity since its discovery. In addition, the thiocarbonylthio end group inherent to the chain end can be modified in a number of ways, including aminolysis or reduction to a thiol<sup>28</sup> which in turn opens up enormous possibilities for end modification of RAFT-synthesised polymers.<sup>29</sup>

#### **1.4. Post-polymerisation modification**

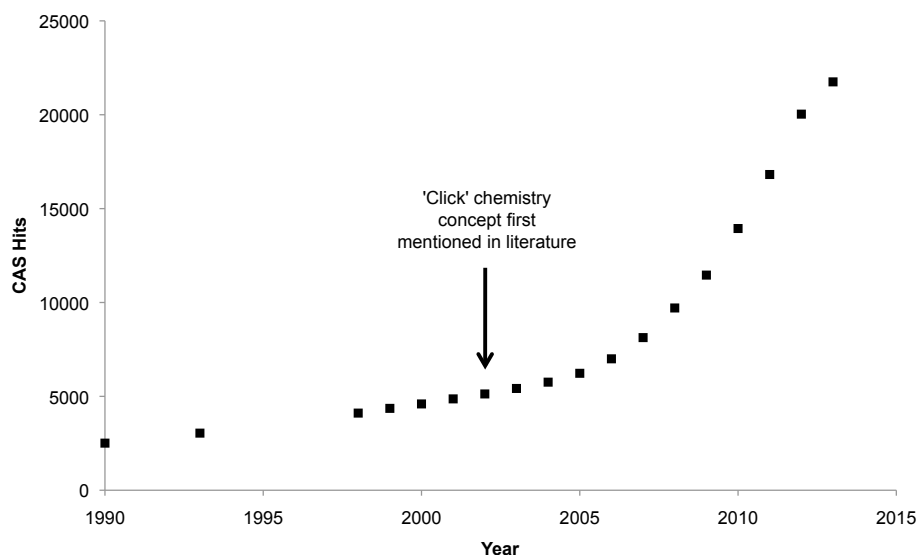
Even with the increasing sophistication of the many and varied polymerisation techniques, it is often advantageous to modify, functionalise or conjugate synthesised polymers to species of interest *after* polymerisation. This could be for several reasons: the conjugate or functionality of interest is unstable to polymerisation conditions, or a library of polymers from a single, well-defined scaffold polymer is the goal. Both the design and polymerisation of novel functional monomers, and the post-polymerisation modification of existing polymers are equally valid approaches, and one may be more appropriate than the other for any given project.

However, more so than in traditional organic synthesis, modification of polymer scaffolds requires reliable reactions that go to high conversions

and require minimal work-up, as chromatographic separation of polymeric species is difficult, and may require specialised equipment to carry out effectively.

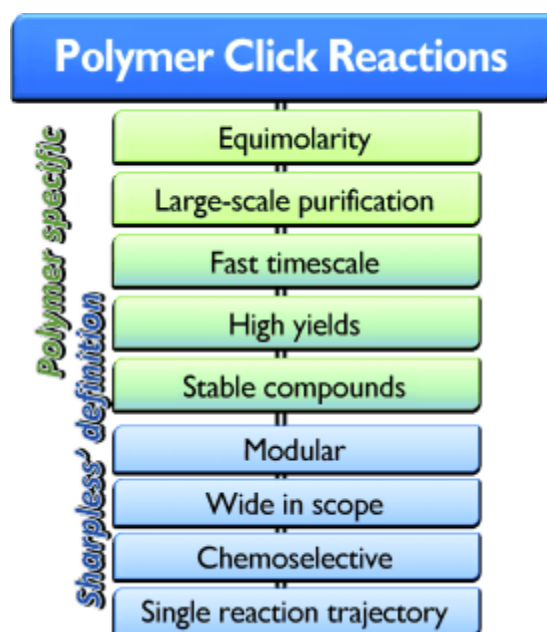
### **1.5. 'Click' Reactions**

The concept of a 'Click' reaction was first conceived in 2001,<sup>30</sup> although many reactions that fall under the Click umbrella were well known and used long before then. The criteria for a reaction to be a Click reaction were outlined by Sharpless and coworkers as: "the reaction must be modular, wide in scope, give very high yields, generate only inoffensive byproducts that can be removed by nonchromatographic methods, and be stereospecific. The required process characteristics include simple reaction conditions (ideally, the process should be insensitive to oxygen and water), readily available starting materials and reagents, the use of no solvent or a solvent that is benign (such as water) or easily removed, and simple product isolation." The concept has been widely embraced, exemplified by the number of results in the CAS database when searching for the keyword 'click' in publication titles (over 22,000 as of June 2013, Figure 1.5).



**Figure 1.5 Number of results returned by the CAS database for the search term ‘click’ — cumulative hits to year end (as of June 2013)**

Click reactions have had a particular impact on polymer and materials science, as the opportunity to readily modify polymer chain ends or pendent groups offers an unprecedented ability to fine-tune bulk or microscopic polymer properties. Sharpless’ requirement for simple product separation by nonchromatographic methods is particularly pertinent as purification methods such as distillation are not feasible for polymeric materials and thus if purification is required, (selective) precipitation is the only relatively simple option. This implies that the reaction should proceed to full conversion with equimolar amounts of starting materials in order to obtain a pure product. With these two points highlighted, an expanded set of criteria for polymer click reactions have been proposed,<sup>31</sup> and are shown in Figure 1.6.



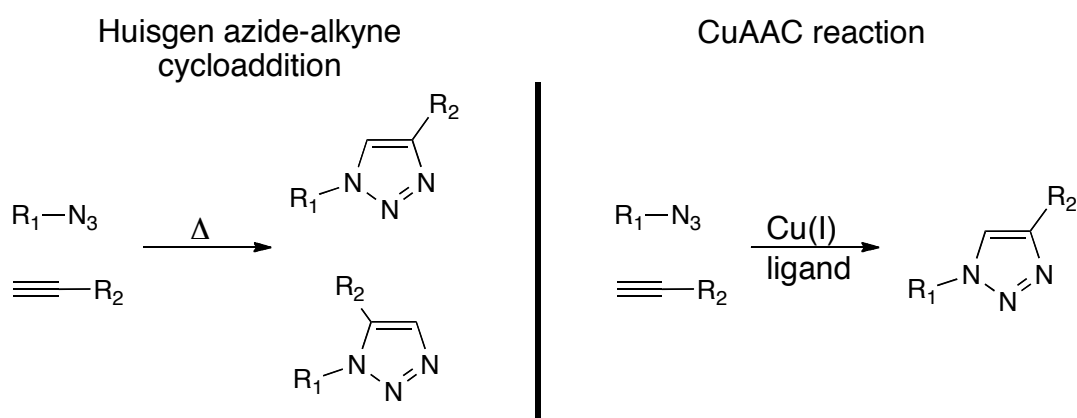
**Figure 1.6 Polymer-specific click criteria — blue are Sharpless' original criteria, green are ones particularly important or specific to polymer click reactions<sup>31</sup>**

Due to the enormous range and number of publications involving click chemistry, it is beyond the scope of this thesis to review even a small portion of them; however, several reviews have been published highlighting the many and varied applications of click chemistries to polymer and materials science.<sup>32</sup> A survey of several reactions that have been referred to as click reactions in the literature follows. All of these reactions fulfil several of the Sharpless criteria for a click reaction, but in some cases there are criteria that have not strictly been fulfilled.



### 1.5.1. Copper catalysed azide–alkyne (CuAAC)

Arguably, the copper-catalysed azide–alkyne cycloaddition (CuAAC)<sup>33</sup> has become the *de facto* standard for many applications where click reactions are required, and thus has become almost synonymous with the term ‘Click reaction’. The reaction is a variant of the Huisgen (thermal) 1,3 dipolar cycloaddition between an azide and terminal alkyne, catalysed by Cu(I) that is usually produced by the reduction of a Cu(II) species *in situ* and stabilised by a complexing ligand. The reaction product is exclusively a 1,4-triazole in the copper-catalysed case.



**Scheme 1.4 Comparison between thermal (Huisgen, left) and copper-catalysed (CuAAC, right) azide–alkyne 1,3-cycloadditions**

The CuAAC reaction is far and away the most popular and widely-used click reaction in materials science; it has been used to synthesise polymers in a step-growth manner<sup>34</sup> as well as dendrimers,<sup>35</sup> but its main use has undoubtedly been for the functionalisation of already existing polymers. In this regard, polymer–polymer conjugation<sup>36</sup> and star polymer synthesis,<sup>37</sup>

polymer cyclisation,<sup>38</sup> conjugation to peptides/proteins<sup>39</sup> and carbon nanotubes,<sup>40</sup> single polymer chain collapse,<sup>41</sup> and functionalisation of self-assembled amphiphilic copolymers<sup>42</sup> are just some of the applications the CuAAC reaction has been used for.

However, it is not without its drawbacks. Although it undoubtedly fulfils all of the requirements of a click reaction, the requirement for a metal catalyst and its subsequent complete removal can be a deterrent to its use, whether this is a perceived or actual problem for the application in question. Additionally, there are some concerns over the stability and explosive nature of low molecular weight azido species, often used to introduce the azide click handle.<sup>43</sup> Finally, there is, as yet, no universal Cu(I) complex that has been identified as a suitable 'off the shelf' catalyst or precatalyst for CuAAC under all conditions; thus, in organic media particularly, conditions need to be tailored for each new reaction.

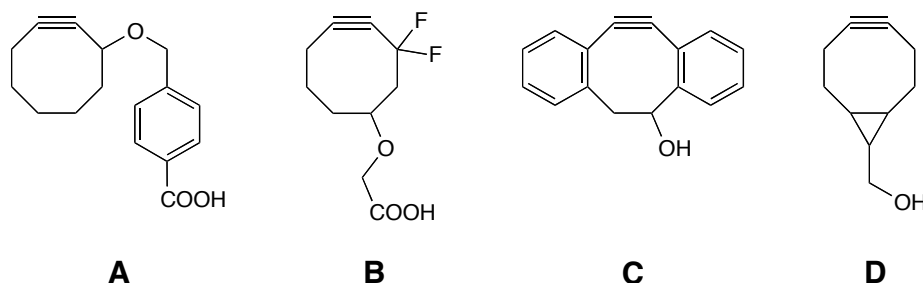
Therefore many groups have focused attention on reactions that display similar click characteristics to the CuAAC reaction, but require no metal catalyst.<sup>44</sup>

## **1.5.2. Dipolar cycloadditions**

### **1.5.2.1. Copper-free azide–alkyne**

Given the undeniable popularity of the CuAAC reaction, it is not surprising that considerable attention has been given to adapting the cycloaddition between azides and alkynes such that no Cu(I) catalyst is required.

Cyclooctynes have proved the most fruitful avenue of exploration, with both strain-promoted (SPAAC) and electronically-promoted versions of the azide–cyclooctyne reaction reported as being highly efficient.

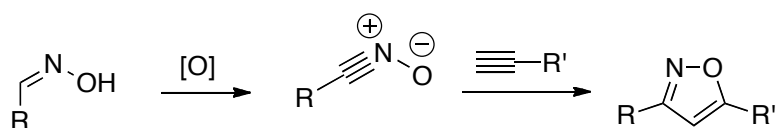


**Figure 1.7 Alkynes used in strain-promoted azide–alkyne (SPAAC) reactions**

The initial report, where **A** was synthesised, functionalised and used for cell labelling, showed the potential for utilising strain rather than a copper catalyst for azide–alkyne cycloadditions, but was a little sluggish.<sup>45</sup> Since then, it has been shown that fluorinated (**B**)<sup>46</sup> and more strained bicyclic dibenzylcyclooctyne-<sup>47</sup> and dicyclononyne-<sup>48</sup> based structures (**C** and **D**) result in greatly enhanced rates of the SPAAC reaction.

The main drawback to SPAAC is the challenging, lengthy and time consuming multi-step syntheses of functional cyclooctynes; and whilst some have very recently become commercially available, they are almost all prohibitively expensive. Additionally, long term storage of highly reactive cyclooctynes is no trivial matter.<sup>49</sup>

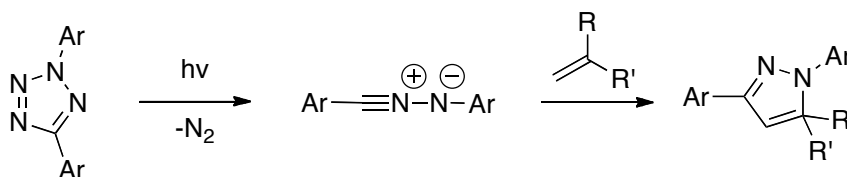
### 1.5.2.2. Nitrile Oxide–Alkyne



**Scheme 1.5 Nitrile oxide-alkyne 1,3 dipolar cycloaddition**

A slight variant on the CuAAC reaction is the cycloaddition between alkynes and nitrile oxides,<sup>50</sup> which has been used as a step-growth polymerisation reaction,<sup>51</sup> and to end-cap or functionalise polyrotaxanes<sup>52</sup> and can be either copper-catalysed<sup>53</sup>, or uncatalysed.<sup>54</sup> However, whilst the reaction can be carried out under mild conditions and has been used for surface functionalisation<sup>55</sup> and polymer end-functionalisation,<sup>56</sup> it has yet to find more widespread use in macromolecular synthesis; this could be due to the requirement for *in situ* generation of the nitrile oxide from an oxime, which are themselves susceptible to hydrolysis or rearrangement.

### 1.5.2.3. Tetrazole–ene



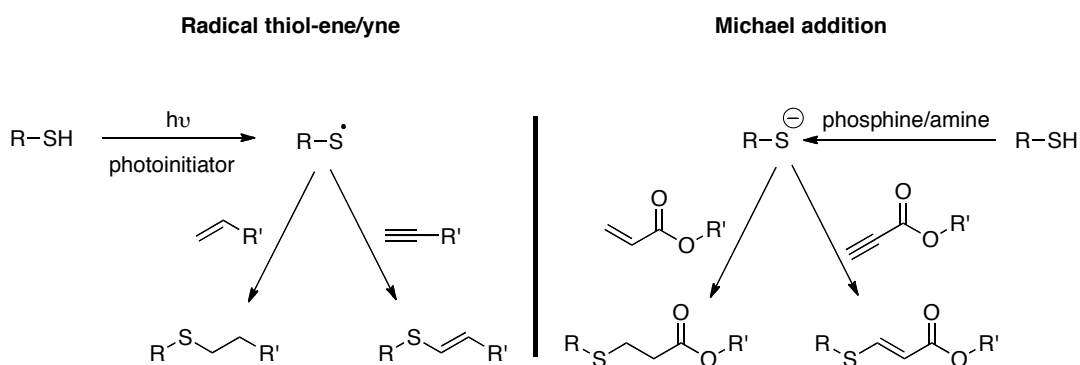
**Scheme 1.6 Nitrile imine-mediated tetrazole–ene cycloaddition (NITEC) reaction**

Another dipolar cycloaddition that occurs under benign conditions, with only molecular N<sub>2</sub> as a byproduct is the UV-initiated decomposition of a tetrazole to a nitrile imine, which reacts with an alkene in a Nitrile Imine-mediated Tetrazole-Ene Cycloaddition (NITEC). The NITEC reaction has been used for polymer–polymer coupling and grafting onto surfaces,<sup>57</sup> and modification of proteins,<sup>58</sup> and has the added advantage that the tetrazoles are profluorescent in nature.

### 1.5.3. Thiol-based reactions

#### 1.5.3.1. Thiol–ene/yne

The thiol–ene and thiol–yne reactions<sup>59</sup> have emerged as some of the most prominent ‘metal-free click’ reactions in recent years. There are two variants: the radical and the nucleophilic Michael addition thiol–ene/yne (Scheme 1.7).



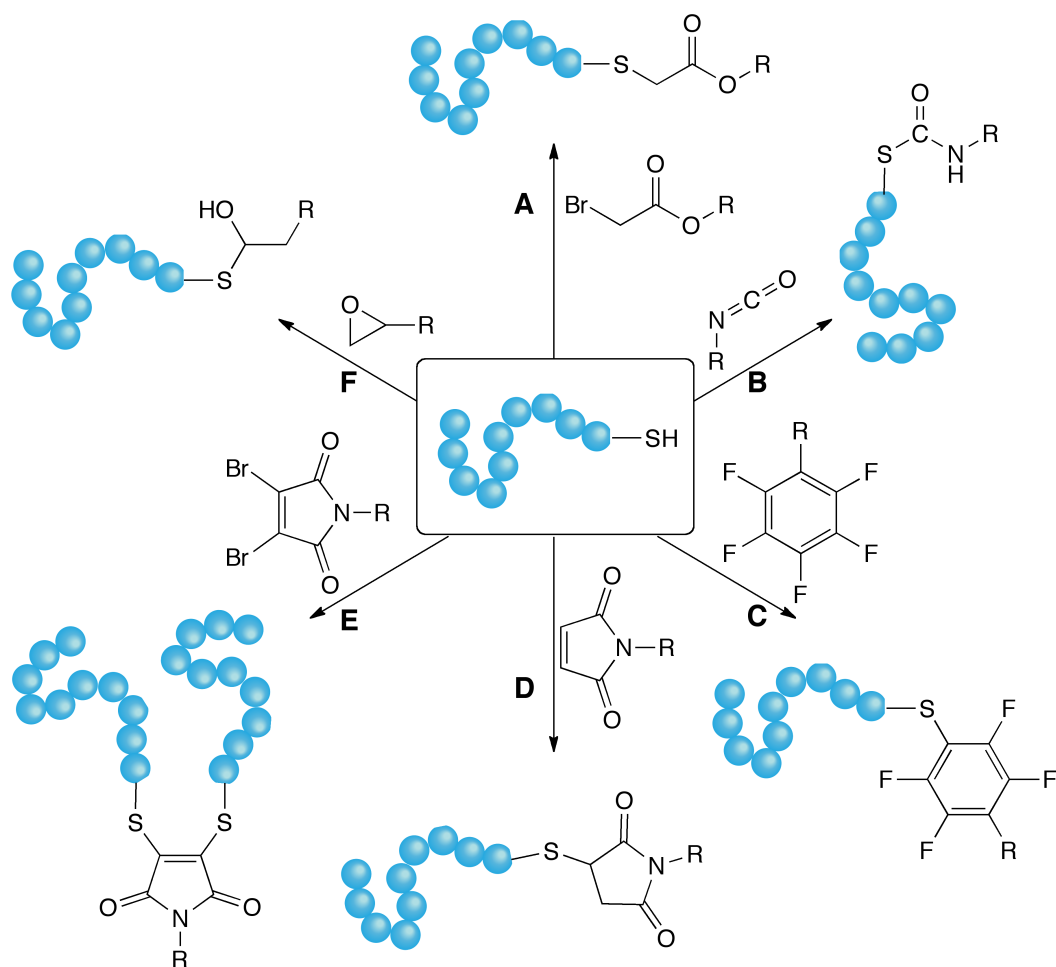
**Scheme 1.7 Thiol–ene/yne (left) and thiol Michael addition (right) click reactions**

As alluded to above, thiol ene/yne reactions have been particularly used in tandem with RAFT-synthesised polymers due to the thiocarbonylthio group functioning as a masked thiol, revealed by reduction. However, it has been shown that, due to side reactions, radical-based thiol–ene reactions cannot enable efficient polymer–polymer coupling,<sup>60</sup> although there are many examples of its use when functionalisation or polymer linking is done using an excess of small molecule thiol/alkene.<sup>61</sup> Michael addition reactions using thiols require catalysts and/or initiators to proceed at acceptable rates, which can lead to purification issues.<sup>62</sup> Whilst the alkene-based Michael reaction is more prevalent in the literature, there has been a recent report of using the nucleophilic Michael thiol–alkyne reaction to modify polymer chain ends and perform polymer–polymer coupling of two PEG chains, in which no issues with catalyst removal post-reaction were reported, and coupling was achieved in a highly efficient, click manner.<sup>63</sup>

#### **1.5.3.2. Other thiol-based click reactions**

There are several other thiol-based reactions that have been denoted as click reactions in the literature, summarised in Scheme 1.8.

The appeal of  $\alpha$ -bromo esters lies in both their reaction with thiols (**A** in Scheme 1.8) and their ability to act as an initiator in ATRP; this has been exploited to synthesise both dendrimers and dendritic macromolecules using a sequential ‘click-and-grow’ approach.<sup>64</sup> Hyperbranched polymers have also been prepared in a similar manner.<sup>65</sup>



**Scheme 1.8 Thiol-based click reactions (A) thiol–bromoester, (B) thiol–isocyanate, (C) thiol–pentafluorostyrene, (D) thiol–maleimide, (E) thiol–bromomaleimide and (F) thiol–epoxide**

Isocyanates are also well known to react rapidly with thiols (**B** in Scheme 1.8), and this has been used to end-functionalise PNIPAM synthesised by RAFT,<sup>66</sup> and also perform a one-pot RAFT polymerisation/functionalisation process.<sup>67</sup>

The reaction of thiols with pentafluorostyrene (PFS) (**C** in Scheme 1.8) has been used to prepare glycopolymers<sup>68</sup> using a pentafluorostyrene based

(co)polymer and a thioglycoside; however further studies on the reactions of PFS-based polymers showed poor conversions and therefore cast doubt on whether this should truly be considered a click reaction.<sup>69</sup>

The reaction between thiols and maleimide (**D** in Scheme 1.8) might be more properly considered a specific Michael-type thiol–ene reaction, but nevertheless it has carved out its own niche in the polymer functionalisation community. It was first explored for the functionalisation of poly(lactide),<sup>70</sup> and has since been applied to the functionalisation of polyurethanes<sup>71</sup> and in tandem with RAFT-synthesised polymers using the latent thiol functionality.<sup>72</sup>

More recently, dibromomaleimides (**E** in Scheme 1.8) have been shown to react in a click manner with thiols, with either single substitution or disubstitution possible;<sup>73</sup> dibromomaleimide-functionalised polymers have been prepared and functionalised with a variety of small molecule thiols.<sup>74</sup>

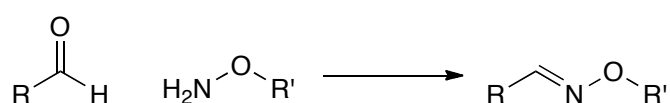
The nucleophilic attack of thiols on epoxides (**F** in Scheme 1.8) has been used to end-functionalise both thiol-terminated<sup>75</sup> and epoxide-terminated and main chain epoxide-bearing polymers.<sup>76</sup> It has also been exploited as a ‘healant’ in self-curing polymer systems.<sup>77</sup>

The versatility of thiols has led to their widespread use in polymer and materials science,<sup>78</sup> however their versatility can also mean that reactions in more complex environments, such as cell media, become non-specific and seriously hindered. In a wider sense, thiol-containing compounds also suffer from significant disulfide formation, especially in oxophilic solvents, so are impractical for long-term storage and ‘off-the shelf’ usage.



#### 1.5.4. Oxime ligation

Oxime ligation (Scheme 1.9), the catalyst-free reaction between aldehydes/ketones and aminooxy functionalities, was one of the reactions selected by Sharpless in the original click chemistry paper<sup>30</sup> as being highly efficient and therefore a quintessential click reaction; however it has yet to find a great deal of use in macromolecular synthesis. One group in particular has used it primarily for protein-based conjugation and in a variety of permutations; for example polymer end-functionalisation and conjugation to a protein,<sup>79</sup> hydrogel formation and functionalisation,<sup>80</sup> patterning of a surface with proteins,<sup>81</sup> and aldehyde<sup>82</sup> and ketone<sup>83</sup> functionalised polymers by RAFT for side-chain functionalisation.

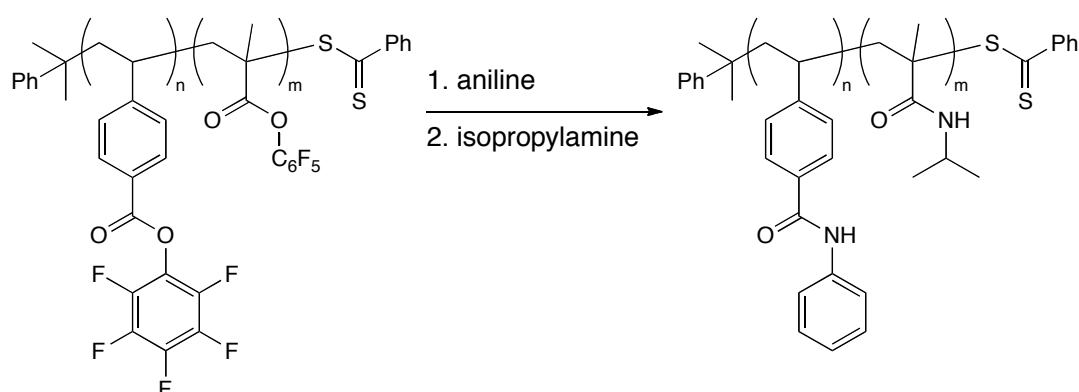


**Scheme 1.9 Oxime bond formation from aldehyde and aminooxy functionalities**

The reason for the apparent reticence in the wider adoption of oxime ligation in macromolecular synthesis could be that oximes can be susceptible to both hydrolysis and further rearrangement, making the linkage potentially neither stable and irreversible, nor controllably and reliably reversible, thereby providing the ‘worst of both worlds’ for potential applications.

### 1.5.5. Activated esters

Activated esters such as *N*-hydroxysuccinimide (NHS) esters have long been used in chemical biology to expedite ester or amide formation during peptide synthesis. Polymers bearing NHS ester groups have also been synthesised and used for protein conjugation,<sup>84</sup> however polymers containing multiple NHS groups tend only to be soluble in highly polar solvents such as DMSO and DMF, and suffer from side reactions with incidental nucleophiles or trace amounts of water, thus limiting their general applicability.



**Scheme 1.10 Reaction of PFP styrenic and methacrylic esters selectively with two different amines in a sequential manner<sup>85</sup>**

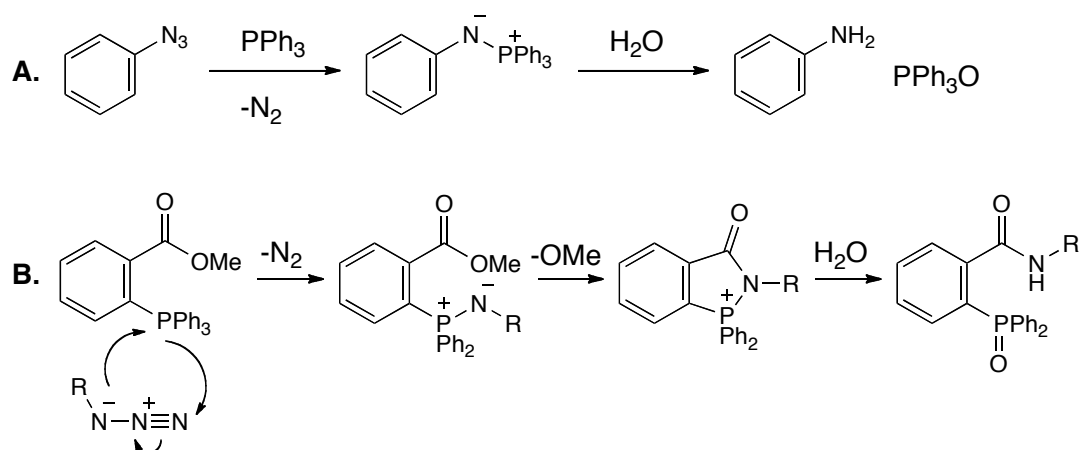
Pentafluorophenyl (PFP) esters have also been shown to be highly reactive towards amines, going to high conversions under mild conditions in a click manner. Styrenic and methacrylate<sup>86</sup> PFP monomers have been polymerised in a controlled manner by RAFT,<sup>85</sup> and their reactions with

amines — only aliphatic amines in the case of the methacrylate PFP monomer — shown to be quantitative at room temperatures.

Additionally, it has also been shown that the styrenic pentafluorophenyl ester is more reactive than the (meth)acrylate pentafluorophenyl ester, leading to the possibility for sequential functionalisation of a block copolymer scaffold using aromatic amines for the styrenic segment and aliphatic amines for the methacrylic segment, as shown in Scheme 1.10.<sup>85</sup>

Whilst the reaction with amines is fast, efficient and easily quantified using  $^{19}\text{F}$  NMR spectroscopy, the PFP can also react with hydroxy groups and thiols, so it is arguably not very orthogonal to other reactions and may not be useful for functionalisation in a more complex environment.

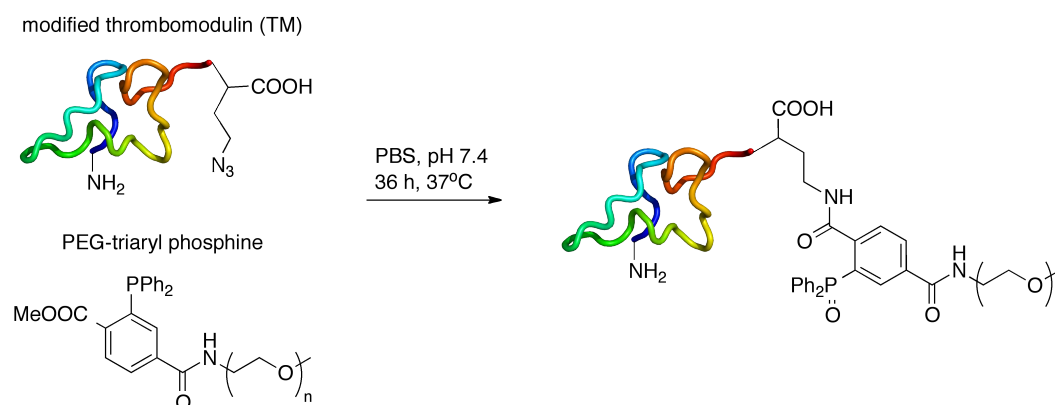
### 1.5.6. Staudinger Ligation



Scheme 1.11 Staudinger elimination (A), Staudinger-Bertozzi ligation (B)<sup>87</sup>

The Staudinger ligation (based on, but different to, the Staudinger elimination reaction) was developed in the Bertozzi lab as a bioorthogonal click reaction.<sup>88</sup> The reaction is between an aryl phosphine and an azide, and in the case where there is an ester in the *meta* position to the aryl phosphine, rearrangement occurs to form a thermodynamically favoured phosphine oxide, and the desired amide linkage, as shown in Scheme 1.11.

Thus far, this reaction has found limited use in polymer and materials chemistry, most probably due to the oxidative instability of the phosphines and also because it is carried out in aqueous/mixed aqueous-organic media, and most polymer families have at best limited solubility in water. Regarding polymers specifically, its prime use thus far has been for polymer–protein ligation, such as the site-specific PEGylation of a protein using a genetically encoded azide, and a phosphine-functionalised PEG.<sup>89</sup>

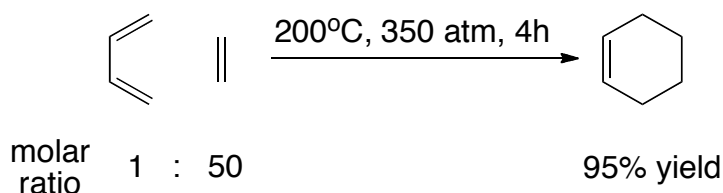


**Figure 1.8 PEG–protein ligation using the Staudinger ligation<sup>89</sup>**

### 1.5.7. Diels-Alder/hetero-Diels-Alder

The Diels-Alder (DA) reaction is a pericyclic reaction between a dienophile and conjugated diene, and since its discovery in 1928<sup>90</sup> has had a huge impact on organic synthesis and beyond. The creation of two carbon–carbon bonds and installation of potentially four stereocentres in one, atom-efficient, reaction step is a powerful and attractive feature for many chemists, and it has found extensive use in many areas of chemistry.<sup>91</sup> A testament to the incredible impact the DA reaction has had is that examples of its use in an industrial (> 1kg) setting can be found in their hundreds.<sup>92</sup>

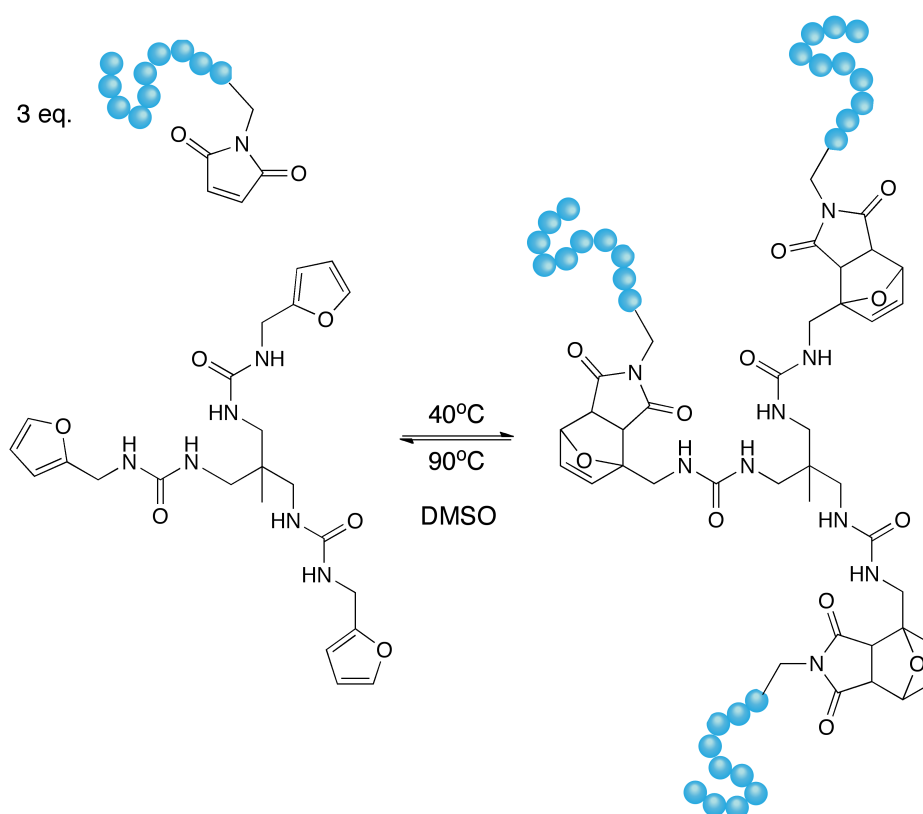
Although occasional questions remain over whether every DA reaction is concerted or synchronous to some extent, the generally accepted mechanism is a [4+2] cycloaddition between a diene and dienophile. The canonical form of a DA reaction is the reaction between butadiene and ethylene to form cyclohexene. However, both the diene and the dienophile display a very low reactivity as the gap between the HOMO<sub>diene</sub> and LUMO<sub>dienophile</sub> is very large; indeed, a successful reaction can only be observed with high pressures and an unusually high butadiene: ethylene molar ratio.<sup>93</sup>



**Scheme 1.12 DA reaction between butadiene and ethylene to form cyclohexene**

More typical are DA reactions where the diene bears an electron donating group and/or the dienophile an electron withdrawing group. Such modifications result in a smaller HOMO–LUMO gap and therefore faster and more favourable reactions.

The most common DA reaction pairs are furan–maleimide and anthracene–maleimide; furan–maleimide particularly so in the area of self-healing materials as its retro DA (rDA) reaction occurs at low temperatures (<100 °C), making it relatively easy to take advantage of its reversible nature.<sup>94</sup>



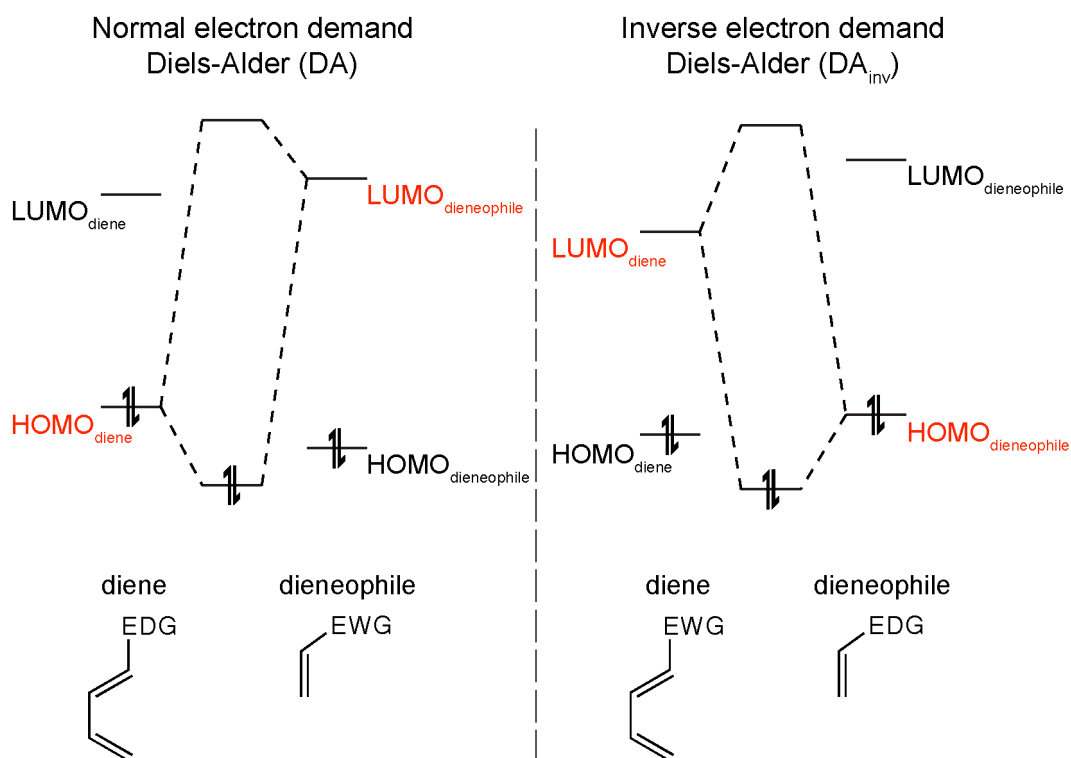
**Scheme 1.13** Reversible formation by DA/rDA reactions of 3-armed stars using a trifunctional furan core and maleimide-terminated polymers<sup>95</sup>

Examples of the DA (and rDA) reaction in use in macromolecular synthesis include the formation of triblock copolymers in tandem with the CuAAC reaction,<sup>96</sup> reversible star polymer formation (Scheme 1.13),<sup>95</sup> formation of cyclic polymers by reaction of maleimides with cyclopentadiene,<sup>97</sup> and graft polymers using maleimide-functionalised PS backbones reacted with anthracene-terminated PEG or PMMA.<sup>98</sup>

The Diels-Alder reaction is not limited to carbon-carbon bonds only, and the hetero Diels-Alder (HDA) reaction has been married with RAFT-synthesised polymers to great effect. Certain RAFT end groups (dithioesters substituted with strongly electron withdrawing groups) are able to undergo HDA reactions with cyclopentadiene-terminated groups, and this has been used to form block copolymers,<sup>99</sup> functionalise carbon nanotubes<sup>100</sup> and grafting of a cellulose surface with polymer chains.<sup>101</sup>

### **1.5.8. Inverse Diels-Alder reaction**

The Diels-Alder reaction with inverse electron demand ( $DA_{inv}$ ) is comparatively recent compared with its conventional cousin, being first experimentally demonstrated only in 1959.<sup>102</sup> In order for the electronics to be reversed, a dramatic lowering of the LUMO of the diene and/or raising of the HOMO of the dienophile must occur relative to 'normal' reactivity. This can occur when the diene is electron deficient, the dienophile electron rich or strained, or a combination of both.



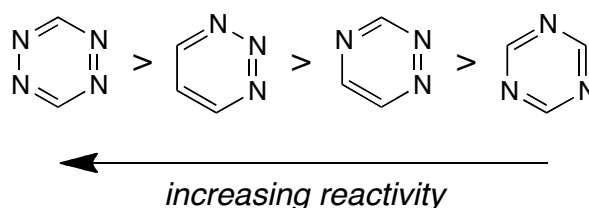
**Figure 1.9 Frontier molecular orbital diagrams for normal (left) and inverse (right) electron demand Diels-Alder reactions**

### 1.5.8.1. Diene Reactivity

Introduction of heteroatoms to the diene lower both the HOMO and LUMO energies, making the orbital overlap for an inverse electron demand Diels-Alder reaction much more favourable. Several examples of DA<sub>inv</sub> reactions with, for example, enones as the diene exist but, uncatalysed, they are generally hindered by poor reactivity and competing polymerisation reactions, resulting in low conversions and multiple byproducts. Lewis acid and organocatalysis improves yields and selectivity greatly, but not to the extent that these reactions could be classed as click reactions.<sup>103</sup>



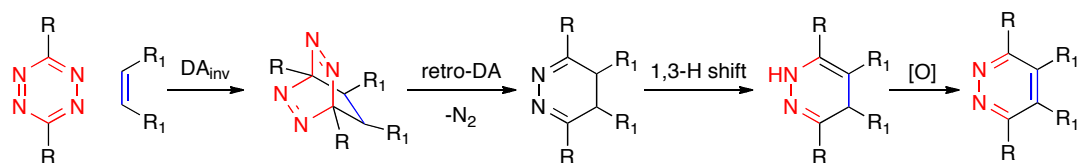
However, combining multiple heteroatoms into the diene, and constraining it into the *cis* position by inclusion into a cyclic structure makes the  $\text{DA}_{\text{inv}}$  reaction much more favourable. In addition to this, the presence of two or more nitrogen atoms in the heterocycle means that expulsion of  $\text{N}_2$  *via* a retro Diels-Alder reaction (rDA) is highly entropically favoured. Thus the reaction is altered from a single, reversible  $\text{DA}_{\text{inv}}$  reaction to a tandem, irreversible  $\text{DA}_{\text{inv}}$ –rDA reaction. This has enormous ramifications for its use, as the reaction is driven to higher conversions than it would be were it to be solely a reversible  $\text{DA}_{(\text{inv})}$  reaction, and the linkage formed is irreversible. To this end, triazines and tetrazines have found great use in  $\text{DA}_{\text{inv}}$  reactions, in which their relative reactivities are shown in Figure 1.10.



**Figure 1.10 Aza-dienes commonly used in  $\text{DA}_{\text{inv}}$ –rDA reactions. Left to right:  
1,2,4,5-tetrazine, 1,2,3-triazine, 1,3,4-triazine, 1,3,5-triazine**

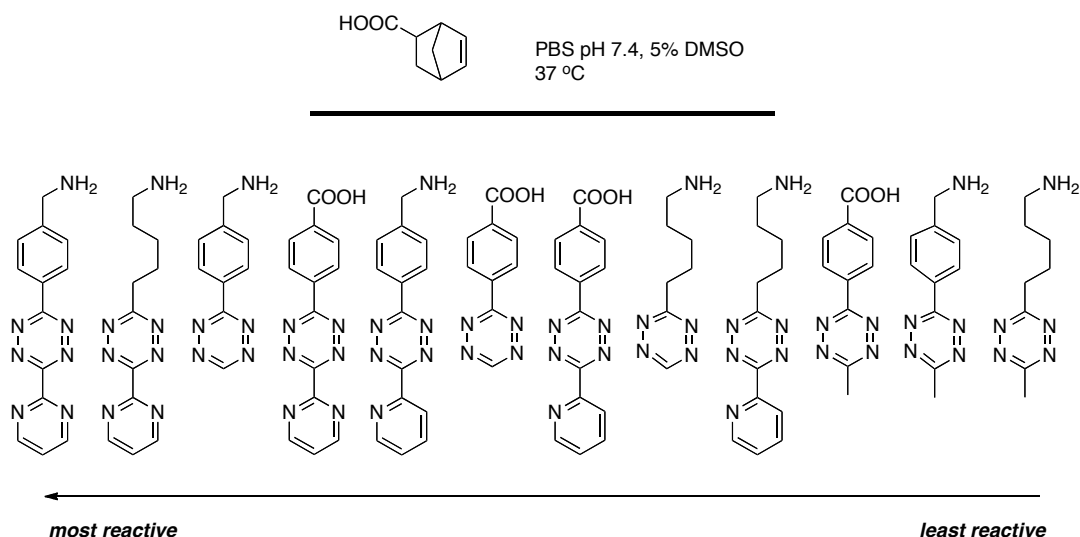
The reaction between tetrazines and strained or electron rich alkenes (Carbonyl-Lindsey reaction)<sup>102</sup> is particularly fast, and has therefore received more attention than the equivalent triazine reactions. The reaction sequence –  $\text{DA}_{\text{inv}}$  reaction, followed by a rDA to expel one molecule of  $\text{N}_2$ , a 1,3 H shift to yield a dihydropyridazine and finally an oxidation step that is

dependent on the reaction conditions employed – is shown below in Scheme 1.14.



**Scheme 1.14 General reaction between a symmetrical 1,2,4,5-tetrazine and alkene — multiple regioisomers are formed if asymmetric reagents are used**

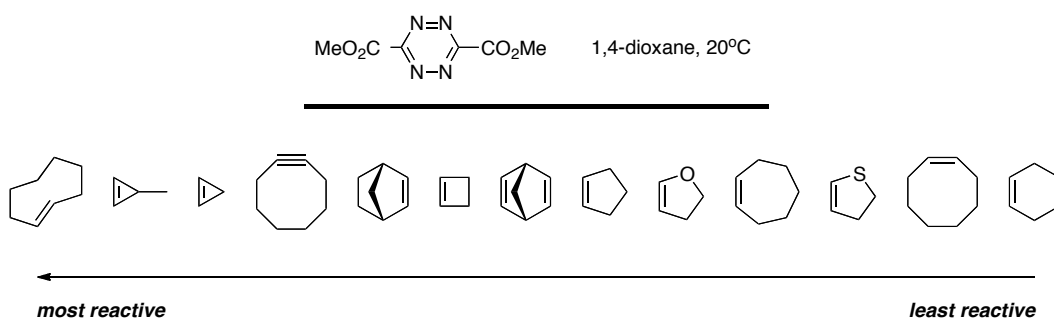
Whilst the tetrazine moiety is itself a voracious diene in the DA<sub>inv</sub> reaction, its reactivity can be further fine tuned by the addition of electron-withdrawing substituents. When initial research was being carried out into reaction rates, only a select few tetrazines were available, but recently a much larger number of tetrazines have been synthesised, and so more detailed investigations into reactivity using asymmetrical tetrazines have been carried out (Figure 1.11).<sup>104</sup> As would be expected, electron-withdrawing substituents further increase the tetrazine reactivity, with the notable exception of a proton substituent, which shows unusually high reactivity compared to theoretical values; this is hypothesised to be due to the lack of steric hindrance. However, reactive tetrazines are, by their very nature, less stable and therefore more susceptible to incidental attack from nucleophiles in the reaction medium.



**Figure 1.11 Reactivity of tetrazines in aqueous buffer solutions<sup>104</sup>**

### 1.5.8.2. *Dienophile Reactivity*

The choice of dienophile also greatly affects the rate of reaction; adding electron donating groups to the alkene and/or incorporating it into a strained ring greatly enhances reactivity, as shown by an early study which investigated the reactivity trends of various cyclic dienophiles with a symmetrical tetrazine (Figure 1.12).<sup>105</sup>



**Figure 1.12 Reactivity of various cyclic dienophiles<sup>105</sup>**

In addition, a more recent investigation looked into tuning the rates of various cyclooctene/yne derivatives for cell labelling purposes, and their findings are shown in Figure 1.13.<sup>106</sup>

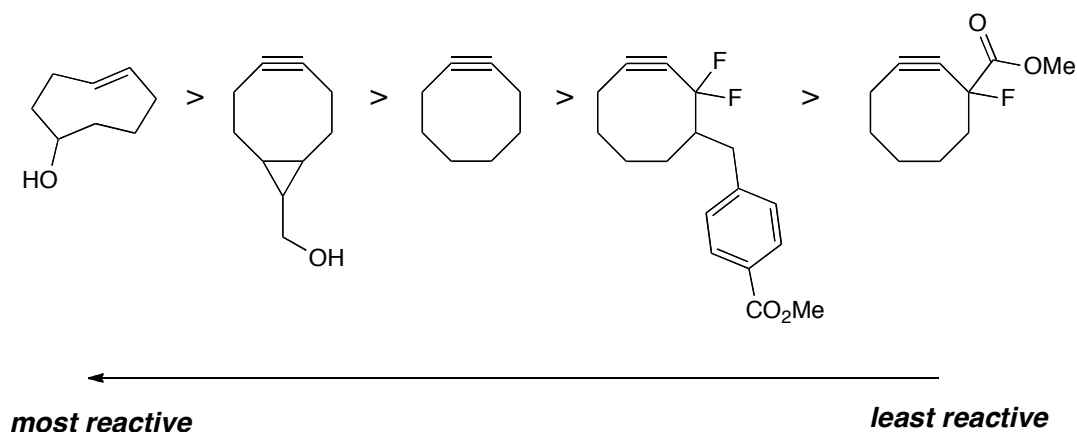
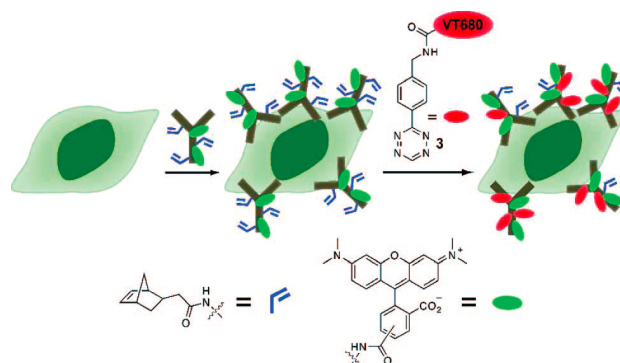


Figure 1.13 Cyclooctene/octyne reactivity rates with dipyrityl tetrazine in methanol<sup>106</sup>

## 1.6. Tetrazine DA<sub>inv</sub> applications

A vast quantity of the initial work on tetrazine DA<sub>inv</sub> reactions was performed in the group of Dale Boger on the synthesis of various natural product targets.<sup>107</sup> Presently, tetrazine DA<sub>inv</sub> reactions are most utilised in the field of bioorthogonal chemistry.<sup>108</sup> The first demonstration of its use was in modifying a large, *trans*-cyclooctene functionalised protein in cell media with a fluorescent tetrazine,<sup>109</sup> and this was extended to fluorescent labelling of proteins inside a cell and on the cell surface.<sup>110</sup> Another group has focused on using the tetrazine reaction as a “bioshuttle” for cancer therapeutics, to deliver a drug of interest to a specifically alkene-labelled cell line.<sup>111</sup>

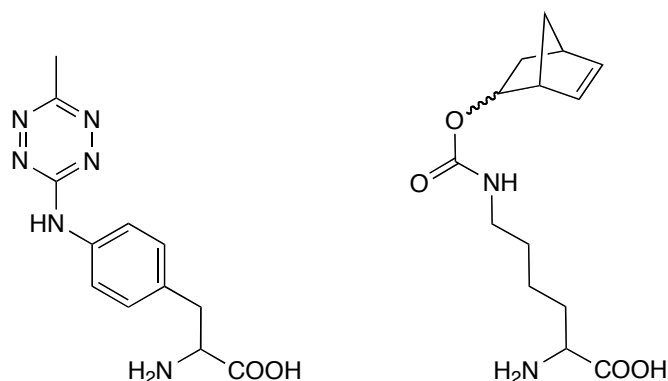


**Figure 1.14 Cellular imaging using Tz–Nb DA<sub>inv</sub>**<sup>112</sup>

Live cell imaging has also been achieved using a ‘pretargeted’ approach (Figure 1.14), whereby cells of interest are modified using a norbornene, then subsequently a fluorescent tetrazine enables labelling of live cells *in situ*.<sup>112</sup> This strategy has also been extended to using *trans*-cyclooctenes,<sup>113</sup> multi-target imaging using tetrazine and SPAAC reactions,<sup>114</sup> and also tetrazine–fluorophore conjugates that display “turn-on” fluorescence properties, such that fluorescent labelling is only achieved after the DA<sub>inv</sub> reaction has taken place.<sup>115</sup>

A step further than the “pretargeted approach”, and the state of the art in bioorthogonal labelling, is to genetically encode unnatural amino acids, so that one of the ligation partners is directly expressed – as opposed to having two separate reactions; one to attach a ligation partner, the next to perform the actual labelling. This has recently been achieved using the tetrazine–norbornene reaction, with one group encoding a norbornene-functional amino acid<sup>116</sup> and another encoding a tetrazine-functional amino

acid<sup>117</sup> and subsequently using the DA<sub>inv</sub> reaction to fluorescently tag proteins in a site-specific manner *in vivo*.

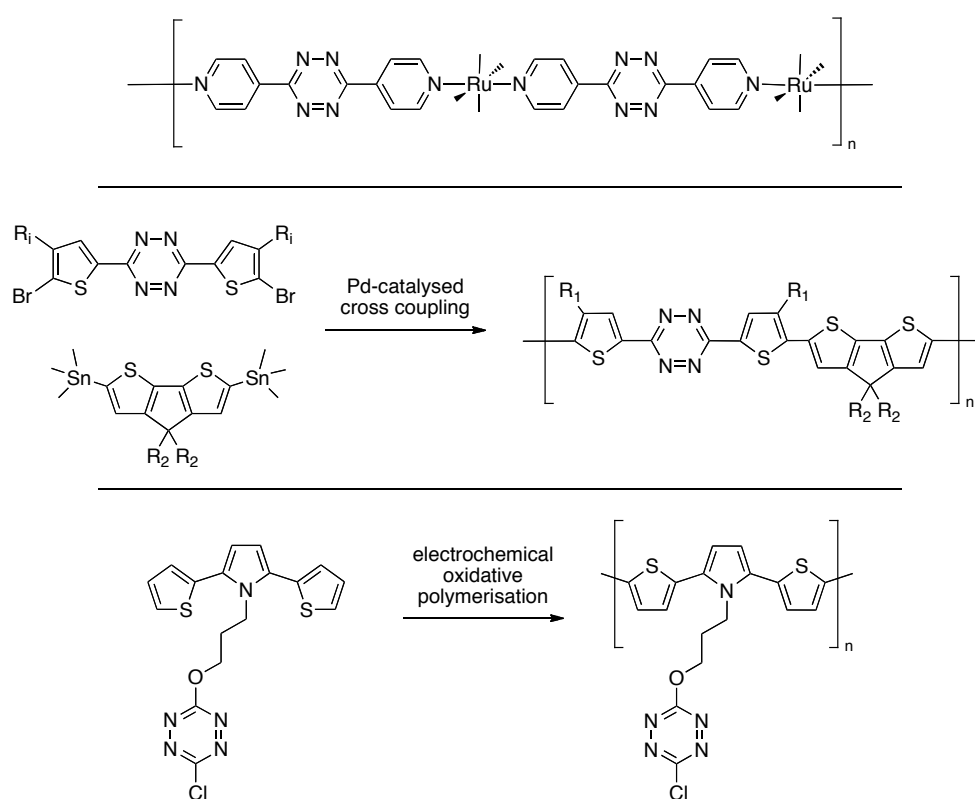


**Figure 1.15 Tetrazine-<sup>117</sup> and norbornene-functionalised<sup>116</sup> unnatural amino acids genetically encoded for *in vivo* labelling using complementary norbornene- or tetrazine-functionalised fluorescent tags**

Cyclopropenes<sup>118</sup> and highly strained bicyclic cyclopropane-*trans*-cyclooctenes<sup>119</sup> have also been developed to be used as highly reactive dienophiles for such cellular chemical reporting purposes.

The DA<sub>inv</sub> reaction between tetrazines and norbornenes has also been used for conjugation of polymeric imidazole ligands to quantum dots,<sup>120</sup> modifying multiwalled carbon nanotubes,<sup>121</sup> labelling of DNA with a fluorescent tetrazine,<sup>122</sup> and remarkably the use of pendent alkenes as the dienophile also resulted in the post-synthetic modification of MOFs using the tetrazine DA<sub>inv</sub>.<sup>123</sup>

Thus far there has been limited application of tetrazine  $DA_{inv}$  reactions to polymers and materials, aside from one early report where a tetrazine was covalently attached to a polymer bead,<sup>124</sup> to be used as a reagent in solid-supported diazine synthesis. In another group, functionalisation of alkyne-terminated polymers with commercially available dipyridyl tetrazine to form pyradizines afforded a metal-complexable end group; this was complexed with silver to provide supramolecular star polymers.<sup>125</sup>

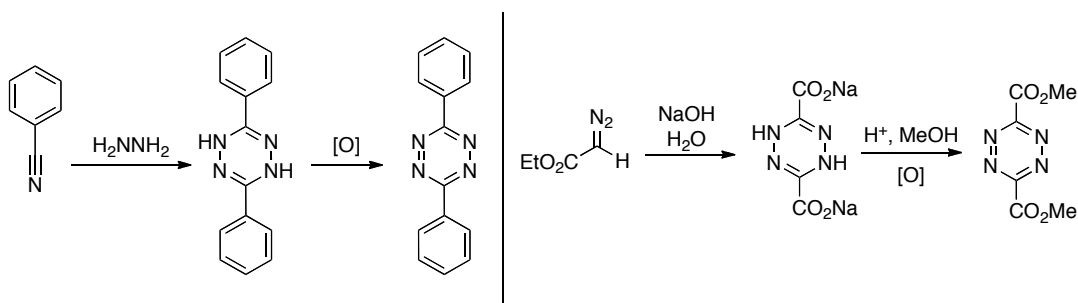


**Scheme 1.15 Tetrazine-based polymers for optoelectronics: metal-conjugated (top),<sup>126</sup> incorporated along the backbone (centre)<sup>127</sup> and as a pendent functionality (bottom)<sup>128</sup>**

There have been some reports on tetrazine-based polymers; however these aim to exploit the electrochemical properties of the tetrazine functionality rather than its intrinsic reactivity. Both metal-coordinated polymers<sup>126</sup> and covalent polymers have been reported — with both the tetrazine conjugated along the polymer backbone<sup>127</sup> and as a pendent functionality<sup>128</sup> — but synthesised in a non-controlled manner (Scheme 1.15).

Since publication of parts of this thesis detailing the use of the DA<sub>inv</sub> reaction in polymer–polymer coupling (Chapter 2), further reports have also utilised this ability to facilitate the counting of polymer loops in a gel system,<sup>129</sup> in hydrogel<sup>130</sup> and polymer gel<sup>131</sup> formation.

## 1.7. Tetrazine synthesis



**Scheme 1.16 Pinner synthesis of aromatic-substituted tetrazine (left), dimerisation of ethyl diazoacetate to form dicarboxy tetrazine (right)**

A general, and the most widely used, method to prepare symmetrical tetrazines is the Pinner synthesis, first reported in 1897; this report detailed the dimerisation of aromatic nitriles using hydrazine, followed by oxidation



from the dihydropyridazine to the tetrazine.<sup>132</sup> An alternative route to symmetrical tetrazines is the base-promoted dimerisation of ethyl diazoacetate to form dicarboxy tetrazine.<sup>133</sup>

Asymmetrical tetrazines are more difficult to synthesise than their symmetrical counterparts, and initial routes to asymmetrically substituted tetrazines involved the desymmetrisation of chlorine-,<sup>134</sup> thioester- and ester-substituted tetrazines, with generally low yields over multistep syntheses.<sup>135</sup>

Recently, efforts to expand the range of unsymmetrical tetrazines available<sup>136</sup> have resulted in the metal-catalysed synthesis of a wider range of tetrazines bearing functional handles being developed.<sup>104,137</sup> In some cases, the yields obtained are low but overall the synthesis, being a one-step process with relatively simple column chromatography purification, is an improvement over previous methods.

Some of the interest in synthesising the tetrazine<sup>138</sup> moiety stems from the fact that it is a high nitrogen material that finds use in explosive materials,<sup>139</sup> and therefore care must be taken when handling tetrazine-based materials. However it also should be noted that, in all but the most extremely substituted nitrogen rich cases, the decomposition temperature of tetrazines is well above 200 °C.<sup>139</sup> Thus when using tetrazines as a click reagent, *i.e.* for room temperature reactions, and during synthesis at temperatures below 100 °C, safety concerns over violent decomposition are minimised.

## **1.8. Conclusions**

In this chapter we have outlined the definition of the term 'click reaction', and listed some examples of reactions that have been considered to have click characteristics. We have described the background and history of the inverse electron demand Diels-Alder reaction between tetrazines and strained alkenes, and demonstrated that it could be denoted as a click reaction. Especially considering the recent developments in the synthesis of functional tetrazines, we conjecture that this click reaction, as yet underused in the field of polymer and materials science, could find applications in a range of syntheses and functionalisations, to be illustrated in the following chapters of this thesis.

## 1.9. References

- (1) Staudinger, H. *Ber. Dtsch. Chem. Ges.* **1920**, 53, 1073-1085.
- (2) (a) Carothers, W. H. *J. Am. Chem. Soc.* **1929**, 51, 2548-2559. (b) Carothers, W. H. *Chem. Rev.* **1931**, 8, 353-426.
- (3) Flory, P. J.; Rehner, J. J. *J. Chem. Phys.* **1943**, 11, 512-520.
- (4) Darling, T. R.; Davis, T. P.; Fryd, M.; Gridnev, A. A.; Haddleton, D. M.; Ittel, S. D.; Matheson, R. R.; Moad, G.; Rizzardo, E. *J. Polym. Sci., Part A: Polym. Chem.* **2000**, 38, 1706-1708.
- (5) McNaught, A. D.; Wilkinson, A. *IUPAC. Compendium of Chemical Terminology, 2nd Ed. (the "Gold Book")*; doi:10.1351/goldbook.L03597.
- (6) Quirk, R. P.; Lee, B. *Polym. Int.* **1992**, 27, 359-367.
- (7) Szwarc, M. *Nature* **1956**, 178, 1168-1169.
- (8) (a) Ovitt, T. M.; Coates, G. W. *J. Am. Chem. Soc.* **1999**, 121, 4072-4073. (b) Connor, E. F.; Nyce, G. W.; Myers, M.; Möck, A.; Hedrick, J. L. *J. Am. Chem. Soc.* **2002**, 124, 914-915. (c) Dove, A. P. *ACS Macro Lett.* **2012**, 1, 1409-1412.
- (9) Bielawski, C. W.; Grubbs, R. H. *Prog. Polym. Sci.* **2007**, 32, 1-29.
- (10) Webster, O. W.; Hertler, W. R.; Sogah, D. Y.; Farnham, W. B.; RajanBabu, T. V. *J. Am. Chem. Soc.* **1983**, 105, 5706-5708.
- (11) Jenkins, A. D.; Jones, R. G.; Moad, G. *Pure Appl. Chem.* **2010**, 82, 483-491.

- (12) (a) Otsu, T.; Yoshida, M. *Makromol. Chem., Rapid Commun.* **1982**, *3*, 127-132. (b) Otsu, T.; Yoshida, M.; Tazaki, T. *Makromol. Chem., Rapid Commun.* **1982**, *3*, 133-140.
- (13) Kato, M.; Kamigaito, M.; Sawamoto, M.; Higashimura, T. *Macromolecules* **1995**, *28*, 1721-1723.
- (14) Matyjaszewski, K.; Gaynor, S.; Wang, J. *Macromolecules* **1995**, *28*, 2093-2095.
- (15) Fischer, H. *Chem. Rev.* **2001**, *101*, 3581-3610.
- (16) Dong, H.; Tang, W.; Matyjaszewski, K. *Macromolecules* **2007**, *40*, 2974-2977.
- (17) Pintauer, T.; Matyjaszewski, K. *Chem. Soc. Rev.* **2008**, *37*, 1087-1097.
- (18) Hawker, C. J.; Bosman, A. W.; Harth, E. *Chem. Rev.* **2001**, *101*, 3661-3688.
- (19) (a) Georges, M. K.; Veregin, R. P. N.; Kazmaier, P. M.; Hamer, G. K. *Macromolecules* **1993**, *26*, 2987-2988. (b) Hawker, C. J. *J. Am. Chem. Soc.* **1994**, *116*, 11185-11186.
- (20) (a) Benoit, D.; Chaplinski, V.; Braslau, R.; Hawker, C. J. *J. Am. Chem. Soc.* **1999**, *121*, 3904-3920. (b) Benoit, D.; Grimaldi, S.; Robin, S.; Finet, J.-P.; Tordo, P.; Gnanou, Y. *J. Am. Chem. Soc.* **2000**, *122*, 5929-5939.
- (21) Grubbs, R. B. *Polym. Rev.* **2011**, *51*, 104-137.

- (22) Chiefari, J.; Chong, Y. K.; Ercole, F.; Krstina, J.; Jeffery, J.; Le, T. P. T.; Mayadunne, R. T. A.; Meijs, G. F.; Moad, C. L.; Moad, G.; Rizzardo, E.; Thang, S. H. *Macromolecules* **1998**, *31*, 5559-5562.
- (23) Corpart, P.; Charmot, D.; Biadatti, T.; Zard, S.; Michelet, D. *Rhodia Chimie Int. Appl.* **1997**, WO 9858974.
- (24) (a) Buback, M.; Janssen, O.; Oswald, R.; Schmatz, S.; Vana, P. *Macromol. Symp.* **2007**, *248*, 158-167. (b) Geelen, P.; Klumperman, B. *Macromolecules* **2007**, *40*, 3914-3920. (c) Konkolewicz, D.; Hawket, B. S.; Gray-Weale, A.; Perrier, S. *Macromolecules* **2008**, *41*, 6400-6412. (d) Konkolewicz, D.; Hawket, B. S.; Gray-Weale, A.; Perrier, S. *J. Polym. Sci., Part A: Polym. Chem.* **2009**, *47*, 3455-3466. (e) Klumperman, B.; van den Dungen, E. T. A.; Heuts, J. P. A.; Monteiro, M. J. *Macromol. Rapid Comm.* **2010**, *31*, 1846-1862.
- (25) Barner-Kowollik, C.; Buback, M.; Charleux, B.; Coote, M. L.; Drache, M.; Fukuda, T.; Goto, A.; Klumperman, B.; Lowe, A. B.; McLeary, J. B.; Moad, G.; Monteiro, M. J.; Sanderson, R. D.; Tonge, M. P.; Vana, P. *J. Polym. Sci., Part A: Polym. Chem.* **2006**, *44*, 5809-5831.
- (26) McLeary, J. B.; Calitz, F. M.; McKenzie, J. M.; Tonge, M. P.; Sanderson, R. D.; Klumperman, B. *Macromolecules* **2005**, *38*, 3151-3161.
- (27) (a) Wood, M. R.; Duncalf, D. J.; Rannard, S. P.; Perrier, S. *Org. Lett.* **2006**, *8*, 553-556. (b) Skey, J.; O'Reilly, R. K. *Chem. Commun.* **2008**, *44*, 4183-4185. (c) Benaglia, M.; Chiefari, J.; Chong, Y. K.; Moad, G.; Rizzardo, E.; Thang, S. H. *J. Am. Chem. Soc.* **2009**, *131*, 6914-6915. (d) Keddie, D.

J.; Moad, G.; Rizzardo, E.; Thang, S. H. *Macromolecules* **2012**, *45*, 5321-5342.

(28) Spruell, J. M.; Levy, B. A.; Sutherland, A.; Dichtel, W. R.; Cheng, J. Y.; Stoddart, J. F.; Nelson, A. J. *Polym. Sci., Part A: Polym. Chem.* **2009**, *47*, 346-356.

(29) (a) Willcock, H.; O'Reilly, R. K. *Polym. Chem.* **2010**, *1*, 149-157. (b) Harvison, M. A.; Roth, P. J.; Davis, T. P.; Lowe, A. B. *Aust. J. Chem.* **2011**, *64*, 992-1006. (c) Moad, G.; Rizzardo, E.; Thang, S. H. *Polym. Int.* **2011**, *60*, 9-25.

(30) Kolb, H. C.; Finn, M. G.; Sharpless, K. B. *Angew. Chem., Int. Ed.* **2001**, *40*, 2004-2021.

(31) Barner-Kowollik, C.; Du Prez, F. E.; Espeel, P.; Hawker, C. J.; Junkers, T.; Schlaad, H.; Van Camp, W. *Angew. Chem., Int. Ed.* **2011**, *50*, 60-62.

(32) (a) Iha, R. K.; Wooley, K. L.; Nystroem, A. M.; Burke, D. J.; Kade, M. J.; Hawker, C. J. *Chem. Rev.* **2009**, *109*, 5620-5686. (b) Durmaz, H.; Sanyal, A.; Hizal, G.; Tunca, U. *Polym. Chem.* **2012**, *3*, 825-835. (c) Mansfeld, U.; Pietsch, C.; Hoogenboom, R.; Becer, C. R.; Schubert, U. S. *Polym. Chem.* **2010**, *1*, 1560-1598. (d) Lutz, J.-F. *Angew. Chem., Int. Ed.* **2007**, *46*, 1018-1025. (e) Binder, W. H.; Sachsenhofer, R. *Macromol. Rapid Comm.* **2007**, *28*, 15-54. (f) Binder, W. H.; Sachsenhofer, R. *Macromol. Rapid Comm.* **2008**, *29*, 952-981. (g) Sumerlin, B. S.; Vogt, A. P. *Macromolecules* **2010**, *43*, 1-13.

- (33) Rostovtsev, V. V.; Green, L. G.; Fokin, V. V.; Sharpless, K. B. *Angew. Chem., Int. Ed.* **2002**, *41*, 2596-2599.
- (34) van Steenis, D. J. V. C.; David, O. R. P.; van Strijdonck, G. P. F.; van Maarseveen, J. H.; Reek, J. N. H. *Chem. Commun.* **2005**, *41*, 4333-4335.
- (35) Wu, P.; Feldman, A. K.; Nugent, A. K.; Hawker, C. J.; Scheel, A.; Voit, B.; Pyun, J.; Fréchet, J. M. J.; Sharpless, K. B.; Fokin, V. V. *Angew. Chem., Int. Ed.* **2004**, *43*, 3928-3932.
- (36) Opsteen, J. A.; van Hest, J. C. M. *Chem. Commun.* **2005**, *41*, 57-59.
- (37) Gao, H.; Matyjaszewski, K. *Macromolecules* **2006**, *39*, 4960-4965.
- (38) (a) Laurent, B. A.; Grayson, S. M. *J. Am. Chem. Soc.* **2006**, *128*, 4238-4239. (b) Laurent, B. A.; Grayson, S. M. *J. Am. Chem. Soc.* **2011**, *133*, 13421-13429.
- (39) (a) Li, M.; De, P.; Gondi, S. R.; Sumerlin, B. S. *Macromol. Rapid Comm.* **2008**, *29*, 1172-1176. (b) Dirks, A. J.; van Berkel, S. S.; Hatzakis, N. S.; Opsteen, J. A.; van Delft, F. L.; Cornelissen, J. J. L. M.; Rowan, A. E.; van Hest, J. C. M.; Rutjes, F. P. J. T.; Nolte, R. J. M. *Chem. Commun.* **2005**, *41*, 4172-4174.
- (40) Li, H.; Cheng, F.; Duft, A. M.; Adronov, A. *J. Am. Chem. Soc.* **2005**, *127*, 14518-14524.
- (41) (a) de Luzuriaga, A. R.; Ormategui, N.; Grande, H. J.; Odriozola, I.; Pomposo, J. A.; Loinaz, I. *Macromol. Rapid Comm.* **2008**, *29*, 1156-1160.

- (b) Sanchez-Sanchez, A.; Asenjo-Sanz, I.; Buruaga, L.; Pomposo, J. A. *Macromol. Rapid Comm.* **2012**, *33*, 1262-1267.
- (42) (a) O'Reilly, R. K.; Joralemon, M. J.; Wooley, K. L.; Hawker, C. J. *Chem. Mater.* **2005**, *17*, 5976-5988. (b) O'Reilly, R. K.; Joralemon, M. J.; Hawker, C. J.; Wooley, K. L. *Chem. Eur. J.* **2006**, *12*, 6776-6786.
- (43) Bräse, S.; Gil, C.; Knepper, K.; Zimmermann, V. *Angew. Chem., Int. Ed.* **2005**, *44*, 5188-5240.
- (44) Becer, C. R.; Hoogenboom, R.; Schubert, U. S. *Angew. Chem., Int. Ed.* **2009**, *48*, 4900-4908.
- (45) Agard, N. J.; Prescher, J. A.; Bertozzi, C. R. *J. Am. Chem. Soc.* **2004**, *126*, 15046-15047.
- (46) Baskin, J. M.; Prescher, J. A.; Laughlin, S. T.; Agard, N. J.; Chang, P. V.; Miller, I. A.; Lo, A.; Codelli, J. A.; Bertozzi, C. R. *Proc. Natl. Acad. Sci. U. S. A.* **2007**, *104*, 16793-16797.
- (47) Ning, X.; Guo, J.; Wolfert, M. A.; Boons, G.-J. *Angew. Chem., Int. Ed.* **2008**, *47*, 2253-2255.
- (48) Dommerholt, J.; Schmidt, S.; Temming, R.; Hendriks, L. J. A.; Rutjes, F. P. J. T.; van Hest, J. C. M.; Lefebvre, D. J.; Friedl, P.; van Delft, F. L. *Angew. Chem., Int. Ed.* **2010**, *49*, 9422-9425.
- (49) Sletten, E. M.; Nakamura, H.; Jewett, J. C.; Bertozzi, C. R. *J. Am. Chem. Soc.* **2010**, *132*, 11799-11805.



- (50) Zlatopolskiy, B. D.; Kandler, R.; Kobus, D.; Mottaghy, F. M.; Neumaier, B. *Chem. Commun.* **2012**, 48, 7134-7136.
- (51) Lee, Y.-G.; Koyama, Y.; Yonekawa, M.; Takata, T. *Macromolecules* **2009**, 42, 7709-7717.
- (52) Lee, Y.-G.; Koyama, Y.; Yonekawa, M.; Takata, T. *Macromolecules* **2010**, 43, 4070-4080.
- (53) Himo, F.; Lovell, T.; Hilgraf, R.; Rostovtsev, V. V.; Noodleman, L.; Sharpless, K. B.; Fokin, V. V. *J. Am. Chem. Soc.* **2004**, 127, 210-216.
- (54) Singh, I.; Vyle, J. S.; Heaney, F. *Chem. Commun.* **2009**, 45, 3276-3278.
- (55) Wendeln, C.; Singh, I.; Rinnen, S.; Schulz, C.; Arlinghaus, H. F.; Burley, G. A.; Ravoo, B. J. *Chem. Sci.* **2012**, 3, 2479-2484.
- (56) Singh, I.; Zarafshani, Z.; Lutz, J.-F.; Heaney, F. *Macromolecules* **2009**, 42, 5411-5413.
- (57) Dietrich, M.; Delaittre, G.; Blinco, J. P.; Inglis, A. J.; Bruns, M.; Barner-Kowollik, C. *Adv. Func. Mat.* **2012**, 22, 304-312.
- (58) Song, W.; Wang, Y.; Qu, J.; Madden, M. M.; Lin, Q. *Angew. Chem., Int. Ed.* **2008**, 47, 2832-2835.
- (59) (a) Hoyle, C. E.; Lee, T. Y.; Roper, T. *J. Polym. Sci., Part A: Polym. Chem.* **2004**, 42, 5301-5338. (b) Kade, M. J.; Burke, D. J.; Hawker, C. J. *J.*

*Polym. Sci., Part A: Polym. Chem.* **2010**, *48*, 743-750. (c) Lowe, A. B. *Polym. Chem.* **2010**, *1*, 17-36.

(60) Koo, S. P. S.; Stamenovic, M. M.; Prasath, R. A.; Inglis, A. J.; Du Prez, F. E.; Barner-Kowollik, C.; Van Camp, W.; Junkers, T. *J. Polym. Sci., Part A: Polym. Chem.* **2010**, *48*, 1699-1713.

(61) (a) Campos, L. M.; Killops, K. L.; Sakai, R.; Paulusse, J. M. J.; Damiron, D.; Drockenmuller, E.; Messmore, B. W.; Hawker, C. J. *Macromolecules* **2008**, *41*, 7063-7070. (b) Gress, A.; Voelkel, A.; Schlaad, H. *Macromolecules* **2007**, *40*, 7928-7933. (c) ten Brummelhuis, N.; Diehl, C.; Schlaad, H. *Macromolecules* **2008**, *41*, 9946-9947. (d) Chan, J. W.; Yu, B.; Hoyle, C. E.; Lowe, A. B. *Chem. Commun.* **2008**, *44*, 4959-4961. (e) Yu, B.; Chan, J. W.; Hoyle, C. E.; Lowe, A. B. *J. Polym. Sci., Part A: Polym. Chem.* **2009**, *47*, 3544-3557.

(62) Li, G.-Z.; Randev, R. K.; Soeriyadi, A. H.; Rees, G.; Boyer, C.; Tong, Z.; Davis, T. P.; Becer, C. R.; Haddleton, D. M. *Polym. Chem.* **2010**, *1*, 1196-1204.

(63) Truong, V. X.; Dove, A. P. *Angew. Chem., Int. Ed.* **2013**, *52*, 4132-4136.

(64) (a) Rosen, B. M.; Lligadas, G.; Hahn, C.; Percec, V. *J. Polym. Sci., Part A: Polym. Chem.* **2009**, *47*, 3940-3948. (b) Rosen, B. M.; Lligadas, G.; Hahn, C.; Percec, V. *J. Polym. Sci., Part A: Polym. Chem.* **2009**, *47*, 3931-3939.

- (65) Xu, J.; Tao, L.; Boyer, C.; Lowe, A. B.; Davis, T. P. *Macromolecules* **2009**, *43*, 20-24.
- (66) Li, H.; Yu, B.; Matsushima, H.; Hoyle, C. E.; Lowe, A. B. *Macromolecules* **2009**, *42*, 6537-6542.
- (67) Gody, G.; Rossner, C.; Moraes, J.; Vana, P.; Maschmeyer, T.; Perrier, S. *J. Am. Chem. Soc.* **2012**, *134*, 12596-12603.
- (68) Becer, C. R.; Babiuch, K.; Pilz, D.; Hornig, S.; Heinze, T.; Gottschaldt, M.; Schubert, U. S. *Macromolecules* **2009**, *42*, 2387-2394.
- (69) ten Brummelhuis, N.; Weck, M. *ACS Macro Lett.* **2012**, *1*, 1216-1218.
- (70) Pounder, R. J.; Stanford, M. J.; Brooks, P.; Richards, S. P.; Dove, A. P. *Chem. Commun.* **2008**, *44*, 5158-5160.
- (71) Billiet, L.; Gok, O.; Dove, A. P.; Sanyal, A.; Nguyen, L.-T. T.; Du Prez, F. E. *Macromolecules* **2011**, *44*, 7874-7878.
- (72) Li, M.; De, P.; Gondi, S. R.; Sumerlin, B. S. *J. Polym. Sci., Part A: Polym. Chem.* **2008**, *46*, 5093-5100.
- (73) (a) Jones, M. W.; Strickland, R. A.; Schumacher, F. F.; Caddick, S.; Baker, J. R.; Gibson, M. I.; Haddleton, D. M. *Chem. Commun.* **2012**, *48*, 4064-4066. (b) Jones, M. W.; Strickland, R. A.; Schumacher, F. F.; Caddick, S.; Baker, J. R.; Gibson, M. I.; Haddleton, D. M. *J. Am. Chem. Soc.* **2011**, *134*, 1847-1852.

- (74) Robin, M. P.; Jones, M. W.; Haddleton, D. M.; O'Reilly, R. K. *ACS Macro Lett.* **2011**, *1*, 222-226.
- (75) Harvison, M. A.; Davis, T. P.; Lowe, A. B. *Polym. Chem.* **2011**, *2*, 1347-1354.
- (76) De, S.; Khan, A. *Chem. Commun.* **2012**, *48*, 3130-3132.
- (77) Yuan, Y. C.; Rong, M. Z.; Zhang, M. Q.; Chen, J.; Yang, G. C.; Li, X. M. *Macromolecules* **2008**, *41*, 5197-5202.
- (78) Hoyle, C. E.; Lowe, A. B.; Bowman, C. N. *Chem. Soc. Rev.* **2010**, *39*, 1355-1387.
- (79) Heredia, K. L.; Tolstyka, Z. P.; Maynard, H. D. *Macromolecules* **2007**, *40*, 4772-4779.
- (80) Grover, G. N.; Lam, J.; Nguyen, T. H.; Segura, T.; Maynard, H. D. *Biomacromolecules* **2012**, *13*, 3013-3017.
- (81) (a) Christman, K. L.; Broyer, R. M.; Schopf, E.; Kolodziej, C. M.; Chen, Y.; Maynard, H. D. *Langmuir* **2010**, *27*, 1415-1418. (b) Paulöhr, T.; Delaittre, G.; Bruns, M.; Meißler, M.; Börner, H. G.; Bastmeyer, M.; Barner-Kowollik, C. *Angew. Chem., Int. Ed.* **2012**, *51*, 9181-9184.
- (82) Alconcel, S. N. S.; Kim, S. H.; Tao, L.; Maynard, H. D. *Macromol. Rapid Comm.* **2013**, *34*, 983-989.
- (83) Liu, J.; Li, R. C.; Sand, G. J.; Bulmus, V.; Davis, T. P.; Maynard, H. D. *Macromolecules* **2012**, *46*, 8-14.

- (84) Chenal, M.; Boursier, C.; Guillaneuf, Y.; Taverna, M.; Couvreur, P.; Nicolas, J. *Polym. Chem.* **2011**, *2*, 1523-1530.
- (85) Nilles, K.; Theato, P. *J. Polym. Sci., Part A: Polym. Chem.* **2010**, *48*, 3683-3692.
- (86) Eberhardt, M.; Théato, P. *Macromol. Rapid Comm.* **2005**, *26*, 1488-1493.
- (87) Sletten, E. M.; Bertozzi, C. R. *Acc. Chem. Res.* **2011**, *44*, 666-676.
- (88) Sletten, E. M.; Bertozzi, C. R. *Angew. Chem., Int. Ed.* **2009**, *48*, 6974-6998.
- (89) Cazalis, C. S.; Haller, C. A.; Sease-Cargo, L.; Chaikof, E. L. *Bioconjugate Chem.* **2004**, *15*, 1005-1009.
- (90) Diels, O.; Alder, K. *Justus Liebigs Ann. Chem.* **1928**, *460*, 98-122.
- (91) Nicolaou, K. C.; Snyder, S. A.; Montagnon, T.; Vassilikogiannakis, G. *Angew. Chem., Int. Ed.* **2002**, *41*, 1668-1698.
- (92) Funel, J.-A.; Abele, S. *Angew. Chem., Int. Ed.* **2013**, *52*, 3822-3863.
- (93) El-Ghatta, H.; Forrer, J. K.; Swiss patent CH597113: 1978.
- (94) Gandini, A. *Prog. Polym. Sci.* **2013**, *38*, 1-29.
- (95) Aumsuwan, N.; Urban, M. W. *Polymer* **2009**, *50*, 33-36.
- (96) Durmaz, H.; Dag, A.; Altintas, O.; Erdogan, T.; Hizal, G.; Tunca, U. *Macromolecules* **2006**, *40*, 191-198.

- (97) Glassner, M.; Blinco, J. P.; Barner-Kowollik, C. *Macromol. Rapid Comm.* **2011**, 32, 724-728.
- (98) Gacal, B.; Durmaz, H.; Tasdelen, M. A.; Hizal, G.; Tunca, U.; Yagci, Y.; Demirel, A. L. *Macromolecules* **2006**, 39, 5330-5336.
- (99) (a) Sinnwell, S.; Inglis, A. J.; Davis, T. P.; Stenzel, M. H.; Barner-Kowollik, C. *Chem. Commun.* **2008**, 44, 2052-2054. (b) Inglis, A. J.; Sinnwell, S.; Stenzel, M. H.; Barner-Kowollik, C. *Angew. Chem., Int. Ed.* **2009**, 48, 2411-2414. (c) Inglis, A. J.; Stenzel, M. H.; Barner-Kowollik, C. *Macromol. Rapid Comm.* **2009**, 30, 1792-1798. (d) Oehlenschlaeger, K. K.; Mueller, J. O.; Heine, N. B.; Glassner, M.; Guimard, N. K.; Delaittre, G.; Schmidt, F. G.; Barner-Kowollik, C. *Angew. Chem., Int. Ed.* **2013**, 52, 762-766.
- (100) Zydzia, N.; Preuss, C. M.; Winkler, V.; Bruns, M.; Hübner, C.; Barner-Kowollik, C. *Macromol. Rapid Comm.* **2013**, 34, 672-680.
- (101) Goldmann, A. S.; Tischer, T.; Barner, L.; Bruns, M.; Barner-Kowollik, C. *Biomacromolecules* **2011**, 12, 1137-1145.
- (102) Carboni, R. A.; Lindsey, R. V., Jr. *J. Am. Chem. Soc.* **1959**, 81, 4342-4346.
- (103) Jørgensen, K. A. *Angew. Chem., Int. Ed.* **2000**, 39, 3558-3588.
- (104) Karver, M. R.; Weissleder, R.; Hilderbrand, S. A. *Bioconjugate Chem.* **2011**, 22, 2263-2270.

- (105) Thalhammer, F.; Wallfahrer, U.; Sauer, J. *Tet. Lett.* **1990**, *31*, 6851-6854.
- (106) Chen, W.; Wang, D.; Dai, C.; Hamelberg, D.; Wang, B. *Chem. Commun.* **2012**, *48*, 1736-1738.
- (107) (a) Boger, D. L.; Boyce, C. W.; Labroli, M. A.; Sehon, C. A.; Jin, Q. *J. Am. Chem. Soc.* **1999**, *121*, 54-62. (b) Boger, D. L.; Soenen, D. R.; Boyce, C. W.; Hedrick, M. P.; Jin, Q. *J. Org. Chem.* **2000**, *65*, 2479-2483. (c) Boger, D. L.; Wolkenberg, S. E. *J. Org. Chem.* **2000**, *65*, 9120-9124. (d) Boger, D. L.; Hong, J. *J. Am. Chem. Soc.* **2001**, *123*, 8515-8519. (e) Hamasaki, A.; Zimpleman, J. M.; Hwang, I.; Boger, D. L. *J. Am. Chem. Soc.* **2005**, *127*, 10767-10770. (f) Boger, D. L.; Zhang, M. *J. Am. Chem. Soc.* **1991**, *113*, 4230-4234.
- (108) Jewett, J. C.; Bertozzi, C. R. *Chem. Soc. Rev.* **2010**, *39*, 1272-1279.
- (109) Blackman, M. L.; Royzen, M.; Fox, J. M. *J. Am. Chem. Soc.* **2008**, *130*, 13518-13519.
- (110) Liu, D. S.; Tangpeerachaikul, A.; Selvaraj, R.; Taylor, M. T.; Fox, J. M.; Ting, A. Y. *J. Am. Chem. Soc.* **2012**, *134*, 792-795.
- (111) (a) Wiessler, M.; Waldeck, W.; Kliem, C.; Pipkorn, R.; Braun, K. *Int. J. Med. Sci.* **2010**, *7*, 19-28. (b) Pipkorn, R.; Waldeck, W.; Diding, B.; Koch, M.; Mueller, G.; Wiessler, M.; Braun, K. *J. Pept. Sci.* **2009**, *15*, 235-241.
- (112) Devaraj, N. K.; Weissleder, R.; Hilderbrand, S. A. *Bioconjugate Chem.* **2008**, *19*, 2297-2299.

- (113) Devaraj, N. K.; Upadhyay, R.; Haun, J. B.; Hilderbrand, S. A.; Weissleder, R. *Angew. Chem., Int. Ed.* **2009**, *48*, 7013-7016.
- (114) Karver, M. R.; Weissleder, R.; Hilderbrand, S. A. *Angew. Chem., Int. Ed.* **2012**, *51*, 920-922.
- (115) Devaraj, N.; Hilderbrand, S.; Upadhyay, R.; Mazitschek, R.; Weissleder, R. *Angew. Chem., Int. Ed.* **2010**, *49*, 2869-2872.
- (116) (a) Lang, K.; Davis, L.; Torres-Kolbus, J.; Chou, C.; Deiters, A.; Chin, J. W. *Nat. Chem.* **2012**, *4*, 298-304. (b) Plass, T.; Milles, S.; Koehler, C.; Szymański, J.; Mueller, R.; Wießler, M.; Schultz, C.; Lemke, E. A. *Angew. Chem., Int. Ed.* **2012**, *51*, 4166-4170.
- (117) Seitchik, J. L.; Peeler, J. C.; Taylor, M. T.; Blackman, M. L.; Rhoads, T. W.; Cooley, R. B.; Refakis, C.; Fox, J. M.; Mehl, R. A. *J. Am. Chem. Soc.* **2012**, *134*, 2898-2901.
- (118) (a) Patterson, D. M.; Nazarova, L. A.; Xie, B.; Kamber, D. N.; Prescher, J. A. *J. Am. Chem. Soc.* **2012**, *134*, 18638-18643. (b) Yang, J.; Šečkutė, J.; Cole, C. M.; Devaraj, N. K. *Angew. Chem., Int. Ed.* **2012**, *51*, 7476-7479.
- (119) Taylor, M. T.; Blackman, M. L.; Dmitrenko, O.; Fox, J. M. *J. Am. Chem. Soc.* **2011**, *133*, 9646-9649.
- (120) Han, H.-S.; Devaraj, N. K.; Lee, J.; Hilderbrand, S. A.; Weissleder, R.; Bawendi, M. G. *J. Am. Chem. Soc.* **2010**, *132*, 7838-7839.



- (121) Hayden, H.; Gun'ko, Y. K.; Perova, T. S. *Chem. Phys. Lett.* **2007**, *435*, 84-89.
- (122) Schoch, J.; Wiessler, M.; Jäschke, A. *J. Am. Chem. Soc.* **2010**, *132*, 8846-8847.
- (123) Chen, C.; Allen, C. A.; Cohen, S. M. *Inorg. Chem.* **2011**, *50*, 10534-10536.
- (124) Panek, J. S.; Zhu, B. *Tet. Lett.* **1996**, *37*, 8151-8154.
- (125) (a) Hoogenboom, R.; Moore, B. C.; Schubert, U. S. *Chem. Commun.* **2006**, *42*, 4010-4012. (b) Hoogenboom, R.; Wouters, D.; Schubert, U. S. *Macromolecules* **2003**, *36*, 4743-4749.
- (126) Hanack, M.; Lange, A.; Grosshans, R. *Synt. Met.* **1991**, *45*, 59-70.
- (127) Li, Z.; Ding, J.; Song, N.; Du, X.; Zhou, J.; Lu, J.; Tao, Y. *Chem. Mat.* **2011**, *23*, 1977-1984.
- (128) Li, H.; Zhou, Q.; Audebert, P.; Miomandre, F.; Allain, C.; Yang, F.; Tang, J. *J. Electroanal. Chem.* **2012**, *668*, 26-29.
- (129) Zhou, H.; Woo, J.; Cok, A. M.; Wang, M.; Olsen, B. D.; Johnson, J. A. *Proc. Natl. Acad. Sci. U. S. A.* **2012**, *109*, 19119-19124.
- (130) Alge, D. L.; Azagarsamy, M. A.; Donohue, D. F.; Anseth, K. S. *Biomacromolecules* **2013**, *14*, 949-953.
- (131) Zhou, H.; Johnson, J. A. *Angew. Chem., Int. Ed.* **2013**, *52*, 2235-2238.

- (132) Pinner, A. *Justus Liebigs Ann. Chem.* **1897**, 297, 221-271.
- (133) Boger, D. L.; Coleman, R. S.; Panek, J. S.; Huber, F. X.; Sauer, J. J. *Org. Chem.* **1985**, 50, 5377-5379.
- (134) (a) Qing, Z.; Audebert, P.; Clavier, G.; Miomandre, F.; Tang, J.; Vu, T. T.; Méallet-Renault, R. *J. Electroanal. Chem.* **2009**, 632, 39-44. (b) Audebert, P.; Miomandre, F.; Clavier, G.; Vernières, M.-C.; Badré, S.; Méallet-Renault, R. *Chem. Eur. J.* **2005**, 11, 5667-5673.
- (135) (a) Sakya, S. M.; Groskopf, K. K.; Boger, D. L. *Tet. Lett.* **1997**, 38, 3805-3808. (b) Boger, D. L.; Schaum, R. P.; Garbaccio, R. M. *J. Org. Chem.* **1998**, 63, 6329-6337. (c) Hamasaki, A.; Ducray, R.; Boger, D. L. *J. Org. Chem.* **2006**, 71, 185-193.
- (136) Clavier, G.; Audebert, P. *Chem. Rev.* **2010**, 110, 3299-3314.
- (137) Yang, J.; Karver, M. R.; Li, W.; Sahu, S.; Devaraj, N. K. *Angew. Chem., Int. Ed.* **2012**, 51, 5222-5225.
- (138) Saracoglu, N. *Tetrahedron* **2007**, 63, 4199-4236.
- (139) Löbbecke, S.; Pfeil, A.; Krause, H. H.; Sauer, J.; Holland, U. *Propellants Explos. Pyrotech.* **1999**, 24, 168-175.

## **Chapter 2. Tetrazine–norbornene reaction in polymer functionalisation and polymer– polymer coupling**

### **2.1. Abstract**

In this chapter, the application of the tetrazine–norbornene reaction to polymer–polymer coupling and functionalisation is demonstrated. Coupling was shown to take place equally effectively in organic and aqueous media, with no heating, reagent or external stimulus necessary to force the reaction to proceed to very high conversions.

The work in this chapter was carried out in collaboration with Dr Pieter Espeel and Milan Stamenovic from Professor Filip Du Prez's group at Ghent University, and Dr Ian Barker from Dr Andrew Dove's group at Warwick University. The synthesis and characterisation of norbornene-terminated polystyrene and poly(NIPAM) was carried out by Milan Stamenovic, and the LC-MS small molecule solvent screen was carried out by Pieter Espeel. Norbornene-terminated poly(valerolactone)s and poly(caprolactone) synthesis was carried out by Ian Barker.

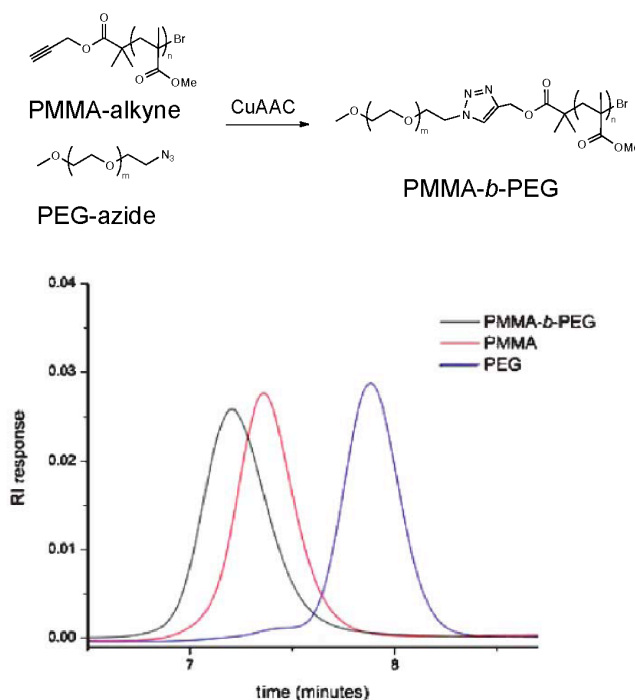
## 2.2. Background

The 'Click' philosophy has arguably had more impact in polymer and materials chemistry than any other area of chemistry, as the efficiency of such reactions proffers an enhanced ability to readily modify polymer chain ends or carry out polymer–polymer conjugation. Since single reactive sites on any given polymer chain are less accessible than on small molecules, and separation of polymeric species is much more difficult than separating small molecule species from each other, the key Click elements of 100% conversion, fast kinetics and orthogonality mean that polymer modification is reliably achievable without tedious and time-consuming workup requirements.<sup>1</sup>

Whilst many block copolymers can be readily synthesised by chain extension using CRP techniques, there are some combinations of monomers which are generally incompatible and thus modular synthesis is an attractive alternative.

As discussed in the introduction, the CuAAC reaction<sup>2</sup> has become the *de facto* standard for many reactions where Click conditions are required. It was the first method employed for the modular synthesis of block copolymers<sup>3</sup> where alkyne-functionalised ATRP initiators were used to synthesise PS and PMMA with a terminal alkyne; these polymers were then coupled to azide-functionalised PS and PEG blocks. Purification was carried out using scavenger resins and/or washing procedures, so it is difficult to assess the efficiency of the reaction; however the SEC traces of the purified copolymers show little to no trace of residual homopolymer

(Figure 2.1). The methodology was also extended to form triblock copolymers,<sup>4</sup> albeit again with purification procedures (washing and column chromatography) after formation of the triblock.



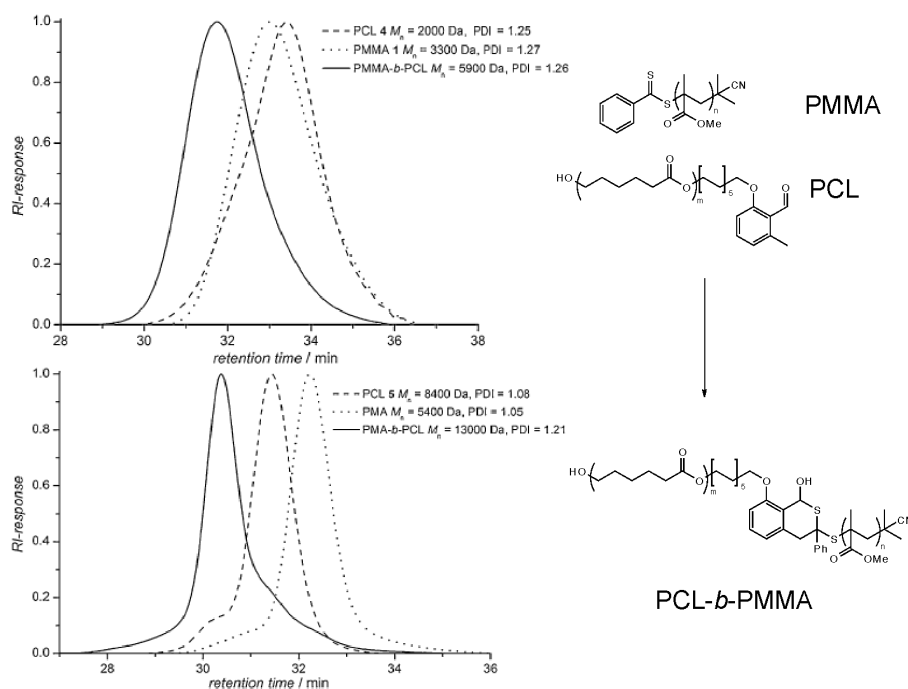
**Figure 2.1 Diblock copolymer formation using the CuAAC reaction to ligate PEG and PMMA homopolymers<sup>3</sup>**

However, also discussed in the introduction, there are some limitations on the use of the CuAAC reaction, particularly with regard to the use and removal of a copper catalyst. In addition to those, to polymers, the azide handle is incompatible with radical polymerisation of vinyl monomers, so it must be introduced in a post-polymerisation step, thus increasing the number of synthetic steps required.<sup>5</sup> There have been several alternatives

to the CuAAC reaction used in polymer functionalisation and polymer–polymer coupling.

Taking advantage of the ability of the dithioester or trithiocarbonate inherent to RAFT-synthesised polymers to act as a dienophile in hetero Diels-Alder (HDA) reactions, Barner-Kowollik *et. al.* have developed particularly electron-deficient dithioesters to facilitate polymer–polymer coupling *via* their “ultra fast” RAFT-HDA method.<sup>6</sup> Polymer–polymer coupling was demonstrated using equimolar amounts of RAFT polymer and cyclopentadiene-functionalised polymer, in under 10 minutes at room temperature; the downside being that the reaction requires trifluoroacetic acid (1.5 eq.) as a catalyst, the cyclopentadiene is tricky to incorporate onto the polymer end (post-polymerisation modification in two steps), and that the RAFT agent employed is somewhat unusual in nature.

The latter two drawbacks have recently been overcome using a photoenol as an alternative to the cyclopentadiene, which enables a commercially available RAFT agent to be used as the dienophile; in this case irradiation with UV light was required to facilitate the reaction (Figure 2.2).<sup>7</sup> The linkage formed between polymers has also been shown to degrade above 80 °C,<sup>8</sup> although this degradation can be made reversible by judicious choice of the RAFT agent.<sup>9</sup>



**Figure 2.2 Example SEC traces for polymer–polymer coupling by light-induced RAFT-HDA methodology<sup>7</sup>**

Aside from the RAFT-HDA reaction, Diels-Alder reactions between anthracene and maleimide,<sup>10</sup> Heck coupling<sup>11</sup> and Atom Transfer Nitroxide Radical Coupling (ATNRC) reaction<sup>12</sup> have also all been used to synthesise block copolymers; and in many cases the methodology has been extended to form triblock copolymers or star polymers using a ‘double click’ strategy.<sup>13</sup> However, aside from the sole example using Heck coupling, it is unusual to see block copolymers using these strategies formed from equimolar amounts of their constituent homopolymers, and thus purification processes are required after the synthesis. The radical thiol–ene reaction, although a popular click reaction, has been shown to be insufficiently efficient to enable polymer–polymer coupling.<sup>14</sup>

Although a wide range of chemistries (“click” or otherwise) have been explored for the synthesis of block copolymers, it was highlighted in recent reviews that the tetrazine–norbornene DA<sub>inv</sub> reaction has not yet been applied to polymer synthesis,<sup>15</sup> despite being fast, quantitative and producing only N<sub>2</sub> as a byproduct. Thus we were motivated to investigate polymer functionalisation and polymer–polymer ligation using the DA<sub>inv</sub> reaction between tetrazine and norbornene. We opted for norbornene as the dieneophile, over the more reactive *trans*-cyclooctene, as the synthesis and manipulation of norbornenes is considerably easier, and norbornene is already well established in the polymer world due to its use as a Ring-Opening Metathesis Polymerisation (ROMP) motif;<sup>16</sup> it has been used in tandem with both ATRP<sup>17</sup> and RAFT polymerisations<sup>18</sup> for the formation of ROMP-CRP graft polymers.

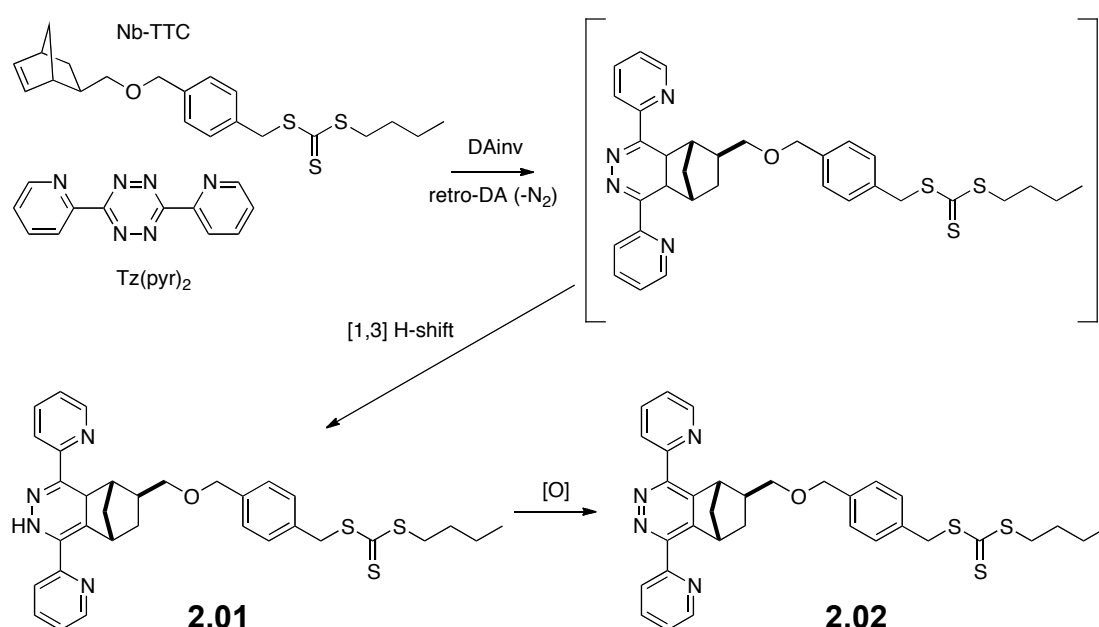
## **2.3. Results and discussion**

### **2.3.1. Small molecule studies**

The aim of investigating an equivalent small molecule reaction to the polymer–polymer one was twofold: firstly to ensure that there was no cross-reaction or other adverse reactions involving the RAFT group and the tetrazine, and secondly to explore the scope of the reaction with regard to solvent choice. Since the reaction between tetrazines and norbornenes is so favourable, side reactions or loss of orthogonality was not anticipated, however, unusual reactivity of tetrazines with aldehydes and ketones has been observed under certain reaction conditions (microwave irradiation).<sup>19</sup>



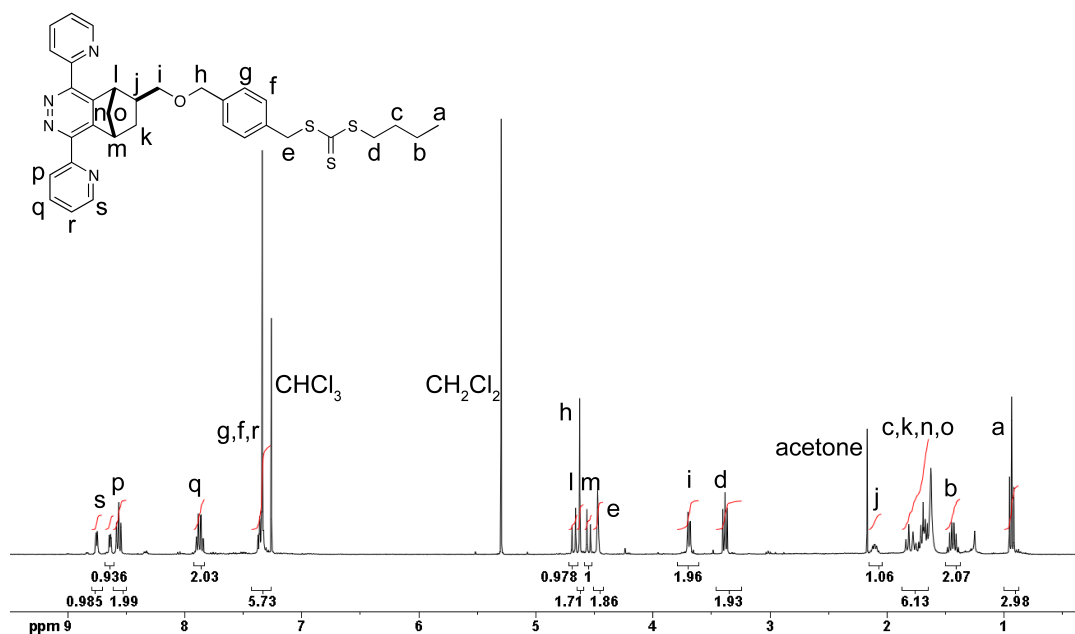
The norbornene-terminated polymers used in the study were synthesised *via* RAFT polymerisation using a previously reported norbornene-functionalised trithiocarbonate, Nb-TTC, synthesised at Ghent University.<sup>20</sup> Thus this species was used as the dienophile partner. Commercially available dipyridyl tetrazine was used as the diene, as it is known to have markedly increased reactivity in the DA<sub>inv</sub> reaction compared to diphenyl tetrazine, the only other readily commercially available tetrazine at the time.<sup>21</sup>



**Scheme 2.1** Reaction between norbornene-functionalised RAFT agent (Nb-TTC) and dipyridyl 1-2-4-5-tetrazine (Tz(pyr)<sub>2</sub>)

Addition of dipyridyl tetrazine to Nb-TTC in equimolar quantities in CH<sub>2</sub>Cl<sub>2</sub> demonstrated the orthogonality of the DA<sub>inv</sub> reaction to the trithiocarbonate group. Whilst there are several stereo- and regio-isomers of the

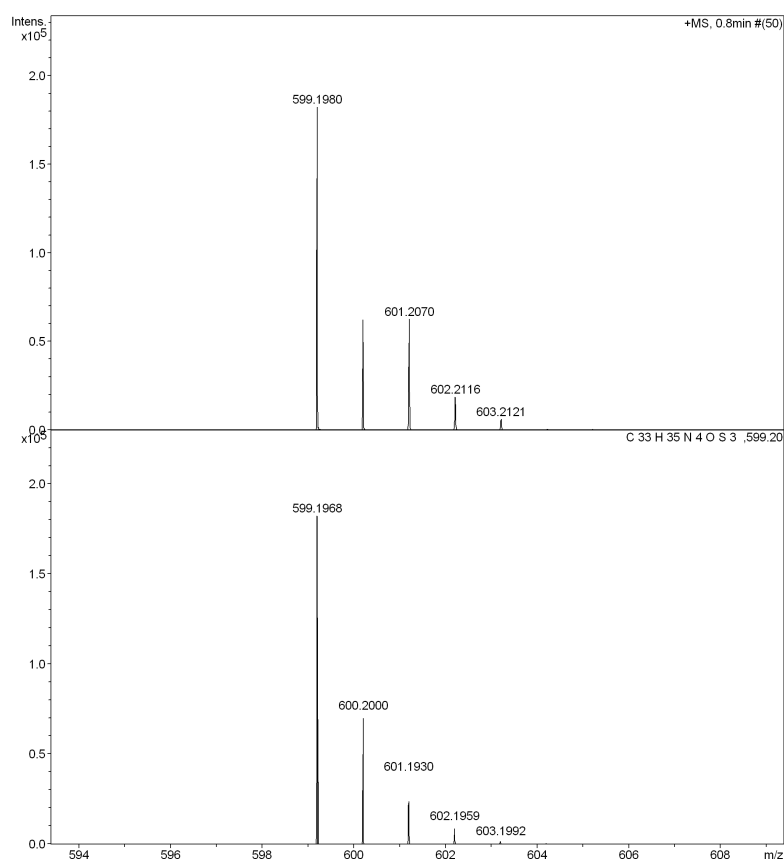
dihydropyradizine product **2.01**, when they were passed over a silica plug to isolate them, incidental oxidation meant that only the fully oxidised pyradizine was formed (single isomer **2.02**).



**Figure 2.3**  $^1\text{H}$  NMR spectrum ( $\text{CDCl}_3$ ) of conjugation product **2.02**

The  $^1\text{H}$  NMR spectrum of **2.02** in Figure 2.3 demonstrated the complete loss of the characteristic Nb alkene signals at 6.1 ppm, whilst the signals arising from the methylene protons adjacent to the trithiocarbonate moiety (d and e in Figure 2.3) remained unaffected, demonstrating the orthogonality to the RAFT end group. Since the isolated product was a single isomer of the fully oxidised pyradizine, it was possible to fully assign the  $^1\text{H}$  NMR spectrum – this is generally difficult to impossible when a mixture of *exo* and *endo* isomers of the dihydropyradizines are present.

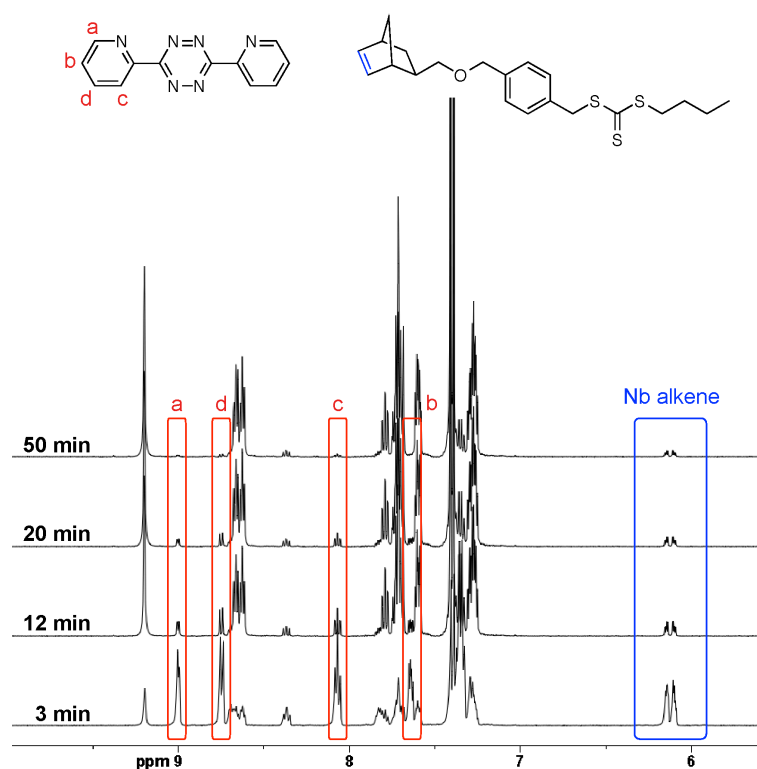
The expected mass of the oxidised addition product was observed by high resolution mass spectrometry (found  $m/z$  599.1980 for  $[M+H]^+$ , expected  $m/z$  599.1973), shown in Figure 2.4.



**Figure 2.4 HRMS for small molecule product 2.02 (top); predicted mass spectrum for formula  $C_{33}H_{35}N_4OS_3$   $[M+H]^+$  (bottom)**

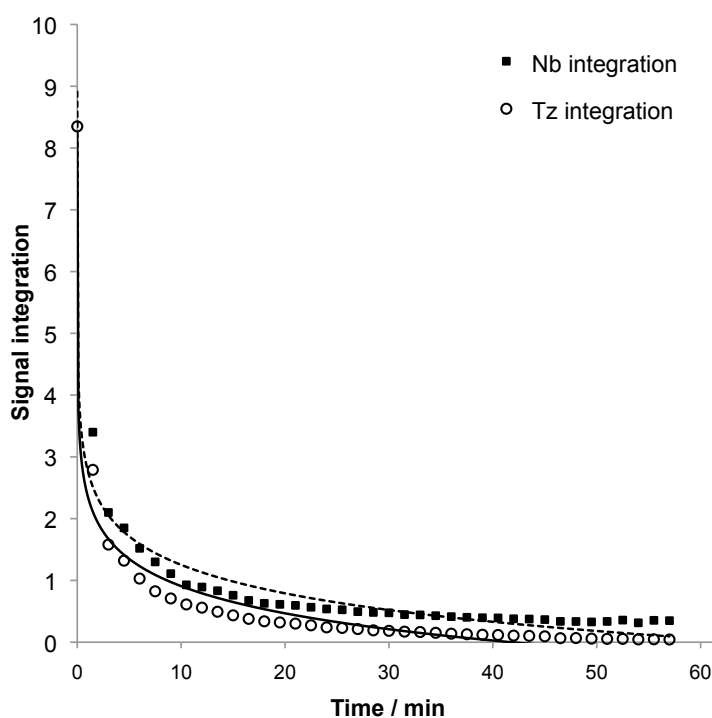
Solvent screening on the model system was also carried out by Dr Pieter Espeel (Ghent University) to determine the range of solvents in which the reaction can be performed as well as elucidate any effect on reaction rate. The same reaction detailed above was performed and the conversion analysed by LC-MS; the reaction rate was found to be affected by the

solvent according to the following order: DMSO > DMF  $\approx$  EtOH > 1,4-dioxane  $\approx$  THF  $\approx$  CH<sub>2</sub>Cl<sub>2</sub> (data shown in Appendix 2.6, Figure 2.26). The fact that the reaction can be performed in a broad range of solvents is a positive one though, as often polymer–polymer couplings are limited by the solubility and/or polymer–solvent interaction of the constituent homopolymers.



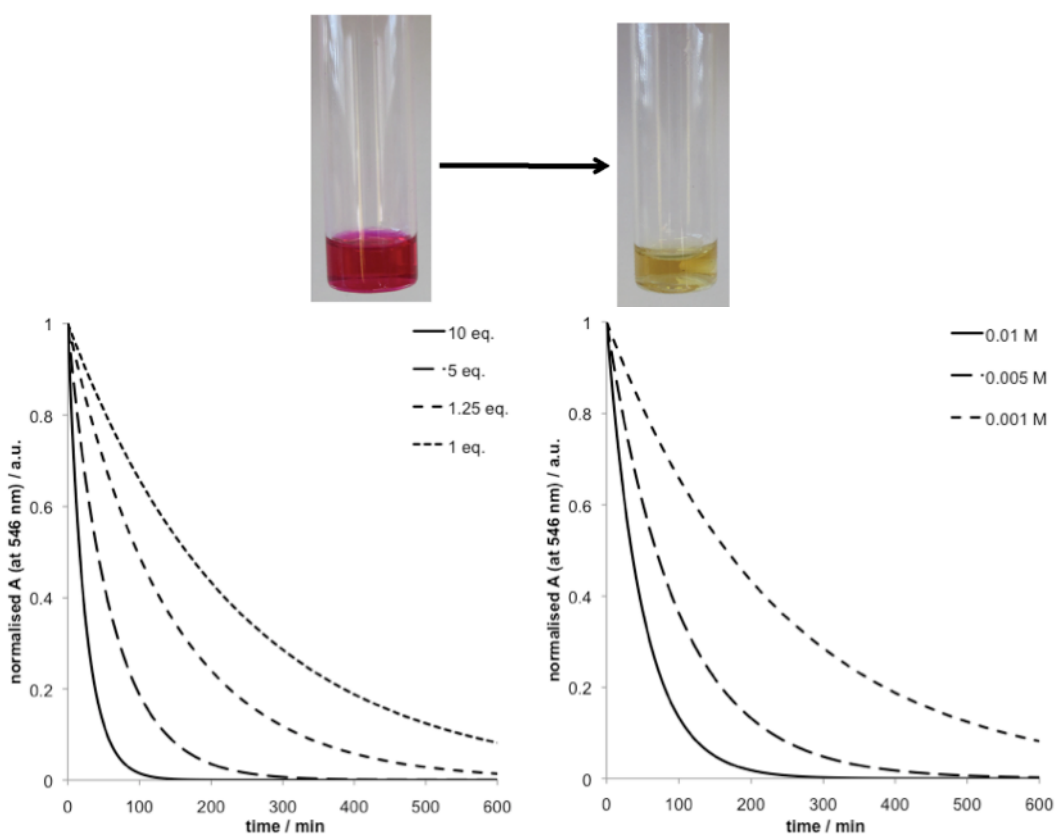
**Figure 2.5** Section of the <sup>1</sup>H NMR spectra (CD<sub>2</sub>Cl<sub>2</sub>) of the reaction mixture forming 2.01 and 2.02 (mixture of stereo- and regio-isomers) over time, with signals arising from the starting materials highlighted.

To explore the rate of the tetrazine–norbornene reaction, *in situ* monitoring by  $^1\text{H}$  NMR and UV/vis spectroscopies was carried out on the model system in  $\text{CH}_2\text{Cl}_2$  ( $\text{CD}_2\text{Cl}_2$  for the NMR experiment). At a concentration of 0.06 M (with equimolar starting materials), the reaction was essentially complete within 1 hour (Figure 2.6), with no starting materials detectable by  $^1\text{H}$  NMR spectroscopy. The integrations of the Nb alkene and Tz pyridyl signals (from the proton labeled d in Figure 2.5) were taken relative to the residual solvent peak (normalised to 1). Due to the complex mixture of stereo-/regio-isomers formed, consumption of starting materials was a more appropriate method for monitoring the reaction than formation of products.



**Figure 2.6 Kinetics of the equimolar small molecule reaction at 0.06 M monitored by  $^1\text{H}$  NMR spectroscopy. To the obtained data points have been fitted logarithmic curves; solid line = Tz integration, dotted line = Nb integration**

The coupling reaction progress is also characterised by a distinctive color change that can be monitored by UV/vis spectroscopy utilising the weak absorbance at 546 nm. This was possible over a range of tetrazine concentrations (0.01 M to 0.001 M). The rather stronger absorbance at 340 nm can also be used for reaction monitoring at much lower concentrations,<sup>22</sup> however the strong absorbance from the Nb–TTC trithiocarbonate group overlaps with this peak significantly so is not possible in this case.



**Figure 2.7** UV/vis absorbance at 546 nm against time for the reaction of Nb–TTC with Tz(pyr)<sub>2</sub>, varying equivalents of Nb–TTC at constant [Tz] (left) and concentration of both Nb–TTC and Tz in equimolar amounts (right). The colour change corresponding to the change in absorbance is shown at the

top

The same reaction as described previously was carried out at 25 °C in CH<sub>2</sub>Cl<sub>2</sub>. The concentration of tetrazine and norbornene, and equivalents of tetrazine relative to Nb–TTC (0.001 M) were varied, and the absorbance at 546 nm measured every 60 s over the timeframe. The data were baseline subtracted, the baseline taken to be the absorbance at 546 nm after several days, and normalised such that the highest absorbance was equal to unity. An exponential curve fit was applied to the data, with R<sup>2</sup> values all greater than 0.98.

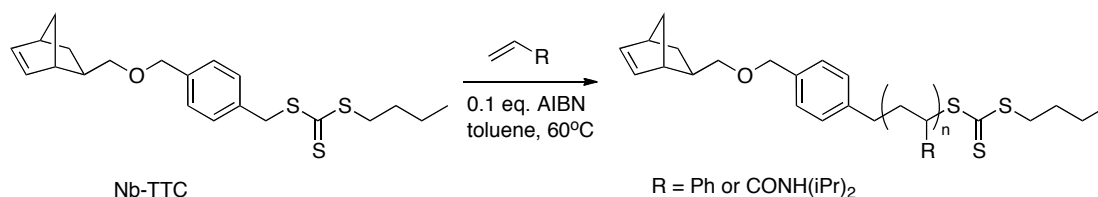
The UV/vis data shown in Figure 2.7 demonstrated that, as would be expected, the rate of coupling increased with higher concentration and equivalents of tetrazine with respect to the Nb group.

## **2.3.2. Functionalised polymer synthesis**

### **2.3.2.1. Norbornene-terminated polymers**

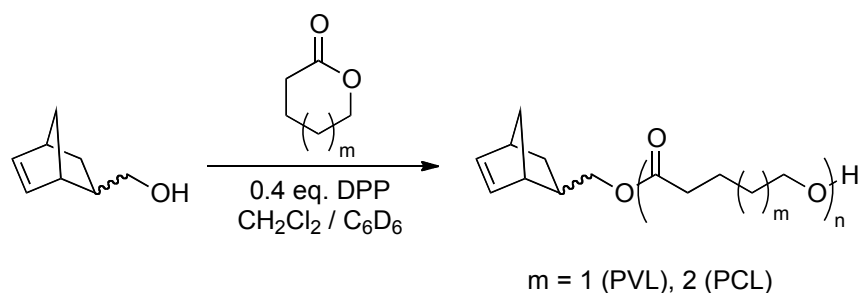
Norbornene-functionalised polystyrene (PS–Nb) and poly(*N*-isopropylacrylamide) (PNIPAM–Nb) were synthesised *via* RAFT polymerisation by Milan Stamenovic at Ghent University, in a similar manner to that described previously.<sup>18,20,23</sup> The general synthetic approach is shown in Scheme 2.2; the only significant consideration when compared to a ‘normal’ RAFT polymerisation was that the Nb alkene can react with the radicals present in the polymerisation when there is a dearth of vinyl groups available to propagate the growing polymer chain, and so conversions were kept low (~30%) to minimise this. This is an oft-observed phenomenon and

stopping the polymerisations at low conversions is the only method described in the literature to deal with the issue.<sup>18,23-24</sup>



**Scheme 2.2 General RAFT synthesis of Nb-terminated PS and PNIPAM (2.03, 2.04 and 2.05)**

Poly( $\epsilon$ -caprolactone) (PCL–Nb) and poly( $\delta$ -valerolactone) (PVL–Nb) of varying molecular weights were synthesised by Ian Barker (Dove group, Warwick University) *via* ring-opening polymerisation (ROP) catalysed by diphenyl phosphate (DPP) using 5-norbornene methyl alcohol (a mixture of *endo* and *exo* isomers) as an initiator (Scheme 2.3).<sup>25</sup> Unlike the RAFT polymerisations using the norbornenyl-functionalised initiator Nb–TTC, the norbornene is not degraded by the initiator or catalyst, therefore these polymers were assumed to have (close to) 100% end group fidelity.

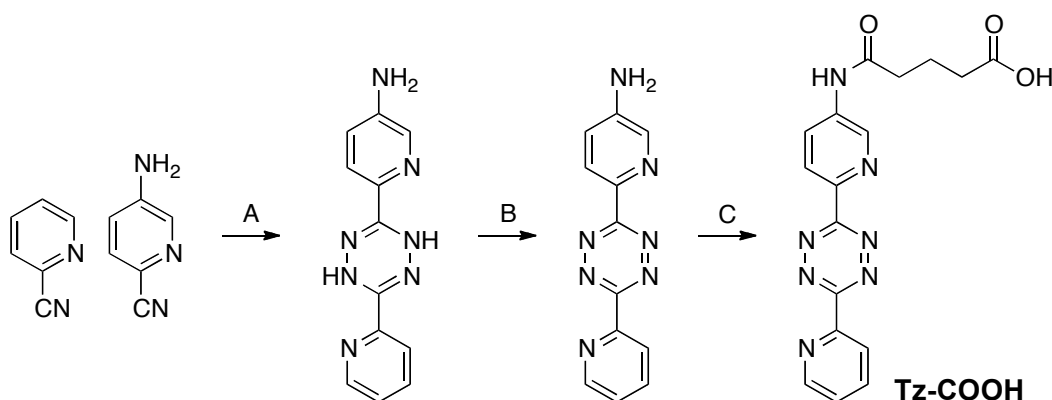


**Scheme 2.3 Synthesis by ROP of Nb-terminated PVL and PCL (2.06–2.09)**



### 2.3.2.2. Tetrazine-terminated polymers

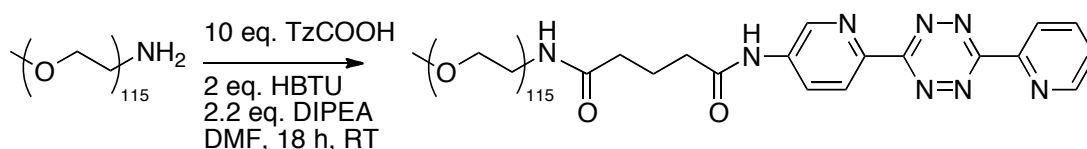
Due to its reactive nature, it is not possible to carry out vinyl polymerisations in the presence of a tetrazine moiety.<sup>26</sup> Control experiments were carried out at typical RAFT polymerisation temperatures (60–90 °C) and equivalents of vinyl monomer (50–200 eq.), but complete degradation of the tetrazine was visually confirmed by loss of the purple colour from the solution, and only took between 4 minutes at 90 °C and 2–3 hours at 60 °C. Since, particularly for end group modification and polymer–polymer coupling, end group fidelity is extremely important, incorporation of the tetrazine into a RAFT, ATRP or NMP initiator is inappropriate, as the reaction of tetrazine with the vinyl groups of the monomer is only exacerbated by the ratio of monomer to initiator in a typical polymerisation. Thus to access tetrazine-terminated polymers with good end group fidelity, both post-polymerisation modification and ROP using an alcohol-functionalised tetrazine were carried out.



**Scheme 2.4** Synthesis of Tz–COOH in three steps. Conditions: (A) 5 eq. hydrazine monohydrate, reflux, overnight; (B) 2 eq. DDQ, toluene, reflux, overnight; (C) 5 eq. glutaric anhydride, THF, 70 °C, overnight.

A commercially available PEG–NH<sub>2</sub> was coupled with an acid-functionalised tetrazine, which was synthesised according to modified literature precedents (Scheme 2.4).<sup>22,27</sup>

Coupling to the PEG–NH<sub>2</sub> was attempted using EDCI/DMAP (2.1 eq./0.2 eq.), but did not result in high enough conversions, even with a 50-fold excess of Tz–COOH, so HBTU was used as a coupling agent instead (Scheme 2.5).



**Scheme 2.5 Synthesis of tetrazine-terminated PEG 2.10**

The PEG–Tz 2.10 was obtained in 65% yield, and end group fidelity was confirmed by <sup>1</sup>H NMR spectroscopy — comparing the integral of the PEG backbone methylene signal (460 protons) to the new signals arising from the Tz–COOH showed that it possessed end group fidelity of greater than 99%. New signals from the pyridyl protons (7H shown in expanded 7.5–11.5 ppm region of Figure 2.8) and the ‘linker’ signals (labelled in expanded region from 1.5–4.5 ppm) are clearly seen in the <sup>1</sup>H NMR spectrum.

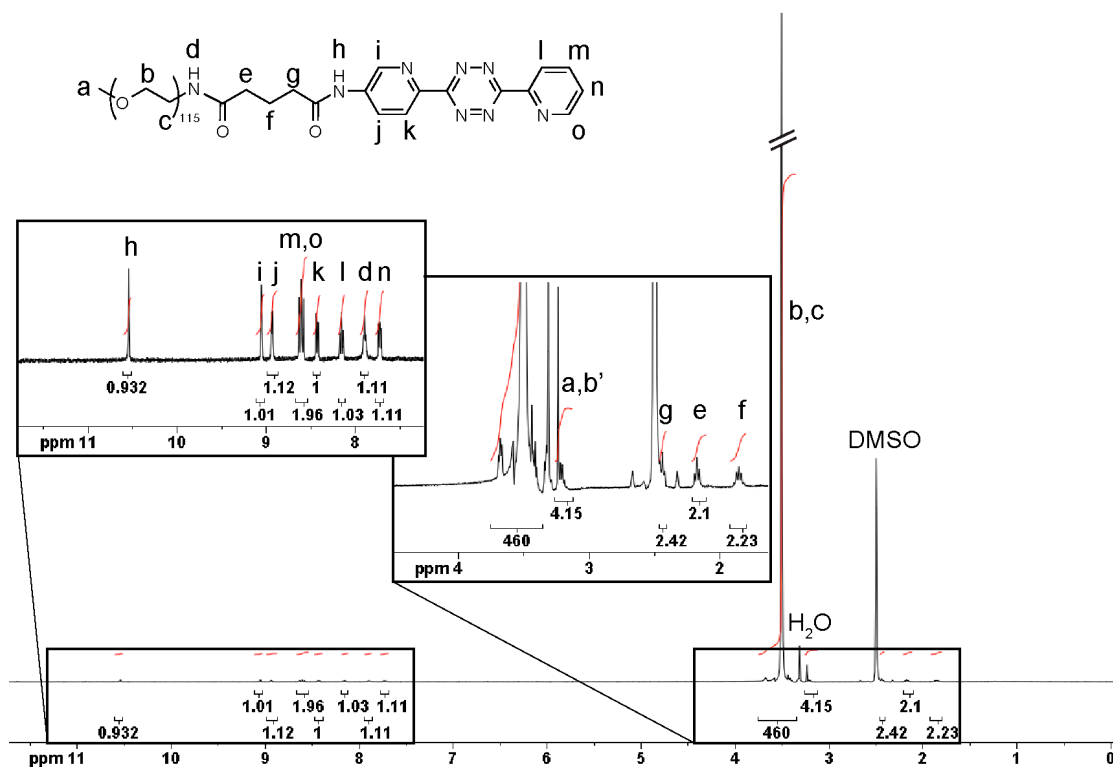
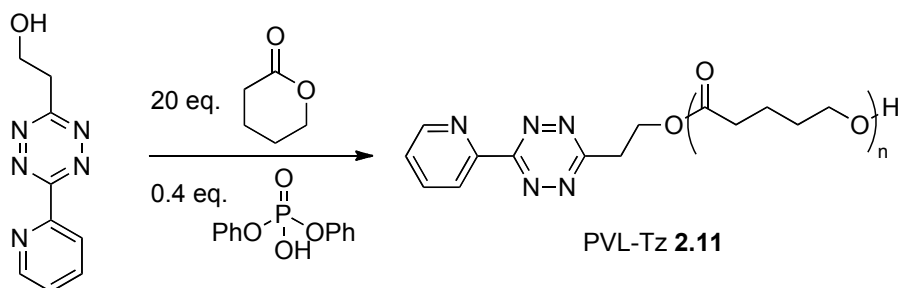


Figure 2.8  $^1\text{H}$  NMR spectrum ( $\text{DMSO-d}_6$ ) of PEG-Tz 2.10



Scheme 2.6 Synthesis of PVL-Tz 2.11 by acid-catalysed ROP

PVL-tetrazine **2.11** was synthesised by Ian Barker at Warwick University using ROP from an alcohol-functionalised tetrazine, synthesised by Pieter Espeel at Ghent University from a literature precedent (Scheme 2.6).<sup>28</sup>

A summary of all of the synthesised polymers and their properties is shown in Table 2.1.  $M_n$  values are calculated by  $^1\text{H}$  NMR spectroscopy, and all  $M_w/M_n$  values calculated by SEC (eluting in THF, relative to PS standards), except for the PNIPAM–Nb **2.05**, which was calculated by SEC eluting in DMF, relative to PMMA standards.  $^1\text{H}$  NMR spectra for polymers **2.03**, **2.05**, **2.06**, **2.07** and **2.11** are shown in Appendix 2.6).

**Table 2.1 Polymers synthesised and used in this chapter**

<b>Sample</b>	<b>Polymer type</b>	<b><math>M_n</math> / kDa</b>	<b><math>M_w/M_n</math></b>	<b>% chain end functionality</b>
<b>2.03</b>	PS–Nb	5.6	1.33	95
<b>2.04</b>	PS–Nb	14.5	1.25	83
<b>2.05</b>	PNIPAM–Nb	16.4	1.21	90
<b>2.06</b>	PCL–Nb	5.6	1.05	100
<b>2.07</b>	PVL–Nb	4.9	1.08	100
<b>2.08</b>	PVL–Nb	10.7	1.07	100
<b>2.09</b>	PVL–Nb	31.0	1.08	100
<b>2.10</b>	PEG–Tz	5.4	1.04	99
<b>2.11</b>	PVL–Tz	1.7	1.23	100

### 2.3.3. End group modification

Since not only polymer–polymer coupling but also the fast and quantitative end-modification of polymers is a desirable target, the same conditions as in the small molecule study ( $\text{CH}_2\text{Cl}_2$ , ambient conditions, equimolar amounts of Tz and Nb) were utilised to functionalise three different Nb-terminated polymers **2.03**, **2.04** and **2.05** with dipyrindyl tetrazine.

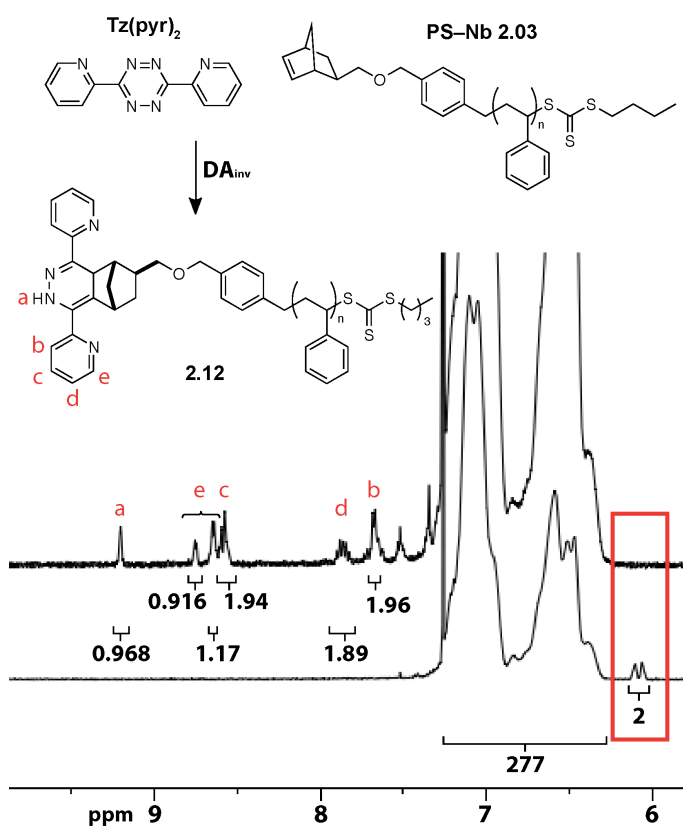


Figure 2.9 Partial  $^1\text{H}$  NMR (400 MHz,  $\text{CDCl}_3$ ) spectrum of PS-Nb **2.03** pre- (bottom) and post- (top) reaction with 1 eq. **Tz(pyr)<sub>2</sub>**. Quantitative functionalisation is shown by the disappearance of norbornenyl 2H (red box, 6.1 ppm), and appearance of 9H (a–e) from the clicked tetrazine.

Confirmation of the coupling reaction is made simple as a result of distinct signals in the  $^1\text{H}$  NMR spectrum in regions that generally contain few other signals. Without any workup or purification of the polymer **2.12**, the norbornenyl resonance at 6.1 ppm disappears completely, and new signals between 7.6–9.3 ppm, which can be readily assigned to the clicked tetrazine end groups (Figure 2.9), appear concomitantly. End group modification of a higher molecular weight PS–Nb, **2.04**, (14.5 kDa) and PNIPAM–Nb **2.05** (16.4 kDa) showed a similar pattern of signals in the  $^1\text{H}$  NMR spectrum, showing that end-functionalisation was just as effective for higher molecular weights.

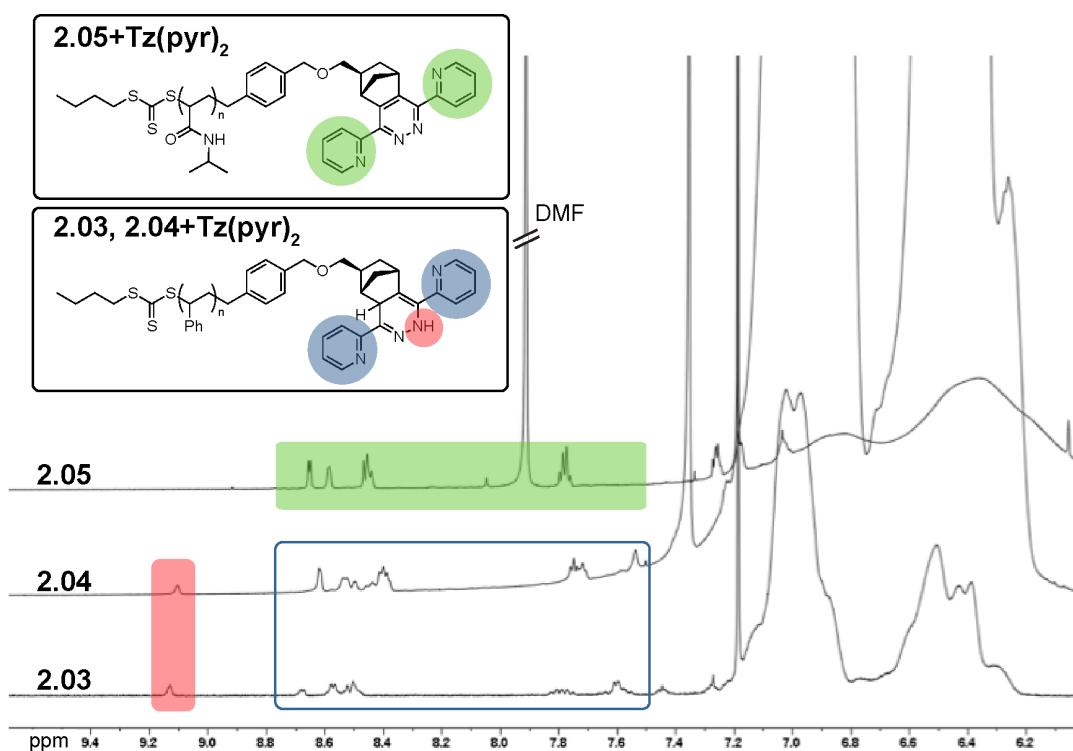
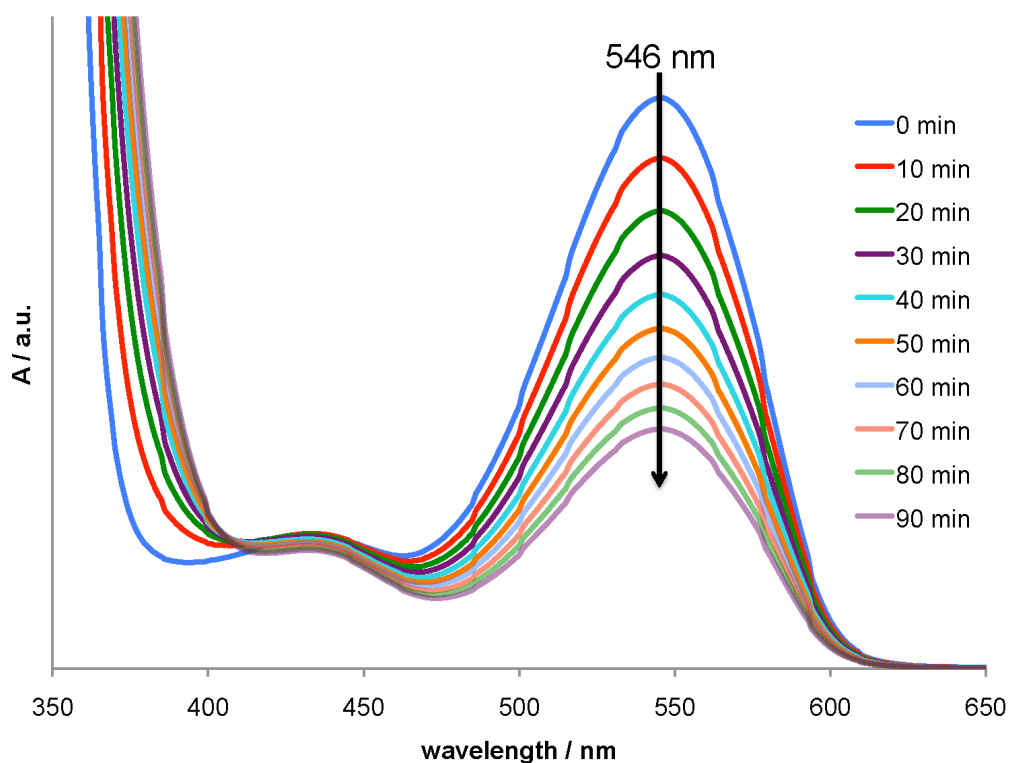


Figure 2.10 Section of  $^1\text{H}$  NMR spectra ( $\text{CDCl}_3$ ) showing near identical tetrazine functionalisation peaks between 7.4 and 9.2 ppm for polymers **2.03**–

**2.05**

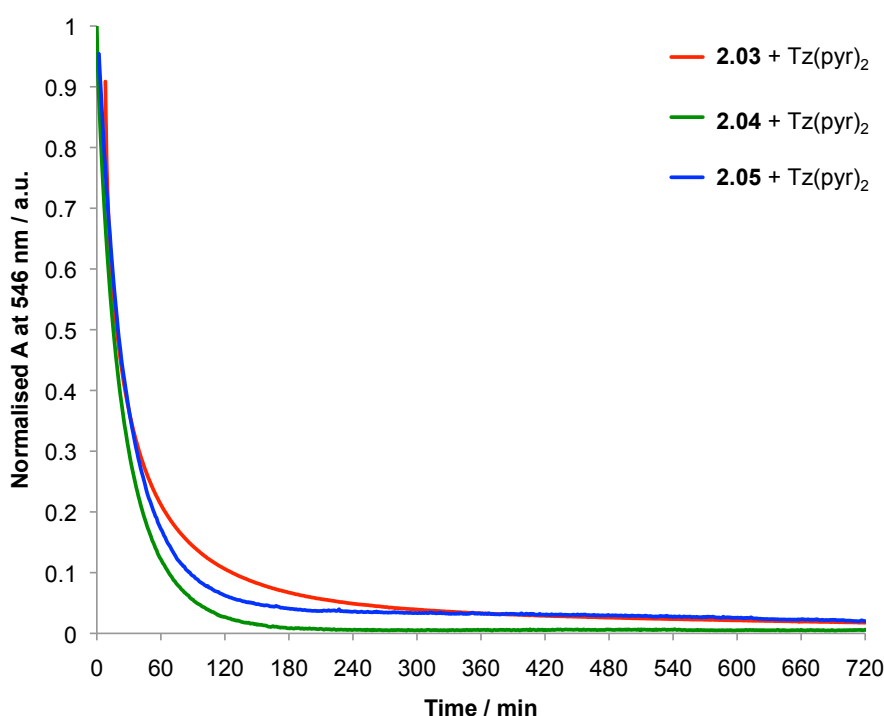
These polymers were recovered after the reaction by precipitation from methanol (for PS) and diethyl ether (PNIPAM) respectively; the only difference in the resulting  $^1\text{H}$  NMR spectra is the lack of dihydropyridazine proton at 9.1 ppm for the PNIPAM **2.05**, which gave the fully oxidised product probably due to the difference in workup procedure.

As with the small molecule coupling reactions described in Section 2.3.1, the polymer end functionalisation can also be followed by UV/vis spectroscopy, monitoring the absorbance at 546 nm, which corresponds with a colour change from pink to yellow-orange (Figure 2.11).



**Figure 2.11** Section of UV/vis spectra for reaction of PS 2.03 with Tz(pyr)<sub>2</sub> showing the change in absorbance at 546 nm with time

When the absorbance at 546 nm was plotted against time and the data normalised to lie between 0 and 1 (Figure 2.12), little to no difference was found in the reaction rate between the small molecule model reaction described earlier and the reaction rate for polymer–small molecule coupling, or between the polymers of different types and molecular weights. Even for the functionalisation of a 16.4 kDa PNIPAM (polymer **2.05**), the equimolar coupling reaction reached over 90% conversion in just 3 hours.

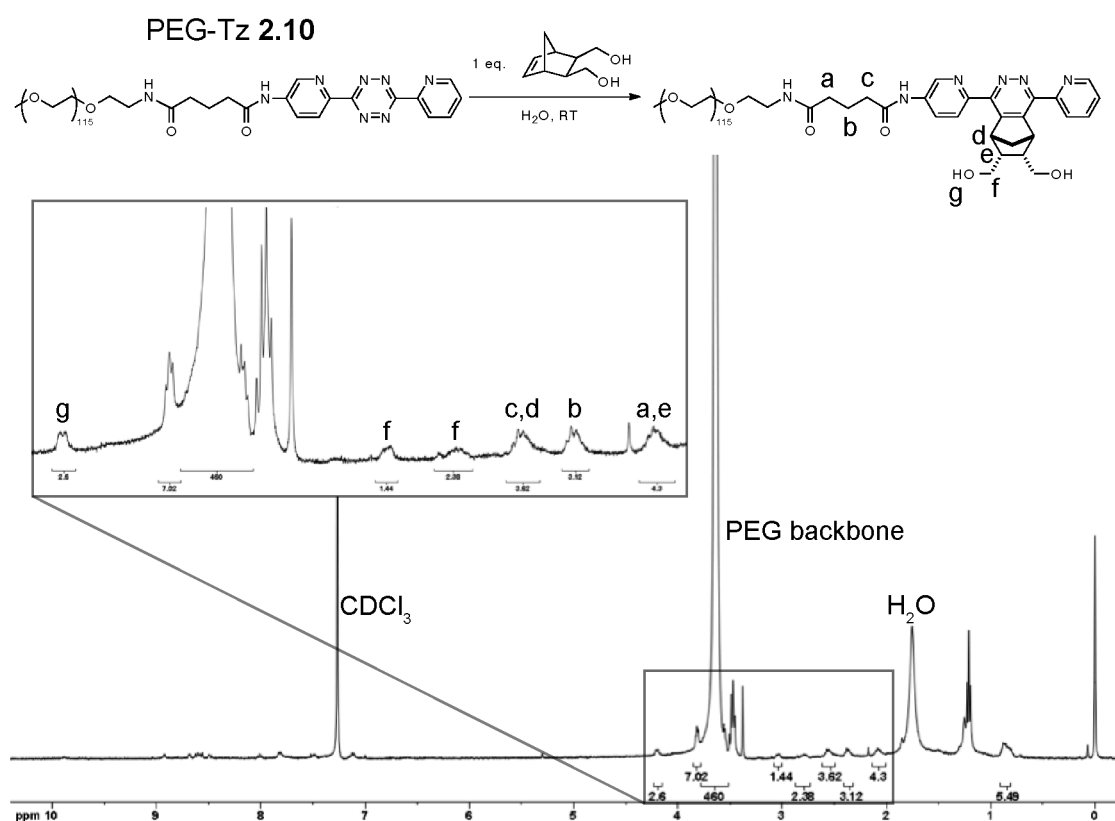


**Figure 2.12 UV/vis absorbance at 546 nm against time for the reaction of polymers 2.03–2.05 with Tz(pyr)<sub>2</sub>**

To further explore the potential scope of the reaction, end-functionalisation of PEG–Tz **2.10** with a water-soluble Nb-containing compound (5-norbornene-2-*endo*,3-*endo*-dimethanol) was carried out in water. The



reaction proceeded at a very similar rate when compared to the polymer functionalisations in organic media, and the product was analysed by  $^1\text{H}$  NMR spectroscopy and MALDI-ToF mass spectrometry. As with functionalisation of the PNIPAM **2.05**, only the fully oxidised product was observed in the  $^1\text{H}$  NMR and MALDI-ToF mass spectra, as evidenced by the lack of characteristic signal at *ca.* 9.2 ppm in the  $^1\text{H}$  NMR spectrum (Figure 2.13), and single isotope distributions per repeat unit in the MALDI-ToF mass spectrum (Figure 2.14).



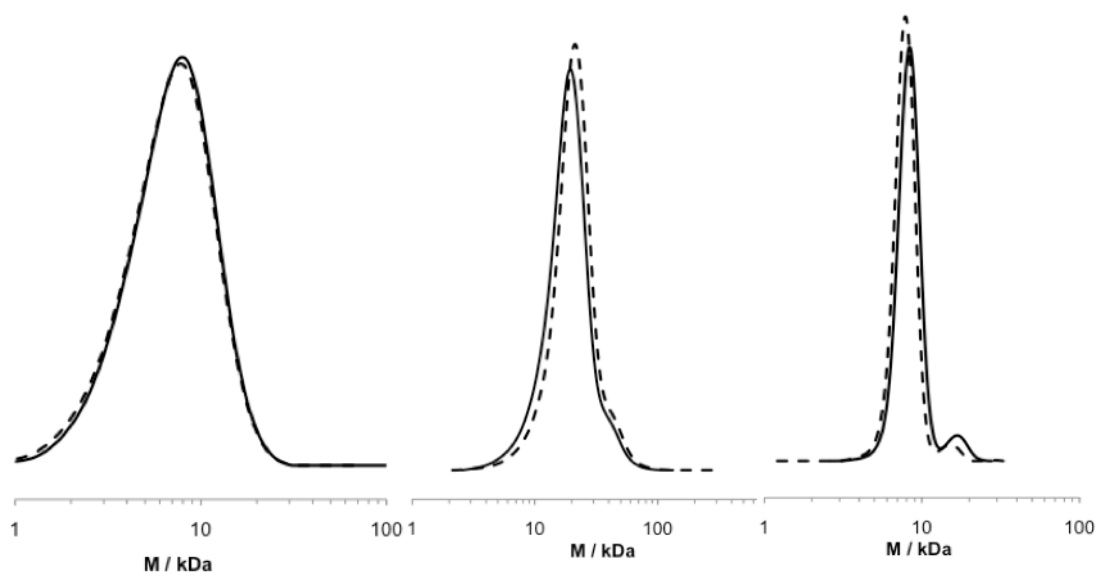
**Figure 2.13**  $^1\text{H}$  NMR spectrum ( $\text{CDCl}_3$ ) of polymer **2.10** functionalised with norbornene dimethanol in water; the expanded view from 2.0–4.2 ppm shows new signals from the reacted norbornene dimethanol

The figure displays two mass spectra. The top spectrum (blue) is for the poly(2-vinylpyridine) derivative, showing a complex pattern of peaks with a prominent peak at approximately 5200 Da. An inset shows a zoomed-in view of the peak at 5200 Da, labeled with  $+Na^+$  and  $+K^+$ , indicating the presence of sodium and potassium adducts. The bottom spectrum (red) is for the precursor poly(2-vinylpyridine), showing a similar pattern of peaks with a prominent peak at approximately 4700 Da. A double-headed arrow indicates the mass difference between the two spectra, labeled 'Mass increase'.

**Mass increase**  
Expected: 471.1907 Da  
Found: 471.2941 Da  
(average of 32 peaks)

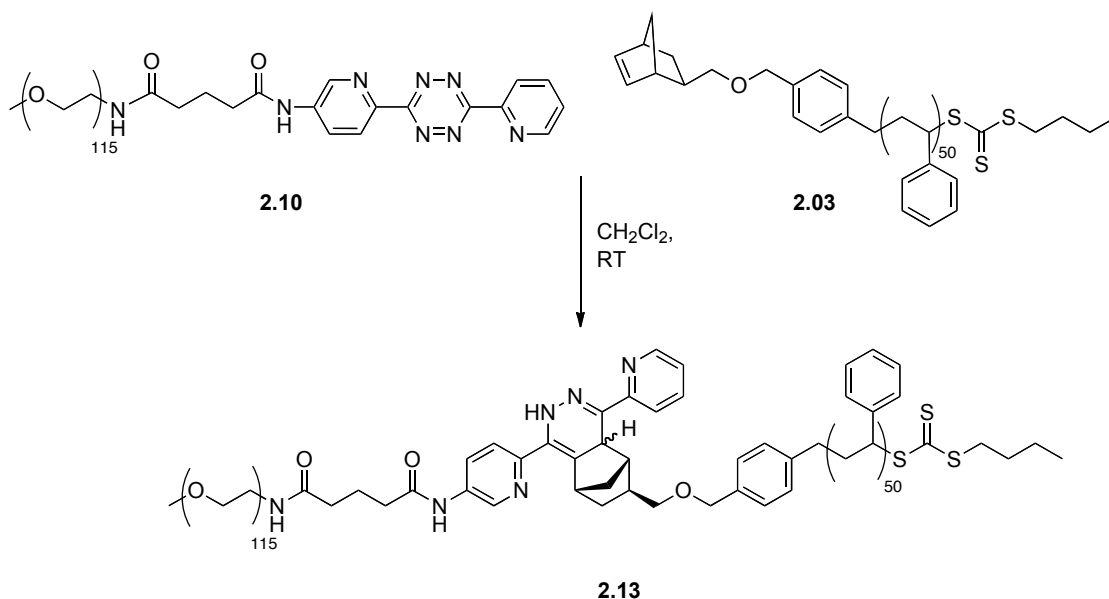
80

The SEC traces (Figure 2.15) of the starting Nb-terminated polymers **2.03** and **2.05**, Tz-terminated polymer **2.10** and their end-functionalised counterparts showed no broadening in dispersity or significant change in molecular weights, indicative that no deleterious side reactions were occurring.



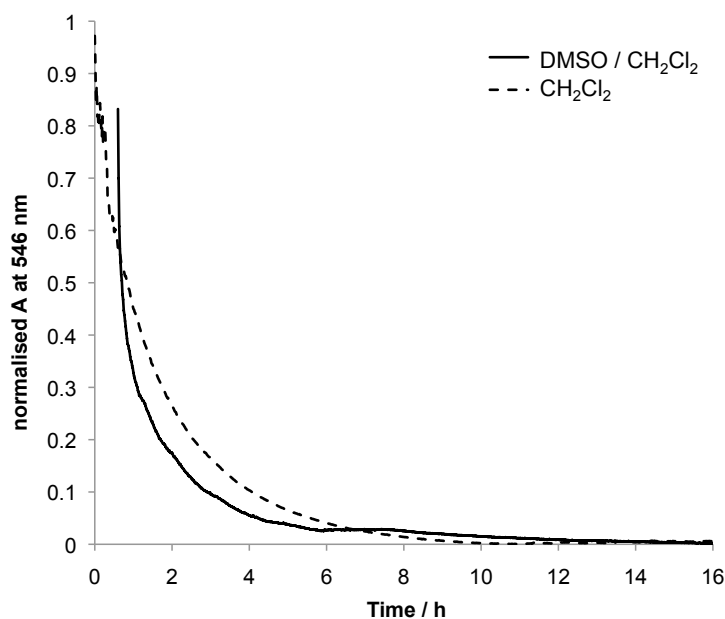
**Figure 2.15 SEC (normalised  $dw/d\log M$  vs.  $\log M$ ) traces for polymer end-functionalisation — dotted line is the starting polymer, solid line is the end-functionalised polymer. Left: PS–Nb **2.03** (THF as SEC eluent) functionalised with dipyriddy tetrazine; centre: PNIPAM–Nb **2.05** (DMF as SEC eluent) functionalised with dipyriddy tetrazine; right: PEG–Tz **2.10** (THF as SEC eluent) functionalised with norbornene dimethanol.**

### 2.3.4. Polymer–polymer coupling



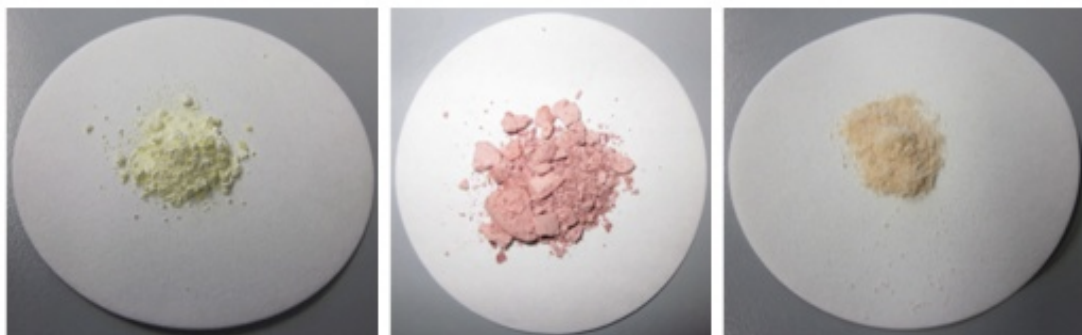
**Scheme 2.7 Polymer–polymer coupling between 2.03 and 2.10**

The same reaction protocol as described for the polymer functionalisation in organic solvent (0.01 M in  $CH_2Cl_2$ , room temperature) was carried out for the conjugation of PEG–Tz **2.10** and PS–Nb **2.03** to afford an amphiphilic block copolymer **2.13** (Scheme 2.7), in  $CH_2Cl_2$  as that is a common solvent for both PS and PEG. Given the results of the solvent screening, we also performed the reaction in a 1:1  $CH_2Cl_2$ /DMSO mixture to expedite the reaction — pure DMSO would be impossible due to the insolubility of PS in that media. In both cases, the resulting SEC traces were identical, although the reaction proceeded faster in the mixed solvent than in pure  $CH_2Cl_2$ .



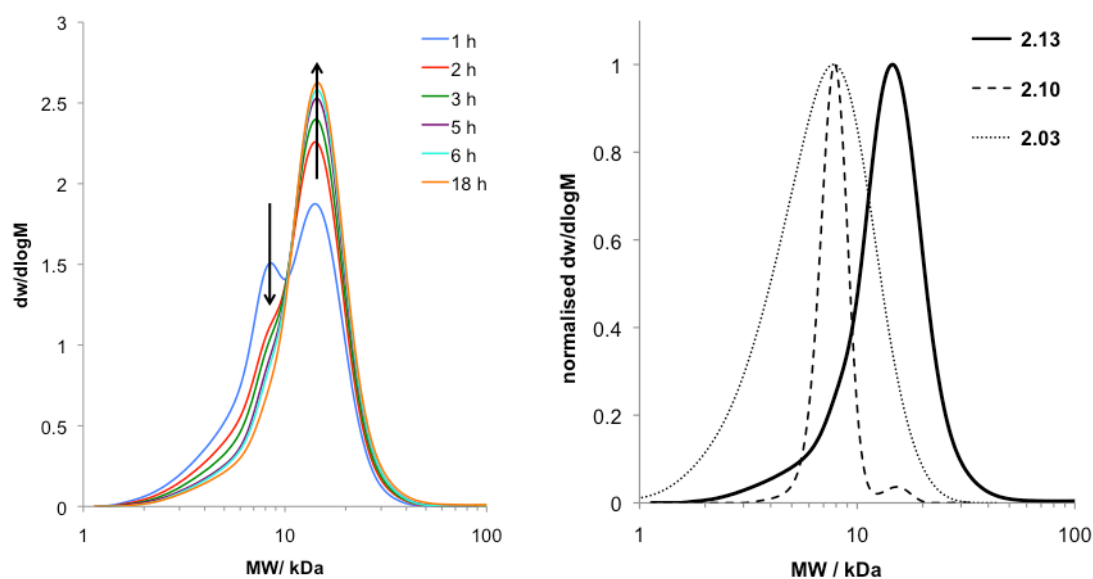
**Figure 2.16 UV/vis absorbance at 546 nm for the coupling of PS–Nb 2.03 and PEG–Tz 2.10 in CH<sub>2</sub>Cl<sub>2</sub> (dotted line) and a 1:1 DMSO/CH<sub>2</sub>Cl<sub>2</sub> mixture (solid line)**

Although not ‘ultra-fast’ like the RAFT-HDA reaction or the reaction between tetrazines and *trans*-cyclooctenes,<sup>15a</sup> the reaction proceeded to 95% conversion in 6 hours in CH<sub>2</sub>Cl<sub>2</sub> and within 4 hours in CH<sub>2</sub>Cl<sub>2</sub>/DMSO (Figure 2.16), and more importantly, at equimolar ratios of functionality. The observed colour change corresponding to the change in UV/vis absorbance can also be clearly seen in the recovered polymers in Figure 2.17.



**Figure 2.17 Photographs of dried polymers 2.03 (left), 2.10 (centre) and 2.13 (right) showing the colour change arising from the Tz–Nb reaction**

#### **2.3.4.1. SEC**



**Figure 2.18 Evolution of the PS-*b*-PEG conjugation SEC (THF eluent) traces with time, showing disappearance of the homopolymer in parallel with appearance of the diblock peak (left), and SEC traces of unpurified diblock PS-*b*-PEG 2.13 and the constituent homopolymers 2.03 and 2.10 (right)**

Evolution of the SEC traces with time provided an excellent method with which to follow this reaction (Figure 2.18, left). As can be seen in Figure 2.18, right, without any purification the ligation of the two homopolymers to form PEG-*b*-PS **2.13** appears to have worked well. Indeed, inspection of the SEC traces ( $dw/d\log M$ ) is the most common method for establishing visually the success or otherwise of polymer–polymer coupling. However, a unimodal trace with a ‘nice shape’ is not enough to quantify the degree of conjugation<sup>30</sup> — although indeed such a unimodal distribution is displayed by the conjugated polymer **2.13** — as it is possible to obtain bimodal SEC traces from a 100% efficient click reaction, provided the dispersities of the starting polymers are sufficiently broad and there is a significant difference in molecular weights between them.<sup>30</sup> When investigating the change in (apparent) molecular weights resulting from polymer conjugation, instinctively the experimenter’s eye tends to be drawn to the  $M_p$  values of the homo- and block copolymers, and whether they appear to have combined in an additive fashion. However, unless the polymers are truly monodisperse, as the combination of homopolymers is actually a convolution rather than addition of SEC traces, it is actually the  $M_n$  values of the constituent homopolymer that add together to give the  $M_n$  of the block copolymer (Table 2.2). In the case of **2.13**, we can see that the resulting  $M_n$  value is very close to the theoretical value, which indicates that the conjugation occurred with very high efficiency. Convolution of the SEC traces should also give an  $M_w/M_n$  value that is obtained *via* an additive method weighted to the square of the weight fraction of the constituent homopolymers; this is shown in Equation 2.1 and is the means by which the

theoretical  $M_w/M_n$  was calculated, and therefore  $M_w$  extrapolated in Table 2.2.<sup>31</sup>

**Equation 2.1 Calculation of theoretical  $M_n$  and  $M_w/M_n$  values for a diblock copolymer formed from ligation of homopolymers A and B, where  $w$  is the weight fraction of A and B polymers in the final copolymer**

$$M_n^{diblock} = M_n^A + M_n^B$$

$$1 + \left( \frac{M_w}{M_n} \right)^{diblock} = (w^A)^2 \left( \frac{M_w^A}{M_n^A} - 1 \right) + (w^B)^2 \left( \frac{M_w^B}{M_n^B} - 1 \right)$$

$$w^A = \frac{M_n^A}{M_n^{diblock}}$$

$$w^B = \frac{M_n^B}{M_n^{diblock}}$$

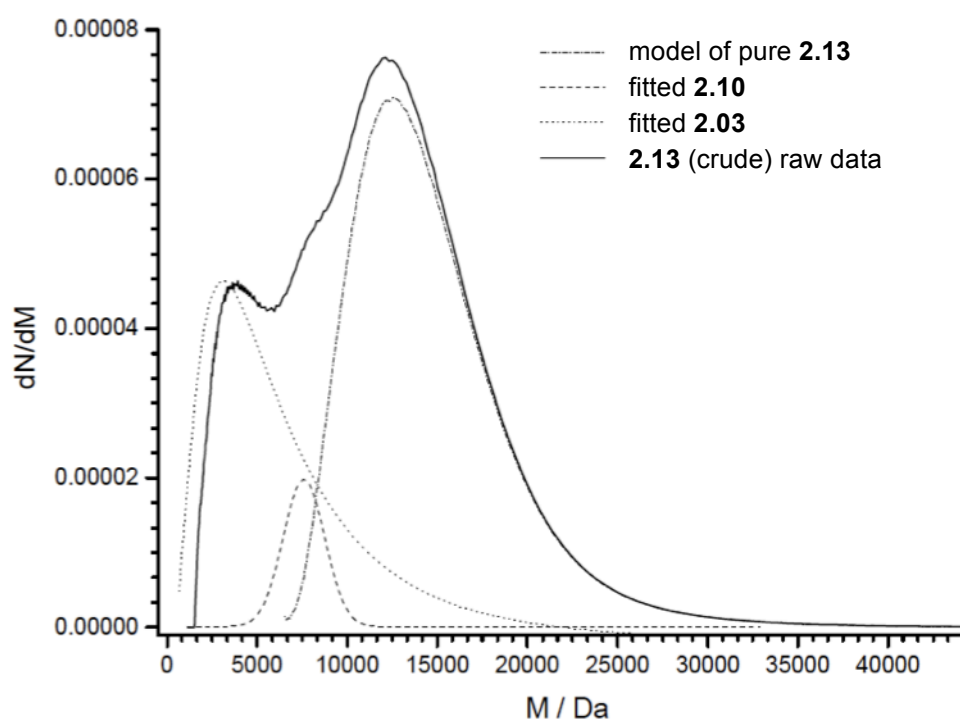
**Table 2.2 Molecular weights and dispersities of homopolymers 2.03 and 2.10, and crude diblock 2.13, calculated by SEC relative to PS standards**

Polymer	$M_p$ / kDa	$M_n$ / kDa	$M_w$ / kDa	$M_w/M_n$
<b>2.03</b>	7.73	5.31	7.53	1.42
<b>2.10</b>	7.93	7.75	8.12	1.04
<b>2.13</b>	14.6	11.8	15.0	1.27
<i>Theoretical 2.13</i>	-	13.1	15.6	1.19



Another factor that needs to be taken into account when performing SEC by refractive index (RI) detection is the  $dn/dc$  values of the homo- and copolymers. Unless the same type of polymer are being coupled together, differences in  $dn/dc$  further confound efforts to quantify success based purely on the SEC traces. In this case, the PEG–Tz **2.10** has a much lower  $dn/dc$  than the PS–Nb **2.03**, so any residual PEG homopolymer in **2.13** would be artificially masked relative to the block copolymer **2.13** and any residual **2.03**.

To investigate the SEC traces further, the number distributions were estimated from the  $dw/d\log M$  distributions arising from SEC analysis, by dividing through by  $M^2$  for every point (Figure 2.19).



**Figure 2.19** Number distributions of polymers **2.03**, **2.10** and **2.13** derived from the  $w\log M$  distribution

When inspecting the number distribution, although there are some inaccuracies in obtaining it indirectly *via* the  $dw/d\log M$  distribution usually resulting in a slight overemphasis of the magnitude of the low molecular weight region, it is clear that there is some residual homopolymer present in the sample. It cannot be discerned whether this is a result of unfunctionalised/dead homopolymer, or unreacted homopolymer though. Fitting Gaussian-like curves to the number distributions and subtracting them from the raw data gave a probable distribution for the 'pure' block copolymer **2.13** (a convolution of distributions **2.03** and **2.10**). The  $dn/dc$  value for the pure block copolymer was taken to be an average of the  $dn/dc$  values for the homopolymers **2.03** and **2.10**, as the weight fractions were approximately the same.<sup>32</sup>

**Table 2.3** Relative integrals from number distributions in Figure 2.19 and calculated fraction of homo- and block copolymer chains

<b>Polymer</b>	<b><i>Area fraction</i></b>	<b><i>dn/dc</i></b>	<b><i>Num%</i></b>
<b>Crude 2.13</b>	1.00	-	100
<b>2.03</b>	0.318	0.184	23
<b>2.10</b>	0.059	0.074	11
<b>Model 'pure' 2.13</b>	<i>0.623</i>	<i>0.129</i>	66

Adjusting for  $dn/dc$ , the number fraction of pure copolymer chains was calculated to be 66% (Table 2.3) – this is an estimate likely to be on the low side due to the aforementioned overemphasis on low molecular weight polymer chains in the distributions.

#### 2.3.4.2. LC-SEC

An arguably superior method than deconvolution of SEC traces is physical deconvolution of the polymers based on hydrophilicity, before SEC analysis of the component parts — LC-SEC analysis.<sup>33</sup> Analysis was carried out by Edwin Mes at Dow Chemical Company using non-critical conditions. Under these conditions, PEG homopolymer did not elute in the timeframe of the LC detection, but some uncoupled PS **2.03** was detected, as seen in Figure 2.20, peak 2.

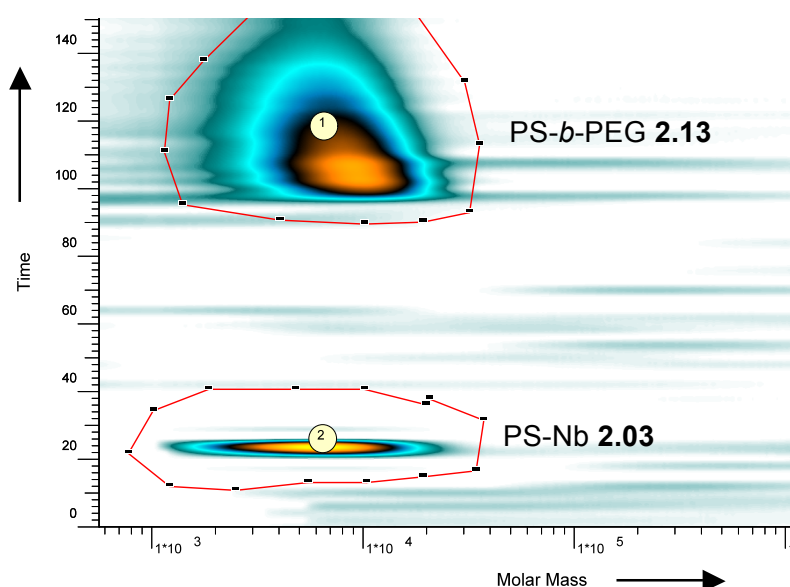


Figure 2.20 LC-SEC chromatogram under non-critical conditions

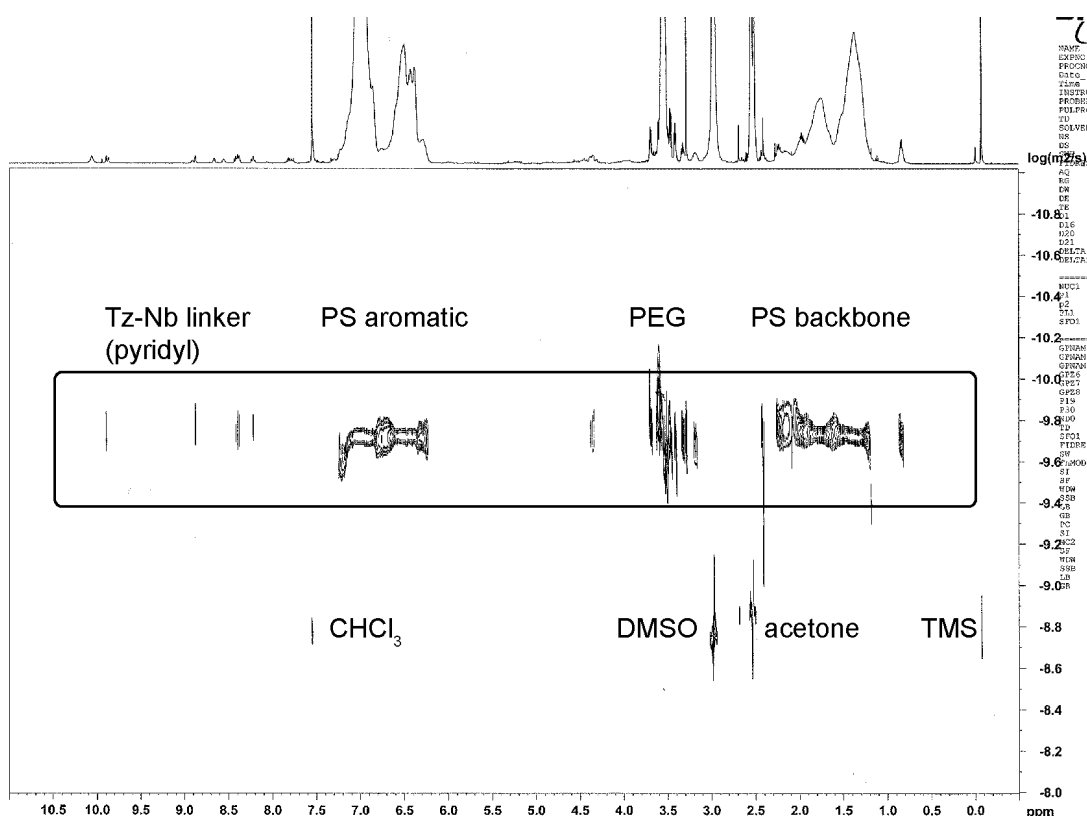
Again, the detection mode employed in the SEC was RI detection, and so the volume fractions of the two detected peaks were adjusted to take the  $dn/dc$  of the PS **2.03** and PS-*b*-PEG **2.13** (predicted  $dn/dc$ ) into account; this gave a diblock copolymer volume fraction of 81%.

**Table 2.4 Volume fractions of peaks detected in LC-SEC chromatogram**

<b>Polymer</b>	<b>Peak</b>	<b>Vol fraction</b>	<b><math>dn/dc</math></b>	<b>Vol%</b>
<b>2.03</b>		0.139	0.129	18.7
<b>2.13</b>		0.861	0.184	81.3

#### **2.3.4.3. DOSY NMR**

Diffusion-Ordered NMR Spectroscopy (DOSY)<sup>34</sup> was also used to investigate the crude diblock copolymer **2.13**. Although it is possible to use DOSY to determine polymer molecular weights,<sup>35</sup> it has thus far not been demonstrated for block copolymers; and as it would require calibration with polymers of similar architecture it is probably impractical. However, we were able to qualitatively determine that coupling between the PS and PEG blocks had been successful, as the data fit well to a single population model. This can be confirmed by observing in Figure 2.21 that the PEG backbone signals, the PS backbone and aromatic signals, and the linker signals all appear at the same diffusion coefficient.



**Figure 2.21 DOSY NMR spectrum (500 MHz,  $\text{CDCl}_3$ ) of crude 2.13**

Using the Speedy Component Resolution (SCORE) algorithm<sup>36</sup> embedded within the DOSY Toolbox program,<sup>37</sup>  $D_{\text{PEG-PS}} = 1.73 \times 10^{-10} \text{ m}^2\text{s}^{-1}$ . Using the same algorithm, the diffusion coefficient of the PEG homopolymer ( $\sim 5 \text{ kDa}$ ) was calculated to be  $1.19 \times 10^{-10} \text{ m}^2\text{s}^{-1}$ . The diffusion coefficient of a 5.6 kDa PS homopolymer is  $1.43 \times 10^{-10} \text{ m}^2\text{s}^{-1}$ ,<sup>35c</sup> and these  $D$  values combined give good evidence that PS-*b*-PEG copolymer has indeed been formed in significant yield, otherwise fitting to a single component model would give wildly implausible diffusion coefficients.

#### 2.3.4.4. $^1\text{H}$ NMR Spectroscopy

The final block copolymer **2.13** was also purified by repeated precipitation from methanol to remove any PS homopolymer, followed by extensive dialysis against a gradient of 20% THF in water to 100% deionised water to remove any PEG homopolymer. The diblock copolymer was recovered by freeze-drying and the  $^1\text{H}$  NMR (Figure 2.22) spectrum analysed to show that the expected block ratios were present.

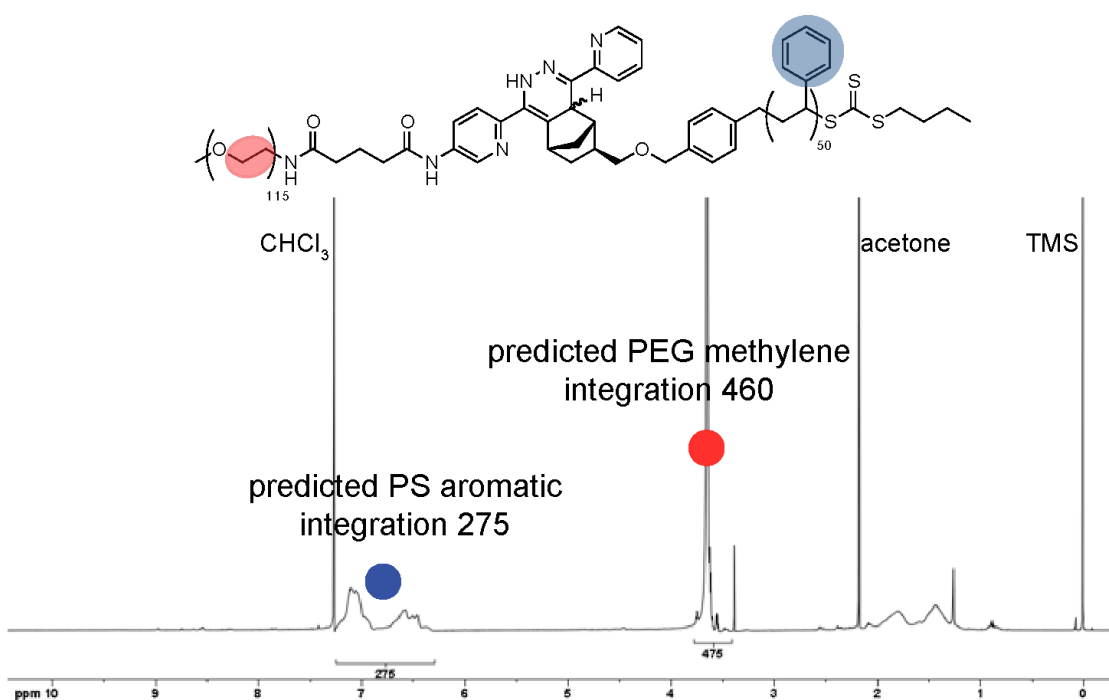
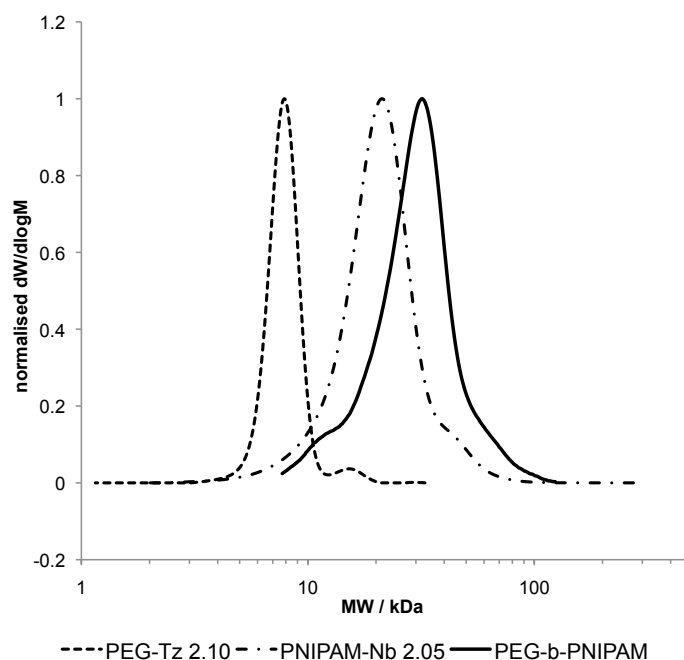


Figure 2.22  $^1\text{H}$  NMR spectrum ( $\text{CDCl}_3$ ) of purified PS-*b*-PEG **2.13**, showing expected relative integrals of PS aromatic peaks and PEG backbone peak

### 2.3.5. Polymer–polymer coupling in water

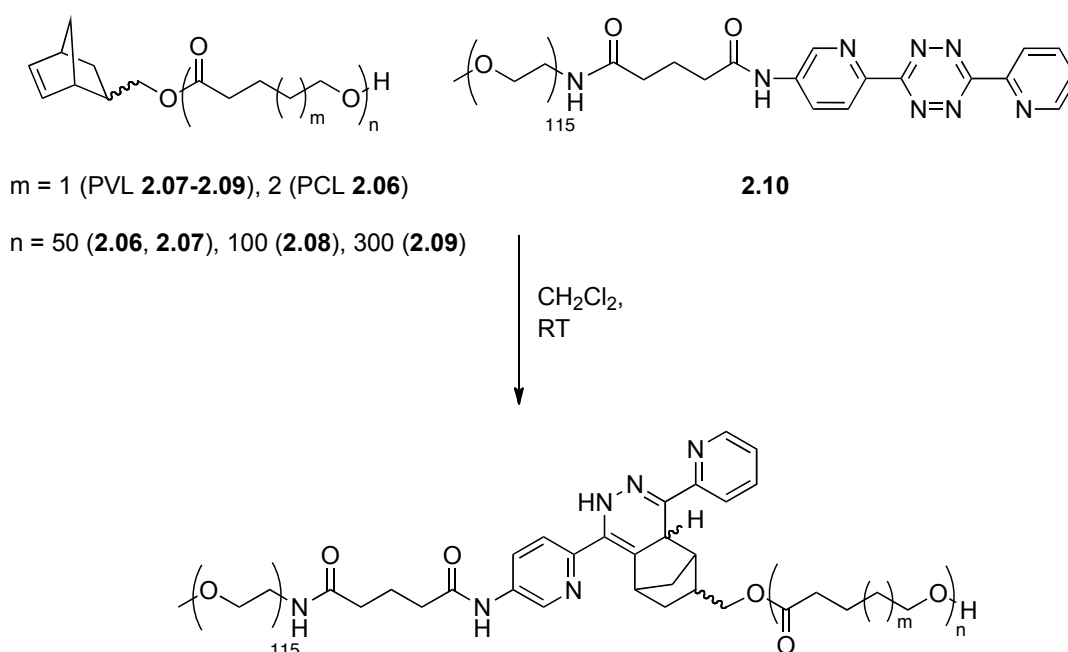
Given that the coupling of **2.03** and **2.10** proceeded with high efficiency according to several different analytical methods, and that the Tz–Nb reaction occurs readily in water (Section 2.3.3), we also attempted polymer–polymer coupling in water, using PNIPAM–Nb, **2.05** and PEG–Tz **2.10**. SEC analysis revealed a clear shift in molecular weight (Figure 2.23), although a slight low molecular weight shoulder can be seen, which we attribute to the fact that **2.05** contained a higher proportion of dead or unfunctionalised chains than **2.03** (10% vs. 5%). The agreement between the theoretical  $M_n$  value (26.6 kDa) and the actual obtained  $M_n$  value (25.9 kDa relative to PMMA standards in DMF eluent) was also close.



**Figure 2.23 SEC traces (DMF eluent) for polymers 2.05, 2.10 and the resulting diblock PEG-*b*-PNIPAM**

No modification to reaction conditions was made relative to the polymer–polymer coupling in  $\text{CH}_2\text{Cl}_2$ , and it was qualitatively observed that the reaction rate was broadly similar, as the colour change observed as previously occurred over a similar timescale (reaction was left stirring at room temperature in air overnight).

### 2.3.6. Polymer–polymer coupling of poly(ester)s

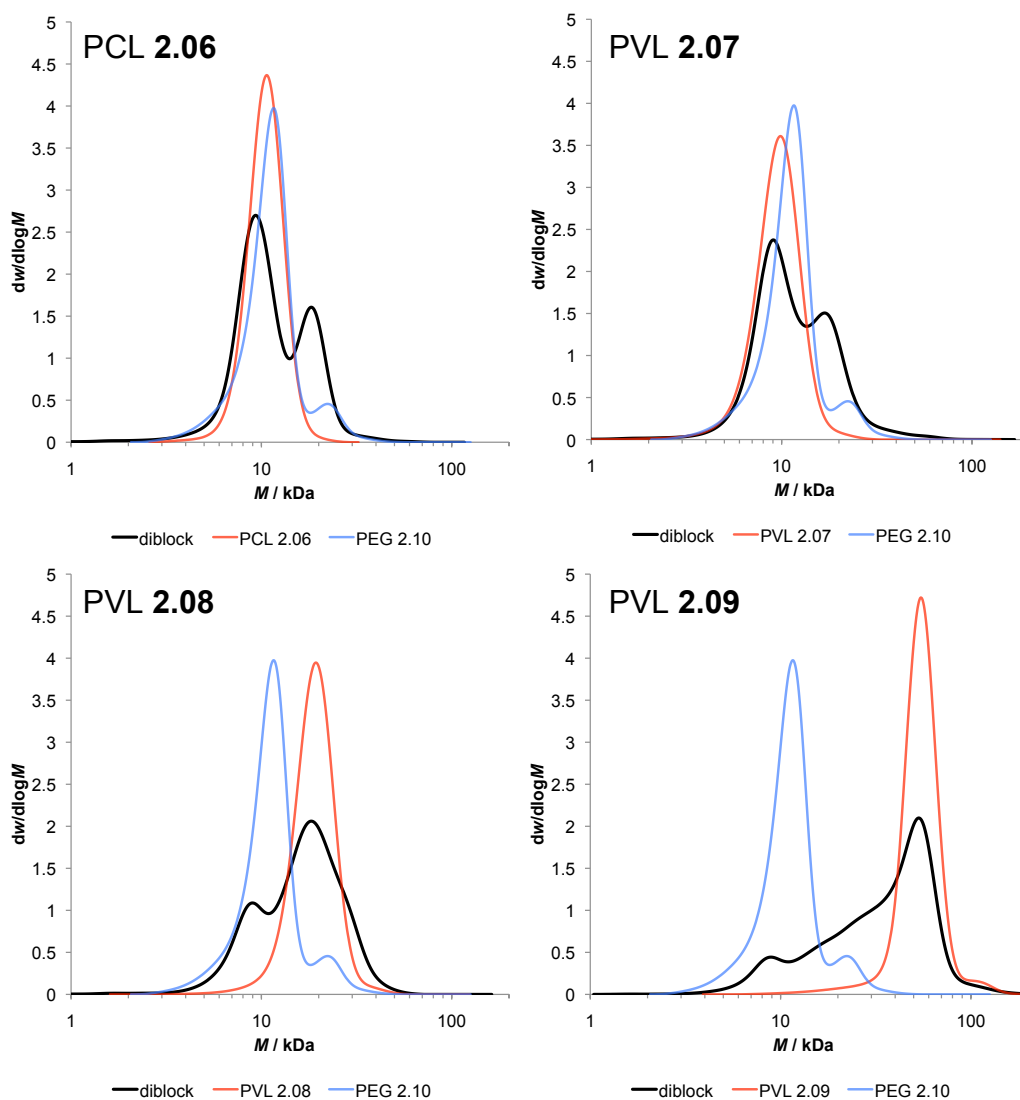


**Scheme 2.8 Attempted couplings of Nb-terminated poly(ester)s **2.06–2.09** and PEG–Tz **2.10****

Couplings of a variety of PVL–Nb polymers (5, 11 and 31 kDa, **2.07–2.09** in Table 2.1) and PCL–Nb, **2.06**, with PEG–Tz **2.10** were also attempted in  $\text{CH}_2\text{Cl}_2$  (Scheme 2.8). The reactions were stirred until the colour change



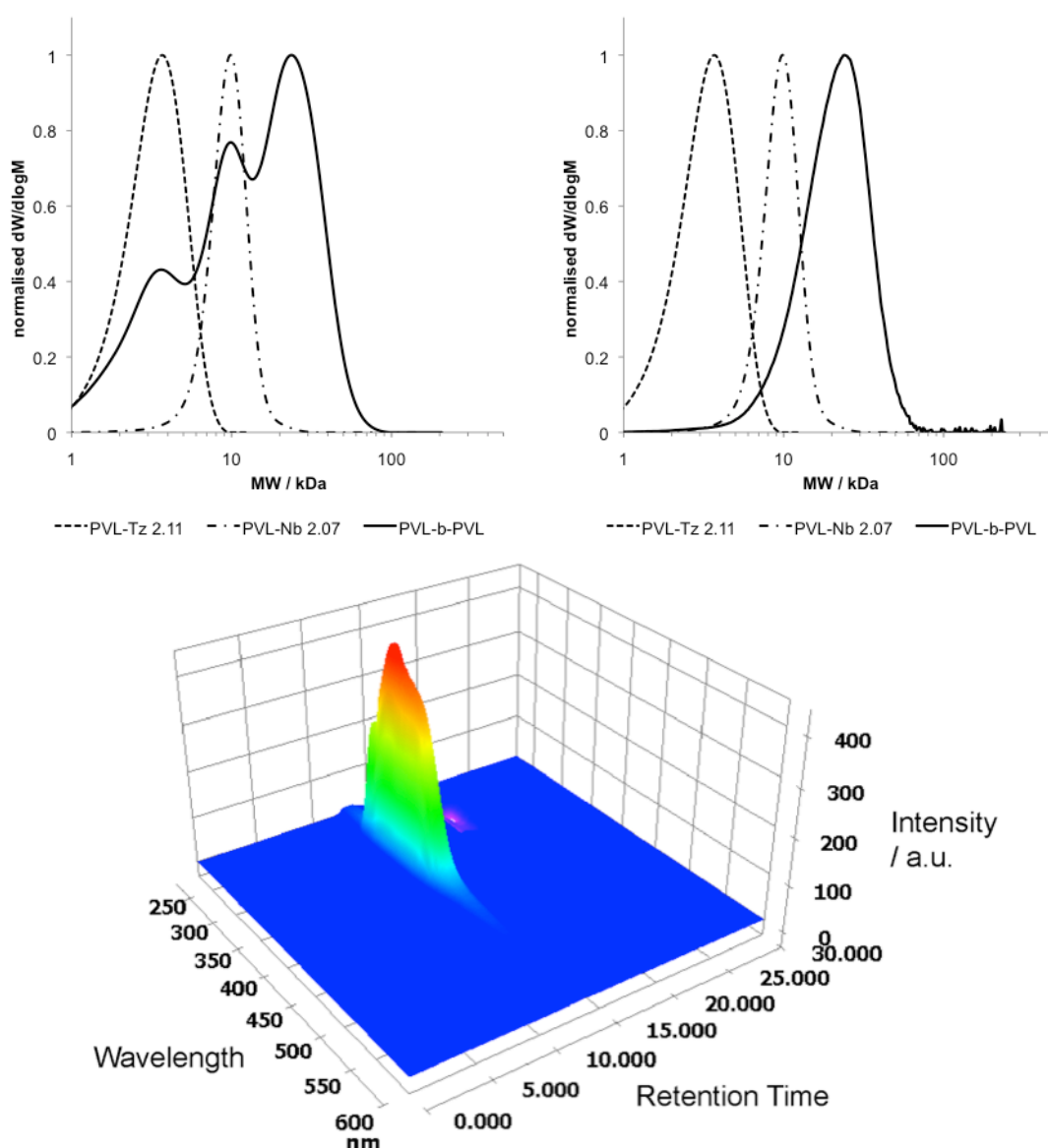
from pink to orange was observed. Using RI detection on the SEC, it was observed that the PCL and PVL couplings appeared to be less efficient than the PS and PNIPAM couplings described previously, with very obvious amounts of starting material present in all cases (Figure 2.24). We hypothesised that this could be because  $\text{CH}_2\text{Cl}_2$  is not an optimum reaction solvent for these polymers (PVL, PCL) and thus the end group is not accessible for reaction, or because of some form of end group degradation that did not occur for the conjugations using RAFT-synthesised polymers. That the reaction solution decoloured over time would suggest that degradation is the likely culprit, however we have yet to furnish a reason why this would be the case with the poly(esters) and not the RAFT-synthesised polymers, given that the tetrazine (dipyridyl functionalised) moiety was the same in both cases, and it was at the same concentration in  $\text{CH}_2\text{Cl}_2$ .



**Figure 2.24 SEC traces (THF eluent, PMMA standards) of the crude reaction mixtures (black line) formed between Nb-terminated poly(esters) 2.06–2.09 (red line) and PEG–Tz 2.10 (blue line)**

Coupling of PVL–Tz **2.11** and PVL–Nb **2.07** proceeded in a similar unsatisfactory fashion when initially analysed by SEC (RI detection, Figure 2.25, top left). If the conjugations were successful, yet the end groups were being degraded before full conversion was achieved, then employing UV detection at 320 nm ( $\lambda_{\text{max}}$  for the Tz–Nb conjugate functionality) on the SEC

would give only a single polymer population, arising from conjugated diblock; the polyesters have no characteristic UV/vis absorbance, and any unconjugated PEG–Tz can be easily identified from its absorbance at 546 nm in addition to the absorbance at 320 nm.



**Figure 2.25** SEC traces by RI detection (top left) and UV detection at 320 nm (top right) for the conjugation of PVL–Nb 2.07 and PVL–Tz 2.11. The full SEC-UV spectrum (bottom), shows a lack of unreacted Tz at any retention time

We thus used UV detection on the SEC at 320 nm (Figure 2.25, top right) and indeed a monomodal Gaussian trace was observed at higher molecular weight than the two starting homopolymers ( $M_n$  11.6 kDa, theoretical  $M_n$  11.8 kDa). Analysing the UV/vis spectra for all retention times (Figure 2.25, bottom) revealed no signal at 546 nm, demonstrating that all tetrazine had been consumed, either by conjugation or degradation. We hypothesise therefore that the Tz–Nb click reaction has reached full conversion with what tetrazine was available, but that degradation prevented effective copolymer formation. This degradation of the tetrazine over the course of the reaction could be because the alcohol-functionalised tetrazine used as the end group of PVL **2.11** is less stable than the dipyridyl tetrazine end of PEG **2.10** used previously.<sup>38</sup>

## **2.4. Conclusions**

In summary, we have demonstrated the utility and scope of the 'spring loaded' and additive-free tetrazine–norbornene click reaction, as applied to a range of polymer–polymer conjugations and polymer end-functionalisations in both water and a range of organic solvents. We propose that this reaction offers some advantages over existing click methodologies for functionalisation and coupling of polymers, particularly with regard to sensitive substrates or applications where external stimuli, catalysts or reagents are not desirable. The limitations of this conjugation strategy lie primarily in the relative difficulty of the synthesis of the tetrazine starting materials, especially given their sensitivity under polymerisation conditions.

## **2.5. Experimental**

### **2.5.1. Materials and Methods**

All chemicals and reagents, except for amine-terminated poly(ethylene glycol) that was purchased from IRIS Biotech, were purchased from Aldrich and used as received unless otherwise stated.

Nuclear magnetic resonance ( $^1\text{H}$  and  $^{13}\text{C}$  NMR) spectra were recorded at 400 or 500 MHz in  $\text{CDCl}_3$  or  $\text{DMSO-}d_6$  solution at 20 °C on a Bruker DPX-400 or Bruker AM-500 spectrometer. Chemical shifts are reported as  $\delta$  in parts per million (ppm) and referenced to the chemical shift of the residual solvent resonances ( $\text{CDCl}_3$   $^1\text{H}$ :  $\delta$  = 7.26 ppm;  $^{13}\text{C}$   $\delta$  = 77.16 ppm;  $\text{DMSO-}d_6$   $^1\text{H}$ :  $\delta$  = 2.50 ppm;  $^{13}\text{C}$   $\delta$  = 39.52 ppm). Coupling constants ( $J$ ) are given in Hz. The resonance multiplicities are described as s (singlet), d (doublet), app t (apparent triplet), q (quartet) or m (multiplet). For acquired  $^{13}\text{C}$  NMR experiments, multiplicities were distinguished using an ATP pulse sequence whereby methylene and quaternary carbon signals appear 'up' (u) and methyl and methane carbons 'down' (dn). Diffusion ordered spectra were acquired using the standard Bruker 2D sequence for diffusion measurements using stimulated echo and LED, and processed using Bruker Topspin and DOSY Toolbox softwares, assuming a single population of molecules.

THF SEC analyses were performed in HPLC grade THF containing 2% triethyl amine (TEA) at 30 °C, at a flow rate of 1.0 mL/min on a set of two PLgel 5  $\mu\text{m}$  Mixed-D columns. Polystyrene or poly(methyl methacrylate) standards were used for calibration and samples were injected using a PL

AS RT autosampler. DMF SEC analyses were performed in *N*-dimethylformamide (DMF) containing LiBr (0.42 g/L) at 30 °C, at a flow rate of 1.0 mL/min on a set of two PLgel 5 µm Mixed-D columns with a refractive index (RI) detector. Poly(methyl methacrylate) (PMMA) standards were used for calibration, and molecular weight and dispersity indices were determined using Cirrus SEC software. A Shimadzu SPD-M20A prominence diode array detector was coupled to the THF SEC, and LC Solution software used to process the resulting data.

High resolution mass spectra (HRMS) were collected using a Bruker MaXis UHR-ESI-TOF. MALDI mass spectra were acquired by MALDI-ToF (matrix-assisted laser desorption and ionisation time-of-flight) mass spectrometry using a Bruker Daltonics Ultraflex II MALDI-ToF mass spectrometer, equipped with a nitrogen laser delivering 2 ns laser pulses at 337 nm with positive ion ToF detection performed using an accelerating voltage of 25 kV. Solutions of dithranol as matrix, sodium chloride as cationisation agent and analyte were mixed prior to being spotted on the MALDI plate and air-dried. The samples were measured in reflectron ion mode and calibrated by comparison to SpheriCal (Polymer Factory) single molecular weight dendrimer standards. Elemental analyses were performed by Warwick Analytical Service.

UV/vis spectroscopy was carried out on a Perkin Elmer Lambda 35 UV/vis spectrometer, equipped with a PTP-1+1 Peltier temperature programmer and stirring system, and a PCB 1500 water system to maintain the desired temperature throughout the experiments. Quartz cuvettes transparent

above 230 nm were used for all experiments, and recorded absorbance values corrected for background and solvent absorbance.

## 2.5.2. Syntheses

Acid-functionalised tetrazine (**Tz-COOH**) was synthesised according to slightly modified literature procedures.<sup>22,27</sup>

### 2.5.2.1. 6-(6-(pyridin-2-yl)-1,4-dihydro-1,2,4,5-tetrazin-3-yl)pyridin-3-amine

2-cyanopyridine (3.00 g, 28.8 mmol), 5-amino-2-cyanopyridine (3.40 g, 28.8 mmol) and hydrazine monohydrate (5.6 mL, 120 mmol) were heated to reflux at 90 °C for 12 h. The resulting precipitate was concentrated *in vacuo* onto silica gel deactivated with triethylamine and purified by flash column chromatography (50% acetone in hexane,  $R_f$  0.3) to give the intermediate product (2.18 g, 8.61 mmol, 30% yield).  $^1\text{H}$  NMR (400 MHz, DMSO- $d_6$ )  $\delta$  (ppm): 8.71 (1H, s), 8.65 (1H, s), 8.62 (1H, d,  $^3J_{\text{H-H}} = 4.8$  Hz), 7.98-7.88 (3H, m), 7.65 (1H, d,  $^3J_{\text{H-H}} = 8.4$  Hz), 7.51 (1H, ddd,  $^3J_{\text{H-H}} = 7.2$  Hz,  $^3J_{\text{H-H}} = 4.8$  Hz,  $^4J_{\text{H-H}} = 1.5$  Hz), 7.00 (1H, dd,  $^3J_{\text{H-H}} = 8.4$  Hz,  $^4J_{\text{H-H}} = 2.7$  Hz), 5.88 (2H, s).  $^{13}\text{C}$  NMR (100 MHz, DMSO- $d_6$ )  $\delta$  (ppm): 148.5 (dn), 147.5 (u), 146.67 (u), 146.63 (u), 146.61 (u), 137.3 (dn), 134.16 (u), 134.07 (dn), 125.1 (dn), 121.8 (dn), 120.8 (dn), 120.3 (dn). HRMS  $m/z$ : expected 254.1149, found 254.1147  $[\text{M}+\text{H}]^+$ . Elemental analysis %: expected C 56.91, H 4.38, N 38.71; found C 57.0, H 4.49, N 37.43.



**2.5.2.2. 6-(6-(pyridin-2-yl)-1,2,4,5-tetrazin-3-yl)pyridin-3-amine**

The intermediate dihydropyridazine (2.00 g, 7.90 mmol) was dissolved in 60 mL toluene (HPLC grade) under N<sub>2</sub>, and 2,3-dichloro-5,6-dicyano-*p*-benzoquinone (DDQ) (3.59 g, 15.8 mmol) was added. The reaction mixture was refluxed for 12 h, the crude product concentrated *in vacuo* onto silica deactivated with EtSiCl<sub>3</sub> and purified by flash column chromatography using a gradient of 20–100% acetone in hexanes. The product was isolated as a red-purple solid (1.38 g, 5.49 mmol, 70% yield). <sup>1</sup>H NMR (400 MHz, DMSO-d<sub>6</sub>) δ (ppm): 8.91-8.89 (1H, m), 8.53 (1H, d, <sup>3</sup>J<sub>H-H</sub> = 8.0 Hz), 8.36 (1H, d, <sup>3</sup>J<sub>H-H</sub> = 8.4 Hz), 8.24 (1H, d, <sup>4</sup>J<sub>H-H</sub> = 2.4 Hz), 8.12 (1H, td, <sup>3</sup>J<sub>H-H</sub> = 8.0 Hz, <sup>4</sup>J<sub>H-H</sub> = 1.6 Hz), 7.70-7.67 (1H, dd, <sup>3</sup>J<sub>H-H</sub> = 7.6 Hz, <sup>3</sup>J<sub>H-H</sub> = 4.8 Hz), 7.12 (1H, dd, <sup>3</sup>J<sub>H-H</sub> = 8.8 Hz, <sup>4</sup>J<sub>H-H</sub> = 2.8 Hz), 6.36 (1H, s). <sup>13</sup>C NMR (100 MHz, DMSO-d<sub>6</sub>) δ (ppm): 162.9 (u), 162.5 (u), 150.44 (u), 150.42 (dn), 148.0 (u), 137.7 (dn), 137.3 (dn), 136.0 (u), 126.2 (dn), 125.7 (dn), 123.7 (dn), 118.9 (dn). HRMS *m/z*: [M+H]<sup>+</sup> expected 252.0998, found 252.0996; [M+Na]<sup>+</sup> expected 274.0817, found 274.0816.

**2.5.2.3. 5-oxo-5-(6-(6-(pyridin-2-yl)-1,2,4,5-tetrazin-3-yl)pyridin-3-ylamino)pentanoic acid (Tz-COOH)**

A mixture of the intermediate dihydropyridazine (1.30 g, 5.18 mmol) and glutaric anhydride (2.95 mg, 25.9 mmol) in THF (300 mL) was heated at 70 °C under reflux for 20 h. After cooling, the solvent was removed *in vacuo* and the resulting solid washed with CH<sub>2</sub>Cl<sub>2</sub> (2 x 300 mL), ethyl acetate (300 mL), before being suspended in diethyl ether and sonicated for 1 hour. The product was isolated by filtration to yield **Tz-COOH** as a purple solid

(1.24 g, 65% yield).  $^1\text{H}$  NMR (400 MHz, DMSO- $d_6$ )  $\delta$  (ppm): 12.11 (1H, s), 10.58 (1H, s), 9.05 (1H, d,  $^4J_{\text{H-H}} = 2.4$  Hz), 8.93 (1H, ddd,  $^3J_{\text{H-H}} = 4.4$  Hz,  $^4J_{\text{H-H}} = 1.6$  Hz), 8.63 (1H, d,  $^3J_{\text{H-H}} = 8.4$  Hz), 8.59 (1H, d,  $^3J_{\text{H-H}} = 7.6$  Hz), 8.43 (1H, dd,  $^3J_{\text{H-H}} = 8.8$  Hz,  $^4J_{\text{H-H}} = 2.4$  Hz), 8.16 (1H, td,  $^3J_{\text{H-H}} = 7.6$  Hz,  $^4J_{\text{H-H}} = 1.6$  Hz), 7.74 (1H, ddd,  $^3J_{\text{H-H}} = 7.6$  Hz,  $^3J_{\text{H-H}} = 4.8$  Hz,  $^4J_{\text{H-H}} = 1.4$  Hz), 2.49 (2H – slightly obscured by DMSO peak, t,  $^3J_{\text{H-H}} = 7.6$  Hz), 2.33 (2H, t,  $^3J_{\text{H-H}} = 7.6$  Hz), 1.86 (2H, quin,  $^3J_{\text{H-H}} = 7.6$  Hz).  $^{13}\text{C}$  NMR (100 MHz, DMSO- $d_6$ )  $\delta$  (ppm): 174.1 (u), 171.9 (u), 163.0 (u), 162.7 (u), 150.6 (dn), 150.2 (u), 143.8 (u), 141.3 (dn), 138.5 (u), 137.8 (dn), 126.6 (dn), 126.1 (dn), 124.9 (dn), 124.2 (dn), 35.4 (u), 32.9 (u), 20.1 (u). HRMS  $m/z$ : expected 366.1315, found 366.1308  $[\text{M}+\text{H}]^+$ ; expected 388.1134, found 388.1130  $[\text{M}+\text{Na}]^+$ .

#### **2.5.2.4. Tetrazine-terminated poly(ethylene glycol) (PEG-Tz 2.10)**

The commercially obtained amine-terminated PEG was checked to ensure 100% amine end group functionality prior to reaction by comparing the integrations of the terminal methyl group at 3.24 ppm with the amine proton signal at 2.75 ppm in DMSO- $d_6$ . MeO-PEG-amine ( $M_p$  5079 Da, 0.900 g, 0.177 mmol), Tz-COOH (0.647 g, 1.77 mmol) and O-benzotriazole- $N,N,N',N'$ -tetramethyl-uronium-hexafluoro-phosphate (0.134 g, 0.354 mmol) were dissolved in anhydrous DMF (50 mL) under a  $\text{N}_2$  atmosphere, and  $N,N$ -diisopropylethylamine (0.0679 mL, 0.390 mmol) was added. The reaction mixture was stirred at room temperature for 18 h, after which the solvent was removed *in vacuo*. The resulting dark sludge was dissolved in THF (100 mL) and filtered twice to recover residual Tz-COOH. The polymer was precipitated three times into diethyl ether (250 mL), dried *in vacuo* and

isolated as a pale pink solid (0.686 g, mmol, 65% yield).  $^1\text{H}$  NMR (500 MHz,  $\text{DMSO-}d_6$ )  $\delta$  (ppm): 10.54 (1H, s), 9.05 (1H, d,  $^4J_{\text{H-H}} = 2.2$  Hz), 8.94 (1H, d,  $^3J_{\text{H-H}} = 4.5$  Hz), 8.62 (1H, d,  $^3J_{\text{H-H}} = 9.2$  Hz), 8.59 (1H, d,  $^3J_{\text{H-H}} = 8.4$  Hz), 8.43 (1H, dd,  $J_1 = 8.7$  Hz,  $J_2 = 2.4$  Hz), 8.16 (1H, dt,  $^3J_{\text{H-H}} = 7.6$  Hz,  $^4J_{\text{H-H}} = 1.6$  Hz), 7.90 (1H, br s), 7.73 (1H, dd,  $^3J_{\text{H-H}} = 7.6$  Hz,  $^4J_{\text{H-H}} = 1.2$  Hz), 3.76-3.39 (495H, br, PEG backbone), 3.31 (2H, m), 3.24 (3H, s), 3.21 (2H, m), 2.44 (2H, t,  $^3J_{\text{H-H}} = 7.4$  Hz), 2.18 (2H, t,  $^3J_{\text{H-H}} = 7.3$  Hz), 1.86 (2H, m).

### 2.5.3. Small molecule kinetics

*Kinetic monitoring by  $^1\text{H}$  NMR spectroscopy:* Nb–TTC (15.0 mg, 0.0382 mmol) and 3,6-dipyridyl-1,2,4,5 tetrazine (9.02 mg, 0.0382 mmol) were dissolved in deuterated dichloromethane (0.7 mL), and the kinetics of the reaction were monitored by integration of the norbornene vinyl signal at 6.08 ppm and one of the pyridyl signals at 8.95 ppm from the tetrazine with respect to the  $d_2$ -dichloromethane solvent peak at 5.32 ppm.

*Kinetic monitoring by UV/vis spectroscopy:* The relevant quantities of the above reagents to give the desired concentration and equivalents were dissolved in  $\text{CH}_2\text{Cl}_2$  and mixed in a cuvette, the temperature maintained at 25 °C over the reaction time. The raw data were normalised to give a relative absorbance of 1 at the reaction start time and 0 after the reaction had ended.

*Product isolation:* The coupling product from the kinetic experiments was purified by flash column chromatography, eluting with 9:1  $\text{CHCl}_3/\text{MeOH}$  ( $R_f$  0.5). Note that only the fully oxidised product, not the dihydropyridazine,

was isolated after the column. HRMS  $m/z$ : expected: 599.1973; found: 599.1980  $[M+H]^+$ .

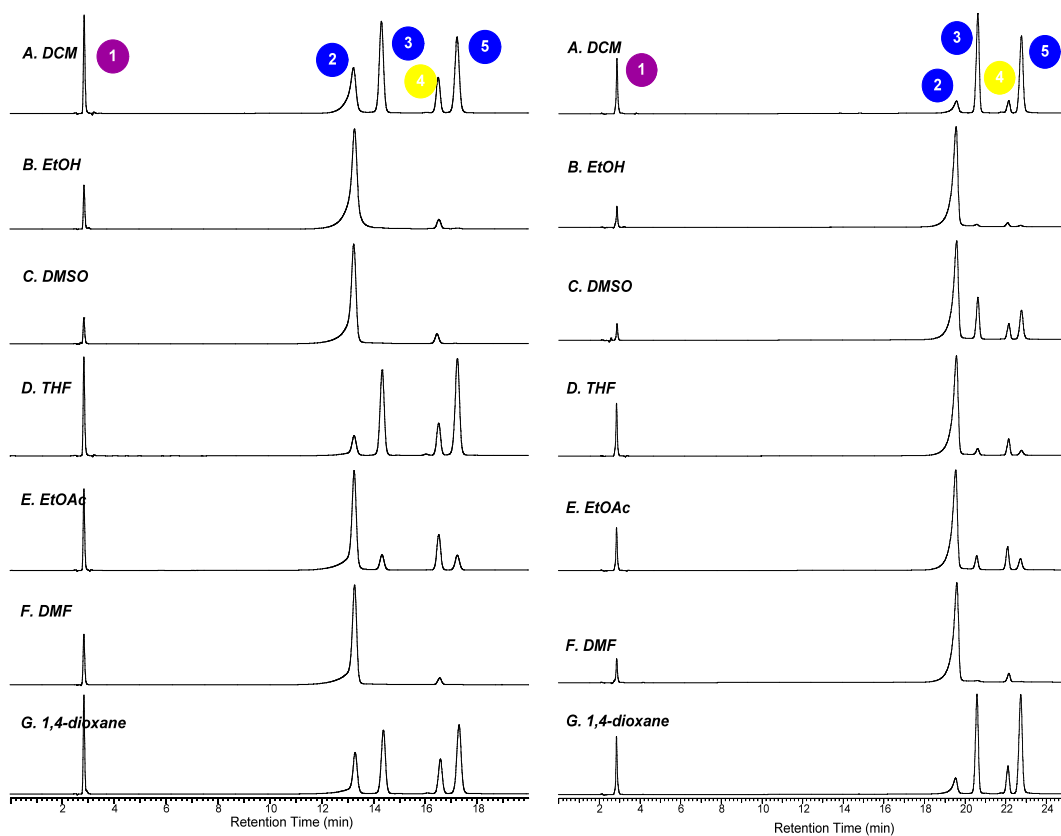
#### **2.5.4. General polymer functionalisation and polymer–polymer coupling**

For all end-functionalisation and polymer–polymer coupling experiments, equimolar amounts of polymer and/or small molecule modifier were dissolved in the desired solvent and stirred at ambient temperature until a colour change from pink to orange was observed.

Purification of block copolymer **2.13** was carried out by precipitation from cold methanol (3 times), followed by extensive dialysis against a 20/80 THF/H<sub>2</sub>O mixture (5 water changes). The polymer was isolated by lyophilisation as a yellow-orange powder.

### **2.6. Appendix: Supplementary Data**

The following data were collected and analysed by Milan Stamenovic and Pieter Espeel at Ghent University (Figure 2.26–Figure 2.28), and Ian Barker at the University of Warwick (Figure 2.29–Figure 2.31).



**Figure 2.26** LC chromatograms (UV detection at 310 nm) of reaction mixture (Scheme 2.1) after 1 hour (left, gradient 90–100% MeCN in H<sub>2</sub>O) and 2 hours (right, gradient 75–100% MeCN in H<sub>2</sub>O). Peak assignments are 1 = Tz(pyr)<sub>2</sub>, 4 = Nb–TTC, 2,3,5 = conjugation products (*m/z* 601)

**Table 2.5** Integration values of Tz peak (1) for each LC chromatogram

Reaction time	area%	area%	area%	area%	area%	area%	area%
	<i>CH<sub>2</sub>Cl<sub>2</sub></i>	<i>EtOH</i>	<i>DMSO</i>	<i>THF</i>	<i>EtOAc</i>	<i>DMF</i>	<i>dioxane</i>
<b>1 h</b>	11.0	6.1	4.9	12.6	9.3	10.6	12.9
<b>2 h</b>	11.2	4.9	2.3	10.3	8.0	4.7	9.1

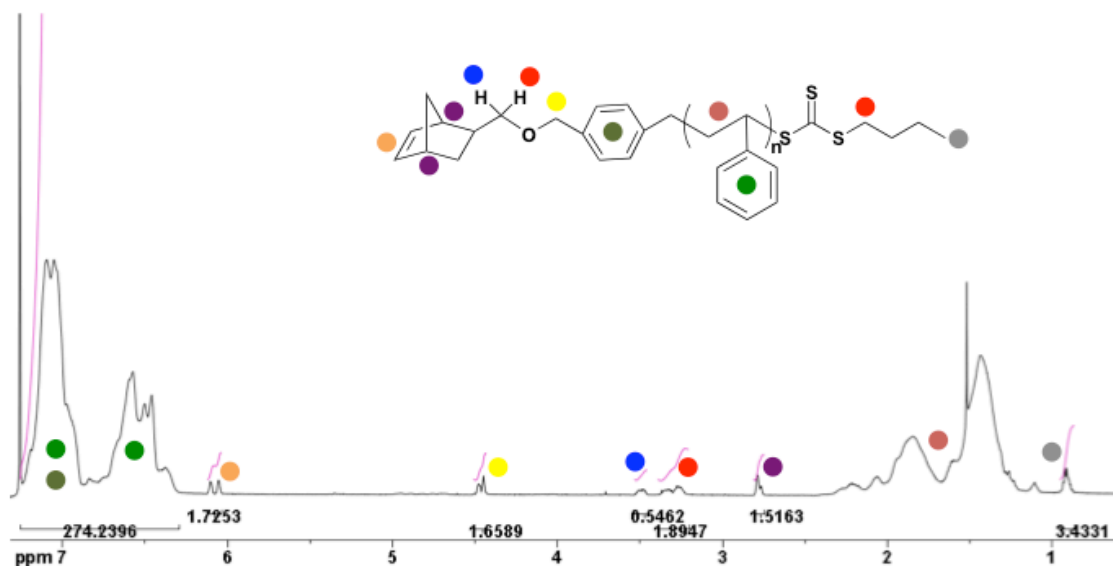


Figure 2.27  $^1\text{H}$ -NMR ( $\text{CDCl}_3$ ) spectrum of PS-Nb 2.03 (DP 55) prepared by RAFT: Nb-TTC CTA, at 70 °C, in bulk, St/Nb-TTC/AIBN = 200/1/0.1

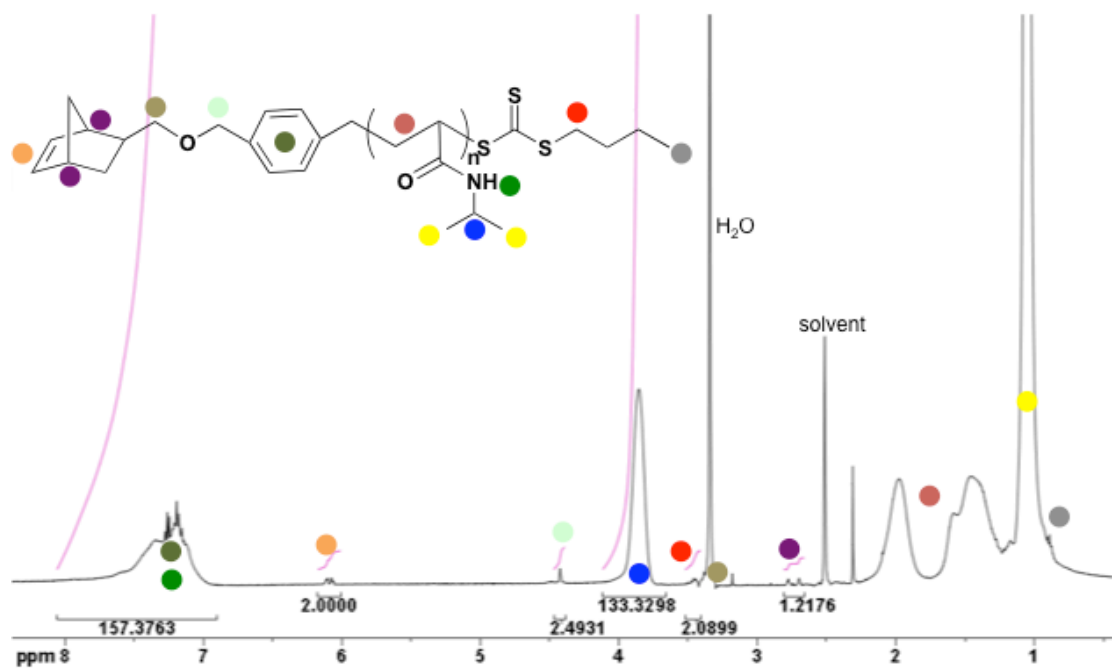


Figure 2.28  $^1\text{H}$ -NMR ( $\text{d}_6\text{-DMSO}$ ) spectrum of PNIPAM-Nb 2.05 (DP 140) prepared by RAFT: Nb-TTC CTA, at 70 °C, in bulk, NIPAM/Nb-TTC/AIBN = 200/1/0.1

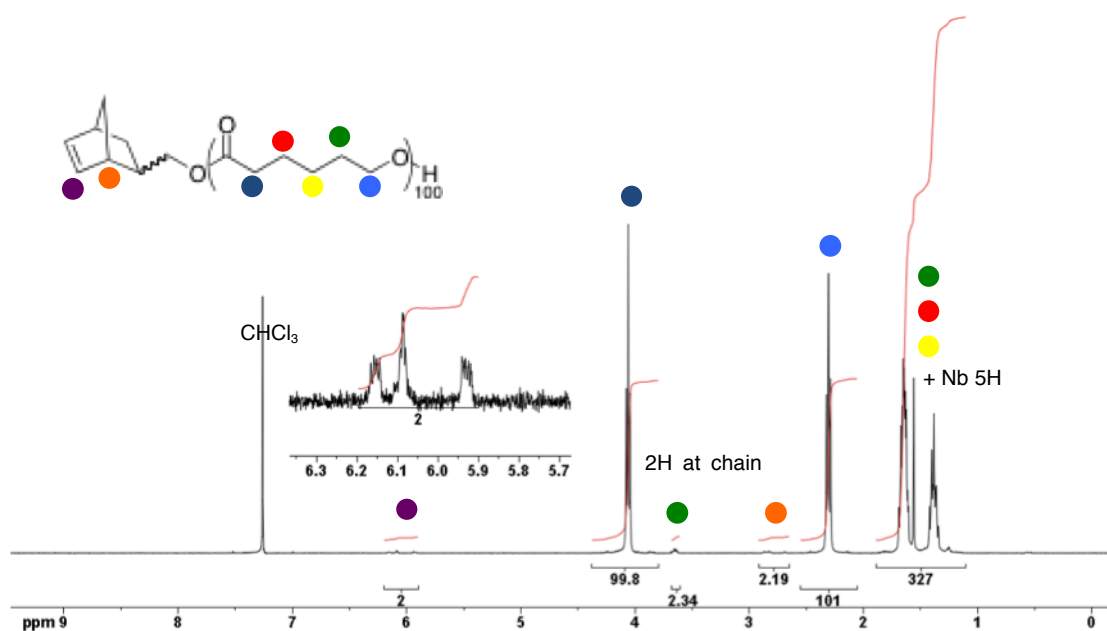


Figure 2.29  $^1\text{H}$  NMR ( $\text{CDCl}_3$ ) spectrum of PCL–Nb 2.06 prepared by ROP. The expansion shows the presence of Nb alkene signals (both *exo* and *endo*)

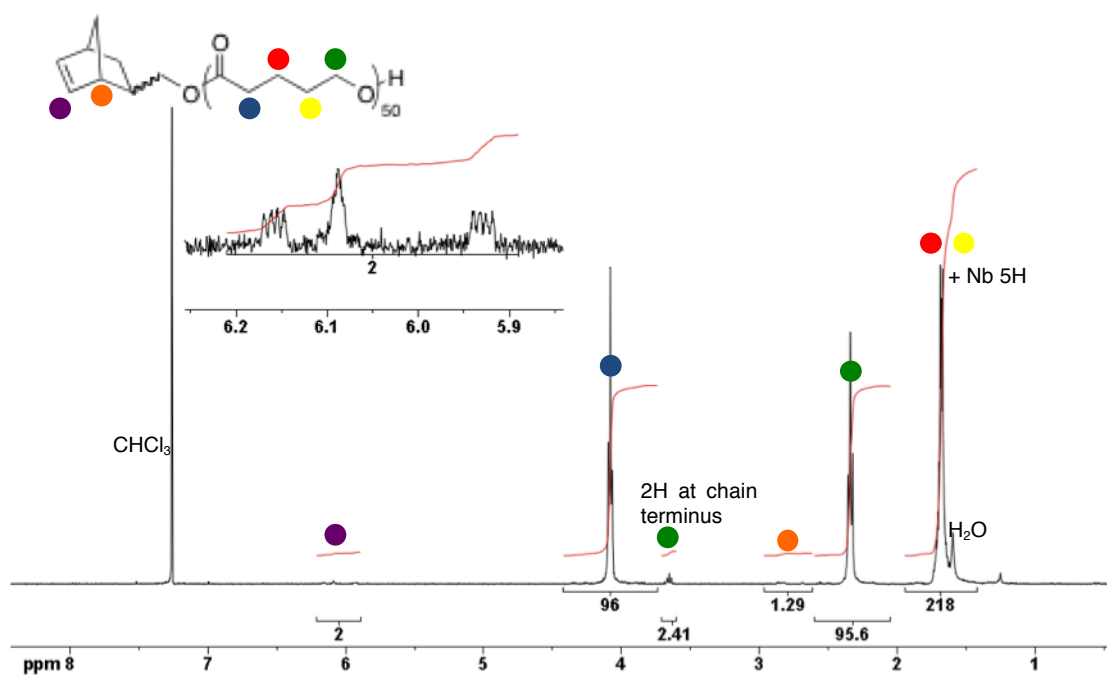
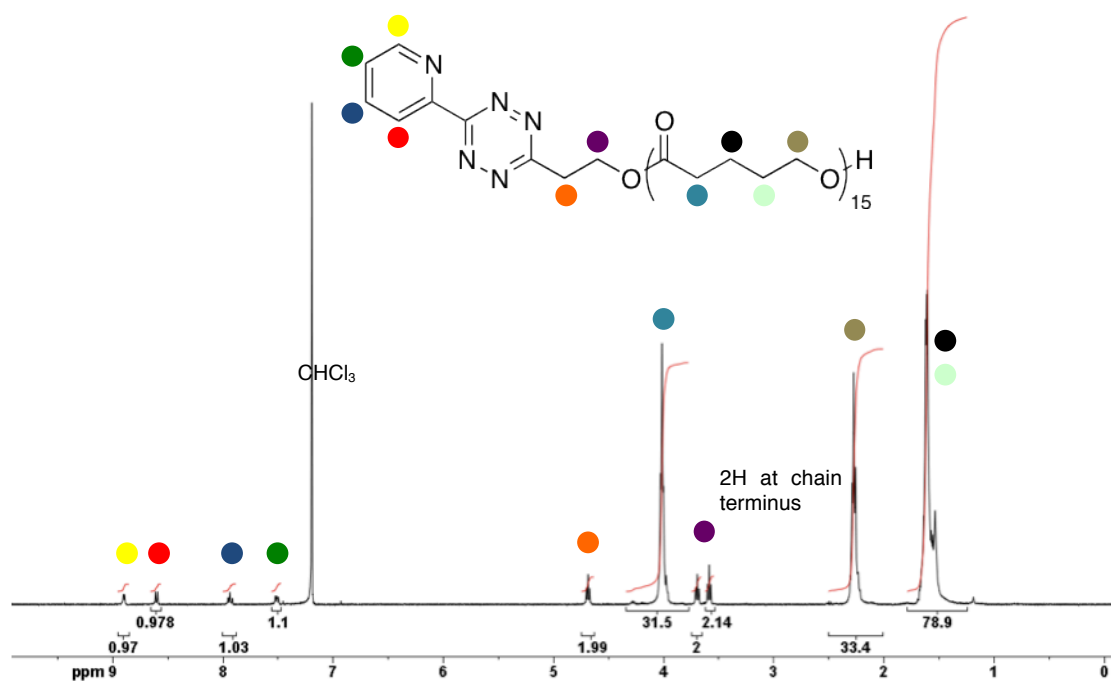


Figure 2.30  $^1\text{H}$  NMR ( $\text{CDCl}_3$ ) spectrum of PVL–Nb 2.07 prepared by ROP. The expansion shows the presence of Nb alkene signals (both *exo* and *endo*)





## 2.7. References

- (1) Golas, P. L.; Matyjaszewski, K. *Chem. Soc. Rev.* **2010**, 39, 1338-1354.
- (2) Rostovtsev, V. V.; Green, L. G.; Fokin, V. V.; Sharpless, K. B. *Angew. Chem., Int. Ed.* **2002**, 41, 2596-2599.
- (3) Opsteen, J. A.; van Hest, J. C. M. *Chem. Commun.* **2005**, 41, 57-59.
- (4) Opsteen, J. A.; van Hest, J. C. M. *J. Polym. Sci., Part A: Polym. Chem.* **2007**, 45, 2913-2924.
- (5) Ladmiral, V.; Legge, T. M.; Zhao, Y.; Perrier, S. *Macromolecules* **2008**, 41, 6728-6732.
- (6) (a) Inglis, A. J.; Sinnwell, S.; Stenzel, M. H.; Barner-Kowollik, C. *Angew. Chem., Int. Ed.* **2009**, 48, 2411-2414. (b) Inglis, A. J.; Stenzel, M. H.; Barner-Kowollik, C. *Macromol. Rapid Comm.* **2009**, 30, 1792-1798. (c) Sinnwell, S.; Inglis, A. J.; Davis, T. P.; Stenzel, M. H.; Barner-Kowollik, C. *Chem. Commun.* **2008**, 44, 2052-2054.
- (7) Oehlenschlaeger, K. K.; Mueller, J. O.; Heine, N. B.; Glassner, M.; Guimard, N. K.; Delaittre, G.; Schmidt, F. G.; Barner-Kowollik, C. *Angew. Chem., Int. Ed.* **2013**, 52, 762-766.
- (8) Sinnwell, S.; Synatschke, C. V.; Junkers, T.; Stenzel, M. H.; Barner-Kowollik, C. *Macromolecules* **2008**, 41, 7904-7912.
- (9) Paulöhr, T.; Inglis, A. J.; Barner-Kowollik, C. *Adv. Mater.* **2010**, 22, 2788-2791.

- (10) Omurtag, P. S.; Gunay, U. S.; Dag, A.; Durmaz, H.; Hizal, G.; Tunca, U. *J. Polym. Sci., Part A: Polym. Chem.* **2013**, *51*, 2252-2259.
- (11) Winkler, M.; Montero de Espinosa, L.; Barner-Kowollik, C.; Meier, M. A. R. *Chem. Sci.* **2012**, *3*, 2607-2615.
- (12) Fu, Q.; Wang, G.; Lin, W.; Huang, J. *J. Polym. Sci., Part A: Polym. Chem.* **2009**, *47*, 986-990.
- (13) Durmaz, H.; Sanyal, A.; Hizal, G.; Tunca, U. *Polym. Chem.* **2012**, *3*, 825-835.
- (14) Koo, S. P. S.; Stamenovic, M. M.; Prasath, R. A.; Inglis, A. J.; Du Prez, F. E.; Barner-Kowollik, C.; Van Camp, W.; Junkers, T. *J. Polym. Sci., Part A: Polym. Chem.* **2010**, *48*, 1699-1713.
- (15) (a) Inglis, A. J.; Barner-Kowollik, C. *Macromol. Rapid Comm.* **2010**, *31*, 1247-1266. (b) Barner-Kowollik, C.; Du Prez, F. E.; Espeel, P.; Hawker, C. J.; Junkers, T.; Schlaad, H.; Van Camp, W. *Angew. Chem., Int. Ed.* **2011**, *50*, 60-62.
- (16) Bielawski, C. W.; Grubbs, R. H. *Prog. Polym. Sci.* **2007**, *32*, 1-29.
- (17) Cheng, C.; Khoshdel, E.; Wooley, K. L. *Macromolecules* **2005**, *38*, 9455-9465.
- (18) Cheng, C.; Khoshdel, E.; Wooley, K. L. *Macromolecules* **2007**, *40*, 2289-2292.

- (19) Hoogenboom, R.; Moore, B. C.; Schubert, U. S. *J. Org. Chem.* **2006**, *71*, 4903-4909.
- (20) Stamenovic, M. M.; Espeel, P.; Camp, W. V.; Du Prez, F. E. *Macromolecules* **2011**, *44*, 5619-5630.
- (21) (a) Devaraj, N. K.; Upadhyay, R.; Haun, J. B.; Hilderbrand, S. A.; Weissleder, R. *Angew. Chem., Int. Ed.* **2009**, *48*, 7013-7016. (b) Carboni, R. A.; Lindsey, R. V., Jr. *J. Am. Chem. Soc.* **1959**, *81*, 4342-4346.
- (22) Blackman, M. L.; Royzen, M.; Fox, J. M. *J. Am. Chem. Soc.* **2008**, *130*, 13518-13519.
- (23) Patton, D. L.; Advincula, R. C. *Macromolecules* **2006**, *39*, 8674-8683.
- (24) (a) Cheng, C.; Qi, K.; Germack, D. S.; Khoshdel, E.; Wooley, K. L. *Adv. Mater.* **2007**, *19*, 2830-2835. (b) Li, A.; Ma, J.; Wooley, K. L. *Macromolecules* **2009**, *42*, 5433-5436. (c) Ma, J.; Cheng, C.; Wooley, K. L. *Aust. J. Chem.* **2009**, *62*, 1507-1519.
- (25) Makiguchi, K.; Satoh, T.; Kakuchi, T. *Macromolecules* **2011**, *44*, 1999-2005.
- (26) Wijnen, J. W.; Zavarise, S.; Engberts, J. B. F. N.; Charton, M. *J. Org. Chem.* **1996**, *61*, 2001-2005.
- (27) Rossin, R.; Renart Verkerk, P.; van den Bosch, S. M.; Vulders, R. C. M.; Verel, I.; Lub, J.; Robillard, M. S. *Angew. Chem., Int. Ed.* **2010**, *49*, 3375-3378.

- (28) Hilderbrand, S.; Devaraj, N.; Weissleder, R.; WO2010051530 (A2): 2010.
- (29) (a) Hoogenboom, R.; Kickelbick, G.; Schubert, U. S. *Eur. J. Org. Chem.* **2003**, 2003, 4887-4896. (b) Kaim, W. *Coord. Chem. Rev.* **2002**, 230, 126-138.
- (30) Barner-Kowollik, C. *Macromol. Rapid Comm.* **2009**, 30, 1625-1631.
- (31) Fukuda, T. *J. Polym. Sci., Part A: Polym. Chem.* **2004**, 42, 4743-4755.
- (32) Gao, H.; Tsarevsky, N. V.; Matyjaszewski, K. *Macromolecules* **2005**, 38, 5995-6004.
- (33) (a) Falkenhagen, J.; Much, H.; Stauf, W.; Müller, A. H. E. *Macromolecules* **2000**, 33, 3687-3693. (b) Perrin, L.; Phan, T. N. T.; Querelle, S.; Deratani, A.; Bertin, D. *Macromolecules* **2008**, 41, 6942-6951. (c) Berek, D. a.; Šišková, A. *Macromolecules* **2010**, 43, 9627-9634.
- (34) Morris, K. F.; Johnson, C. S. *J. Am. Chem. Soc.* **1992**, 114, 3139-3141.
- (35) (a) Li, D.; Kagan, G.; Hopson, R.; Williard, P. G. *J. Am. Chem. Soc.* **2009**, 131, 5627-5634. (b) Bakkour, Y.; Darcos, V.; Li, S.; Coudane, J. *Polym. Chem.* **2012**, 3, 2006-2010. (c) Li, W.; Chung, H.; Daeffler, C.; Johnson, J. A.; Grubbs, R. H. *Macromolecules* **2012**, 45, 9595-9603.
- (36) Nilsson, M.; Morris, G. A. *Anal. Chem.* **2008**, 80, 3777-3782.
- (37) Nilsson, M. *J. Magn. Reson.* **2009**, 200, 296-302.

(38) Karver, M. R.; Weissleder, R.; Hilderbrand, S. A. *Bioconjugate Chem.* **2011**, 22, 2263-2270.

## **Chapter 3. Micelle functionalisation using the tetrazine–norbornene reaction**

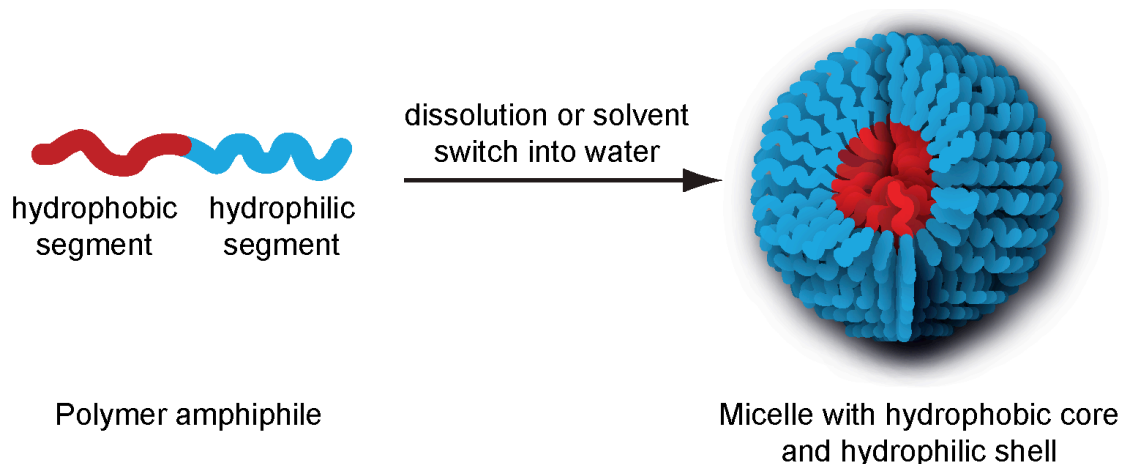
### **3.1. Abstract**

In this chapter the design and synthesis of a polymeric amphiphile bearing two orthogonal 'click-able' functionalities in the two blocks is described. The amphiphile is self-assembled to form a micelle structure with two different functional handles in the core and shell domains, and then orthogonally functionalised using two click reactions. The methodology for separate core-shell functionalisation was extended to a one-pot, sequential addition method for simultaneous core and shell functionalisation using two different ligation partners.

### 3.2. Background

Given that the end-modification and conjugation of polymers has been demonstrated in Chapter 2, we aimed to extend the use of the tetrazine–norborene reaction to functionalise polymeric self-assemblies.

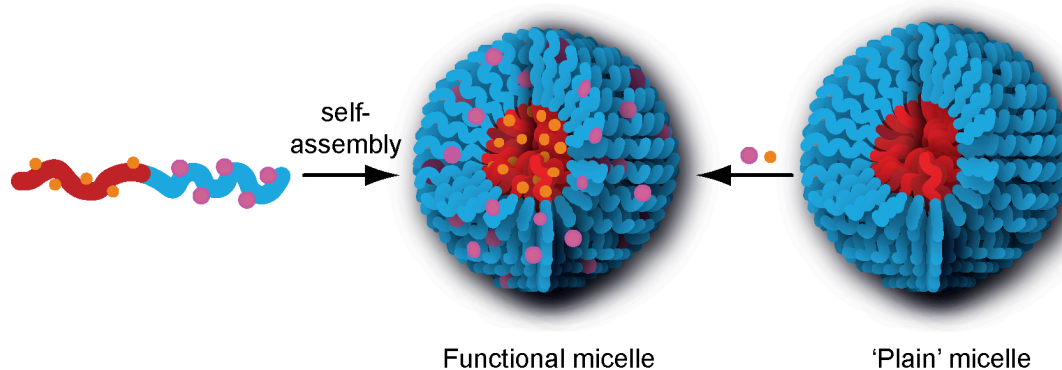
Much like amphiphilic lipids and surfactants, polymer amphiphiles are well-known to assemble in selective solvents into higher-order structures such as micelles, vesicles and cylinders, depending on the volume fraction of hydrophobic to hydrophilic blocks used.<sup>1</sup> Arguably the simplest and most accessible assembly is a spherical micelle structure in water, with a hydrophobic core and hydrophilic shell (Figure 3.1).



**Figure 3.1 Self-assembly of a polymer amphiphile to form a micellar structure**

Polymeric nanostructures generally exhibit superior mechanical properties and are more stable than their small-molecule lipid/surfactant counterparts,<sup>2</sup> which has garnered them significant attention. Inspiration has been drawn from lipid

vesicles to try and use polymeric nanostructures as biomedical transport or delivery vehicles<sup>3</sup> and enzyme-mimicking nanoreactors.<sup>4</sup> As usual, Nature is several steps ahead of synthetic mimics in specificity of design and function; in order to make polymeric nanostructures useful for any application, functionality has to be imparted onto them to, for example, bind to appropriate receptors or respond to stimuli to release their payload. Thus chemical modification is required. This can take place by one of two routes: modification or resynthesis of the original amphiphile followed by self-assembly to form the nanostructure, or direct functionalisation of the micelle *in situ* — these two approaches are illustrated schematically in Figure 3.2. Examples of surface functionalisation of micelles using the pre-assembly approach include saccharide-,<sup>5</sup> peptide-<sup>6</sup> and antigen-decorated<sup>7</sup> nanoparticles. This is often achieved by using a functional initiator or chain transfer agent, and allows for a single modified site per chain expressed at the micelle surface.



**Figure 3.2 Alternative routes to functional micelles**

For situations where functionalisation of the core or shell domains at multiple sites is required, advantages of post-assembly modification over synthesis of new, specifically designed amphiphilic block copolymers are evident. The



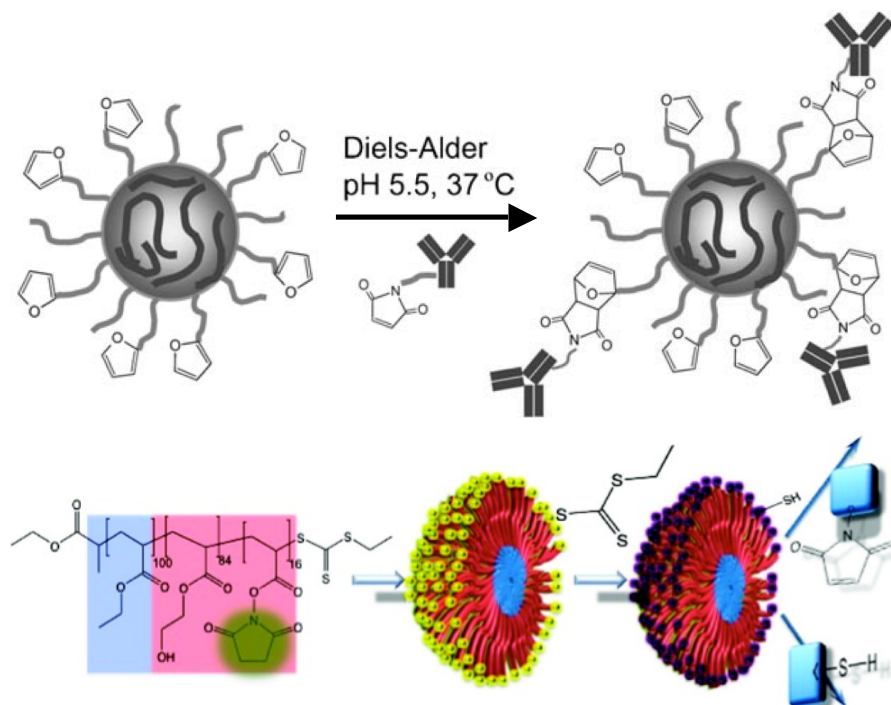
relative timescale and simplicity of modifying one micelle with several different functionalities, compared to synthesising novel monomers, optimising polymerisation conditions and only then self-assembling and purifying the resulting micellar solution means that post-assembly modification is often a faster and easier route.

Another factor in favour of post-assembly modification is that even though a nanostructure is a more complex framework for functionalisation than a single polymer chain, phase segregation of hydrophobic and  $\phi$ -philic reagents can also assist in functionalising the core and shell domains separately.

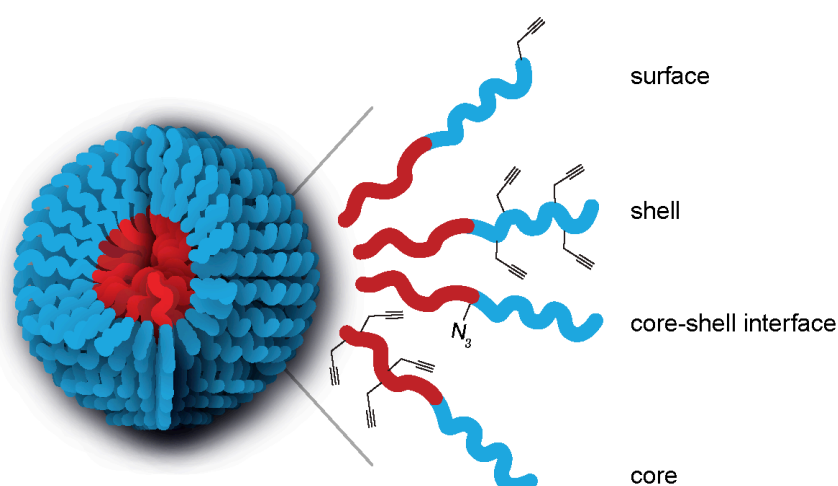
Examples of post-assembly functionalisation include the introduction of chelating ligands for radionuclide imaging agents,<sup>8</sup> nucleic acids,<sup>9</sup> proteins<sup>10</sup> and cancer cell targeting ligands.<sup>11</sup> A variety of chemical methods have been used for micelle and nanostructure functionalisation,<sup>12</sup> however amidation chemistries are employed far more frequently than any other — often for cross-linking purposes<sup>13</sup> and sometimes in tandem with a functionalisation reaction. Since amidation chemistries are not as modular as click reactions, this can lead to uncertainty as to the precise nature of the nanoparticle, for instance exactly how many functionalities have been introduced and whether all of the reactive handles on the micellar scaffold have been consumed. In order to drive the reactions to completion, large excesses of small molecule modifier may also need to be used, which is both wasteful and means that additional purification often needs to be carried out.

Some click-type reactions have been explored for micelle functionalisation: the Diels-Alder reaction between furan and maleimide,<sup>14</sup> thiol-ene reaction<sup>15</sup>

(Figure 3.3) and very recently the strain-promoted cycloaddition between azides and cyclooctynes.<sup>16</sup>



**Figure 3.3** Examples of micelle functionalisation using the Diels-Alder<sup>14</sup> (top) and thiol-ene<sup>15</sup> (bottom) reactions



**Figure 3.4** Examples of functional micelles that exploit the CuAAC reaction to functionalise the micelle surface,<sup>17</sup> shell,<sup>18</sup> core-shell interface<sup>19</sup> and core<sup>20</sup>

Of particular note is the use of the CuAAC reaction, which has been exploited to modify the surface,<sup>17</sup> core,<sup>20</sup> shell<sup>18</sup> and even core-shell interface<sup>19</sup> of micellar structures (Figure 3.4). As mentioned previously though, the presence of a copper catalyst is a deterrent to the use of CuAAC in biologically relevant systems e.g. drug delivery vehicles. Alternatively, “clean, efficient, and bioorthogonal conjugation reactions are required to eliminate undesirable side reactions, minimise nonspecific nanostructure–bioconjugate activity, improve reproducibility in production, and maximise efficacy.”<sup>21</sup>

Since the tetrazine–norbornene reaction has found use as a bioorthogonal reaction,<sup>22</sup> we sought to make use of it to functionalise a polymeric assembly. We also aimed to create a single micelle scaffold containing two orthogonal click handles, segregated into the core and shell respectively, for easy modification in both domains. Such modifications could introduce cargos and/or ligands in a manner that opens up the possibilities for synthesis of micellar libraries in a combinatorial manner.

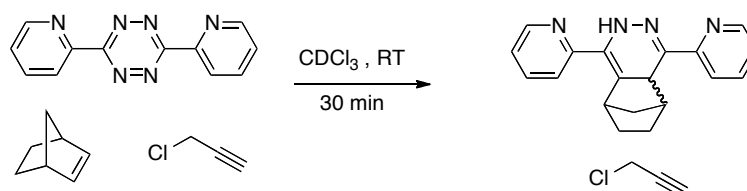
### **3.3. Results and discussion**

We aimed to use the tetrazine–norbornene reaction in tandem with the copper-catalysed azide–alkyne reaction to perform two micelle modifications simultaneously. Whilst the CuAAC reaction is arguably not a bioorthogonal reaction, since it is well understood and has been used for micelle modification before, we opted to use it to provide proof-of-principle for our tandem modification concept. We first investigated the orthogonality of the two

reactions, then explored an appropriate polymer backbone, before self-assembling the amphiphile and carrying out micelle functionalisations.

### 3.3.1. Small molecule model reactions

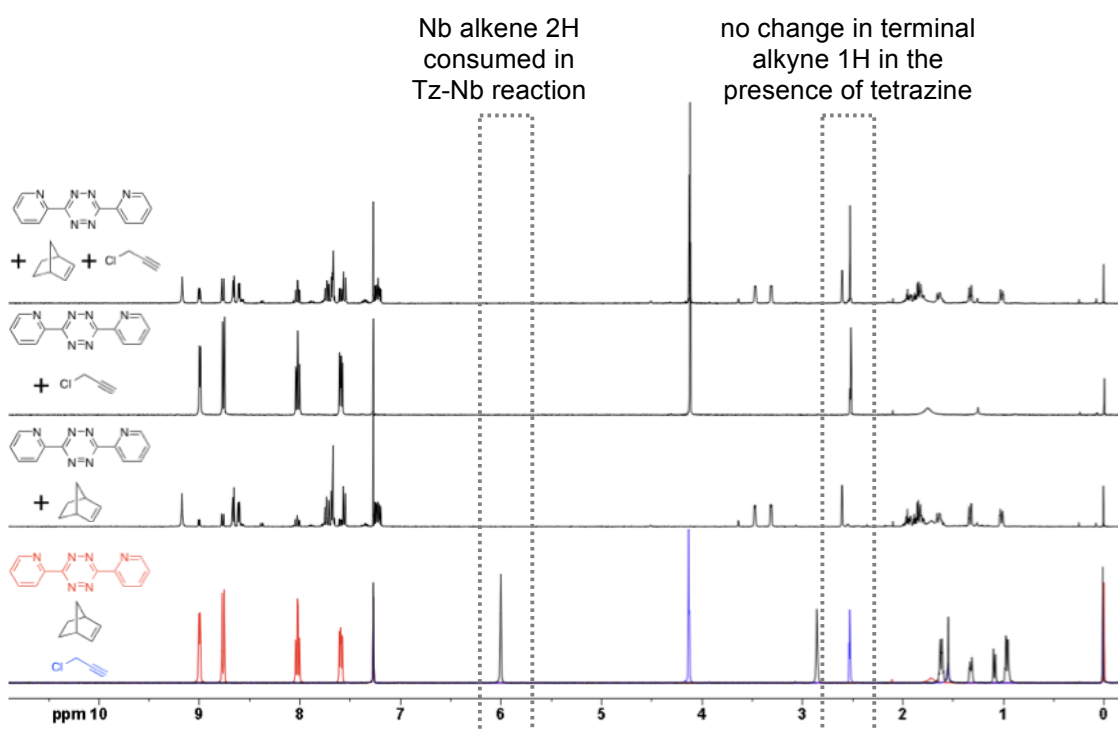
The Tz–Nb reaction has been shown to be a very fast, high-yielding click reaction, but tetrazines can also react with other alkenes and alkynes,<sup>23</sup> albeit at vastly reduced rates and often requiring forcing conditions. Likewise, norbornenes can also react with azides; however examples in the literature predominantly require heating to reflux temperatures and reaction times on the order of days.<sup>24</sup> Thus we considered that the mild reaction conditions employed for both the Tz–Nb reaction and the aqueous CuAAC reaction would not result in any cross-coupling.<sup>25</sup>



**Scheme 3.1 Competition reaction in  $\text{CDCl}_3$  between tetrazine, norbornene and propargyl chloride**

In order to confirm this hypothesis, small molecule competition reactions were carried out. Equimolar amounts of dipyridyl tetrazine and propargyl chloride were dissolved in  $\text{CDCl}_3$  (Scheme 3.1) and stirred for 30 minutes before a  $^1\text{H}$  NMR spectrum was measured. The experiment was then repeated with the addition of one equivalent of norbornene, as a model for the intended core reaction. As shown in Figure 3.5, no change in any chemical shifts were

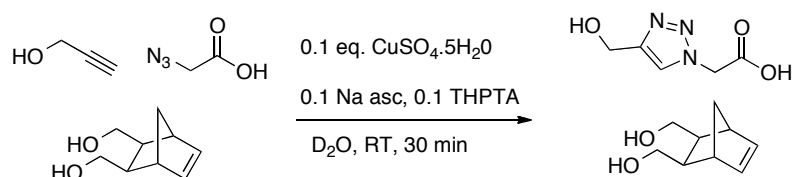
observed in the first experiment, whilst in the second the tetrazine–norbornene reaction proceeded as expected with full consumption of the norbornene signal at 6.0 ppm, leaving the propargyl signals at 2.5 and 4.5 ppm unaffected.



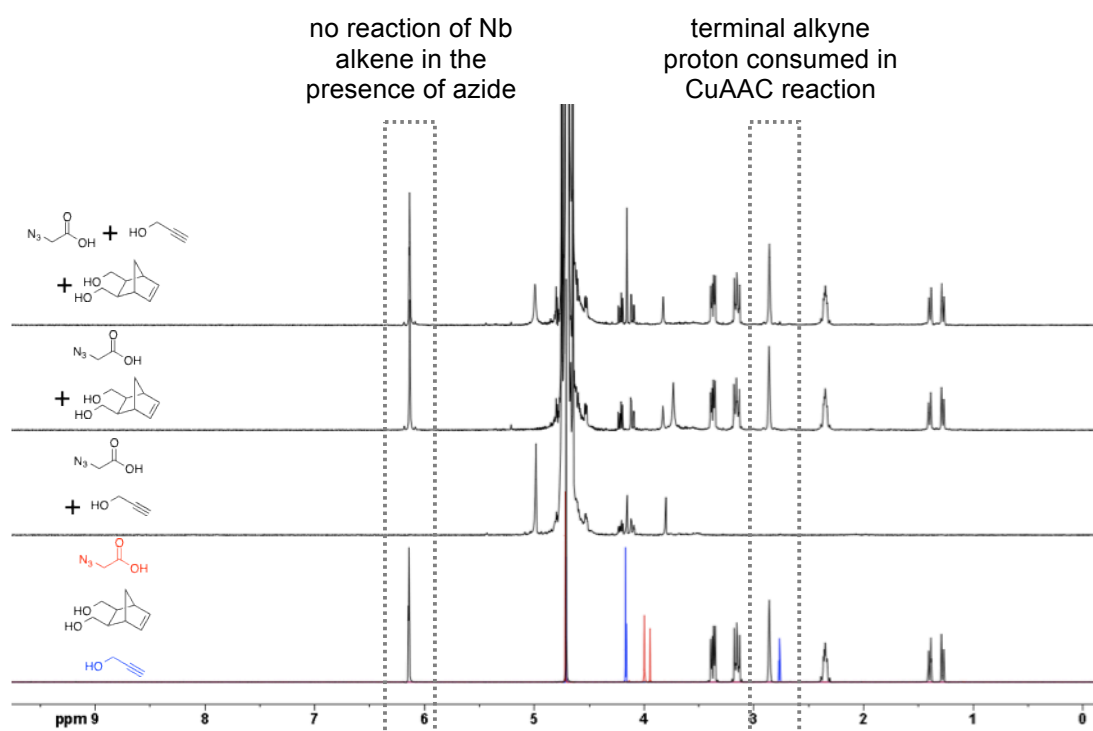
**Figure 3.5** <sup>1</sup>H NMR spectra (CDCl<sub>3</sub>) of tetrazine, propargyl chloride and norbornene individually (*bottom*), clean reaction of norbornene with tetrazine showed by complete consumption of norbornene (*second from bottom*), no reaction of tetrazine with propargyl chloride (*second from top*) and selective reaction of tetrazine with norbornene over propargyl chloride (*top*)

In an analogous manner, a competition reaction between a water-soluble azide, alkyne and functionalised norbornene was carried out in D<sub>2</sub>O as a model for the shell click reaction (Scheme 3.2). When norbornene and 2-azidoacetic acid were combined in equimolar amounts, no reaction of the norbornene double bond (at 6.2 ppm in the <sup>1</sup>H NMR spectrum, Figure 3.6) was observed, whilst the experiment including propargyl alcohol showed a clean

CuAAC reaction in the presence of 5-norbornene-2,2-dimethanol, again with no change in the norbornene double bond.



**Scheme 3.2** Competition reaction in  $\text{D}_2\text{O}$  between water-soluble 2-azidoacetic acid, propargyl alcohol and norbornene *endo*-, *endo*- dimethanol

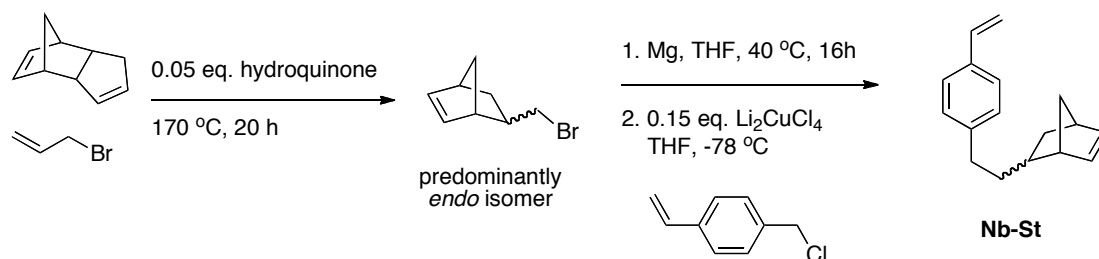


**Figure 3.6**  $^1\text{H}$  NMR spectra ( $\text{D}_2\text{O}$ ) of 2-azidoacetic acid, norbornene dimethanol and propargyl alcohol individually (*bottom*), clean reaction of propargyl alcohol with azidoacetic acid (*second from bottom*), no reaction of azidoacetic acid with norbornene dimethanol (*second from top*) and selective reaction of propargyl alcohol with azidoacetic acid over norbornene dimethanol (*top*)

The competition experiments confirmed that the terminal alkyne remained a spectator in the tetrazine–norbornene reaction, and likewise the norbornene remained uninvolved in the CuAAC reaction.

### 3.3.2. Polymer synthesis and characterisation

In order to install norbornene functionalities in the hydrophobic core of the micelle, and alkyne functionalities in the hydrophilic shell, sequential Reversible Addition-Fragmentation Chain Transfer (RAFT) copolymerisations were carried out to afford an amphiphilic block copolymer. RAFT was chosen as the copolymerisation with styrene of a norbornene-based monomer had been previously reported,<sup>26</sup> and a styrenic core was desirable to ensure that the micelle was kinetically frozen due to the high  $T_g$  of the core.<sup>27</sup>



**Scheme 3.3 Nb–St monomer synthesis**

A styrenic norbornene monomer (Nb–St) was synthesised according to a literature precedent<sup>26a</sup> (Scheme 3.3) and purity confirmed by  $^1\text{H}$  and  $^{13}\text{C}$  NMR spectroscopy; full assignment of the spectral peaks was achieved using COSY and HMQC experiments, and is shown in Figure 3.7. An *exo/endo* mixture of the monomer was isolated, with approximately 88% of the *endo* isomer in the

final product, so small peaks arising from the *exo* isomer can also be seen in the  $^1\text{H}$  and  $^{13}\text{C}$  NMR spectra.

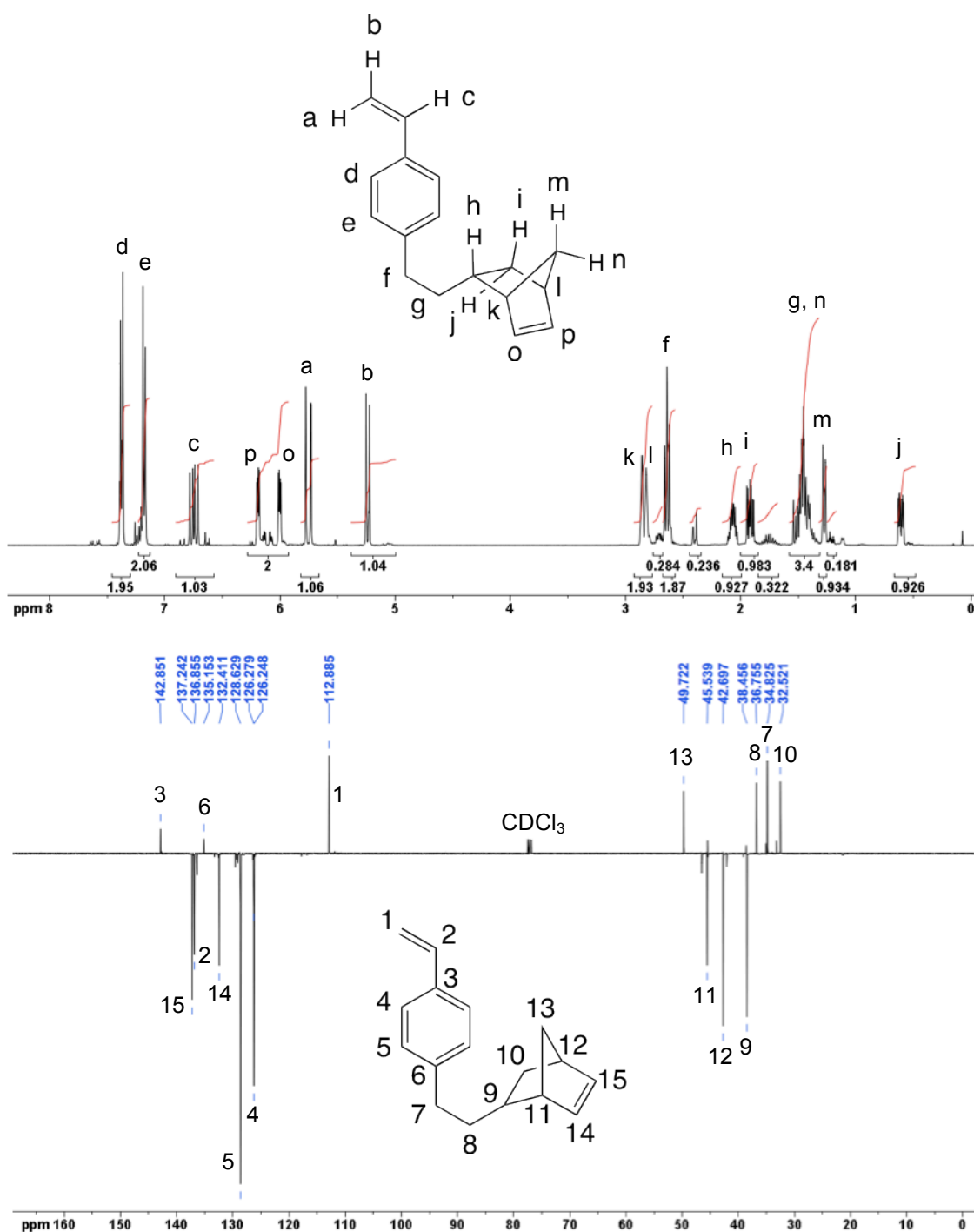
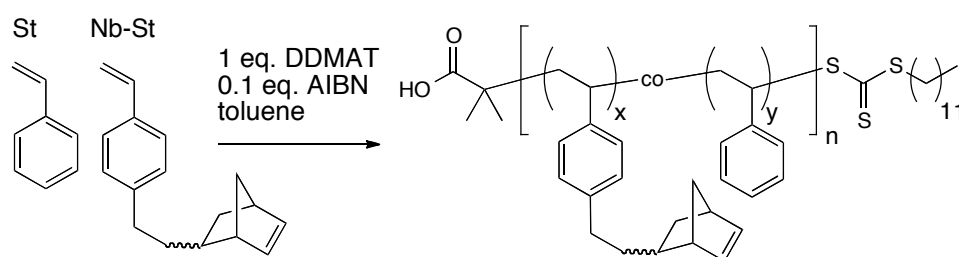


Figure 3.7  $^1\text{H}$  (top) and  $^{13}\text{C}$  (bottom) NMR spectra for Nb-St monomer, peaks for *endo* isomer assigned. In both cases, minor peaks are due to the minority *exo* isomer rather than impurities



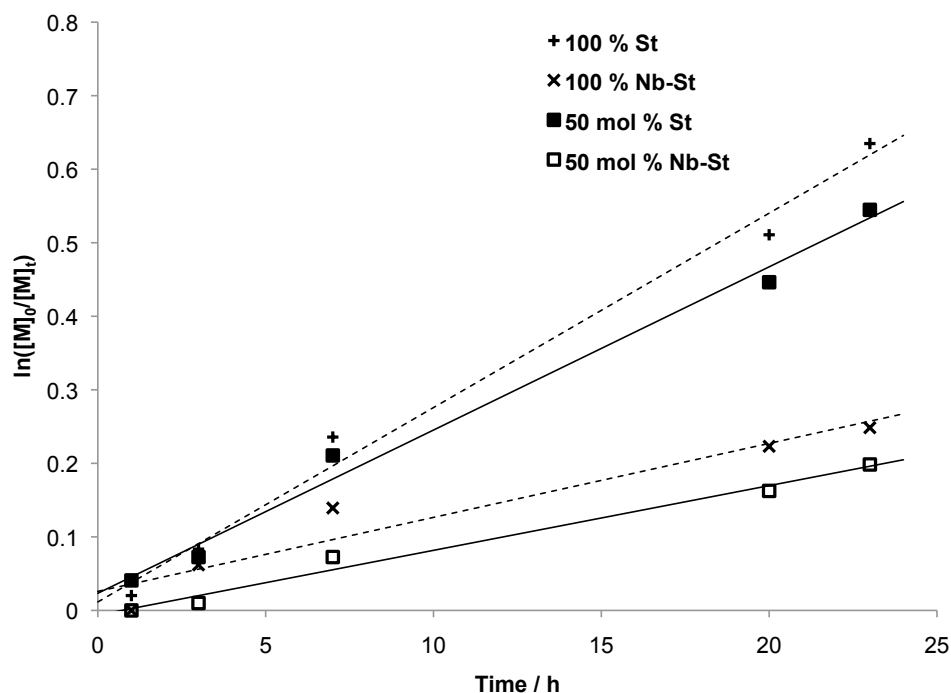
The literature report on the RAFT copolymerisation of Nb–St with styrene (St) was conducted at 120 °C, both in bulk and in toluene (1:1  $v/v$ ); however the bulk polymerisation resulted in pronounced high molecular weight shoulders and therefore we utilised solution polymerisation as an alternative (Scheme 3.4), which was demonstrated to result in much smaller shoulders in the SEC traces. Additionally, it has been shown that lower temperatures (<70 °C) are more suitable to limit adverse reactions of the norbornene group,<sup>28</sup> so we investigated whether lowering the temperature of the copolymerisation would significantly affect the polymerisation kinetics or control when compared with the literature report.



**Scheme 3.4 Copolymerisation of Nb–St and St**

A homopolymerisation of Nb–St and copolymerisation of 50 mol% Nb–St with styrene were carried out in toluene (1:1  $v/v$ ) to assess the kinetics of the reaction. The pseudo first order kinetic plot is shown in Figure 3.8, and the kinetics compared with a homopolymerisation of St. In the 50 mol% copolymerisation, the conversion of Nb–St reached 18% after 23 hours, and the conversion of St reached 42%. The slower conversion of Nb–St than St is in agreement with the reactivity ratios reported in solution as  $r_{\text{Nb–St}} = 0.56$  and  $r_{\text{St}} = 0.94$ .<sup>26a</sup> Crucially, the homo- and copolymerisations still proceeded at a

reasonable rate with no loss of control ( $M_w/M_n$  after 23 hours = 1.13), although the incorporation of Nb–St retarded the polymerisation with respect to a St homopolymerisation.

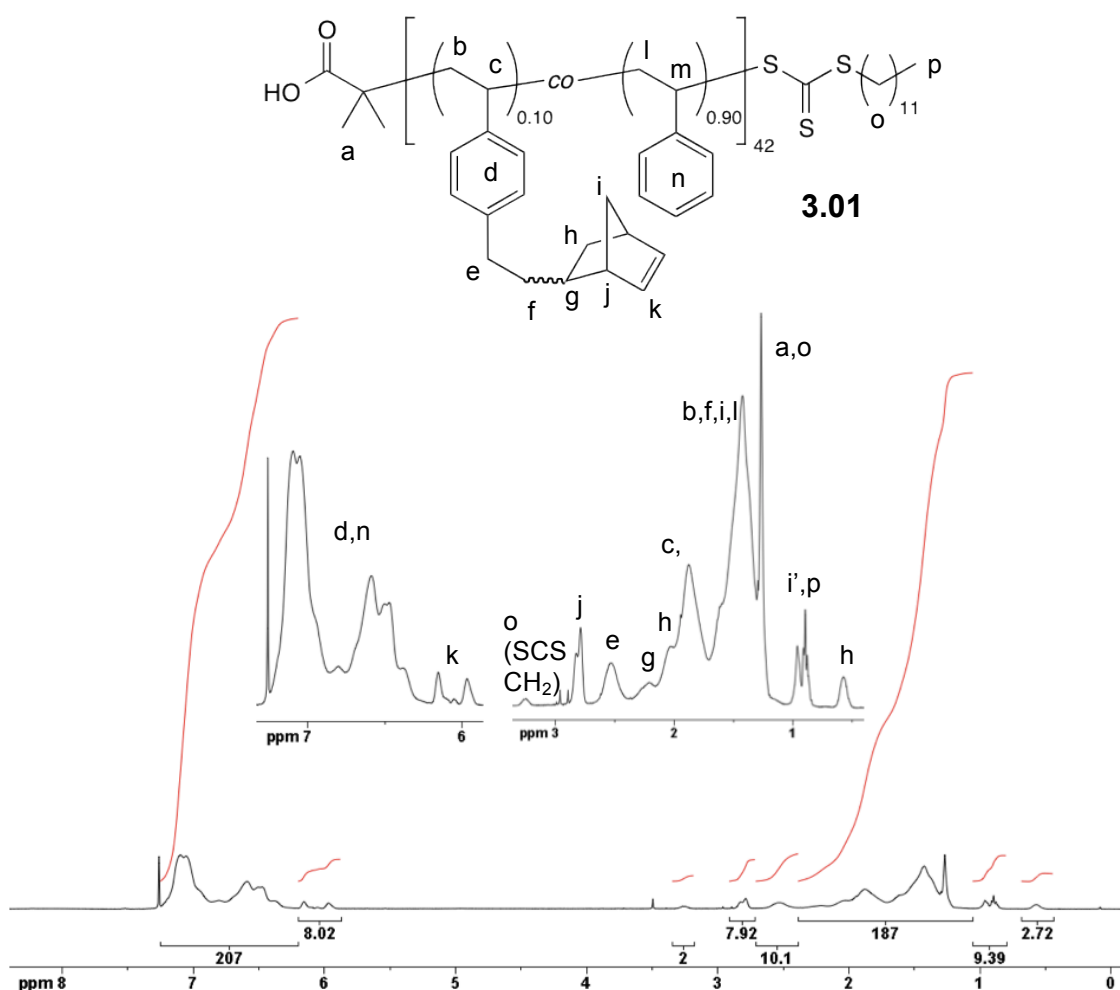


**Figure 3.8** Kinetic plot of  $[M]:[CTA]:[AIBN] = 100:1:0.1$  for 100% St (+), 100% Nb–St (x) and 50 mol% Nb–St:St (□ and ■ respectively). The dotted lines are the linear fits to the 100% St and 100% Nb–St kinetics, the solid lines are the linear fits for each monomer in the 50 mol% St/Nb–St polymerisation

Since the 50 mol% copolymerisation at 70 °C appeared to proceed smoothly, we continued to use this lower temperature in order to limit adverse side reactions of the norbornene group.

To synthesise the hydrophobic block, St was copolymerised with 10 mol% Nb–St monomer in toluene. The conversion after 24 hours was *ca.* 30–40%, and the polymerisation was terminated at that point in order to avoid side reactions involving the norbornene; this is an oft-observed phenomenon at higher

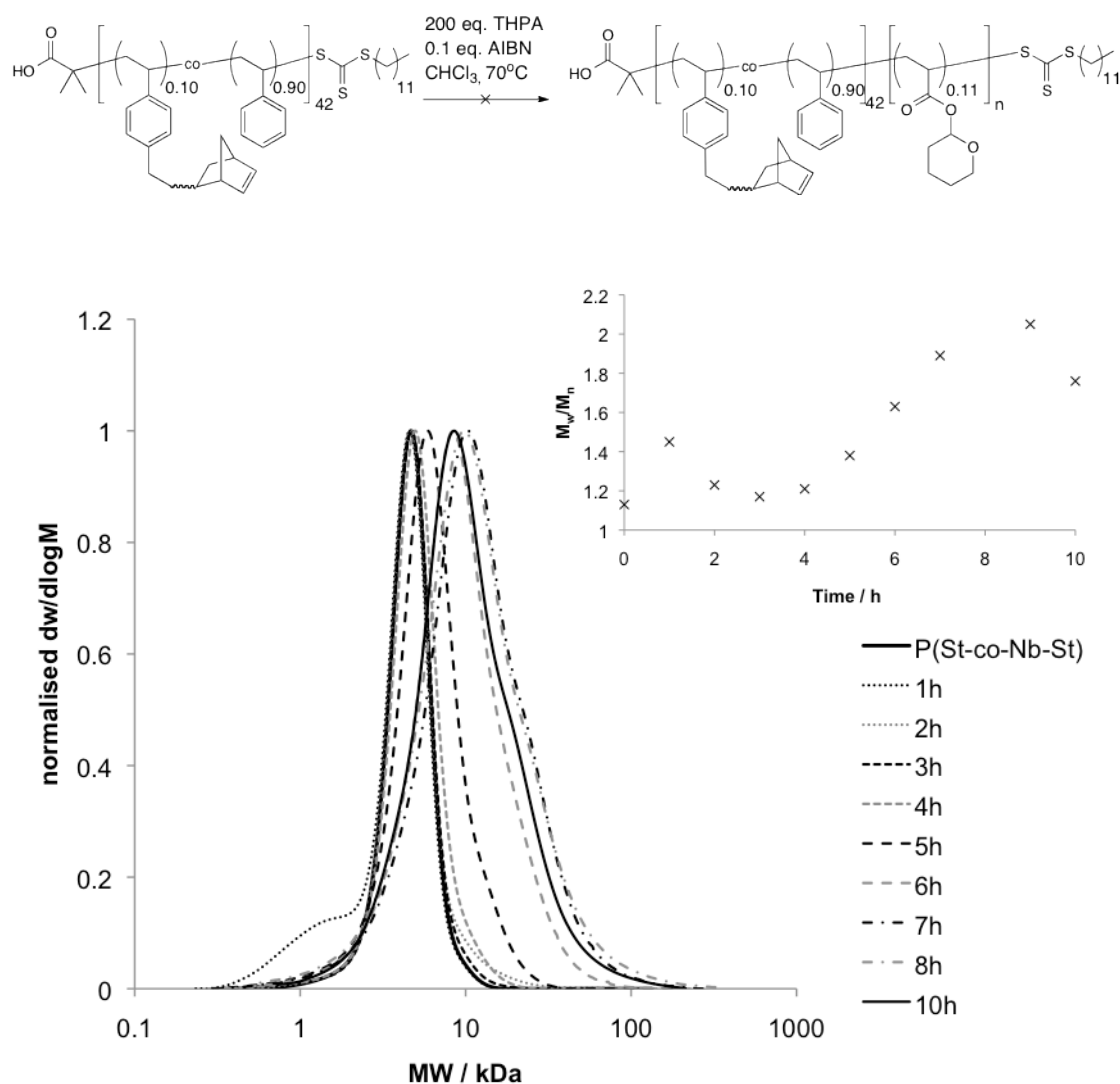
conversions when polymerising Nb-containing monomers.<sup>29</sup> The  $M_n$  of **3.01** was determined by SEC, relative to PS standards, to be 4.1 kDa, ( $M_w/M_n$  1.13). Comparison of the integrals of the methylene adjacent to the trithiocarbonate (3.25 ppm, seen in Figure 3.9) with the Nb signals at 6.0 ppm and the aromatic peaks from 6.2 to 7.2 ppm gave the degree of polymerisation as St = 38, Nb–St = 4 ( $M_n$  5.2 kDa).



**Figure 3.9 Assigned  $^1\text{H}$  NMR spectrum of polymer 3.01, with regions from 0.5–3.3 ppm and 5.9–7.5 ppm expanded**

To furnish the copolymer with a hydrophilic block, two routes were explored: the first being polymerisation of a deprotectable monomer, the second being direct polymerisation of a hydrophilic monomer. For the first route, a number of monomers have been polymerised by RAFT that can be deprotected to form poly(acrylic acid) (PAA): *tert*-butyl acrylate (*t*BuA),<sup>30</sup> tetrahydropyranyl acrylate (THPA),<sup>31</sup> 1-ethoxyethyl acrylate (EEA)<sup>32</sup> among others. In this case *t*BuA is not possible as the deprotection requires strong acid, which would hydrolyse the norbornene double bonds already installed in the styrenic segment.<sup>33</sup>

Chain extension of **3.01** was first attempted with THPA, as the relatively mild conditions needed for deprotection (dilute acid, room temperature) are compatible with the norbornene functionalities. 200 equivalents of THPA relative to macro-CTA **3.01** in dry chloroform (1:1 <sup>w/v</sup>) were used in the polymerisation, and the kinetics monitored by <sup>1</sup>H NMR spectroscopy and SEC (Figure 3.10). The <sup>1</sup>H NMR spectra showed self-catalysed deprotection of the THPA functionalities after only 2 hours polymerisation time, and the SEC traces (Figure 3.10) also demonstrate little success in chain extending with any degree of control, most likely due to uncontrolled deprotection to acrylic acid during polymerisation. In order to rule out the effect of the acid end group on the polymerisation, a chain extension from polystyrene (PS) with a benzylic rather than acidic end group was carried out, but also resulted in low apparent conversions and deprotection of the THPA. Thus it was concluded that THPA is incompatible with this particular chain extension, and an alternative monomer was sought.

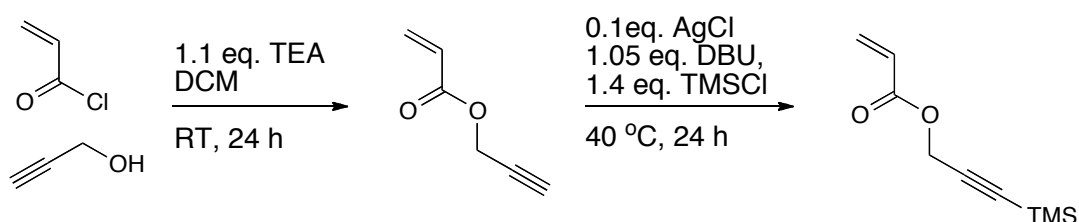


**Figure 3.10 Evolution of SEC traces and  $M_w/M_n$  (inset) with time of TPHA chain extension from poly(St-co-Nb-St)**

EEA was also attempted, however, in accordance with some suggestions in the initial report of its homopolymerisation,<sup>32</sup> deprotection and cross-linking of the resultant PAA occurred during polymerisation, which is extremely undesirable for a polymer destined for self-assembly, so this route was not pursued further.

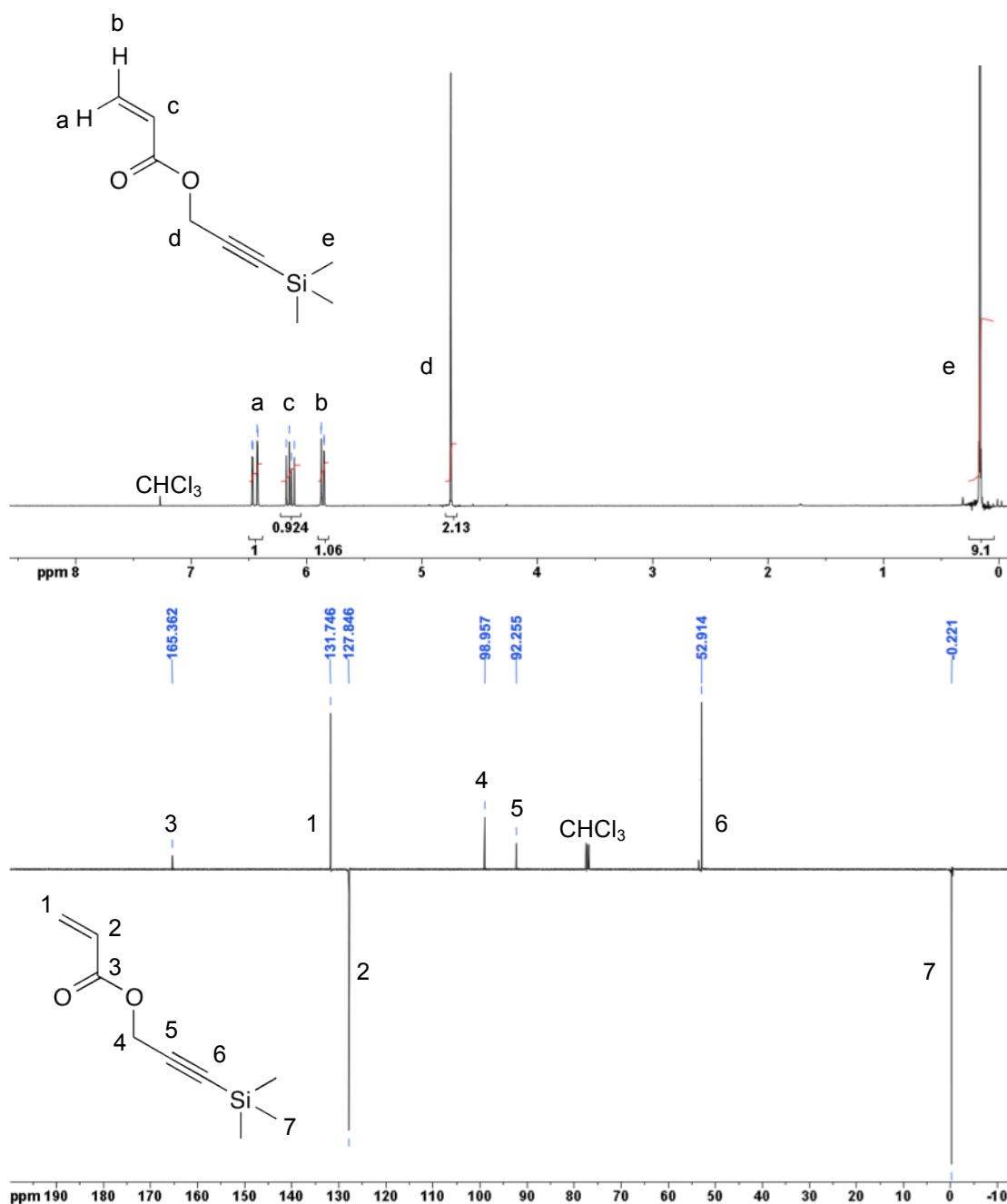
In view of the deprotection and crosslinking issues encountered when using THPA and EEA, and also the propensity of PAA-shell micelles to aggregate if pH and salt concentration are not finely controlled,<sup>34</sup> we turned our attention away from acrylic acid to monomers that can be polymerised by RAFT in organic solvents, yet are also hydrophilic to facilitate self-assembly. Poly(ethylene glycol) (PEG) (meth)acrylates have recently gained attention as potentially biocompatible, hydrophilic monomers that are polymerisable by CRP techniques,<sup>35</sup> RAFT included.<sup>36</sup> The shortest PEG side chain that is water soluble at room temperature is the 3-mer, triethylene glycol acrylate (TEGA), which we opted to use as the hydrophilic segment.

To install alkyne functionalities, a propargyl-based acrylate was copolymerised with TEGA. The propargyl acrylate was trimethyl silane protected, as previous reports using unprotected propargyl acrylate suggest that the resulting dispersities are broad due to alkyne–alkyne coupling.<sup>37</sup> There are conflicting reports that use unprotected propargyl functionalities in a copolymerisation with PEGMA with reportedly good control;<sup>38</sup> however it was envisaged that norbornene–alkyne radical coupling could also occur during polymerisation from the macro-CTA and so we opted for the protected alkyne approach.



**Scheme 3.5 Synthesis of trimethyl silane-protected propargyl acrylate (PA-TMS)**

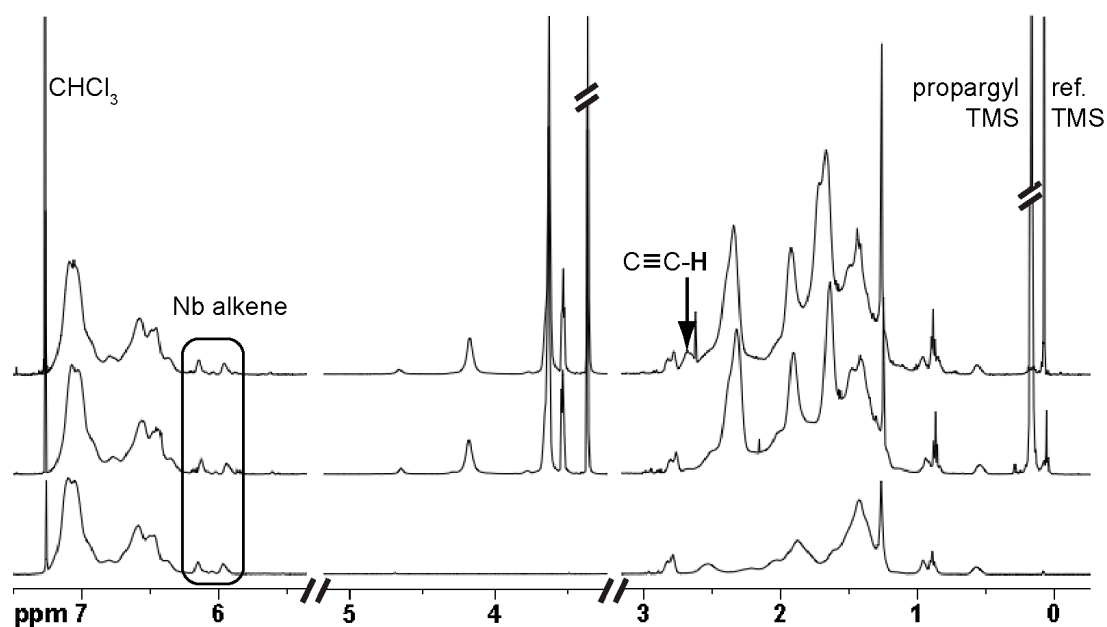
The trimethyl silane-protected alkyne monomer (PA-TMS) was synthesised in two steps in 51% yield from propargyl alcohol and acryloyl chloride, according to literature reports (Scheme 3.5).<sup>39</sup> Purity was confirmed by  $^1\text{H}$  and  $^{13}\text{C}$  NMR spectroscopy, and the assigned spectra are shown in Figure 3.11.



**Figure 3.11 Assigned  $^1\text{H}$  (top) and  $^{13}\text{C}$  (bottom) spectra in  $\text{CDCl}_3$  for PA-TMS monomer**

A copolymerisation of hydrophilic triethylene glycol acrylate (TEGA) and 10 mol% PA-TMS was chain extended from macroCTA **3.01**. Kinetic studies showed that the conversions of PA-TMS and TEGA were approximately equal throughout the polymerisation, suggesting, in the absence of reactivity ratios for the monomers, that the resulting copolymer segment is statistically random.

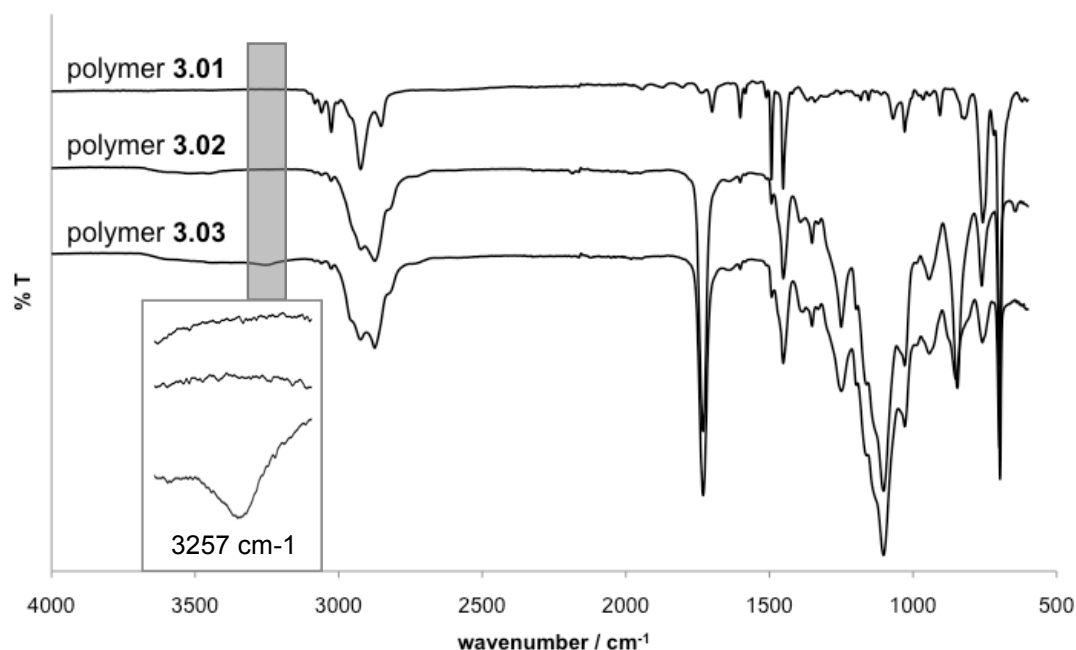
Polymer **3.02** was characterised by  $^1\text{H}$  NMR spectroscopy (Figure 3.12) to determine the block ratios, using the prominent TEGA  $\text{CH}_2$  signal at 4.2 ppm and the PA-TMS  $\text{CH}_2$  signal at 4.6 ppm in comparison to the aromatic protons of the styrenic block. This gave a calculated  $M_n$  of 24.3 kDa. The  $M_n$  by SEC was much lower (14.5 kDa), although as TEGA-co-PA-TMS is vastly different to the PS standards used in the SEC calibration, this is perhaps not surprising.



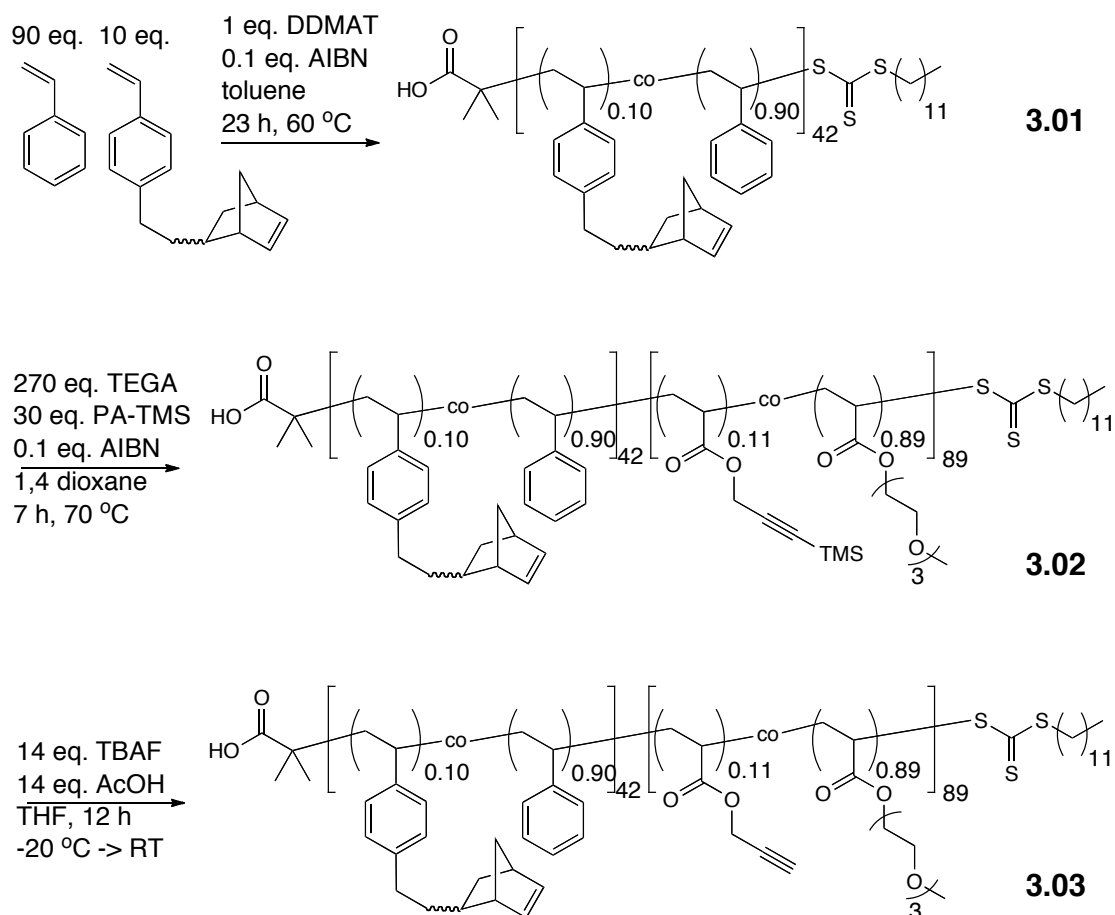
**Figure 3.12**  $^1\text{H}$  NMR spectra ( $\text{CDCl}_3$ ) of polymers **3.01** (bottom), **3.02** (middle) and **3.03** (top). The section from 3.2 to 5.2 ppm the z axis is contracted in order to show the detail in the rest of the spectrum.



The TMS protecting groups were easily removed following the method of Haddleton and coworkers;<sup>40</sup> complete deprotection was confirmed by the disappearance of the TMS methyl signals at 0.2 ppm in the  $^1\text{H}$  NMR spectrum and the appearance of the alkyne proton signal at 2.65 ppm, as highlighted in Figure 3.12. Crucially, the integrations of the norbornenyl alkene signal at 6.0 ppm relative to the aromatic protons remained constant from polymers **3.01**–**3.03** showing that the norbornene functionalities were not affected by the chain extension or deprotection steps. FT-IR analysis of polymer **3.03** also showed the appearance of a characteristic alkyne C–H vibration at  $3257\text{ cm}^{-1}$  (Figure 3.13), not present in the IR spectra of **3.01** or **3.02**. The full synthesis of polymer **3.03** is shown in Scheme 3.6.



**Figure 3.13** FT-IR spectra of polymers **3.01**–**3.03**; segment showing alkyne C–H stretch expanded

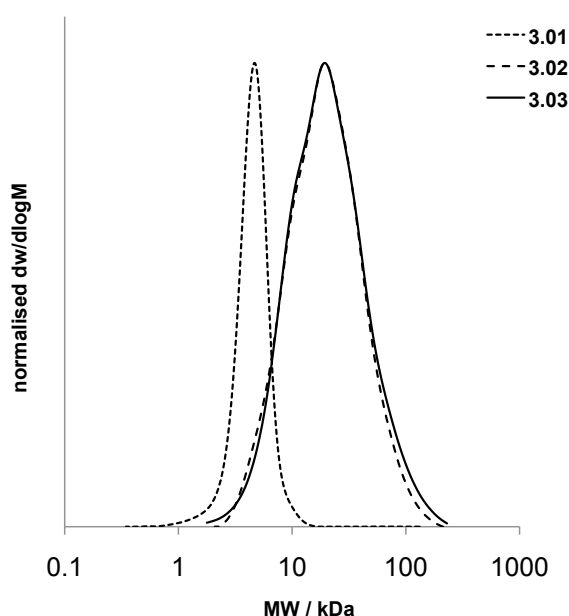


**Scheme 3.6 Synthetic approach to polymers 3.01, 3.02, and 3.03**

The  $M_n$  and  $M_w$  of **3.03** by SEC were virtually unchanged from polymer **3.02**, showing that the deprotection had no adverse effect on the other functionalities on the polymer.

However, the dispersities of the resulting diblock copolymers **3.02** and **3.03** were rather broad (1.71), as shown in Figure 3.14, possibly because of side reactions of the norbornene groups during the chain extension. Whilst this is not an ideal situation, it has previously been shown that broad dispersities in the corona-forming block of a micelle only results in mixed non-spherical morphologies in extreme cases ( $M_w/M_n > 3$  for a PS-PAA block copolymer

system).<sup>41</sup> Broad dispersities in the hydrophilic block of vesicle-forming copolymers also result in vesicles that are smaller than might be expected, but again no change in morphology is observed; indeed the size distribution of the vesicles formed from broad dispersity polymers was narrower than the distribution of the vesicles formed from the copolymers with low dispersity indices.<sup>42</sup> This is in contrast to the effect that the core-forming block dispersity can have on the morphology; in one example, a block copolymer with a hydrophobic block dispersity of 1.74 and narrow dispersity hydrophilic block formed ovoid structures rather than spherical micelles.<sup>43</sup>



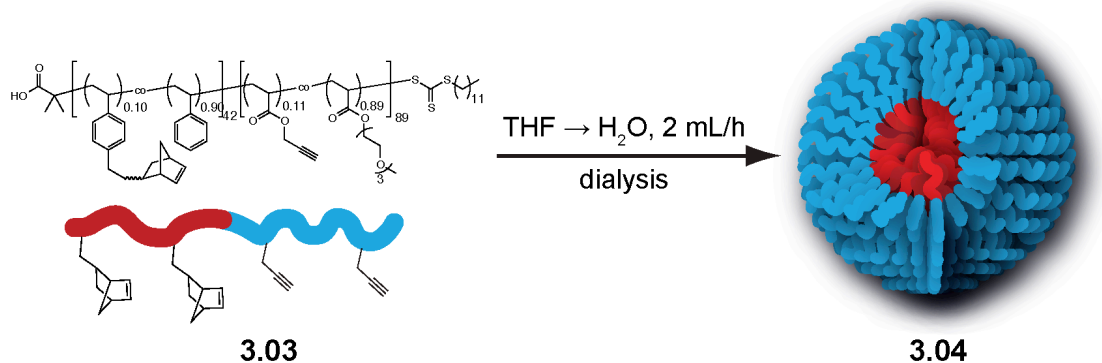
**Figure 3.14 SEC traces of polymers 3.01–3.03**

With these literature examples in mind, we proceeded with self-assembly of the block copolymer **3.03** as the core-forming hydrophobic block was well-defined and the relatively broad dispersity of the final polymer was solely due to the broad dispersity of the corona-forming hydrophilic block, which we

anticipated would not result in deviations from the spherical micelle structures targeted.

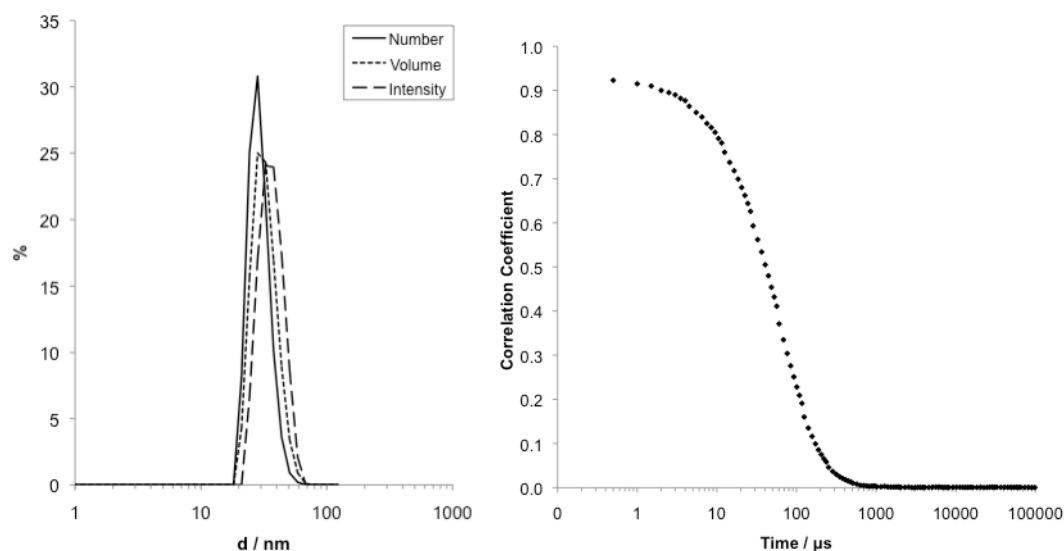
### 3.3.3. Micelle synthesis and characterisation

The amphiphilic block copolymer **3.03** was dissolved in THF (16 mg/mL), followed by slow addition of water at 2 mL/h to form micellar structures **3.04** (Scheme 3.7). Exhaustive dialysis against 18.2 MΩcm<sup>-1</sup> water was carried out, giving a final micelle concentration of 3 mg/mL. The spherical nature and size of the structures was confirmed by dry-state TEM imaging on graphene oxide (GO)<sup>44</sup> and DLS (dynamic light scattering).



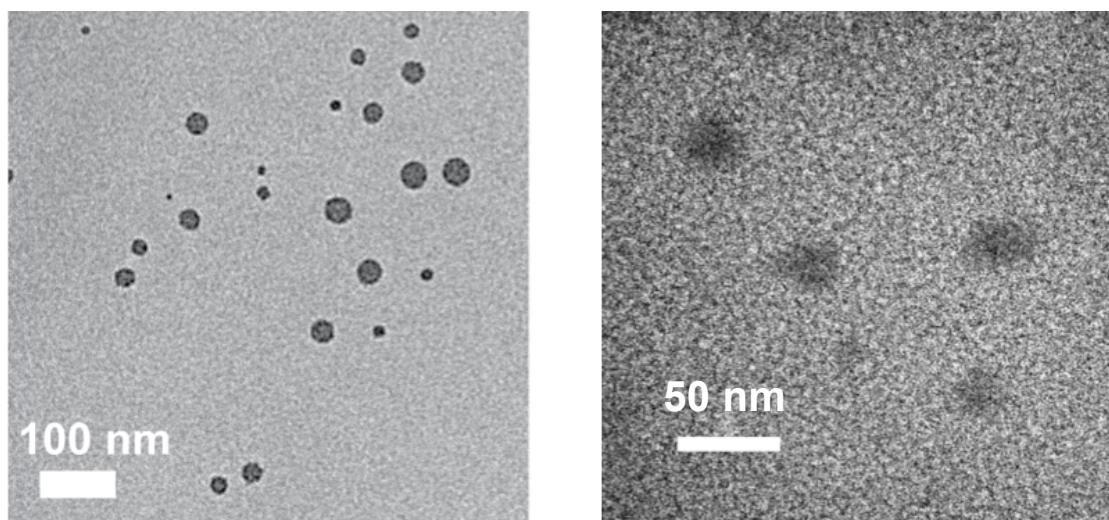
**Scheme 3.7 Formation of micelles 3.04 from polymer 3.03**

The DLS data (Figure 3.15) show a narrow distribution of sizes in a single population ( $D_h$   $32.9 \pm 4.0$  nm), and a smooth correlation function that fits well to a single population model; both of these factors demonstrate that there are no large aggregates in the solution.

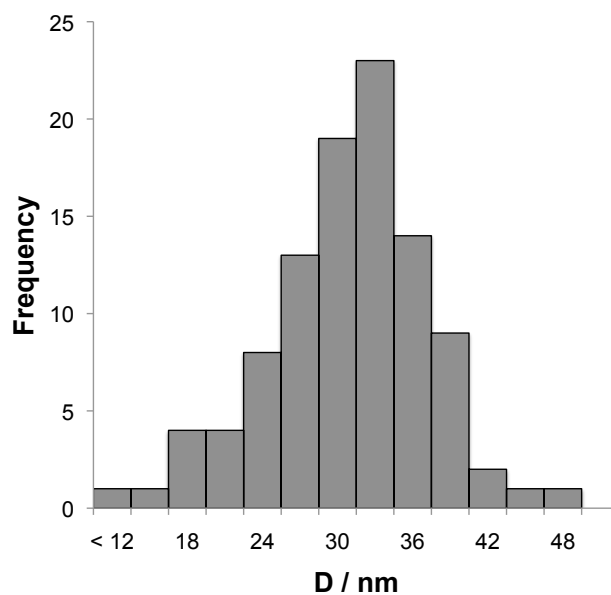


**Figure 3.15 DLS traces (left) and correlogram (right) for the core-shell functionalised micelles 3.04**

TEM images were taken on an atomically thin support of GO, in order to visualise the structures clearly without the need of a heavy metal stain — staining the sample with uranyl acetate resulted in less clear images, as shown in Figure 3.16.



**Figure 3.16 TEM images of micelles 3.04, unstained on GO (left) and stained with uranyl acetate (right)**

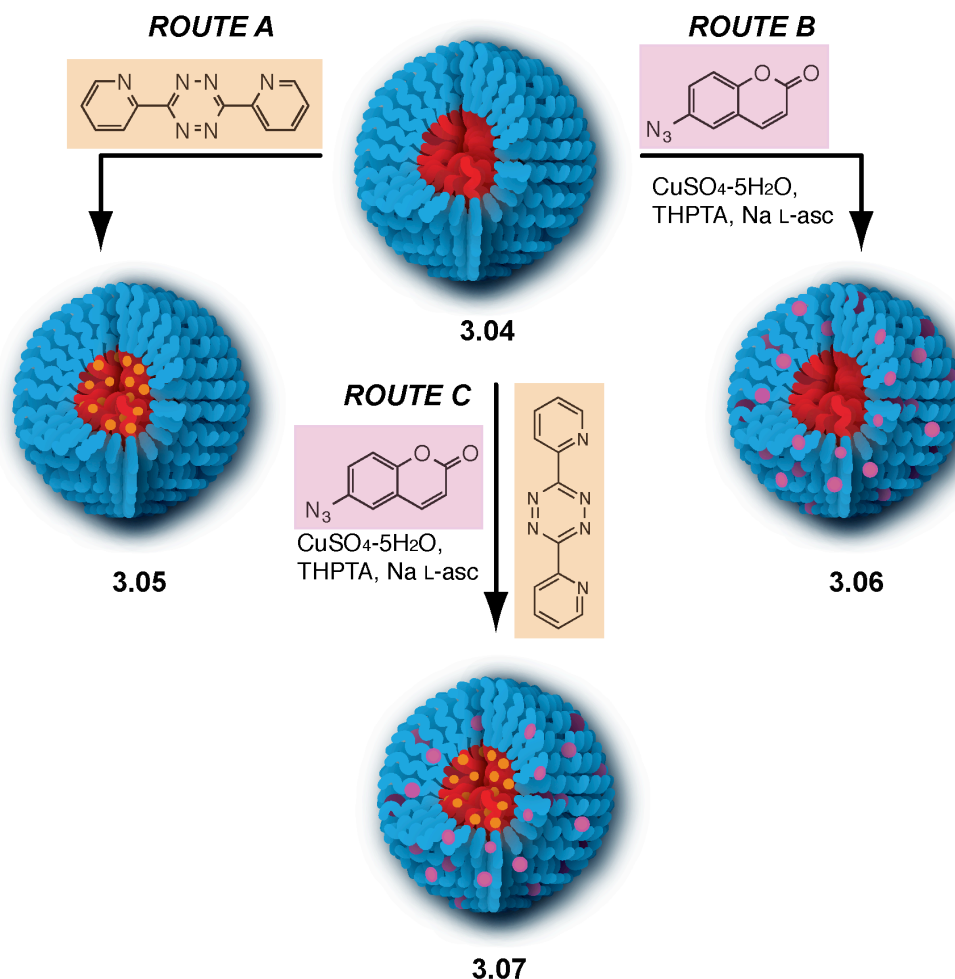


**Figure 3.17 Histogram of 3.04 particle diameters measured from TEM imaging on GO**

The average diameter of the particles **3.04** by TEM was calculated by measuring at least 100 particles from several images. Only spherical structures were observed in the TEM images, and the distribution of sizes is shown ( $D_{av}$   $29.9 \pm 6.9$  nm) in Figure 3.17. The diameter of the particles measured by TEM is slightly less than the diameter measured by DLS, which is expected due to the collapse and drying of the particles onto the TEM grid, in comparison to their fully hydrated state measured by DLS.

### 3.3.4. Micelle functionalisation

The overall synthetic strategy to perform functionalisations on the micelle scaffold **3.04** is shown in Scheme 3.8.

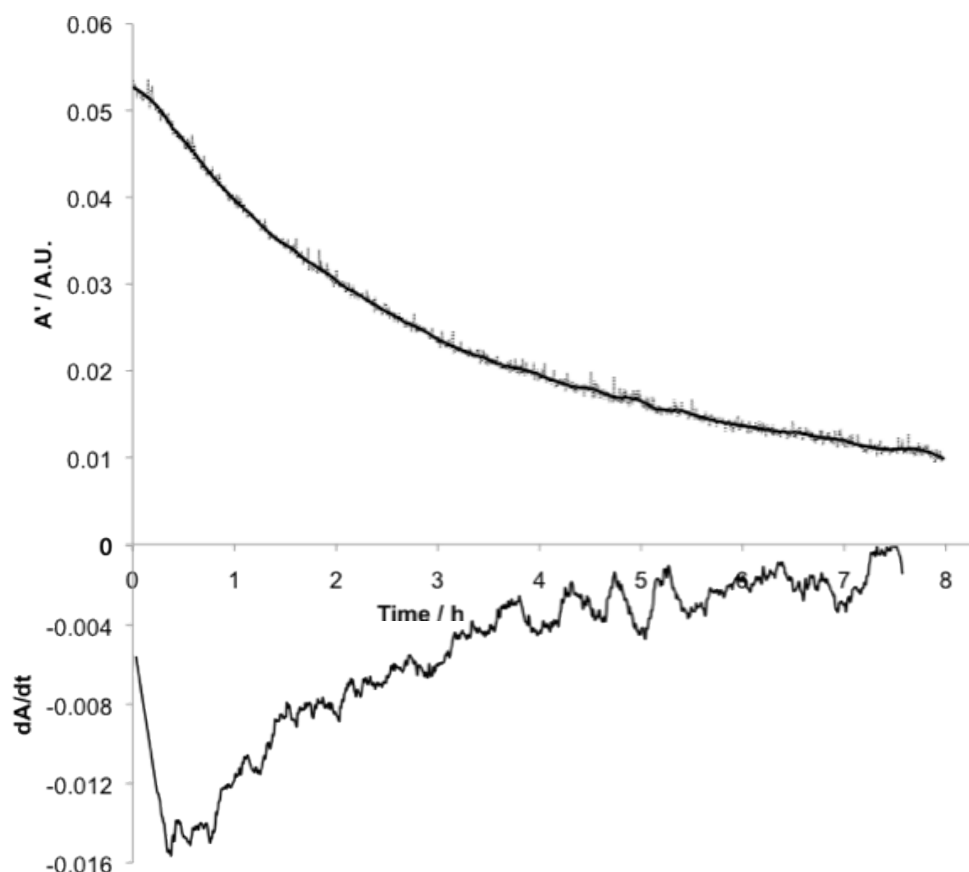


Scheme 3.8 Approach to functionalisation of micelles **3.04**

#### 3.3.4.1. Core Tetrazine–norbornene reaction (route A)

A tetrazine–norbornene click reaction was carried out in the core of the micelle by simple addition of dipyrindyl tetrazine (1.2 eq. relative to norbornene groups) in a minimum volume of THF required to dissolve it due to its poor water solubility. The reaction was carried out at room temperature in air, and

monitored by the reduction in intensity of the UV/vis signal at 546 nm, arising from the colour change from pink to orange that is characteristic of the reaction. The point at which the first derivative of the absorbance against time curve reached zero ( $A$  vs.  $t$  curve in the top of Figure 3.18,  $dA/dt$  curve in the bottom of the Figure) was used to determine the reaction time (approximately 8 hours). Relative to the polymer-polymer coupling or end functionalisation described previously, the concentration of tetrazine used here was much lower, and thus the absorbance at 546 nm also much lower. For this reason, the data were smoothed before calculating the derivative of the graph.

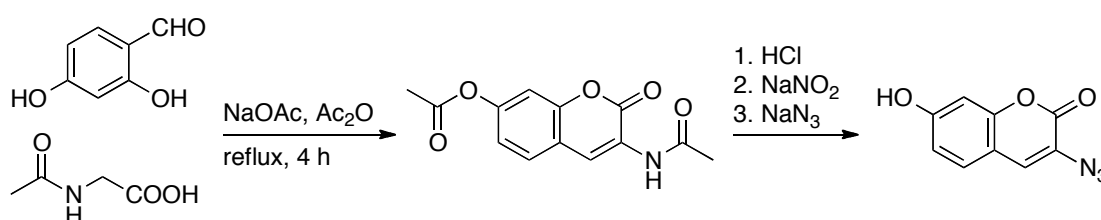


**Figure 3.18 UV/vis absorbance at 546 nm (*top*) for functionalisation of micelles 3.04 to micelles 3.05 with dipyrindyl tetrazine, and first derivative of the smoothed curve (*bottom*) used to determine reaction completion**



### 3.3.4.2. Shell CuAAC (route B)

To investigate the viability of the CuAAC click reaction in the micelle shell, a pro-fluorogenic, water-soluble 3-azido-7-hydroxy-coumarin (coumarin- $N_3$ ) was used for ligation. As previously described in the literature,<sup>19</sup> this coumarin is not fluorescent until clicked with a terminal alkyne, after which it fluoresces strongly with an emission wavelength between 400 and 490 nm. This provides an ideal method to confirm CuAAC functionalisation in the micelle shell.



**Scheme 3.9** Synthesis of pro-fluorescent coumarin- $N_3$

The coumarin- $N_3$  was synthesised in two steps (Scheme 3.9) in 16% overall yield following a literature preparation method, and purity confirmed by <sup>1</sup>H and <sup>13</sup>C NMR spectroscopy; the spectra are shown in Figure 3.19.

To a solution of micelles **3.04** was added coumarin- $N_3$  (1.2 eq. relative to alkyne groups), copper sulfate pentahydrate, water-soluble Cu ligand tris(hydroxypropyl)triazolylmethyl-amine (THPTA) and sodium ascorbate in aqueous solution. The mixture was allowed to stir for several hours, after which the copper was removed by adsorption onto CupriSorb™ beads, and any remaining small molecules removed by extensive dialysis against water.

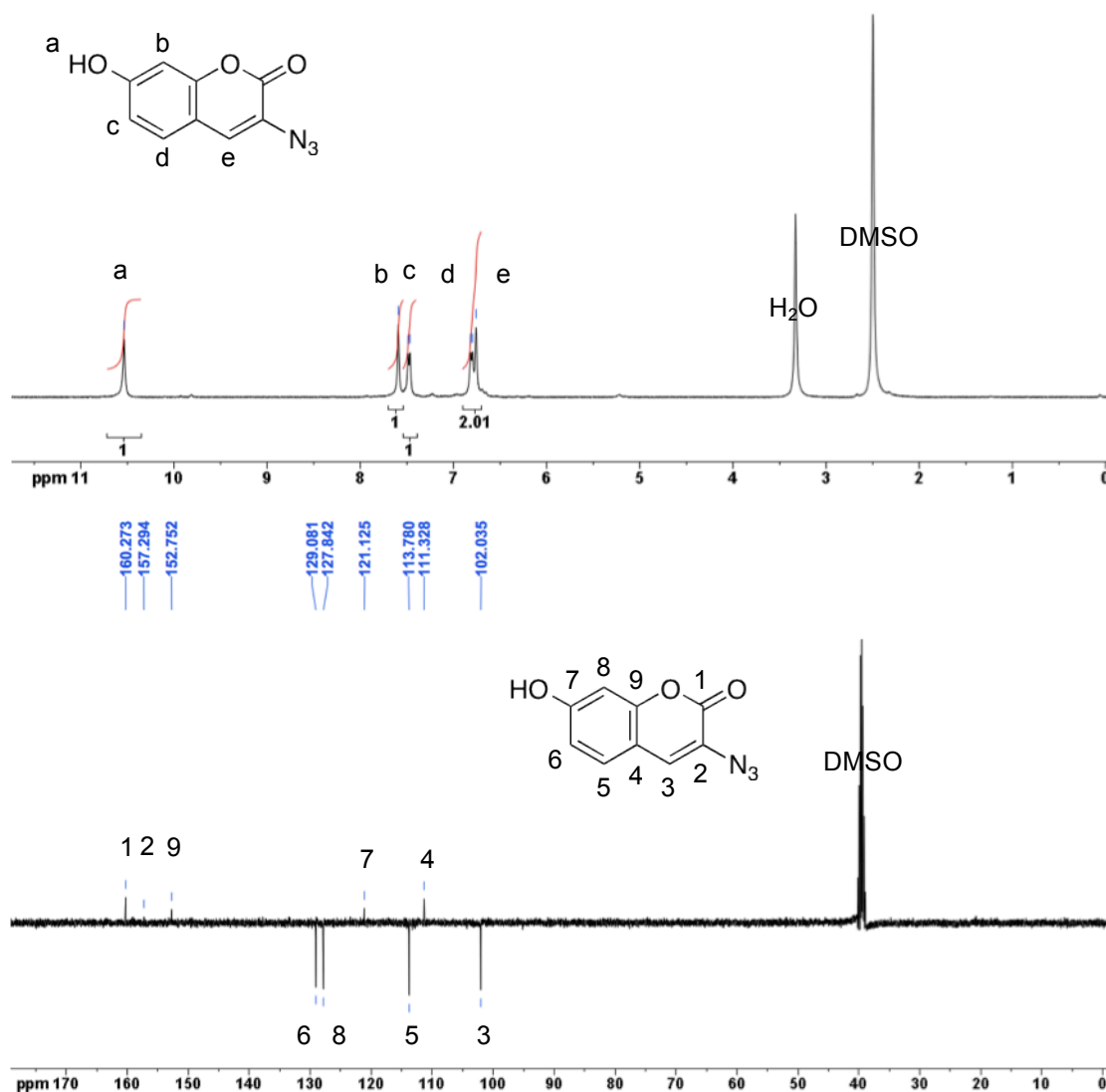


Figure 3.19 <sup>1</sup>H (top) and <sup>13</sup>C (bottom) NMR spectra (DMSO-d<sub>6</sub>) of coumarin-N<sub>3</sub>

#### 3.3.4.3. Tandem core-shell functionalisation (route C)

We first attempted to carry out the tandem reaction by adding all of the CuAAC and Tz-Nb click reagents (1.2 eq. of the coumarin azide and dipyrindyl tetrazine) at the same time, however this lead to reduced efficiency of both reactions – approximately 50%, judged by freeze-drying the resulting micelles

and analysing by  $^1\text{H}$  NMR spectroscopy the remaining Nb alkene signals. Increasing the ratios of the Tz–Nb and CuAAC click reagents to 5 eq. did not result in any increase in conversion relative to using only 1.2 eq. Since tetrazines and related pyridazines are known to form metal complexes,<sup>45</sup> we hypothesise that such a Cu–tetrazine complex was forming and inhibiting both the CuAAC and Tz–Nb reactions, possibly by reducing the phase segregation of the relevant reagents and catalysts between the hydrophobic core and hydrophilic shell. This is in agreement with other recently published work where the CuAAC and Tz–Nb reactions were attempted simultaneously in bioorthogonal labelling reactions.<sup>46</sup>

In order to overcome this, a one-pot, sequential addition strategy was employed as an alternative to an exactly simultaneous addition. The CuAAC reagents were added in aqueous solution to the micelles **3.04**, after which the mixture was stirred for 20 minutes before addition of dipyriddy tetrazine in THF. The micelle solution was allowed to stir for 12 hours before characterisation by DLS and TEM, and analysis of the constituent polymers by  $^1\text{H}$  NMR spectroscopy, SEC and UV/vis spectroscopy of the freeze-dried solution. Reversing the order of addition (i.e. dipyriddy tetrazine followed by CuAAC reagents) resulted in the same high efficiency for the Tz–Nb reaction but greatly reduced CuAAC reaction efficiency.

### 3.3.5. Characterisation of functionalised micelles

The micelles **3.04–3.07** were characterised in their self-assembled state by DLS and TEM to ascertain that no fundamental changes in size or morphology had been induced by functionalisation, and fluorescence spectroscopy to assess the CuAAC shell reaction. A portion of the micelles **3.04–3.07** were also analysed by inductively-coupled plasma mass spectrometry (ICP-MS) to determine how much residual copper was present from the CuAAC reaction. Micelles **3.05–3.07** were then freeze-dried to isolate the constituent polymers, and analysis by SEC, UV/vis,  $^1\text{H}$  NMR, and FT-IR spectroscopies carried out.

#### 3.3.5.1. DLS

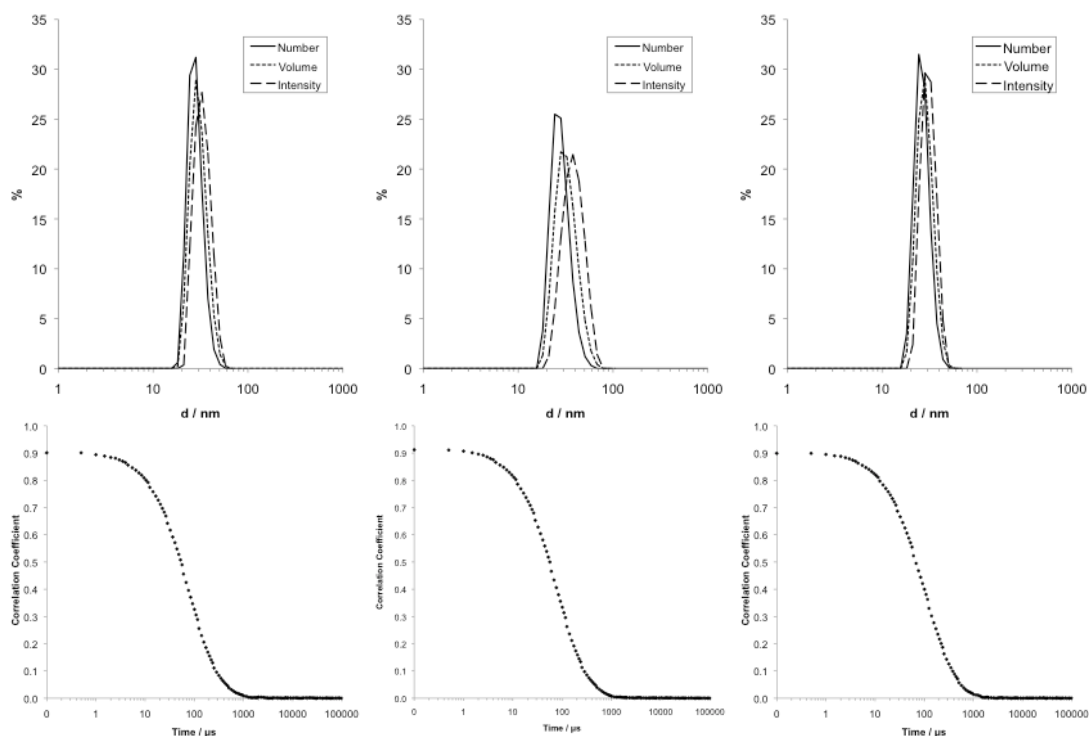


Figure 3.20 DLS traces (top) and correlograms (bottom) for micelles 3.05 (left), 3.06 (centre) and 3.07 (right)

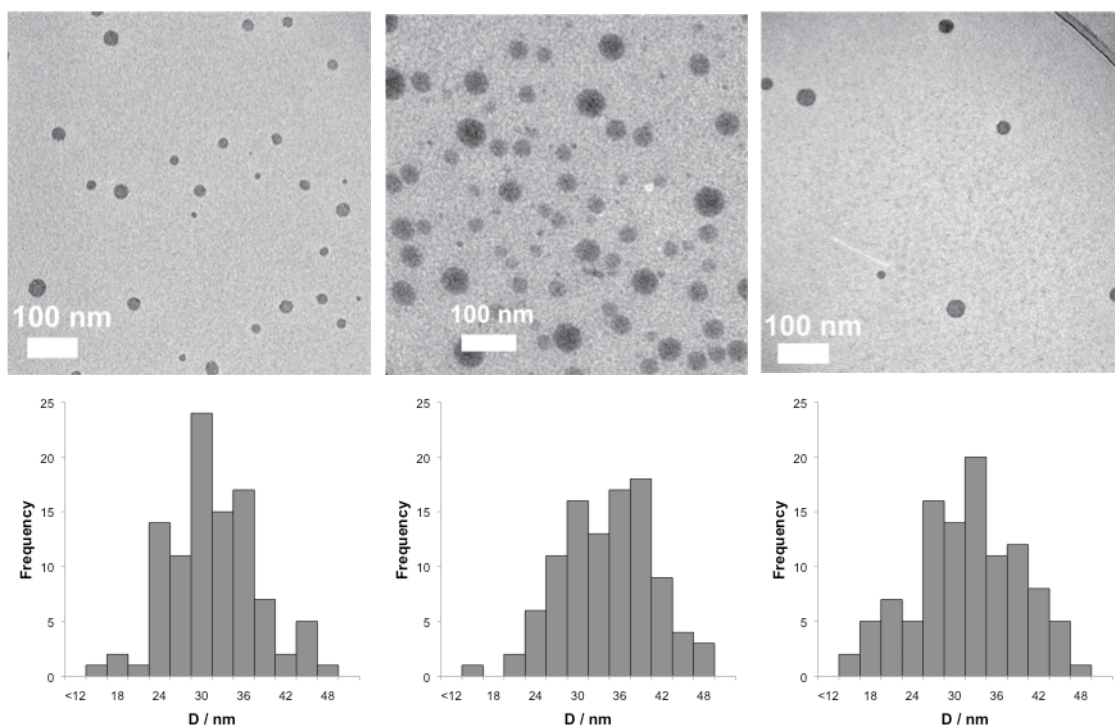
Micelles **3.05**, **3.06** and **3.07** showed no significant changes in size or morphology with respect to the unfunctionalised parent micelles **3.04** (Figure 3.20); hydrodynamic diameters are given in Table 3.1.

### 3.3.5.2. TEM

The average diameters of the micelles were determined by measuring at least 100 particles from TEM images obtained by drop deposition of the micelle solutions onto GO-coated copper grids, without any heavy metal stain being applied. As mentioned with regard to the parent micelles **3.04**, in general the average diameters are smaller than those determined by DLS, probably due to the slight collapse of the particles as they dry onto the grid, relative to their size in the hydrated state measured by light scattering. Representative images of the micelles, and histograms of the size distributions are shown in Figure 3.21, and the average diameters given in Table 3.1.

**Table 3.1**  $D_h$  of micelles **3.04–3.07**, measured by DLS and  $D_{av}$  of micelles **3.04–3.07**, measured by TEM (imaging on GO)

Micelle	$D_h$ / nm	$D_{av}$ / nm
<b>3.04</b>	$32.9 \pm 4.0$	$29.9 \pm 6.9$
<b>3.05</b>	$30.5 \pm 4.4$	$30.1 \pm 6.2$
<b>3.06</b>	$33.4 \pm 4.3$	$33.3 \pm 6.4$
<b>3.07</b>	$28.8 \pm 2.7$	$30.3 \pm 7.5$

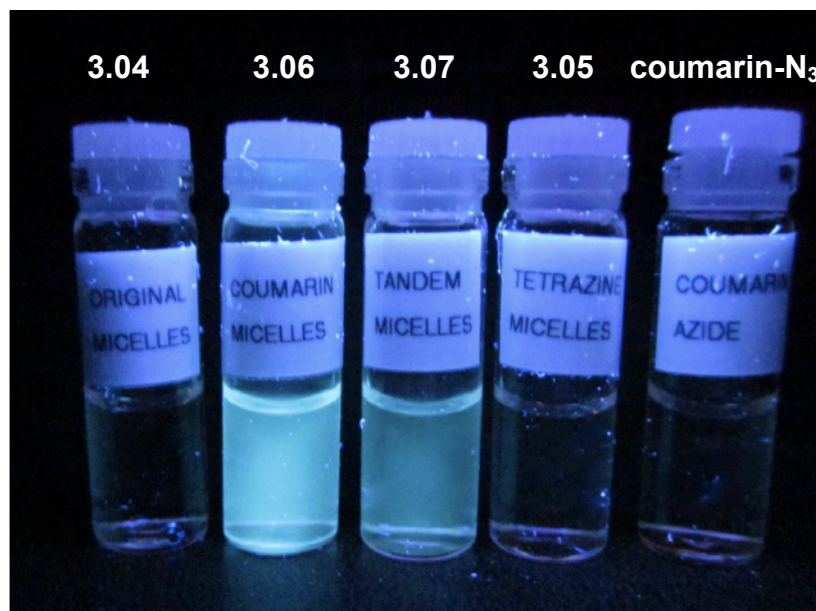


**Figure 3.21 Representative TEM images (top) and size histograms (bottom) of micelles 3.05 (left), 3.06 (centre) and 3.06 (right)**

### 3.3.5.3. *Fluorescence spectroscopy*

Fluorescence spectroscopy was used to assess the success of the CuAAC shell reaction with the pro-fluorescent coumarin. Micelles **3.06** were analysed by fluorescence spectroscopy, exciting at 340 nm, with a peak emission at 473 nm. Interestingly, the excitation and emission maxima found were different to the previously reported values. The closest of these to our current approach is where the coumarin azide was clicked into the core of a micelle<sup>20</sup> ( $\lambda_{\text{ex}} = 496 \text{ nm}$ ,  $\lambda_{\text{em}} = 551 \text{ nm}$ ). We hypothesise that this disparity in wavelengths is due to the difference in coumarin environment between the hydrophobic, styrenic core reported previously, and the hydrophilic micelle shell in this work. Difference in coumarin environment explains this

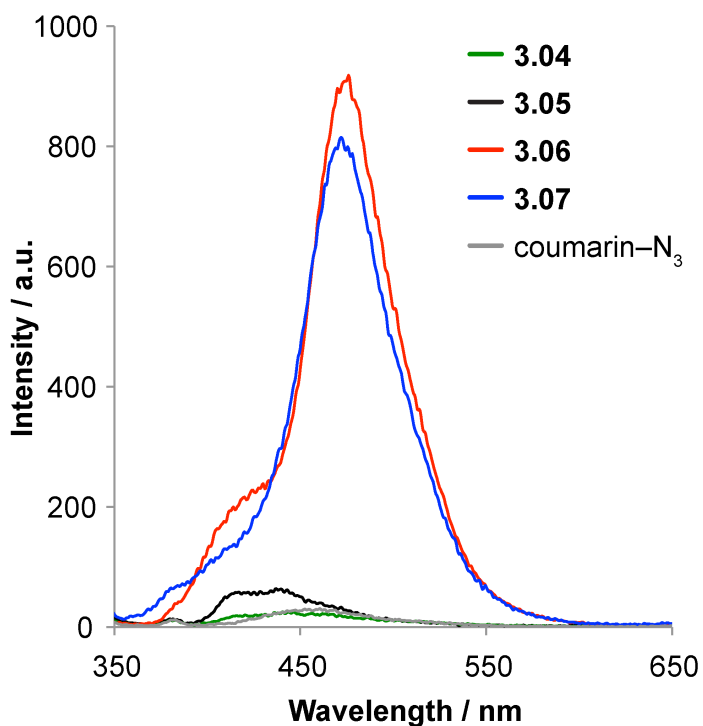
discrepancy rather than failure of the CuAAC reaction, which would result in no fluorescence rather than altered fluorescence properties. It should be noted that the fluorescence is not a quantitative measure of conversion of the CuAAC reaction; rather it was assumed to be 100% efficient as the reaction is so well-documented to be so. Fluorescence was observed by illumination under a hand-held lamp ( $\lambda_{\text{ex}} = 496 \text{ nm}$ ) shown in Figure 3.22; and also measured using a fluorometer to quantitatively judge the relative fluorescence of the shell-functionalised micelles **3.06** to the dual core-shell functionalised micelles **3.07**.



**Figure 3.22** Photograph of micelle solutions under a long wave UV lamp

Importantly, the fluorescence intensity of micelles **3.07** was almost the same as micelles **3.06** at the same dilution — all measurements were carried out at 12.5 nM relative to the (pro)-fluorescent moieties — thus showing that the CuAAC click reaction efficiency was not reduced by the subsequent addition of dipyriddy tetrazine for the core Tz–Nb reaction. Possible influence on the

fluorescence intensity by the core Tz–Nb was ruled out as core-functionalised micelles **3.05** did not have any significant fluorescence emission (Figure 3.23).



**Figure 3.23 Fluorescence emission spectra of micelles 3.04–3.07 and free coumarin-N<sub>3</sub>**

#### **3.3.5.4. ICP-MS**

In order to assess how effective the CupriSorb™ and dialysis was at removing the residual copper from the CuAAC reaction, ICP-MS was used. The micelle solutions were directly infused into the instrument at known concentrations and the copper content calculated with reference to four calibration points. The data were then corrected to a nominal micelle concentration of 1 mg/mL.



**Table 3.2 Approximate copper concentrations in micelle solutions at 1 mg/mL, obtained by ICP-MS**

Micelle	[Cu] / ppb
<b>3.04</b>	20
<b>3.05</b>	20
<b>3.06</b>	740
<b>3.07</b>	820

From these data it is evident that not all of the copper is removed by the purification methods employed — the initial copper concentration was 4.8 ppm — but the level remaining is relatively low (less than the 1.3 ppm upper limit set by the United States Environmental Protection Agency for drinking water).<sup>47</sup> Additionally, there was no significant difference in copper concentration between the shell-functionalised micelles **3.06** and dual-functionalised **3.07**, despite the presence of potentially copper-complexing pyradizines in **3.07** that could preclude efficient removal of the copper catalyst.

#### **3.3.5.5. SEC–UV/vis**

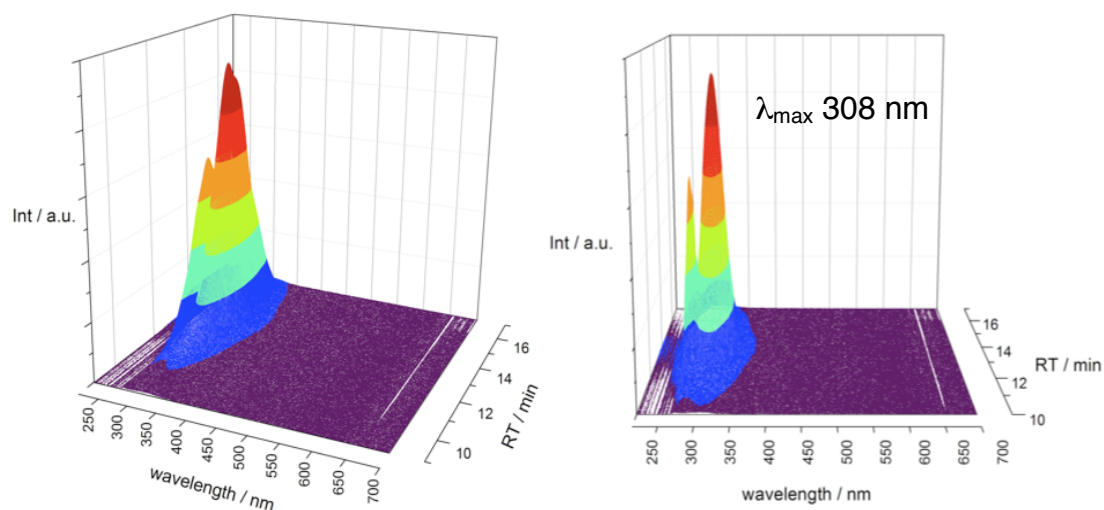
SEC analysis of the parent polymers from micelles **3.05**, **3.06** and **3.07** demonstrated little to no change in the polymer distributions, and slight increases in  $M_n$  relative to the original polymer (Table 3.3), concomitant with

the addition of several dipyridyl tetrazine and/or coumarin units along the backbone.

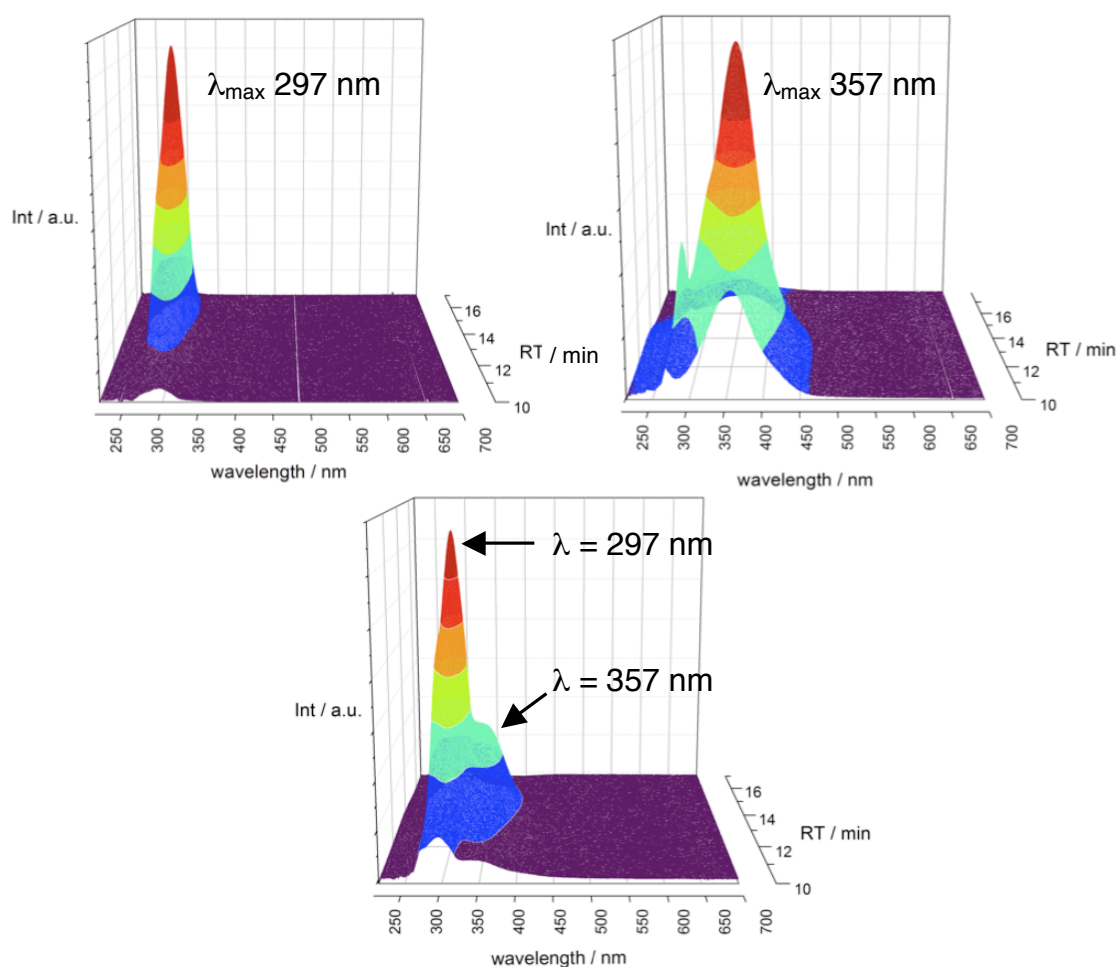
**Table 3.3 Properties of polymers obtained from freeze-dried micelles 3.04–3.07, obtained by SEC eluting in THF (2% TEA) and relative to PS standards**

Polymer from micelle	$M_n$ / kDa	$M_w/M_n$
<b>3.04</b>	14.9	1.71
<b>3.05</b>	15.6	1.76
<b>3.06</b>	15.3	1.76
<b>3.07</b>	15.6	1.79

The SEC used to analyse the polymers is coupled to an online photodiode array (PDA) detector to generate 2D SEC–UV/vis spectra. The spectrum generated from the parent polymer **3.03** (precursor to micelles **3.04**) is shown in Figure 3.24 from two different angles. It shows that the main peak in the UV/vis spectrum arising from the unfunctionalised micelle is at 308 nm (the absorbance is from the RAFT trithiocarbonate end group), and that the UV/vis spectrum is uniform across the molecular weight range of the polymer i.e. all polymer chains in the distribution contain a trithiocarbonate.



**Figure 3.24** Section of 2D SEC-UV/vis spectrum for polymer 3.03 from 200–700 nm in the wavelength domain and 11–17 minutes retention time in the SEC elution time domain



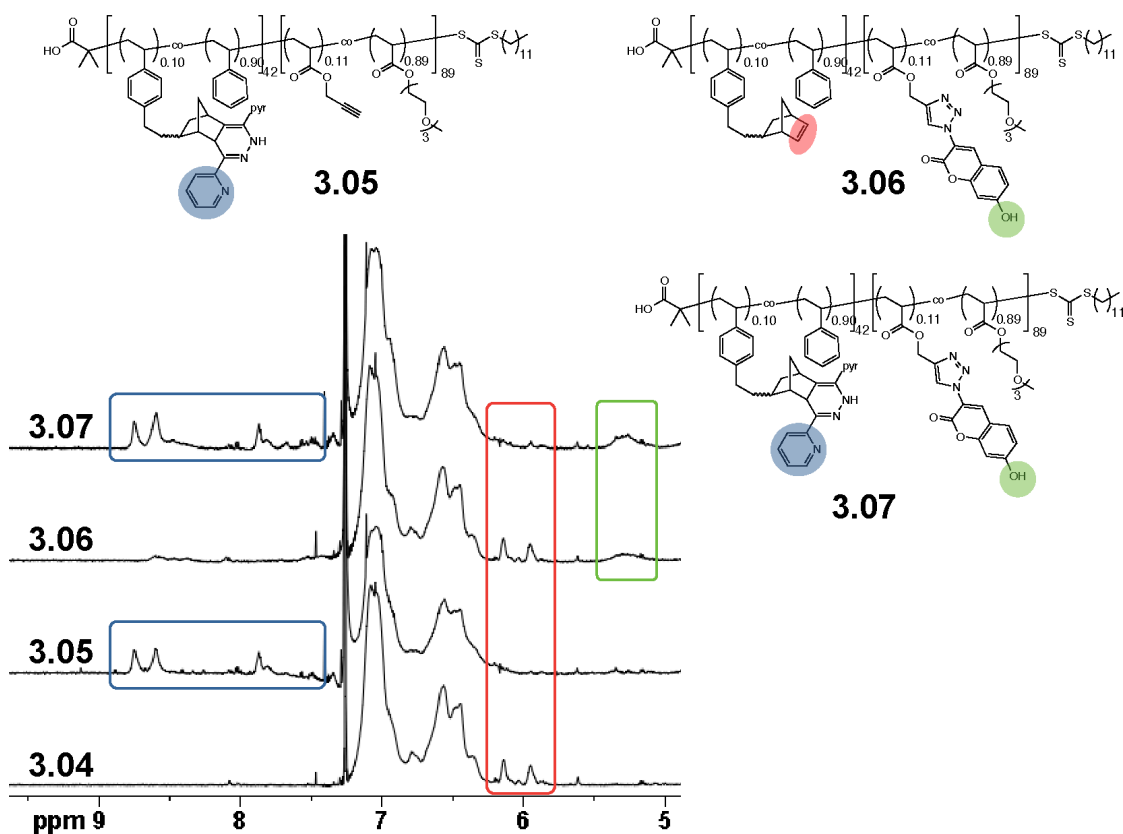
**Figure 3.25** Section of 2D SEC-UV/vis spectrum for freeze-dried micelles 3.05 (top left), 3.06 (top right) and 3.07 (bottom)

Extracting the UV/vis spectra for freeze-dried micelles **3.05**, **3.06** and **3.07** (Figure 3.25) showed that the spectrum resulting from the Tz–Nb reaction had a  $\lambda_{\text{max}}$  at 297 nm, and the CuAAC-clicked coumarin had a  $\lambda_{\text{max}}$  at 357 nm. Both peaks were present in the UV/vis spectrum of freeze-dried micelles **3.07**, showing that both reactions had taken place.

#### **3.3.5.1. $^1\text{H}$ NMR Spectroscopy**

In the  $^1\text{H}$  NMR spectrum (in  $\text{CDCl}_3$ ) of freeze-dried micelles **3.05** (Figure 3.26), complete disappearance of the norbornene alkene at 6.0 ppm was observed, with new signals corresponding to the pendant pyridine groups of the clicked tetrazine, indicating complete functionalisation of the core norbornene moieties in the micelle.

In the  $^1\text{H}$  NMR spectrum of freeze-dried micelles **3.06**, the complete disappearance of the alkyne signal at 2.5 ppm was difficult to confirm due to significant overlap with the polymer backbone and Nb–St signals; reduction in the signal was observed but 100% conversion of alkyne to triazole was unable to be categorically ascertained using only the alkyne proton signal. However, the integral of the aromatic region increased relative to the starting polymer **3.03** due to the aromatic coumarin protons. Importantly, the Nb alkene signals at 6 ppm were still clearly present, indicating that the CuAAC reaction in the shell left the core norbornene moieties unaffected.



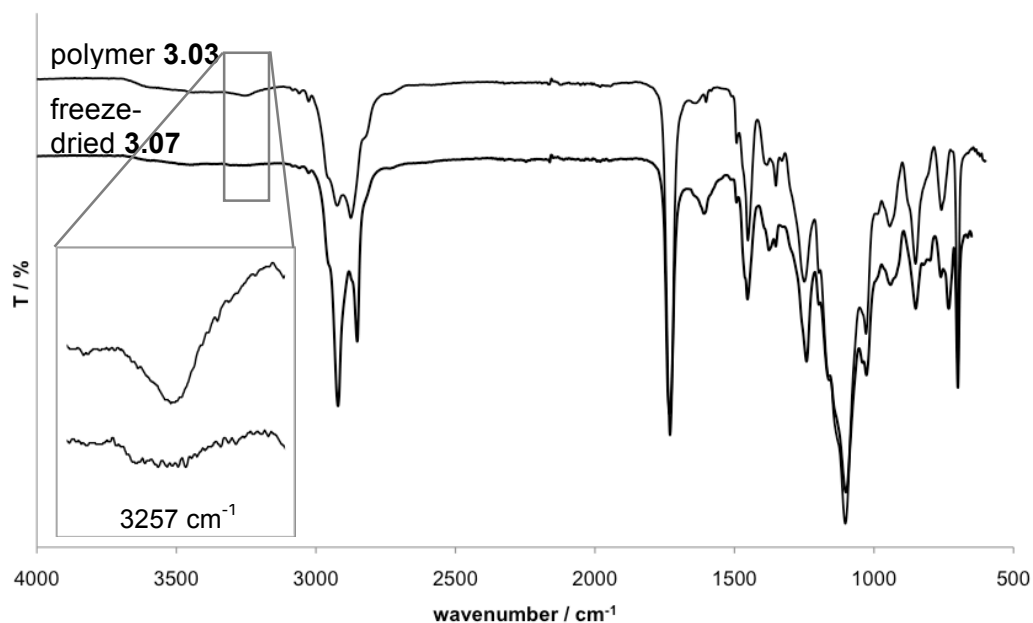
**Figure 3.26** Section of  $^1\text{H}$  NMR spectra ( $\text{CDCl}_3$ ) for polymers isolated by freeze-drying micelles **3.04–3.07**

However, in the  $^1\text{H}$  NMR spectrum of freeze-dried micelles **3.05** and **3.07**, the Nb signal is completely consumed (highlighted by the red box in Figure 3.26). Signals from the clicked dipyridyl tetrazine (blue boxes) are evident in the spectra of **3.05** and **3.07**, and coumarin hydroxyl proton signals (green box) are evident in the spectra of **3.06** and **3.07**.

#### **3.3.5.1. FT-IR**

FT-IR was employed as a means of assessing whether all of the terminal alkyne moieties in the micelle shell had been consumed in the reactions to

form micelles **3.06** and **3.07**. The characteristic alkyne C–H stretch seen in the parent polymer **3.03** at  $3257\text{ cm}^{-1}$  was no longer present in the IR spectrum of freeze-dried **3.07** (Figure 3.27). This evidence, coupled with the fluorescence spectroscopy described above, shows that performing dual functionalisation in a one-pot process does not hinder the shell CuAAC reaction.



**Figure 3.27** FT-IR spectra of parent polymer **3.03** and freeze-dried micelles **3.07**

### **3.4. Conclusions**

We have shown that a single micellar scaffold can be both core- and shell-functionalised in a one-pot process using two orthogonal click reactions. This opens up the potential for functionalisation with a large array of water-soluble azide-bearing compounds for the shell, and hydrophobic tetrazine-bearing compounds for the core. Azides are undemanding to introduce during synthesis, and the increasing array of tetrazines containing functional handles<sup>48</sup> means that potentially any target of interest could be azide- or tetrazine-functionalised and therefore introduced into the micelle in either the core or shell domains. The two reactions occur highly efficiently in a one-pot process with only a slight excess of small molecule reagent, thus significantly reducing the preparation and purification time of functionalised micelles.

### 3.5. Experimental

#### 3.5.1. Materials and methods

All chemicals and reagents were purchased from Sigma-Aldrich and used without further purification unless otherwise stated. Styrene (St) was distilled over  $\text{CaH}_2$ , 2,2'-Azobis(2-methylpropionitrile) (AIBN) was recrystallised twice from methanol and both were stored at 4 °C in the dark before use. 2-azidoacetic acid and tris(hydroxypropyl)triazolylmethyl-amine (THPTA) was synthesised by Diluar Khan,<sup>49</sup> tetrahydropyranyl acrylate (THPA) was synthesised by Kay Doncom<sup>50</sup> and tri(ethylene glycol) acrylate (TEGA) was synthesised by Nikos Petzetakis,<sup>51</sup> all according to published procedures. 2-azidoacetic acid, PA-TMS and TEGA were stored at -20 °C in the dark prior to use. SpectraPor dialysis tubing was purchased from Spectrum Labs, with a molecular weight cut-off of 6–8 kDa. Seachem Cuprisorb™ (a copper-absorbing resin used to halt CuAAC reactions) was purchased from Warehouse Aquatics (UK).

$^1\text{H}$  and  $^{13}\text{C}$  NMR spectra were recorded at 400 or 500 MHz in  $\text{CDCl}_3$  or  $\text{DMSO}-d_6$  solution on a Bruker DPX-400 or DRX-500 spectrometer at 20 °C. Chemical shifts are reported as  $\delta$  in parts per million (ppm) and referenced to the chemical shift of the residual solvent resonances. The resonance multiplicities are described as s (singlet), d (doublet), t (triplet), q (quartet) or m (multiplet).

Molar mass distributions were measured using size exclusion chromatography (SEC). Analyses were performed in HPLC grade THF containing 2 vol% triethyl amine (TEA) at 30 °C, at a flow rate of 1.0 mL/min on a set of two



PLgel 5  $\mu\text{m}$  Mixed-D columns and one PLgel 5  $\mu\text{m}$  guard column with differential refractive index detection. Polystyrene or poly(methyl methacrylate) standards were used for calibration, samples were injected using a PL AS RT autosampler and molecular weight and dispersity indices determined using Cirrus software. A Shimadzu SPD-M20A prominence diode array (PDA) detector was also coupled to the SEC system and used to extract UV/vis spectra for the synthesised polymers. These data were analysed using LC Solution software.

FT-IR spectra were obtained using a Perkin Elmer Spectrum 100 FT-IR. 16 scans from 600 to 4000  $\text{cm}^{-1}$  were taken, and the spectra corrected for background absorbance.

UV/vis measurements were made on a Perkin Elmer Lambda 35 UV/vis spectrometer. Far UV quartz cuvettes (Hellma) were used, and the progress of tetrazine–norbornene reactions was monitored using the Timedrive function, monitoring at 546 nm. The temperature was maintained at 20 °C using a PTP-1+1 Peltier temperature programmer and stirring system, and a PCB 1500 water system. The raw data were normalised to remove the effect of background absorbance from the pure micelle solution. Due to the very low concentrations used, the data were smoothed in Origin Pro 5.1 over 50 points using the Savitzky-Golay function, using a polynomial of order 2, before the first derivative of the resulting curve was calculated.

Hydrodynamic diameters ( $D_h$ ) and size distributions of micelles were determined by DLS on a Malvern Zetasizer Nano ZS operating at 20 °C with a 4 mW He-Ne 633 nm laser module. Samples were filtered through a 0.45  $\mu\text{m}$

nylon filter prior to measurement and disposable plastic sizing cuvettes were used. Measurements were made at a detection angle of 173° (back scattering), and the data analysed using Malvern DTS 5.02 software, using the multiple narrow modes setting. All measurements were made in triplicate, with 10 runs per measurement.

TEM analyses were performed on a JEOL 2011 (LaB<sub>6</sub>) microscope operating at 200 kV, equipped with a GATAN UltraScan 1000 digital camera. Conventional bright field conditions were used to image samples in all cases. TEM grids used were lacey carbon-coated copper grids (Agar Scientific, 400 mesh, S116-4) coated with a thin layer of graphene oxide. Micelle solutions were diluted to 1 mg/mL before 4 µL of each sample was drop-deposited onto the graphene oxide-coated grids and allowed to air dry. No subsequent staining or treatment of the grids was required prior to imaging the samples.<sup>44</sup> Images were analysed using ImageJ software, and a minimum of 100 particles were measured to produce a mean and standard deviation for the particle size ( $D_{av}$ ).

Fluorescence spectra were obtained using a single-beam Perkin-Elmer LS55 fluorometer, using a slit width of 5.0 nm and exciting at 340 nm. Samples were diluted to 12.5 nM with respect to the (pro-)fluorescent group prior to measurement. Emission spectra were collected between 350 and 650 nm.

Residual copper in the micelle solutions was analysed using an Agilent 7500 Series ICP-MS instrument. 4 calibration standards were used as a basic calibration curve for comparison to the micelle solutions, and solutions in water at 0.1 mg/mL were directly infused into the instrument. Results obtained after

calibration were then corrected to give the concentration of copper (in ppb) for a nominal micelle concentration of 1 mg/mL.

### 3.5.2. Competition reactions

3,6-Di-2-pyridyl-1,2,4,5-tetrazine (14.2 mg, 0.0600 mmol) and propargyl chloride (4.48 mg, 0.0600 mmol) were dissolved in CDCl<sub>3</sub> (1.2 mL) and stirred at room temperature for 30 min before a <sup>1</sup>H NMR spectrum was taken. The experiment was repeated with the addition of norbornene (5.65 mg, 0.0600 mmol).

5-Norbornene-2-*endo*,3-*endo*-dimethanol (15.4 mg, 0.100 mmol), 2-azidoacetic acid (10.1 mg, 0.100 mmol), copper sulfate pentahydrate (4.99 mg, 0.0200 mmol), THPTA (8.69 mg, 0.0200 mmol) were dissolved in D<sub>2</sub>O (2 mL), followed by the addition of (+)-sodium L-ascorbate (7.92 mg, 0.0400 mmol). The reaction mixture was stirred at room temperature for 30 min, after which Cuprisorb<sup>TM</sup> was added to scavenge the copper, and a <sup>1</sup>H NMR spectrum was taken. The experiment was repeated with the addition of propargyl alcohol (5.61 mg, 0.100 mmol).

### 3.5.3. Syntheses

#### 3.5.3.1. *p*-norbornenylethylstyrene (Nb–St monomer)

A literature method was followed for the preparation of Nb–Br<sup>52</sup> as a precursor to Nb–St.<sup>26a</sup> Dicyclopentadiene (40 mL, 0.597 mol), allyl bromide (124 mL, 1.43 mol) and hydroquinone (0.394 g, 3.58 mmol) were placed in an oven-

dried tightly sealed flask and heated to 170 °C overnight. Excess allyl bromide was removed *in vacuo* (b.p. 71 °C), and the resulting norbornene bromide (Nb–Br) purified by distillation under reduced pressure twice (99.0 g).

Magnesium turnings (5.00 g, 0.205 mol) were placed in a dry round-bottomed flask under nitrogen, and dry THF (50 mL) added *via* cannula. Nb–Br (28.5 g, 0.152 mol) was added dropwise at 0 °C, before the mixture was warmed slowly to 40 °C and heated overnight. The as-formed Grignard reagent was transferred by cannula to a mixture of 4-chloromethylstyrene (18.6 g, 0.122 mol), Li<sub>2</sub>CuCl<sub>4</sub> (0.334 g, 1.52 mmol) in THF (50 mL) under nitrogen at -78 °C. The reaction mixture was warmed to room temperature and stirred overnight, before being quenched using saturated NH<sub>4</sub>Cl solution. The mixture was extracted with diethyl ether (2 x 100 mL), washed with water, saturated NaHSO<sub>4</sub>, brine (all 100 mL) and dried over MgSO<sub>4</sub>. The monomer was purified by flash column chromatography eluting with petroleum ether 40–60 °C (15.0 g, 66.9 mmol, 44% yield, R<sub>f</sub> 0.45). <sup>1</sup>H NMR (CDCl<sub>3</sub>, 400 MHz, *endo* isomer only) δ (ppm): 7.37 (2H, d, <sup>3</sup>J<sub>H-H</sub> = 8.1 Hz), 7.18 (2H, d, <sup>3</sup>J<sub>H-H</sub> = 8.1 Hz), 6.75 (1H, dd, <sup>3</sup>J<sub>H-H</sub> = 17.6, <sup>3</sup>J<sub>H-H</sub> = 10.8 Hz), 6.00–6.19 (2H, m), 5.75 (1H, d, <sup>3</sup>J<sub>H-H</sub> = 17.6 Hz), 5.24 (1H, d, <sup>3</sup>J<sub>H-H</sub> = 10.8 Hz), 2.84 (2H, d, <sup>3</sup>J<sub>H-H</sub> = 14.8 Hz), 2.64 (2H, d, <sup>3</sup>J<sub>H-H</sub> = 7.9 Hz), 2.04–2.09 (1H, m), 1.92 (1H, m), 1.40–1.54 (3H, m), 1.28 (1H, d, <sup>3</sup>J<sub>H-H</sub> = 8.0 Hz), 0.57 (1H, m). <sup>13</sup>C NMR (CDCl<sub>3</sub>, 100 MHz, *endo* isomer only) δ (ppm): 142.9, 137.2, 136.9, 135.2, 132.4, 128.6, 126.2, 112.9, 49.7, 45.4, 42.7, 38.5, 36.8, 34.8, 32.5.

### 3.5.3.2. 3-(trimethylsilyl)prop-2-ynyl acrylate (PA–TMS)

Synthesis of PA–TMS was carried out according to a literature precedent.<sup>39</sup>

AgCl (1.95 g, 13.6 mmol) was suspended in dry CH<sub>2</sub>Cl<sub>2</sub> (150 mL) under

nitrogen, and propargyl acrylate (15.0 g, 0.136 mol) and 1,8-diazabicyclo[5.4.0]undec-7-ene (21.8 g, 0.143 mol) added. The mixture was heated to 40 °C for 24 h, after which the CH<sub>2</sub>Cl<sub>2</sub> was removed *in vacuo* and the product purified by flash column chromatography, eluting with 25:1 petroleum ether 40–60 °C/diethyl ether (12.7 g, 69.8 mmol, 51% yield). <sup>1</sup>H NMR (CDCl<sub>3</sub>, 400 MHz) δ (ppm): 6.44 (1H, dd, <sup>3</sup>J<sub>H-H</sub> = 17.3 Hz, <sup>2</sup>J<sub>H-H</sub> = 1.4 Hz), 6.13 (1H, dd, <sup>3</sup>J<sub>H-H</sub> = 17.3 Hz, <sup>3</sup>J<sub>H-H</sub> = 10.5 Hz), 4.74 (2H, dd, <sup>3</sup>J<sub>H-H</sub> = 10.5 Hz, <sup>2</sup>J<sub>H-H</sub> = 1.4 Hz), (2H, s), 0.16 (9H, s). <sup>13</sup>C NMR (CDCl<sub>3</sub>, 100 MHz) δ (ppm): 165.4, 131.7, 127.8, 99.0, 92.3, 52.9, -0.2.

### 3.5.3.3. 3-azido-7-hydroxy-chromen-2-one (coumarin–N<sub>3</sub>)

Coumarin–N<sub>3</sub> was synthesised according to the method of Wang *et. al.*<sup>53</sup> 2,4-Dihydroxybenzaldehyde (2.76 g, 20.0 mmol), *N*-acetyl glycine (2.34 g, 20.0 mmol) and sodium acetate (4.92 g, 60.0 mmol) were added to acetic anhydride (100 mL) and the mixture heated to reflux for 4 h. After cooling, the reaction mixture was poured onto ice water, the solid isolated by filtration and washed with further portions of ice water. The yellow precipitate collected was used without further characterisation or purification. Ice water (40 mL) was added, followed by sodium nitrite (2.76 g, 40.0 mmol), with cooling in an ice bath. After 10 minutes of stirring, sodium azide (3.90 g, 60.0 mmol) was added slowly, followed by stirring for a further 15 min. The obtained precipitate was isolated by filtration and dried *in vacuo* (0.608 g, 2.93 mmol, 16% yield). <sup>1</sup>H NMR (DMSO-d<sub>6</sub>, 400 MHz) δ (ppm): 10.5 (1H, s), 7.59 (1H, s), 7.47 (1H, d, <sup>3</sup>J<sub>H-H</sub> = 8.4 Hz), 6.80 (1H, d, <sup>3</sup>J<sub>H-H</sub> = 8.4 Hz), 6.76 (1H, s). <sup>13</sup>C NMR (DMSO-d<sub>6</sub>,

400 MHz)  $\delta$  (ppm): 160.3, 157.3, 152.8, 129.1, 127.8, 121.1, 113.8, 111.3, 102.0.

#### **3.5.3.4. PS(Nb) copolymer 3.01**

In an analogous manner to literature precedent,<sup>26a</sup> styrene (2.92 g, 28.1 mmol), Nb–St (0.700 g, 3.12 mmol), DDMAT (0.114 g, 0.312 mmol) and AIBN (5.12 mg, 0.0312 mmol) were dissolved in toluene (3.5 mL) and subjected to four freeze-evacuate-thaw cycles. The polymerisation ampoule was warmed to room temperature under nitrogen and then immersed in an oil bath at 70 °C for 23 h. Monomer conversions were determined by <sup>1</sup>H NMR spectroscopy to be 29% and 26% for St and Nb–St respectively. The polymer was precipitated 3 times from cold methanol and 3 times from cold pentane before being freeze dried from dioxane and recovered as a yellow powdery solid (1.51 g).  $M_n^{NMR}$  5.2 kDa,  $DP_{St}$  38,  $DP_{Nb-St}$  4;  $M_n^{SEC}$  (eluting in THF, relative to St standards) 4.1 kDa,  $M_w/M_n$  1.13. <sup>1</sup>H NMR (CDCl<sub>3</sub>, 400MHz)  $\delta$  (ppm): 7.25–6.25 (5H<sub>St</sub> + 4H<sub>Nb-St</sub>), 6.2–5.9 (2H<sub>Nb alkene</sub>), 3.25 (2H<sub>end group</sub>), 2.9–2.7 (2H<sub>Nb-St</sub>), 2.7–1.1 (3H<sub>backbone</sub> + 6H<sub>Nb-St</sub> + 26H<sub>end group</sub>), 1.0–0.8 (2H<sub>Nb-St</sub> + 3H<sub>end group</sub>), 0.65–0.45 (1H<sub>endo Nb-St</sub>). IR  $\nu$  (cm<sup>-1</sup>): 3060, 3026, 2924, 2853, 1511, 1452, 757, 697.

#### **3.5.3.5. PS(Nb)-TEGA(PA–TMS) block copolymer 3.02**

**1** (0.200 g, 0.0488 mmol), TEGA (2.10 g, 9.64 mmol), PA–TMS (0.195 g, 1.07 mmol) and AIBN (0.801 mg, 0.00488 mmol) were dissolved in DMF (5 mL) and subjected to four freeze-evacuate-thaw cycles. The polymerisation ampoule was warmed to room temperature, backfilled with nitrogen and then immersed in an oil bath at 70 °C for 9 h. Monomer conversions were

determined to be 32% and 30% for PA-TMS and TEGA respectively. The polymer was precipitated 3 times from cold petroleum ether 40–60 °C/diethyl ether (10:1) before being dried *in vacuo* and recovered as a yellow gummy solid (747 mg).  $M_n^{\text{NMR}}$  24.3 kDa,  $DP_{\text{TEGA}}$  79,  $DP_{\text{PA-TMS}}$  10;  $M_n^{\text{SEC}}$  (eluting in THF, relative to PS standards) 14.5 kDa,  $M_w/M_n$  1.71.  $^1\text{H}$  NMR ( $\text{CDCl}_3$ , 400 MHz)  $\delta$  (ppm): 7.25–6.25 ( $5\text{H}_{\text{St}} + 4\text{H}_{\text{Nb-St}}$ ), 6.2–5.9 ( $2\text{H}_{\text{Nb alkene}}$ ), 4.7–4.5 ( $2\text{H}_{\text{PA-TMS}}$ ), 4.4–3.9 ( $2\text{H}_{\text{TEGA}}$ ), 3.80–3.55 ( $8\text{H}_{\text{TEGA}}$ ), 3.55–3.48 ( $3\text{H}_{\text{TEGA}}$ ), 3.18 ( $2\text{H}_{\text{end group}}$ ), 2.9–2.7 ( $2\text{H}_{\text{Nb-St}}$ ), 2.7–1.1 ( $3\text{H}_{\text{backbone}} + 6\text{H}_{\text{Nb-St}} + 26\text{H}_{\text{end group}}$ ), 1.0–0.8 ( $2\text{H}_{\text{Nb-St}} + 3\text{H}_{\text{end group}}$ ), 0.65–0.45 ( $1\text{H}_{\text{endo Nb-St}}$ ), 0.35–0.0 ( $9\text{H}_{\text{PA-TMS}}$ ). IR  $\nu$  ( $\text{cm}^{-1}$ ): 3036–2801, 1731, 1452, 1250, 1198, 1163, 1103, 1029, 944, 846, 761, 700.

### 3.5.3.6. ***PS(Nb)-TEGA(PA) block copolymer 3.03***

Deprotection of the TMS groups was carried out according to the method of Haddleton *et. al.*<sup>40</sup> Polymer **3.02** (0.500 g, 0.0206 mmol) was dissolved in THF (30 mL) and acetic acid (16.5  $\mu\text{L}$ , 0.288 mmol) added. Nitrogen was bubbled through to degas the solution for 30 minutes, after which it was cooled to -20 °C and TBAF (288  $\mu\text{L}$ , 0.288 mmol) was added slowly over 2 minutes. The mixture was allowed to stir at -20 °C for 30 minutes, then warmed to room temperature and stirred for a further 24 h. The solution was filtered through a short silica gel column, the solvent removed and the polymer isolated as a yellow gummy solid by precipitation from cold petroleum ether 40–60 °C twice (482 mg, 99% yield).  $M_n^{\text{NMR}}$  23.6 kDa,  $DP_{\text{TEGA}}$  79,  $DP_{\text{PA}}$  10;  $M_n^{\text{SEC}}$  (eluting in THF, relative to PS standards) 14.9 kDa,  $M_w/M_n$  1.71. UV/vis  $\lambda_{\text{max}}$  307 nm.  $^1\text{H}$  NMR ( $\text{CDCl}_3$ , 400 MHz)  $\delta$  (ppm): 7.25–6.25 ( $5\text{H}_{\text{St}} + 4\text{H}_{\text{Nb-St}}$ ), 6.2–5.9 ( $2\text{H}_{\text{Nb alkene}}$ ), 4.75–4.55 ( $2\text{H}_{\text{PA}}$ ), 4.4–3.9 ( $2\text{H}_{\text{TEGA}}$ ), 3.80–3.55 ( $8\text{H}_{\text{TEGA}}$ ), 3.55–3.48

( $3H_{\text{TEGA}}$ ), 3.18 ( $2H_{\text{end group}}$ ), 2.9–2.7 ( $2H_{\text{Nb-St}}$ ), 2.7–1.1 ( $3H_{\text{backbone}} + H_{\text{PA}} + 6H_{\text{Nb-St}} + 26H_{\text{end group}}$ ), 1.0–0.8 ( $2H_{\text{Nb-St}} + 3H_{\text{end group}}$ ), 0.65–0.45 ( $1H_{\text{endo Nb-St}}$ ). IR  $\nu$  ( $\text{cm}^{-1}$ ): 3257, 3036–2801, 1731, 1452, 1250, 1198, 1163, 1103, 1029, 944, 846, 761, 700.

### 3.5.3.7. *Formation of micelles 3.04*

Polymer **3.03** (162 mg, 0.00686 mmol), was dissolved in THF (10 mL) with vigorous stirring.  $18.2 \text{ M}\Omega\text{cm}^{-1}$  Type I water (20 mL) was added slowly over 18 h using a peristaltic pump, after which the micelle solution was exhaustively dialysed (6–8 kDa MWCO) against  $18.2 \text{ M}\Omega\text{cm}^{-1}$  Type I water to remove traces of THF. The final volume was 53 mL, giving a concentration of ca. 3 mg/mL.  $D_{\text{h}}^{\text{int}}$   $36.7 \pm 4.9 \text{ nm}$ ,  $D_{\text{h}}^{\text{vol}}$   $32.5 \pm 3.8 \text{ nm}$ ,  $D_{\text{h}}^{\text{num}}$   $29.4 \pm 3.0 \text{ nm}$ . TEM  $D_{\text{av}} = 29.9 \pm 6.9 \text{ nm}$ .

## 3.5.4. **Micelle reactions**

### 3.5.4.1. *Tz–Nb reaction in core (micelles 3.05)*

To **3.04** (7 mL) was added dipyrindyl tetrazine (1.05 mg, 0.00445 mmol, 1.2 eq. relative to number of Nb units) in THF (200  $\mu\text{L}$ ). The mixture was stirred at room temperature for 9 h, before being dialysed (6–8 kDa MWCO) against a gradient of 10% THF in  $18.2 \text{ M}\Omega\text{cm}^{-1}$  Type I water to 100%  $18.2 \text{ M}\Omega\text{cm}^{-1}$  Type I water.  $D_{\text{h}}^{\text{int}}$   $34.9 \pm 4.2 \text{ nm}$ ,  $D_{\text{h}}^{\text{vol}}$   $30.0 \pm 3.8 \text{ nm}$ ,  $D_{\text{h}}^{\text{num}}$   $26.5 \pm 2.9 \text{ nm}$ . TEM  $D_{\text{av}} = 30.1 \pm 6.2 \text{ nm}$ .



The same experiment was carried out in the UV/vis machine to monitor reaction progress, but on a scale whereby 2 mL of **3.04** and dipyridyl tetrazine (0.300 mg, 0.00127 mmol) in 60  $\mu$ L THF was added.

A portion of the micelles **3.05** (3.5 mL) were freeze-dried and the resulting polymer analysed by  $^1\text{H}$  NMR spectroscopy and SEC.  $M_n^{\text{SEC}}$  (eluting in THF, relative to PS standards) 15.6 kDa,  $M_w/M_n$  1.71. UV/vis  $\lambda_{\text{max}}$  297 nm.  $^1\text{H}$  NMR ( $\text{CDCl}_3$ )  $\delta$  (ppm): 9.29–7.66 ( $8\text{H}_{\text{pyridyl}}$ ), 7.25–6.25 ( $5\text{H}_{\text{St}}$  +  $4\text{H}_{\text{Nb-St-Tz}}$ ), 4.75–4.55 ( $2\text{H}_{\text{PA}}$ ), 4.4–3.9 ( $2\text{H}_{\text{TEGA}}$ ), 3.80–3.55 ( $8\text{H}_{\text{TEGA}}$ ), 3.55–3.48 ( $3\text{H}_{\text{TEGA}}$ ), 3.18 ( $2\text{H}_{\text{end group}}$ ), 2.7–1.1 ( $3\text{H}_{\text{backbone}}$  +  $\text{H}_{\text{PA}}$  +  $12\text{H}_{\text{Nb-St-Tz}}$  +  $26\text{H}_{\text{end group}}$ ), 0.81 (t,  $3\text{H}_{\text{end group}}$ ).

#### 3.5.4.2. CuAAC reaction in shell (micelles 3.06)

A solution of coumarin- $\text{N}_3$  (2.21 mg, 0.0107 mmol, 1.2 eq relative to alkynyl functionality), copper sulfate pentahydrate (0.133 mg, 0.00053 mmol) sodium L-ascorbate (0.212 mg, 0.00107 mmol) and THPTA (0.232 mg, 0.00053 mmol) in water (500  $\mu$ L) was added to **3.04** (7 mL) and stirred at room temperature for 3 h. Cuprisorb<sup>TM</sup> was added to stop the reaction and stirring was continued for 15 minutes, after which the Cuprisorb<sup>TM</sup> was removed by filtration and the solution exhaustively dialysed (6–8 kDa MWCO) against  $18.2\text{ M}\Omega\text{cm}^{-1}$  Type I water.  $D_h^{\text{int}}$   $39.0 \pm 4.9\text{ nm}$ ,  $D_h^{\text{vol}}$   $32.8 \pm 4.4\text{ nm}$ ,  $D_h^{\text{num}}$   $28.3 \pm 3.4\text{ nm}$ . TEM  $D_{\text{av}} = 33.3 \pm 6.4\text{ nm}$ . Fluorescence emission  $\lambda_{\text{max}}$  473 nm, excitation at 340 nm.

A portion of the micelles **3.06** (3.5 mL) were freeze-dried and the resulting polymer analysed by  $^1\text{H}$  NMR spectroscopy and SEC.  $M_n^{\text{SEC}}$  (eluting in THF, relative to PS standards) 15.3 kDa,  $M_w/M_n$  1.75. UV/vis  $\lambda_{\text{max}}$  357 nm.  $^1\text{H}$  NMR ( $\text{CDCl}_3$ )  $\delta$  (ppm): 7.25–6.25 ( $5\text{H}_{\text{St}}$  +  $4\text{H}_{\text{Nb-St}}$  +  $5\text{H}_{\text{coumarin}}$ ), 6.2–5.9 ( $2\text{H}_{\text{Nb alkene}}$ ), 5.4–5.0 (br,  $\text{H}_{\text{coumarin-OH}}$ ), 4.75–4.55 ( $2\text{H}_{\text{PA}}$ ), 4.4–3.9 ( $2\text{H}_{\text{TEGA}}$ ), 3.80–3.55

(8H<sub>TEGA</sub>), 3.55–3.48 (3H<sub>TEGA</sub>), 3.18 (2H<sub>end group</sub>), 2.9–2.7 (2H<sub>Nb–St</sub>), 2.7–1.1 (3H<sub>backbone</sub> + 6H<sub>Nb–St</sub> + 26H<sub>end group</sub>), 1.0–0.8 (2H<sub>Nb–St</sub> + 3H<sub>end group</sub>), 0.65–0.45 (1H<sub>endo Nb–St</sub>).

#### 3.5.4.3. Tandem orthogonal reaction (micelles 3.07)

Dipyridyl tetrazine (1.05 mg, 0.00445 mmol) in THF (200 µL), and coumarin–N<sub>3</sub> (2.21 mg, 0.0107 mmol), copper sulfate pentahydrate (0.133 mg, 0.00053 mmol), sodium L-ascorbate (0.212 mg, 0.00107 mmol), THPTA (0.232 mg, 0.00053 mmol) in water (500 µL) were added to **3.04** (7 mL). The solution was stirred at room temperature for 16 h before Cuprisorb™ was added to mop up any remaining copper. The Cuprisorb™ was removed by filtration, and the micelle solution exhaustively dialysed (6–8 kDa MWCO) against a gradient of 10% THF in 18.2 MΩcm<sup>-1</sup> Type I water to 100% 18.2 MΩcm<sup>-1</sup> Type I water.  $D_h^{int}$  31.0 ± 2.7 nm,  $D_h^{vol}$  28.7 ± 2.8 nm,  $D_h^{num}$  26.6 ± 2.5 nm. TEM  $D_{av}$  = 30.3 ± 7.5 nm. Fluorescence emission  $\lambda_{max}$  472 nm, excitation at 340 nm.

A portion of the micelles **3.07** (3.5 mL) were freeze-dried and the resulting polymer analysed by <sup>1</sup>H NMR spectroscopy and SEC.  $M_n^{SEC}$  (eluting in THF, relative to PS standards) 15.6 kDa,  $M_w/M_n$  1.79. UV/vis  $\lambda_{max}$  297 nm. <sup>1</sup>H NMR (CDCl<sub>3</sub>)  $\delta$  (ppm): 9.29–7.66 (8H<sub>pyridyl</sub>), 7.25–6.25 (5H<sub>St</sub> + 4H<sub>Nb–St–Tz</sub> + 5H<sub>coumarin</sub>), 5.4–5.0 (br, H<sub>coumarin–OH</sub>), 4.75–4.55 (2H<sub>PA</sub>), 4.4–3.9 (2H<sub>TEGA</sub>), 3.80–3.55 (8H<sub>TEGA</sub>), 3.55–3.48 (3H<sub>TEGA</sub>), 3.18 (2H<sub>end group</sub>), 2.7–1.1 (3H<sub>backbone</sub> + 12H<sub>Nb–St–Tz</sub> + 26H<sub>end group</sub>), 0.81 (t, 3H<sub>end group</sub>).

### 3.6. References

- (1) Blanz, A.; Armes, S. P.; Ryan, A. J. *Macromol. Rapid Comm.* **2009**, *30*, 267-277.
- (2) Discher, B. M.; Won, Y.-Y.; Ege, D. S.; Lee, J. C.-M.; Bates, F. S.; Discher, D. E.; Hammer, D. A. *Science* **1999**, *284*, 1143-1146.
- (3) Dwars, T.; Paetzold, E. *Angew. Chem., Int. Ed.* **2005**, *44*, 7174-7199.
- (4) Elsabahy, M.; Wooley, K. L. *Chem. Soc. Rev.* **2012**, *41*, 2545-2561.
- (5) Joralemon, M. J.; Murthy, K. S.; Remsen, E. E.; Becker, M. L.; Wooley, K. L. *Biomacromolecules* **2004**, *5*, 903-913.
- (6) Becker, M. L.; Liu, J.; Wooley, K. L. *Biomacromolecules* **2005**, *6*, 220-228.
- (7) Joralemon, M. J.; Smith, N. L.; Holowka, D.; Baird, B.; Wooley, K. L. *Bioconjugate Chem.* **2005**, *16*, 1246-1256.
- (8) (a) Pressly, E. D.; Rossin, R.; Hagooly, A.; Fukukawa, K.-i.; Messmore, B. W.; Welch, M. J.; Wooley, K. L.; Lamm, M. S.; Hule, R. A.; Pochan, D. J.; Hawker, C. J. *Biomacromolecules* **2007**, *8*, 3126-3134. (b) Turner, J. L.; Pan, D.; Plummer, R.; Chen, Z.; Whittaker, A. K.; Wooley, K. L. *Adv. Func. Mat.* **2005**, *15*, 1248-1254. (c) Shrestha, R.; Shen, Y.; Pollack, K. A.; Taylor, J.-S. A.; Wooley, K. L. *Bioconjugate Chem.* **2012**, *23*, 574-585.
- (9) Turner, J. L.; Becker, M. L.; Li, X.; Taylor, J.-S. A.; Wooley, K. L. *Soft Matter* **2005**, *1*, 69-78.

- (10) Liu, H.; Jiang, X.; Fan, J.; Wang, G.; Liu, S. *Macromolecules* **2007**, *40*, 9074-9083.
- (11) (a) Pan, D.; Turner, J. L.; Wooley, K. L. *Macromolecules* **2004**, *37*, 7109-7115. (b) Pan, D.; Turner, J. L.; Wooley, K. L. *Chem. Commun.* **2003**, *39*, 2400-2401.
- (12) Perrier, T.; Saulnier, P.; Benoit, J.-P. *Chem. Eur. J.* **2010**, *16*, 11516-11529.
- (13) (a) Elsabahy, M.; Wooley, K. L. *J. Polym. Sci., Part A: Polym. Chem.* **2012**, *50*, 1869-1880. (b) Kim, Y.; Pourgholami, M. H.; Morris, D. L.; Stenzel, M. H. *Biomacromolecules* **2012**, *13*, 814-825. (c) Read, E. S.; Armes, S. P. *Chem. Commun.* **2007**, *43*, 3021-3035.
- (14) Shi, M.; Wosnick, J. H.; Ho, K.; Keating, A.; Shoichet, M. S. *Angew. Chem., Int. Ed.* **2007**, *46*, 6126-6131.
- (15) (a) Kakwere, H.; Perrier, S. *J. Am. Chem. Soc.* **2009**, *131*, 1889-1895. (b) van der Ende, A. E.; Harrell, J.; Sathiyakumar, V.; Meschievitz, M.; Katz, J.; Adcock, K.; Harth, E. *Macromolecules* **2010**, *43*, 5665-5671.
- (16) Chan, D. P. Y.; Owen, S. C.; Shoichet, M. S. *Bioconjugate Chem.* **2013**, *24*, 105-113.
- (17) O'Reilly, R. K.; Joralemon, M. J.; Hawker, C. J.; Wooley, K. L. *J. Polym. Sci., Part A: Polym. Chem.* **2006**, *44*, 5203-5217.
- (18) O'Reilly, R. K.; Joralemon, M. J.; Wooley, K. L.; Hawker, C. J. *Chem. Mater.* **2005**, *17*, 5976-5988.

- (19) Wang, X.; Liu, L.; Luo, Y.; Zhao, H. *Langmuir* **2008**, *25*, 744-750.
- (20) O'Reilly, R. K.; Joralemon, M. J.; Hawker, C. J.; Wooley, K. L. *Chem. Eur. J.* **2006**, *12*, 6776-6786.
- (21) Algar, W. R.; Prasuhn, D. E.; Stewart, M. H.; Jennings, T. L.; Blanco-Canosa, J. B.; Dawson, P. E.; Medintz, I. L. *Bioconjugate Chem.* **2011**, *22*, 825-858.
- (22) Lim, R. K. V.; Lin, Q. *Chem. Commun.* **2010**, *46*, 1589-1600.
- (23) Thalhammer, F.; Wallfahrer, U.; Sauer, J. *Tet. Lett.* **1990**, *31*, 6851-6854.
- (24) (a) Castillo, J. A.; Borchmann, D. E.; Cheng, A. Y.; Wang, Y.; Hu, C.; Garcia, A. J.; Weck, M. *Macromolecules* **2012**, *45*, 62-69. (b) Sasaki, T.; Eguchi, S.; Yamaguchi, M.; Esaki, T. *J. Org. Chem.* **1981**, *46*, 1800-1804.
- (25) Liang, Y.; Mackey, J. L.; Lopez, S. A.; Liu, F.; Houk, K. N. *J. Am. Chem. Soc.* **2012**, *134*, 17904-17907.
- (26) (a) Chen, L.; Hillmyer, M. A. *Macromolecules* **2009**, *42*, 4237-4243. (b) Chen, L.; Phillip, W. A.; Cussler, E. L.; Hillmyer, M. A. *J. Am. Chem. Soc.* **2007**, *129*, 13786-13787.
- (27) Zhang, L.; Eisenberg, A. *Macromolecules* **1999**, *32*, 2239-2249.
- (28) Stamenovic, M. M.; Espeel, P.; Camp, W. V.; Du Prez, F. E. *Macromolecules* **2011**, *44*, 5619-5630.

- (29) (a) Cheng, C.; Khoshdel, E.; Wooley, K. L. *Macromolecules* **2005**, *38*, 9455-9465. (b) Patton, D. L.; Advincula, R. C. *Macromolecules* **2006**, *39*, 8674-8683.
- (30) Chiefari, J.; Chong, Y. K.; Ercole, F.; Krstina, J.; Jeffery, J.; Le, T. P. T.; Mayadunne, R. T. A.; Meijs, G. F.; Moad, C. L.; Moad, G.; Rizzardo, E.; Thang, S. H. *Macromolecules* **1998**, *31*, 5559-5562.
- (31) Williams, R. J.; O'Reilly, R. K.; Dove, A. P. *Polym. Chem.* **2012**, *3*, 2156-2164.
- (32) Hoogenboom, R.; Schubert, U. S.; Van Camp, W.; Du Prez, F. E. *Macromolecules* **2005**, *38*, 7653-7659.
- (33) Allen, A. D.; Tidwell, T. T. *J. Am. Chem. Soc.* **1982**, *104*, 3145-3149.
- (34) (a) Colombani, O.; Ruppel, M.; Burkhardt, M.; Drechsler, M.; Schumacher, M.; Gradzielski, M.; Schweins, R.; Müller, A. H. E. *Macromolecules* **2007**, *40*, 4351-4362. (b) Colombani, O.; Ruppel, M.; Schubert, F.; Zettl, H.; Pergushov, D. V.; Müller, A. H. E. *Macromolecules* **2007**, *40*, 4338-4350.
- (35) Lutz, J.-F. *J. Polym. Sci., Part A: Polym. Chem.* **2008**, *46*, 3459-3470.
- (36) Grover, G. N.; Lee, J.; Matsumoto, N. M.; Maynard, H. D. *Macromolecules* **2012**, *45*, 4958-4965.
- (37) Sumerlin, B. S.; Tsarevsky, N. V.; Louche, G.; Lee, R. Y.; Matyjaszewski, K. *Macromolecules* **2005**, *38*, 7540-7545.

- (38) Grogna, M.; Cloots, R.; Luxen, A.; Jerome, C.; Passirani, C.; Lautram, N.; Desreux, J.-F.; Collodoro, M.; De Pauw-Gillet, M.-C.; Detrembleur, C. *Polym. Chem.* **2011**, *2*, 2316-2327.
- (39) (a) Lang, A. S.; Neubig, A.; Sommer, M.; Thelakkat, M. *Macromolecules* **2010**, *43*, 7001-7010. (b) Malkoch, M.; Thibault, R. J.; Drockenmuller, E.; Messerschmidt, M.; Voit, B.; Russell, T. P.; Hawker, C. J. *J. Am. Chem. Soc.* **2005**, *127*, 14942-14949.
- (40) Ladmiral, V.; Mantovani, G.; Clarkson, G. J.; Cauet, S.; Irwin, J. L.; Haddleton, D. M. *J. Am. Chem. Soc.* **2006**, *128*, 4823-4830.
- (41) Terreau, O.; Bartels, C.; Eisenberg, A. *Langmuir* **2003**, *20*, 637-645.
- (42) Terreau, O.; Luo, L.; Eisenberg, A. *Langmuir* **2003**, *19*, 5601-5607.
- (43) Schmitt, A. L.; Repollet-Pedrosa, M. H.; Mahanthappa, M. K. *ACS Macro Lett.* **2012**, *1*, 300-304.
- (44) Patterson, J. P.; Sanchez, A. M.; Petzetakis, N.; Smart, T. P.; Epps III, T. H.; Portman, I.; Wilson, N. R.; O'Reilly, R. K. *Soft Matter* **2012**, *8*, 3322-3328.
- (45) (a) Hoogenboom, R.; Kickelbick, G.; Schubert, U. S. *Eur. J. Org. Chem.* **2003**, *2003*, 4887-4896. (b) Hoogenboom, R.; Moore, B. C.; Schubert, U. S. *Chem. Commun.* **2006**, *42*, 4010-4012. (c) Hoogenboom, R.; Wouters, D.; Schubert, U. S. *Macromolecules* **2003**, *36*, 4743-4749.
- (46) Willems, L. I.; Li, N.; Florea, B. I.; Ruben, M.; van der Marel, G. A.; Overkleeft, H. S. *Angew. Chem., Int. Ed.* **2012**, *51*, 4431-4434.

- (47) EPA; 57FR26460, Ed. AWQC ADDENDUM 1989 DRAFT 2002.
- (48) (a) Karver, M. R.; Weissleder, R.; Hilderbrand, S. A. *Bioconjugate Chem.* **2011**, *22*, 2263-2270. (b) Yang, J.; Karver, M. R.; Li, W.; Sahu, S.; Devaraj, N. K. *Angew. Chem., Int. Ed.* **2012**, *51*, 5222-5225.
- (49) Dyke, J. M.; Groves, A. P.; Morris, A.; Ogden, J. S.; Dias, A. A.; Oliveira, A. M. S.; Costa, M. L.; Barros, M. T.; Cabral, M. H.; Moutinho, A. M. C. *J. Am. Chem. Soc.* **1997**, *119*, 6883-6887.
- (50) Chan, T. R.; Hilgraf, R.; Sharpless, K. B.; Fokin, V. V. *Org. Lett.* **2004**, *6*, 2853-2855.
- (51) Ryu, J. H.; Roy, R.; Ventura, J.; Thayumanavan, S. *Langmuir* **2010**, *26*, 7086-7092.
- (52) (a) Stubbs, L. P.; Weck, M. *Chem. Eur. J.* **2003**, *9*, 992-999. (b) Dolman, S. J.; Hultsch, K. C.; Pezet, F.; Teng, X.; Hoveyda, A. H.; Schrock, R. R. *J. Am. Chem. Soc.* **2004**, *126*, 10945-10953.
- (53) Sivakumar, K.; Xie, F.; Cash, B. M.; Long, S.; Barnhill, H. N.; Wang, Q. *Org. Lett.* **2004**, *6*, 4603-4606.



# **Chapter 4. Nanoparticle formation using single chain collapse of norbornene- functionalised polymers**

## **4.1. Abstract**

Single chain polymer nanoparticles (SCPNS) are formed using pendent-norbornene decorated polystyrenes of various molecular weights and incorporation of norbornenes, and a bifunctional tetrazine crosslinker. Characterisation by SEC, DLS, SLS, SANS, TEM and AFM showed that discrete particulate material has been successfully formed, although SCPN formation had a lower molecular weight limit, primarily due to some polymer–polymer coupling or gelation occurring in all samples.

## 4.2. Background

With the increasing sophistication of ‘nano’ chemistry, it is desirable that molecules or particles of any possible size, morphology and functionality can be synthesised. ‘Bottom-up’ techniques such as single molecule dendrimer synthesis give access to molecules up to approximately 5 nm in size,<sup>1</sup> and ‘top-down’ approaches such as self-assembly of amphiphiles or mini-emulsion polymerisations give access to macromolecular constructs down to around 20 nm. However, particles of a size range 5–20 nm have traditionally been difficult to access. Such particles are useful for semiconductor lithography,<sup>2</sup> as sacrificial porogens,<sup>3</sup> and viscosity modifiers.<sup>4</sup>

More recently interest has been growing in mimicking Nature’s folding of proteins and enzymes,<sup>5</sup> using synthetic polymers able to undergo reversible chain collapse. Advances in this respect have been furthered by the ability to selectively insert single, specific, monomer units into a growing polymer chain — so-called ‘sequence-controlled polymerisation’ — which means that reversible ‘folds’, covalent links or other functional units in the collapsed polymer chain can be precisely placed, analogous to protein folding, and one step closer to Nature’s nanomachines such as enzymes, growth factors and oxygen carriers.<sup>6</sup>

Similarly to the small particles used in synthetic applications, enzymes and other naturally folded polymers are also of the size range 5–20 nm. Free polymer chains in solution also display such sizes, dependent on their

molecular weight, polymer–polymer and polymer–solvent interactions (Equation 4.1).

**Equation 4.1 Hydrodynamic diameter of a (linear) polymer chain in solution**

$$D = \left( \frac{12KM_n^{1+\alpha}}{5\pi N_A} \right)^{\frac{1}{3}}$$

$D$  = diameter,  $M_n$  = number average molecular weight  
 $N_A$  = Avogadro's number  
 $\alpha, K$  = Mark – Houwink – Sakurada values

Therefore one can imagine if an individual polymer chain were compacted in order to freeze its diameter in any given solvent, then this would be an appropriate route to spherical or folded particles in the 5–20 nm size range. The theoretical diameter of a fully compacted polymer chain is given in Equation 4.2.

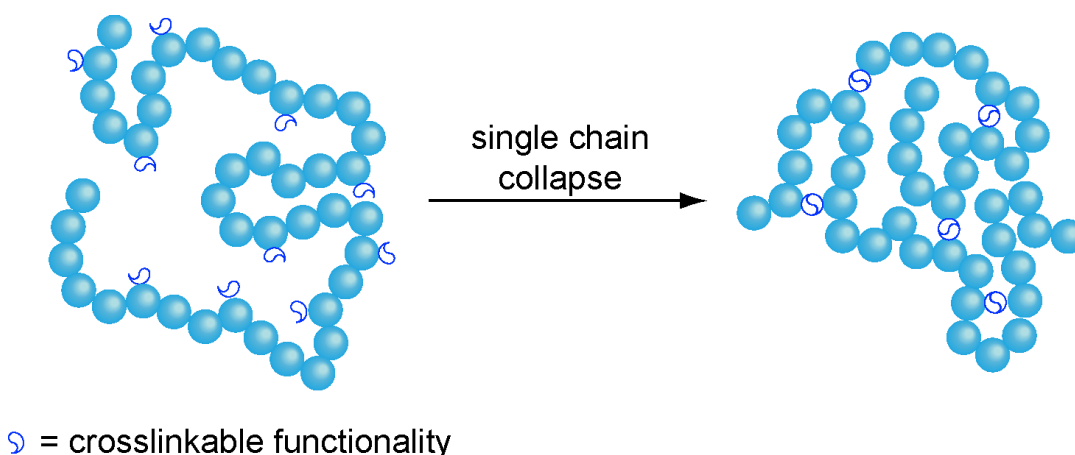
**Equation 4.2 Diameter of a fully compacted polymer chain with no excluded volume**

$$D = \left( \frac{6M_n}{\pi\rho N_A} \right)^{\frac{1}{3}}$$

$D$  = diameter,  $M_n$  = number average molecular weight  
 $\rho$  = polymer density,  $N_A$  = Avogadro's number

For a polystyrene particle, this means that particles of 5 nm diameter can in theory be synthesised by the collapse of a polymer chain of maximum 42 kDa, and particles of 20 nm can be accessed using a polymer chain of 2670 kDa. In practice, however, these lower bounds will probably never be reached for these particles due to topological ‘freezing’ of the particles at

the later stages of formation, so these are upper limits for the molecular weights of polymers required for those sizes.



**Figure 4.1 Self-crosslinking of polymer chains to form defined single polymer chain nanoparticles (SCPNCs)**

Collapse of single chains can be achieved by incorporating pendent crosslinkable functionalities along the polymer backbone, and inducing intramolecular crosslinking such that single polymer chain nanoparticles (SCPNCs) are formed (Figure 4.1). Crosslinking is possible with either self-condensing functionalities that are activated in some way — temperature and UV light are the most common — or by using a bifunctional crosslinker molecule. Examples of crosslinking methods are shown in Figure 4.2.

The first example of single chain collapse to form SCPNCs was by Mercier *et. al.* using AIBN to radically crosslink pendent acrylate functionalities along a PCL or PMMA backbone.<sup>3</sup> This was done under ultradilute conditions ( $<10^{-5}$  M) such that intramolecular crosslinking would

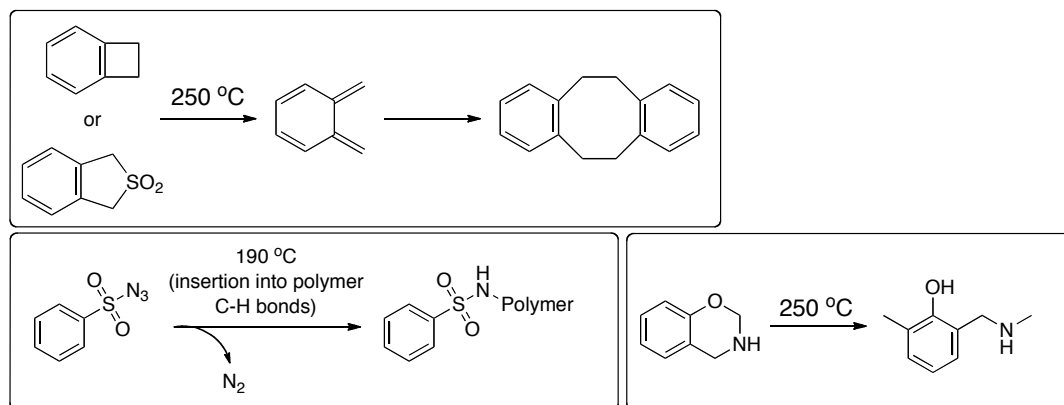
be favoured over intermolecular gel formation. However, these conditions preclude particle synthesis on a large scale simply due to the impractical volumes of solvent involved, and so an alternative slow addition technique was developed shortly afterwards,<sup>7</sup> whereby the dissolved polymer is added slowly to a defined volume of solvent (containing crosslinker if required), at a concentration that would otherwise cause gel formation, but due to the slow addition rate SCPNs form instead. This requires that the reaction forming the SCPNs, be it self-condensation or reaction with a crosslinker, is fast and efficient, which lends itself to click-type reactions.

Aside from radical coupling of vinyl groups,<sup>8</sup> one of the first reactions exploited was the self-condensation of benzocyclobutene (BCB) moieties at 250 °C.<sup>7</sup> An alternative *o*-quinodimethane precursor, benzosulfone, has been used in a similar vein,<sup>9</sup> and substituted benzosulfones have been shown to reduce the temperature required for ring opening down to 150 °C.<sup>10</sup> Similar high temperature approach involved the crosslinking of benzoxazine groups at 250 °C,<sup>11</sup> and of sulfonyl azide groups at 190 °C.<sup>12</sup>

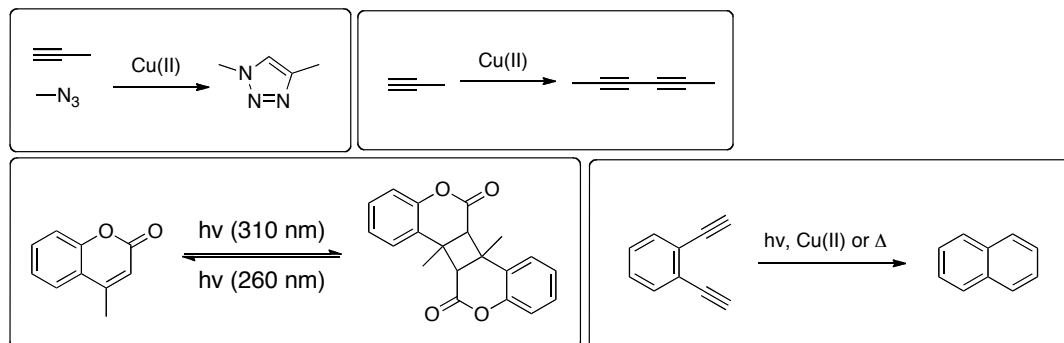
Negating the need for high reaction temperatures, polymerisation of alkyne- and azide-containing monomers into a single chain also enabled the use of the room temperature CuAAC reaction for SCPN formation,<sup>13</sup> and using only alkyne-containing monomers achieved the same result using Glaser-Hay coupling of alkynes.<sup>14</sup> UV-induced photodimerisation of coumarin<sup>15</sup> and cinnamyl<sup>16</sup> groups, and photo-induced Bergman cyclisations<sup>17</sup> have also been employed to circumvent the need for boiling solvents.

Taking inspiration from various polymerisation processes and mechanisms, metathesis of alkenes using the Grubbs catalyst,<sup>18</sup> crosslinking of isocyanates with amines,<sup>19</sup> and oxidative polymerisation of thiophene-type pendent monomers<sup>20</sup> have also been used for SCPN formation.

#### THERMALLY ACTIVATED:



#### ROOM TEMPERATURE:



#### 'POLYMERISATION-INSPIRED':

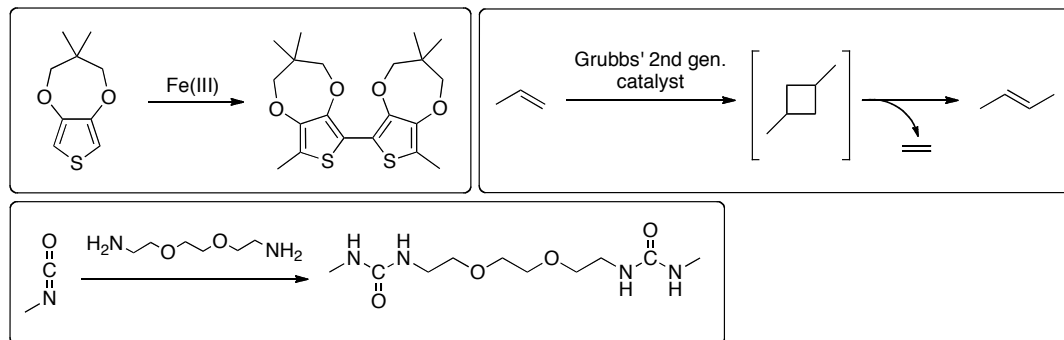


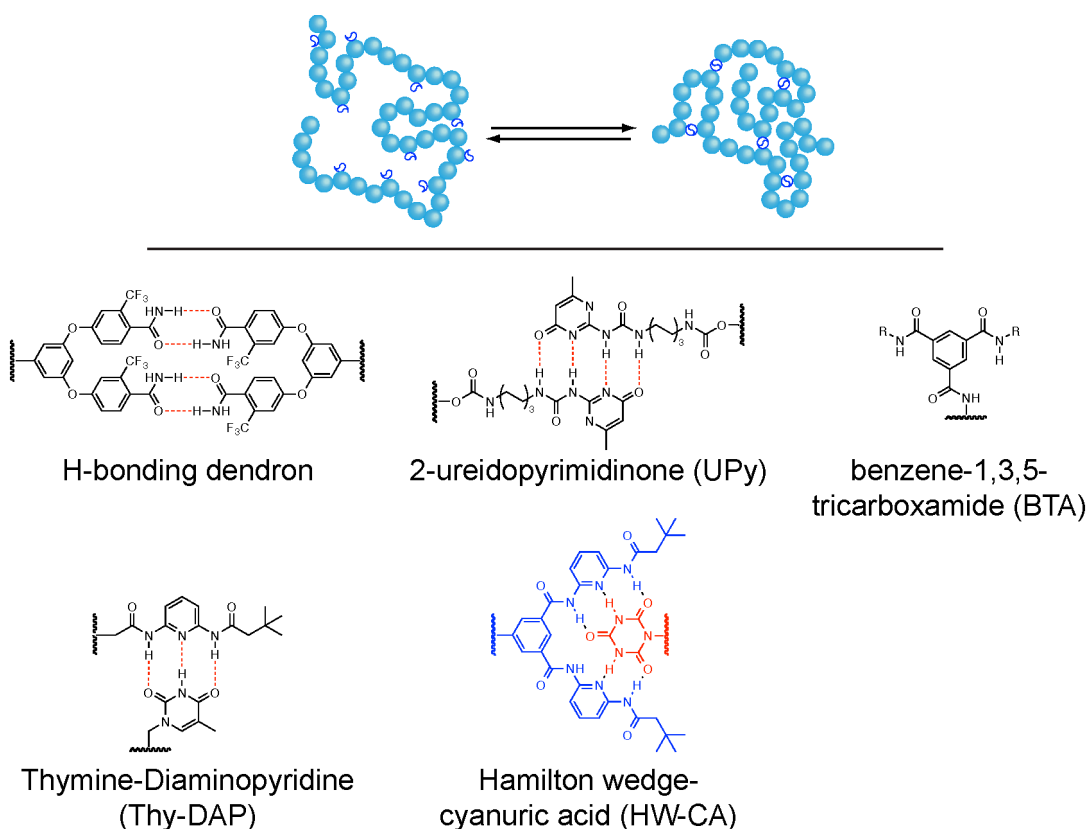
Figure 4.2 Crosslinking reactions employed for the irreversible formation of

SCPNS<sup>8-20</sup>

Another avenue of interest has been using these polymers as a model for naturally occurring folding polymers such as proteins and enzymes. To this end, various H-bonding motifs have been incorporated into polymers to be used as reversible crosslinkers. The first of these was a polymerisable H-bonding dendron, copolymerised by RAFT with PMMA<sup>21</sup> and shown to form SCPNs, in comparison to a control dendron with no H-bonding motifs which showed no morphology change. Meijer and coworkers have used two different self-complementary H-bonding pairs — ureidopyrimidone (UPy) and benzene-1,3,5-tricarboxamide (BTA) — caged by the UV-induced deprotection of *ortho*-nitrobenzyl protecting groups to induce self-assembly of SCPN structures. SCPNs were formed by the self-association of pendent UPy groups on ROMP-,<sup>22</sup> SET-LRP-,<sup>23</sup> NMP- and RAFT-synthesised<sup>24</sup> polymers. BTA groups have an interesting H-bonding mode in that they stack in a helical fashion to form secondary structures.<sup>25</sup> These groups were incorporated into a water-soluble polymer also containing catalyst-based monomers and used for catalytic water-soluble particles, in a step towards enzyme mimics,<sup>26</sup> and into organic-soluble particles and used for metal sensing.<sup>27</sup> Later, it was also shown that the UPy and BTA self-assemblies are orthogonal, so that SCPNs containing both helical stacks and globular areas were formed.<sup>28</sup>

The H-bonding between diaminopyridine (DAP) and thymine (Thy) has been used to form microscopic nanogels by defined gelation of polymers bearing those groups;<sup>29</sup> inspired by this early work, single chain collapse has also been achieved using these moieties.<sup>30</sup> Thy-DAP bonding in tandem with the recognition between a Hamilton wedge (HW) and cyanuric

acid (CA) was also used to form SCPNs with two complementary H-bonding motifs.<sup>31</sup>



**Figure 4.3 H-bonding motifs used for the formation of SCPNs: dendrons,<sup>21</sup>**

**UPy<sup>22-24,28</sup>, BTA,<sup>25-28</sup> Thy-DAP<sup>29-31</sup> and HW-CA<sup>31</sup>**

More unusual methods of SCPN formation include reversible molecular recognition events between viologen and cucurbituril moieties,<sup>32</sup> and the complexation of poly(cyclooctadiene) with rhodium.<sup>33</sup>

More recently, the concept of dynamic covalent chemistry,<sup>34</sup> a combination of the covalent and reversible (H-bonding) motifs described above, has been used to synthesise SCPNs.<sup>35</sup> and this was extended to a system which could reversibly switch between its SCPN state and a networked



hydrogel by heating and cooling respectively. This achieved using polymers possessing a lower critical solution temperature (LCST) in the backbone; upon cooling the SCPNs below their LCST, spontaneous aggregation occurred, increasing the local SCPN concentration and inducing dynamic covalent bond exchange, resulting in a gel structure.<sup>36</sup>

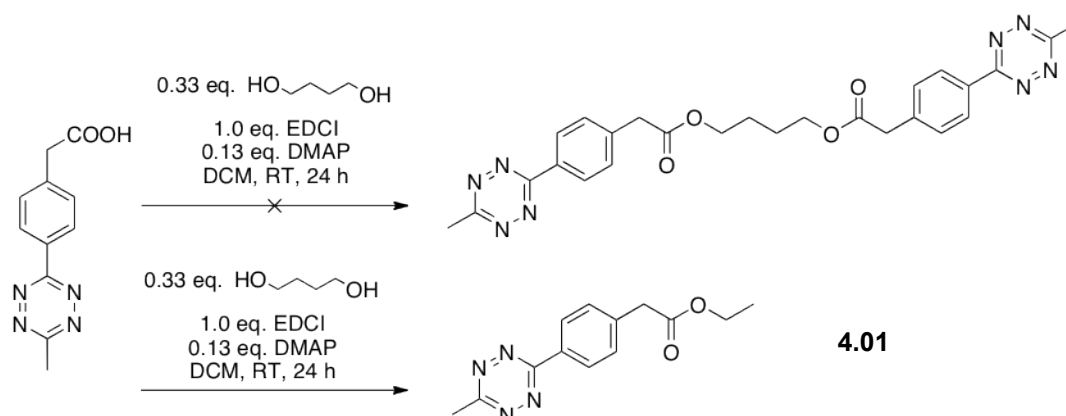
In this work, we aimed to use the Tz–Nb reaction as a crosslinker to form non-dynamic SCPNs as the Tz–Nb reaction has some advantages to those reactions already used for SCPN formation. The high-temperature reactions such as the BCB reactions described above preclude incorporation of many functionalities, should the basic SCPN structure be incorporated into more complex frameworks, so the room temperature nature of the Tz–Nb reaction is advantageous in that respect. The tetrazine and norbornene functionalities, whilst reactive and by extension not stable under *all* conditions, are stable enough that SCPN formation does not have to be run under stringently anhydrous conditions, like the isocyanate–amine reaction does, nor under nitrogen. The Nb functionalities can be incorporated into a polymer by RAFT easily, as described in earlier Chapters, and thus the number of synthetic steps is reduced relative to the SCPN precursors that require post-polymerisation modification to incorporate the reactive functionalities prior to SCPN formation. The catalyst- and additive-free nature of the Tz–Nb reaction also simplifies SCPN synthesis.

## 4.3. Results and discussion

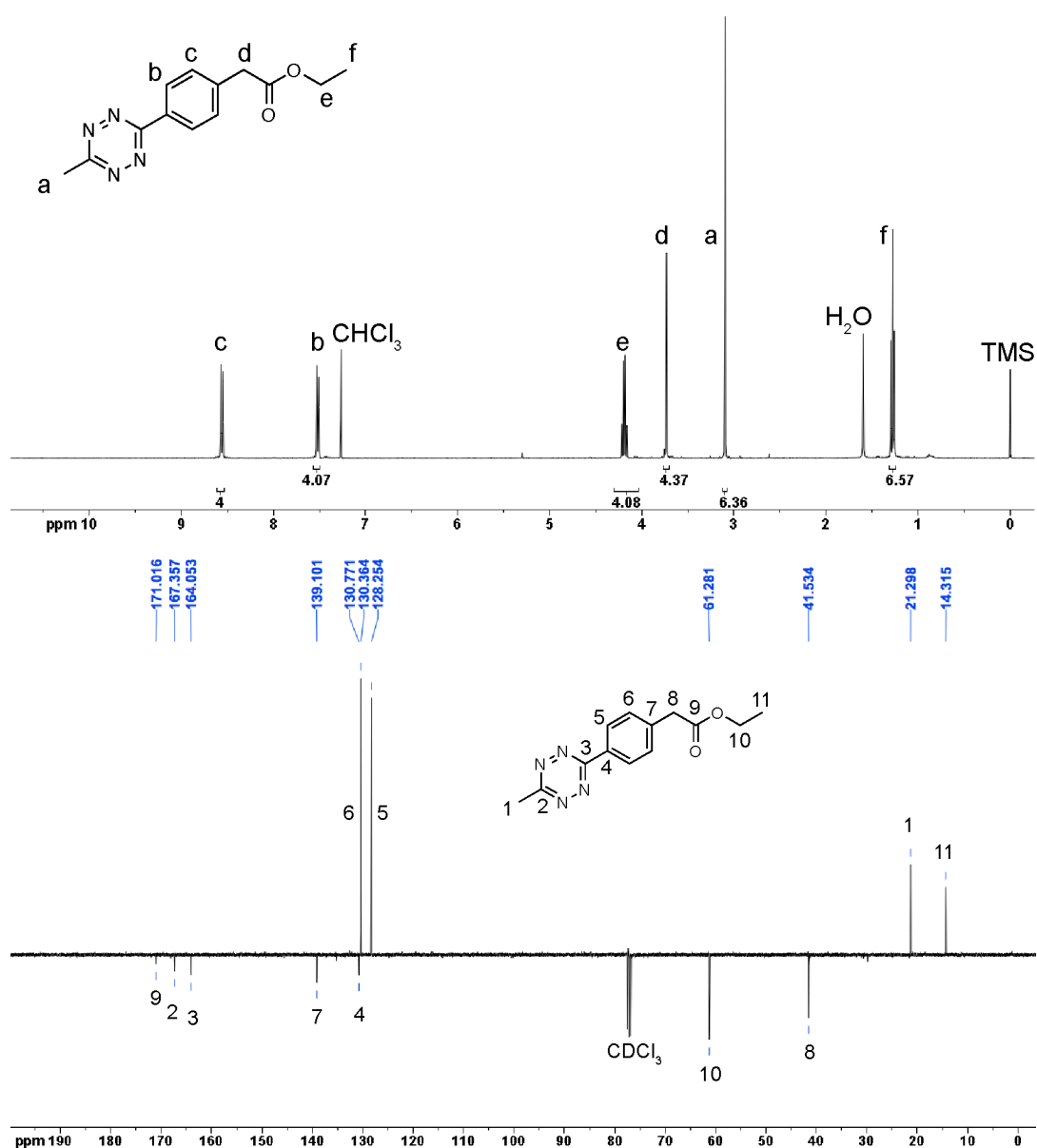
### 4.3.1. Crosslinker Synthesis

Our synthetic strategy hinged upon norbornene-functionalised polystyrenes (the general synthesis of which is described in Chapter 3), and a bifunctional tetrazine-based crosslinker.

To synthesise the crosslinker, we started with a carboxylic acid-functionalised tetrazine, itself synthesised by a recently reported metal-catalysed method in moderate yield.<sup>37</sup> EDCI-mediated coupling with 1,4-butanediol resulted in a most unexpected product, **4.01**. This was ascertained using mass spectrometry (predicted  $m/z$  281.1014, found 281.1009 for  $[M+Na]^+$ ) and the ATP-<sup>13</sup>C NMR spectrum of **4.01**; the signal arising from the unanticipated terminal methyl carbon (labelled 11 in Figure 4.4) showed that it was a methyl rather than the methylene carbon it would be were it incorporated into the butanediol linker segment.



**Scheme 4.1 Attempted synthesis of a bifunctional tetrazine crosslinker, and the unexpected product resulting**

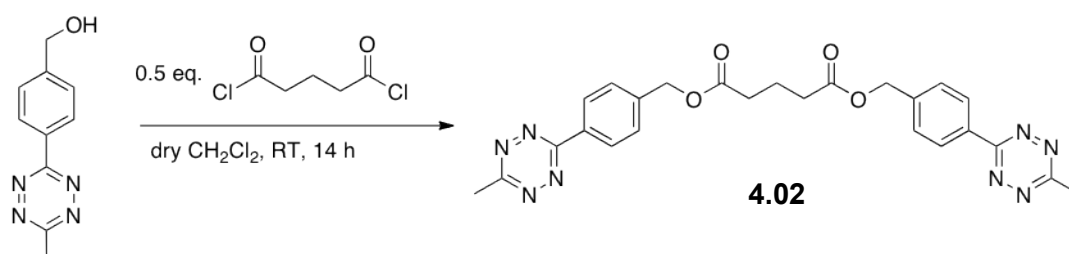


**Figure 4.4 <sup>1</sup>H (top) and <sup>13</sup>C (bottom) NMR spectra (CDCl<sub>3</sub>) of unexpected product 4.01**

We as yet do not have a viable hypothesis for the mechanism that provided this unexpected reaction product, but have noted that this ethyl substitution seems to occur when coupling linear diols using EDCI as a coupling agent, and is eliminated when DCC is used as an alternative coupling agent. We

used **4.01** as a 'dummy' crosslinker in control experiments described later, to ensure that any analytical results are not down to the changes in the side chain of the polymer.

As an alternative, we accessed a slightly different crosslinker using a bifunctional acyl chloride and alcohol-functionalised tetrazine, in order to circumvent any issues with using the EDCI or DMAP catalyst. **4.02** was obtained in moderate yield (38%) as a pink solid, and identity and purity confirmed by  $^1\text{H}$  and  $^{13}\text{C}$  NMR spectroscopy, HRMS and IR spectroscopy.



**Scheme 4.2 Synthesis of bifunctional tetrazine crosslinker 4.02**

Structure and purity were confirmed by  $^1\text{H}$ ,  $^{13}\text{C}$  NMR spectroscopy, FT-IR and HRMS. The FT-IR spectrum revealed formation of an ester by the characteristic carbonyl stretch at  $1733\text{ cm}^{-1}$ , and the expected  $m/z$  of 501 for the  $[\text{M}+\text{H}]^+$  ion was observed in the HMRS. The assigned  $^1\text{H}$  and  $^{13}\text{C}$  NMR spectra are shown in Figure 4.5.

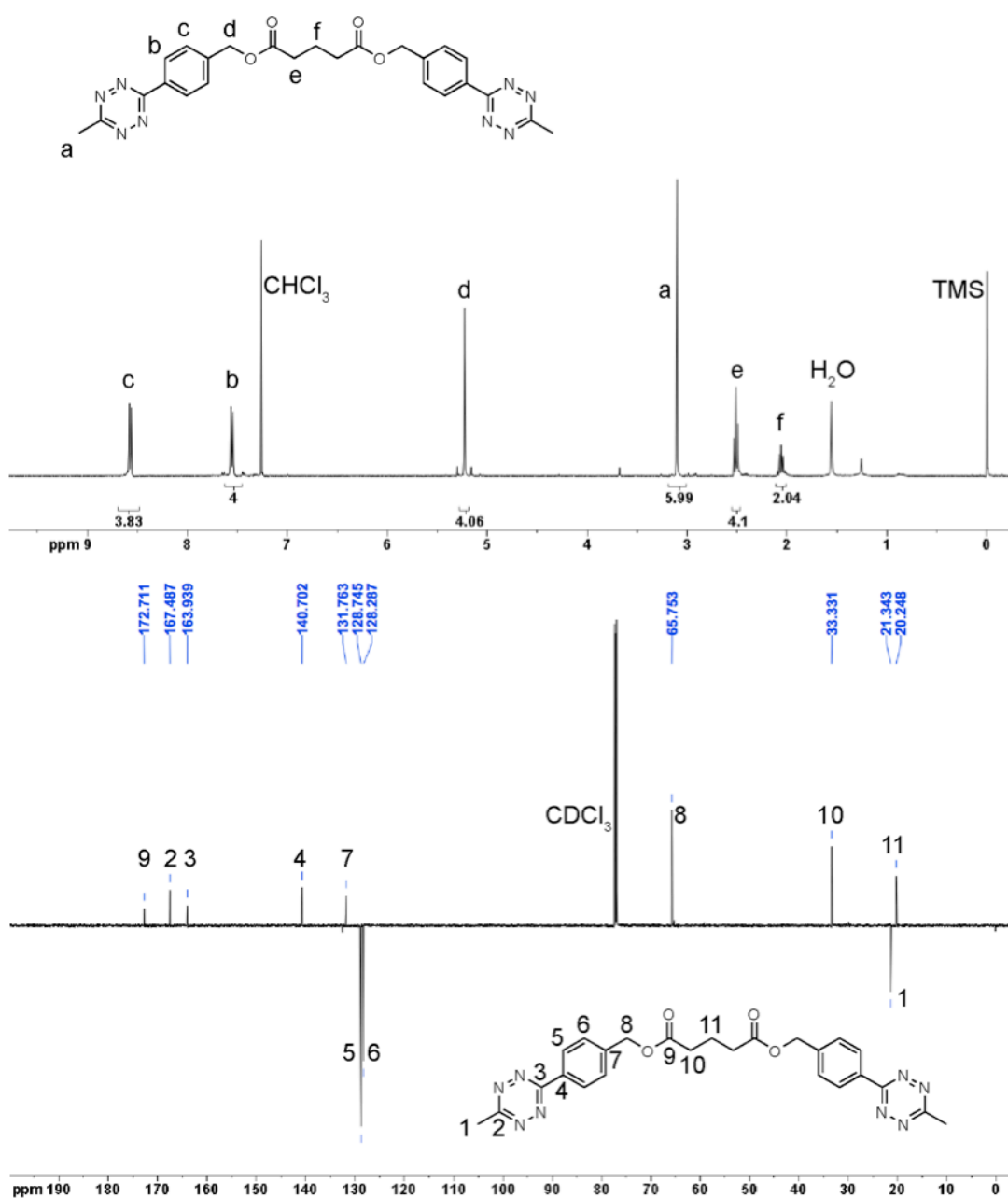


Figure 4.5 <sup>1</sup>H (top) and <sup>13</sup>C (bottom) NMR spectra (CDCl<sub>3</sub>) of Tz–Tz crosslinker

4.02

### 4.3.2. SCPN Synthesis

To form the nanoparticles, the 'slow addition' method rather than the 'ultradilute' method was used; briefly, a solution of poly(Nb–St-co-St) in DMF was added slowly (1 mL/h) to a stirred solution of crosslinker in DMF at 80 °C. Initial trials at room temperature were unsuccessful; qualitatively the colour change indicative of a successful reaction did not occur within 24 hours — and for SCPN formation using slow addition in particular a fast reaction is imperative — and only gelled polymer was obtained when analysing the reaction mixture. Faster rates of addition also resulted in polymer–polymer coupling, evidenced by increases in  $M_w$  compared to the parent linear polymer (although mostly in tandem with decreases in  $M_n$ , showing that some SCPN formation was occurring).

The amounts of polymer and crosslinker were calculated such that  $[Nb] = 0.01$  M in all cases, in accordance with the method of Hawker *et. al.*<sup>3</sup> For ease of calculation, the mol% functionality (as in Table 4.1) was assumed to be equal to the mol% feed in the polymerisation, rather than the mol% calculated by  $^1\text{H}$  NMR spectroscopy in the polymer, which was consistently slightly less than the feed ratio – for example 4.2 mol% calculated instead of the 5.0 mol% in the polymerisation feed.

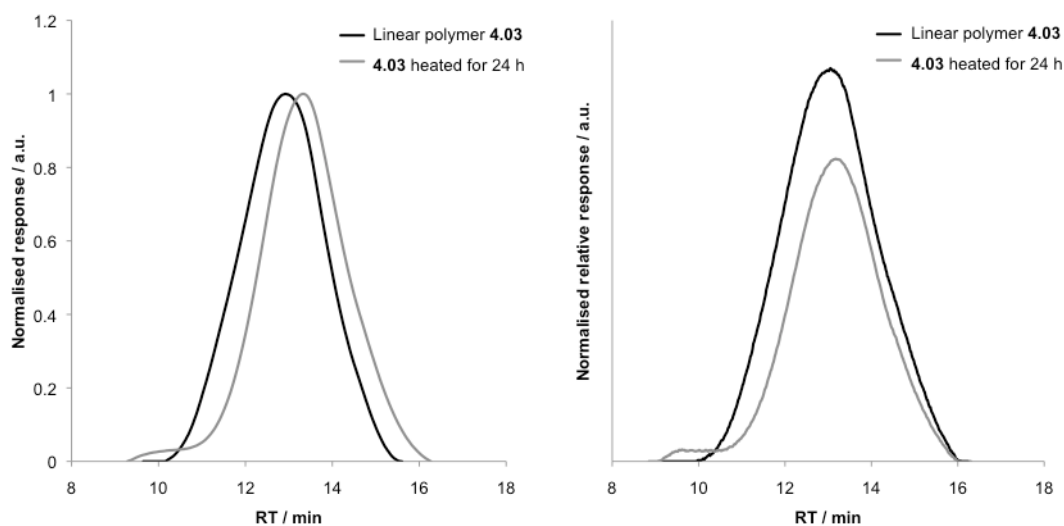
Table 4.1 shows a series of linear polymers subjected to this treatment, varying in molecular weight (ca. 10, 20 and 30 kDa) and incorporation of Nb functionalities (5, 10 and 20 mol%), and the SEC analysis results of the resulting SCPNs. Of these, polymer and SCPN **4.03** (highlighted) are the focus of further analytical techniques in this chapter.

**Table 4.1 Apparent  $M_n$ ,  $M_w$  and  $M_w/M_n$  values by SEC (THF eluent) for equivalent linear polymers and SCPNs, calculated by RI detection relative to PS calibrations**

<b>P</b>	<b>Mol% Nb</b>	<b>Linear Precursor</b>			<b>SCPN</b>		
		$M_n$ / kDa	$M_w$ / kDa	$M_w/M_n$	$M_n$ / kDa	$M_w$ / kDa	$M_w/M_n$
<b>4.03</b>	20	34.1	62.3	1.83	11.7	17.7	1.50
<b>4.04</b>	10	44.3	55.3	1.25	14.9	23.9	1.60
<b>4.05</b>	5	31.3	43.5	1.35	25.5	47.5	1.86
<b>4.06</b>	20	21.6	36.0	1.67	12.0	18.3	1.52
<b>4.07</b>	10	15.7	19.9	1.27	16.3	24.1	1.48
<b>4.08</b>	5	23.9	31.5	1.32	21.5	41.2	1.91
<b>4.09</b>	20	8.8	10.8	1.23	6.5	7.9	1.21
<b>4.10</b>	10	13.3	17.3	1.31	11.8	17.2	1.46
<b>4.11</b>	5	9.1	10.5	1.16	9.5	13.8	1.45
<b>4.12</b>	20	3.8	4.2	1.11	4.2	5.6	1.34
<b>4.13</b>	10	5.0	7.1	1.42	4.9	6.1	1.25
<b>4.14</b>	5	2.3	3.5	1.09	1.4	2.7	1.87

### 4.3.3. Control experiments

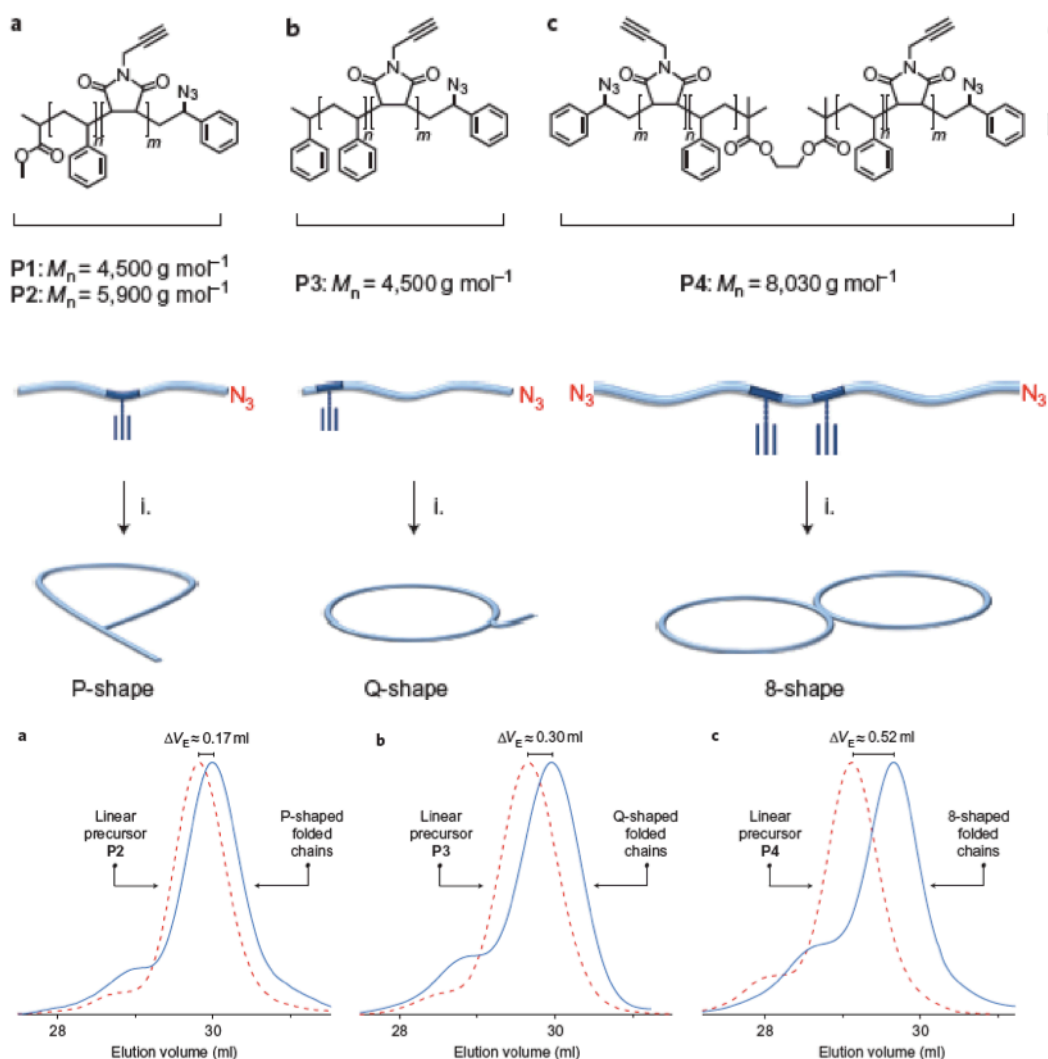
As a control experiment, the linear precursor to the SCPN was heated in DMF at 80 °C for 24 hours. Surprisingly, this yielded a very small shift to an earlier retention time in the SEC ( $\Delta V = 0.12$  mL for polymer **4.03**, Figure 4.6), although this effect was only noticeable on the higher MW polymers (*ca.* 30 kDa) for 10 and 20 mol% functionality. That this shift is accompanied by a reduction in the UV/vis intensity at 309 nm might suggest that the trithiocarbonate is being aminolysed by incidental amines present in the DMF, and the resulting thiol reacting with one of the pendent norbornene groups. If it were the norbornenes reacting with themselves, or the polymer backbone in some fashion, then the net effect would be the same as SCPN formation and therefore a much larger change in retention time would be expected.



**Figure 4.6 SEC traces for linear polymer 4.03 (grey) and after heating at 80 °C for 24 hours in DMF (black), by RI detection (left) and UV detection at 309 nm (right)**



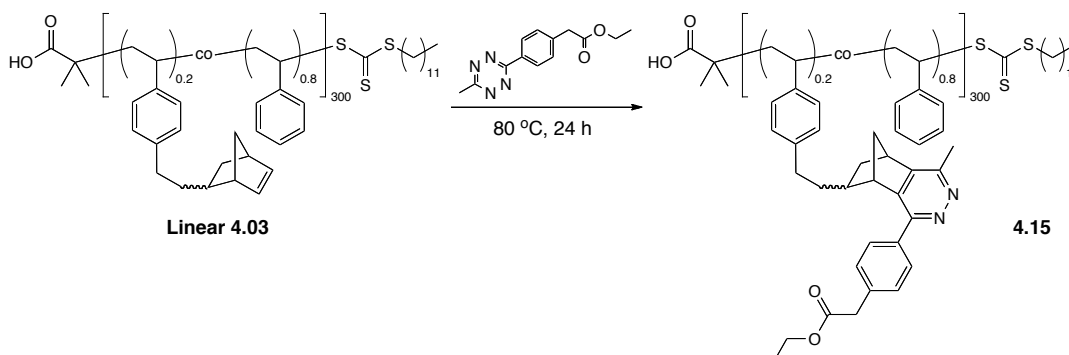
Formation of a single loop within the polymer chain is supported by the work of Lutz *et. al.*<sup>38</sup> (Figure 4.7) where controlled folding of single chains into ‘P-shaped’, ‘Q-shaped’ and ‘8-shaped’ polymers was demonstrated exclusively by small shifts in elution volume, on a similar scale to what we observed in our control experiment.



**Figure 4.7** Single chain folding with only one or two covalent links per chain<sup>38</sup>

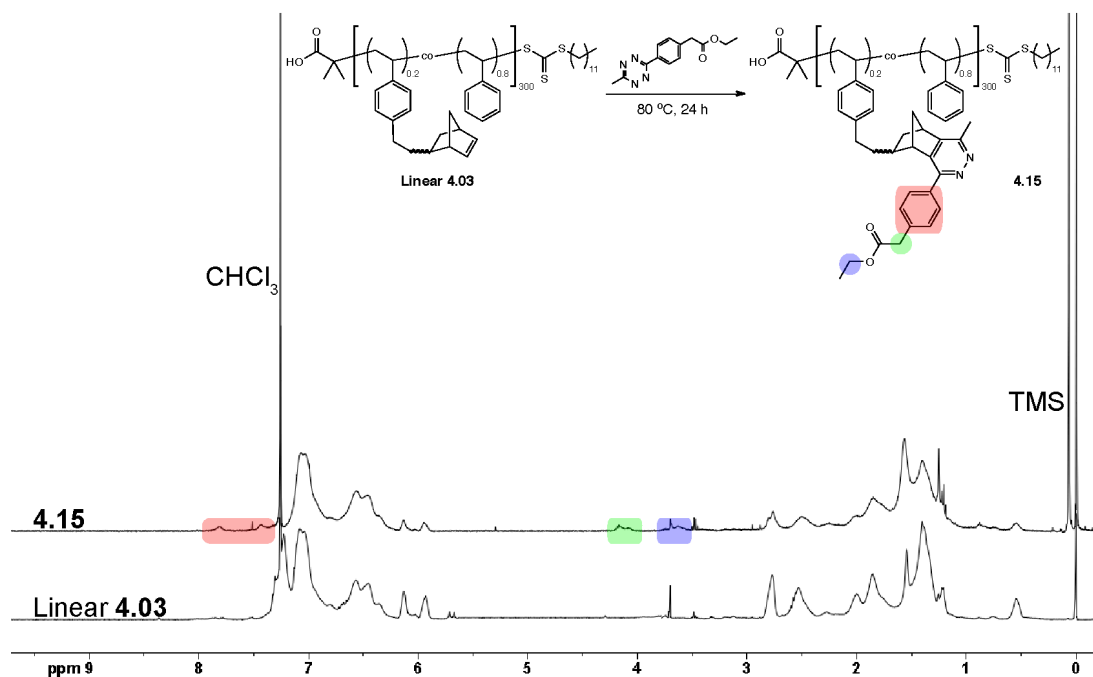
For comparison, observed  $\Delta V$  values for a single loop were 0.17 mL and 0.30 mL depending on the proportion of chain that was incorporated into the cycle, over a 60 minute run time; in our case the  $\Delta V = 0.12$  mL was observed in a 30 minute elution timeframe, which would equate to 0.24 mL in the case of the aforementioned work.

In a further control experiment, we also used the ethyl-substituted tetrazine **4.01** (in equimolar amounts to the number of Nb units present) discussed above to substitute the norbornene units without crosslinking the polymer (Scheme 4.3), in order to avoid erroneously assigning differences in characterisation behaviour to the linear polymer, which were actually due to changes in the backbone character, to SCPN formation.



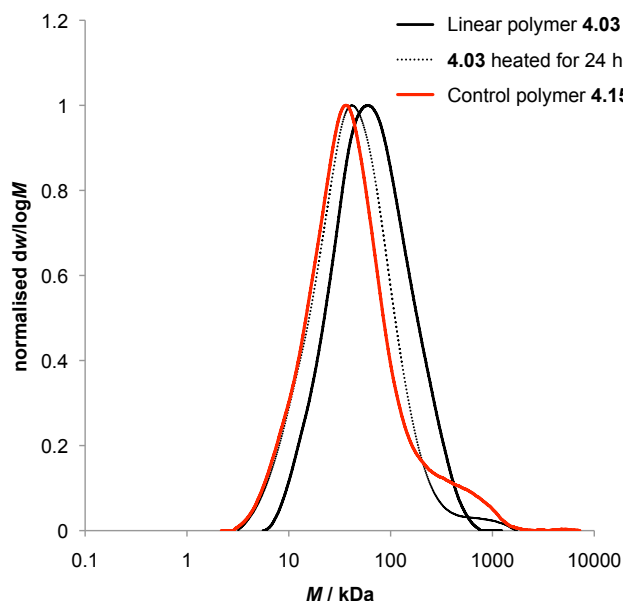
**Scheme 4.3 Formation of substituted, uncrosslinked polymer 4.15**

Successful Tz–Nb reaction was confirmed by  $^1\text{H}$  NMR spectroscopy (Figure 4.8), although it should be noted that there were still 25% Nb units remaining, as calculated relative to the integral of the aromatic protons in the  $^1\text{H}$  NMR spectrum, even though all tetrazine had been consumed.



**Figure 4.8**  $^1\text{H}$  NMR spectra ( $\text{CDCl}_3$ ) of linear polymer 4.03, control polymer 4.15, formed by functionalisation of 4.03 with TzCOOEt 4.01

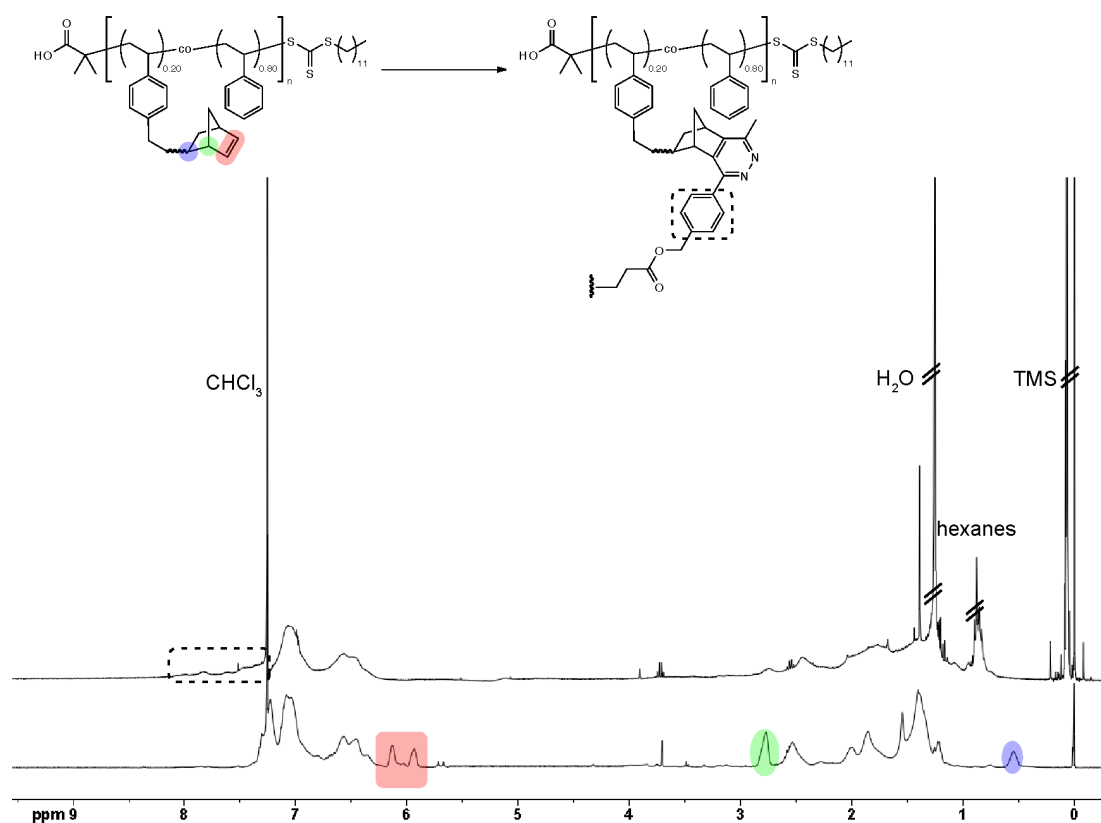
As can be seen from the SEC traces in Figure 4.9, no significant changes are observed when the model tetrazine is conjugated, with respect to the slight change that is observed due to heating the polymer alone. Therefore we were able to conclude that any shifts in retention time greater than 0.12 min (with a flow rate of 1 mL/min) could be assigned to SCPN formation.



**Figure 4.9 SEC (normalised  $dw/d\log M$ ) traces for linear polymer 4.03, 4.03 heated for 24 h, and model substituted polymer 4.15**

#### **4.3.4. SCPN Characterisation**

$^1\text{H}$  NMR spectroscopy in  $\text{CDCl}_3$  showed complete reaction of the Nb units (Figure 4.10), shown by the lack of signal at 6.0 ppm. This was not expected, as molecular simulations<sup>39</sup> and experimental evidence<sup>19</sup> has shown that after a certain degree of crosslinking, some reactive groups become inaccessible and so remain unreacted. However, this observation in the  $^1\text{H}$  NMR spectrum can be rationalised by assuming any unreacted Nb groups are buried within the SCPN and therefore not 'visible' by NMR; this is supported by the observation that the signals associated with the similarly buried crosslinker (expected to be at 3.6 and 4.1 ppm) are also not obvious.

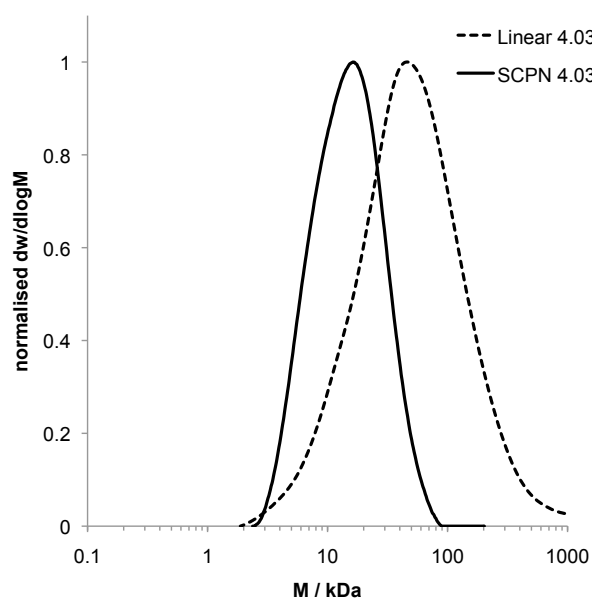


**Figure 4.10**  $^1\text{H}$  NMR ( $\text{CDCl}_3$ ) spectrum of linear polymer (bottom) and SCPN 4.03, with pertinent Nb signals highlighted to demonstrate reaction of the Nb groups

DOSY NMR<sup>40</sup> spectroscopy was also attempted to determine the size difference achieved *via* any differences in diffusion coefficient, however the differences in calculated diffusion coefficient were within experimental error and so this method was deemed unsuitable for probing SCPN formation by polymers of this molecular weight range; although DOSY has however been used as to probe SCPN formation of much larger polymers (150 kDa).<sup>26a</sup>

#### 4.3.4.1. SEC

The primary method for evaluating the success or otherwise of SCPN formation is generally an apparent reduction in the molecular weight and dispersity compared to the parent linear polymers, as displayed by linear and SCPN **4.03** (Figure 4.11).<sup>41</sup> This is because in traditional SEC analysis using polymer standards as calibrants, a given  $D_h$  is correlated to a given molecular weight of calibrant, and therefore when the SCPN is formed and the  $D_h$  decreases, the SEC results are for a free polymer chain of equivalent  $D_h$ , therefore lower molecular weight.

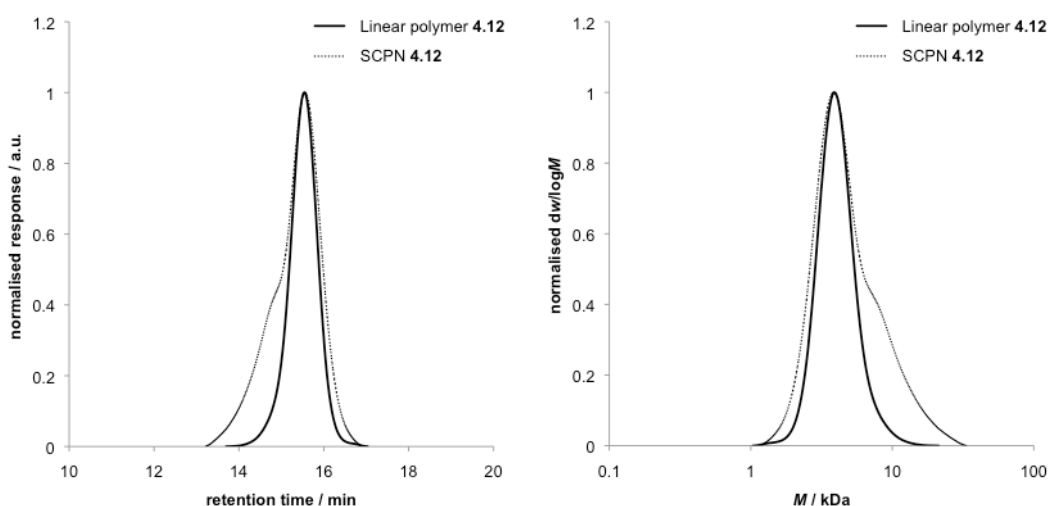


**Figure 4.11 SEC traces (THF, PS standards) for linear and SCPN 4.03; the observed change in  $M_n$  and  $M_w$  is a result of a shift in retention time of 1.2 min**

As can be seen from the results in Table 4.1, there is a reduction in  $M_n$  and  $M_w$  for the majority of samples, showing successful SCPN formation across

a range of molecular weights. As expected, lower incorporations of Nb functionality result in less compacted structures and smaller reductions in  $M_n$  and  $M_w$  compared to their parent polymers. There is not always a reduction in  $M_w/M_n$ , a trend reflected when analysing literature values,<sup>41</sup> due to the large effect that any high molecular weight shoulders arising from small amounts of polymer–polymer coupling can have. In this case, there was a small amount of high molecular weight shoulder apparent in nearly all of the samples, and this means that only the 20 mol% samples have a large enough proportional change in  $M_w$  and  $M_n$  to ‘overcome’ the high molecular weight shoulder and result in a net reduction in  $M_w/M_n$ .

Inspecting the results in Table 4.1, the low molecular weight samples **4.12**–**4.14** in particular do not appear to have successfully formed SCPNs, and upon closer inspection of the SEC traces (Figure 4.12), the only change observable is the formation of a high molecular weight shoulder.



**Figure 4.12** SEC traces for linear and SCPN 4.12 showing RI response vs. retention time (left) and the processed data to give  $dw/d\log M$  vs.  $M$  (right)

The universal formation of the high molecular weight shoulder would appear to mean that SCPN formation is not possible at lower molecular weights, probably because there are fewer Nb units available for crosslinking and therefore every polymer-polymer coupling event that occurs has a far greater effect on the proportion of available functionalities for SCPN formation. The high molecular weight shoulder would also imply that SCPN formation is not perfect and could be improved, perhaps by exploiting a faster reaction pair than the tetrazine–norbornene used in this case.

SEC by RI detection does not give an absolute size of the resulting SCPNs and so we set out to characterise linear and SCPN **4.03** more thoroughly by alternative analysis methods. The smallest possible diameter for SCPN **4.03** (calculated by Equation 4.2), assuming a fully compacted chain is 4.7 nm; the  $D_h$  of the precursor chain in THF (Mark-Houwink-Sakurada coefficients:  $K = 1.41 \times 10^{-8} \text{ m}^3/\text{g}$ ,  $\alpha = 0.70$ )<sup>42</sup> is 9.7 nm, so we would expect a hydrodynamic diameter in the region between those two values.

#### **4.3.4.2.      *Dynamic Light Scattering***

Many reports of single chain collapse use DLS to measure the diameter of SCPN particles.<sup>7,9b,13a,19,35</sup> We carried out DLS analysis at a single angle of 173°, using linear and SCPN sample **4.03**, at 25 °C and 5 mg/mL in CH<sub>2</sub>Cl<sub>2</sub>. Using the automatic cumulant fit method of data analysis the linear polymer  $D_h = 6.5 \text{ nm}$ , SCPN  $D_h = 8.5 \text{ nm}$  and functionalised, uncrosslinked polymer **4.15**  $D_h = 8.5 \text{ nm}$ . DLS data for SCPN **4.03** collected at multiple angles at a single concentration (5 mg/mL) and temperature (25 °C)<sup>43</sup> gave an  $R_h$  of 7.0 nm for SCPN **4.03**. These data are a little contradictory to expectations,



and to each other, and so we therefore investigated their sizes at different temperatures, reasoning that the linear chains might have greater degrees of freedom and may therefore swell upon heating,<sup>26a</sup> whereas the SCPNs may be unable to do so. We repeated the measurements from 10–50 °C, and the cumulant fit  $D_h$  values (average of 3 measurement sets per temperature) are shown in the left of Figure 4.13.

However, there was a small amount of larger particulate matter present that resulted in large dispersities and skewed results (due to the dependence of scattering intensity on  $R^6$ ). Deconvolution of these larger structures from the SCPNs was done by fitting a stretched exponential function to calculate the decay rate ( $\Gamma$  in Equation 4.3) of the smaller structures; this was then used to calculate the  $D_h$  values *via* the Stokes-Einstein equation.

#### **Equation 4.3 Relationship between the decay rate ( $\Gamma$ ) of the DLS**

**autocorrelation function and diffusion coefficient ( $D_t$ ) (top), where**

**$q$  = scattering vector,  $n$  = refractive index of sample,  $\theta$  = measurement angle,**

**$\lambda$  = incident light wavelength and Stokes-Einstein equation to calculate  $R_h$**

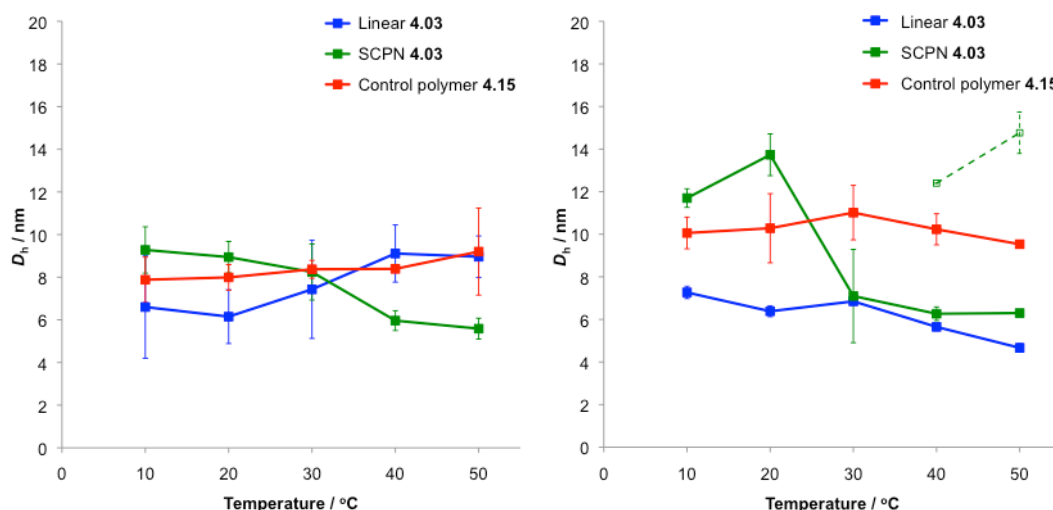
**and  $D_h$  (bottom), where  $k$  = Boltzmann constant,  $T$  = temperature,  $\eta$  = solvent**

**viscosity**

$$\Gamma = q^2 D_t \quad \left( q = \frac{4\pi n}{\lambda} \sin\left(\frac{\theta}{2}\right) \right)$$

$$D_t = \frac{kT}{6\pi\eta R_h}$$

This recalculation showed that in the case of SCPN 4.03, two distinct populations of equal intensity were present at higher temperatures, and the recalculated  $D_h$  values are shown on the right of Figure 4.13.

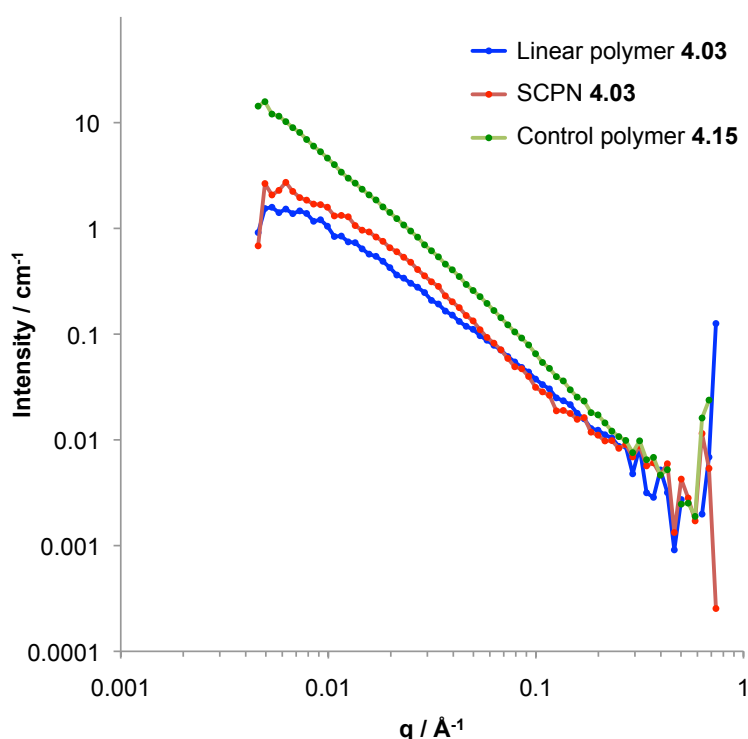


**Figure 4.13**  $D_h$  values at different temperatures calculated using the automatic cumulant fit (left) and by re-fitting the data (right)

Whilst the SCPN  $D_h$  values do not increase with temperature, and actually appear to decrease, in line with our expectations due to the constrained nature of the system, the trends in the data are quite unusual. A variation in  $D_h$  from 10 to 4 nm with temperature, and the appearance of a secondary population in the reanalyzed data (right of Figure 4.13, dashed line) may suggest that the SCPNs form oligomeric aggregates at this concentration, and that these aggregates are broken up by heating. This would give a 'true'  $D_h$  for SCPN 4.03 of 6.5 nm, by averaging the  $D_h$  values obtained by for the unaggregated population.

#### 4.3.4.3. Small Angle Neutron Scattering

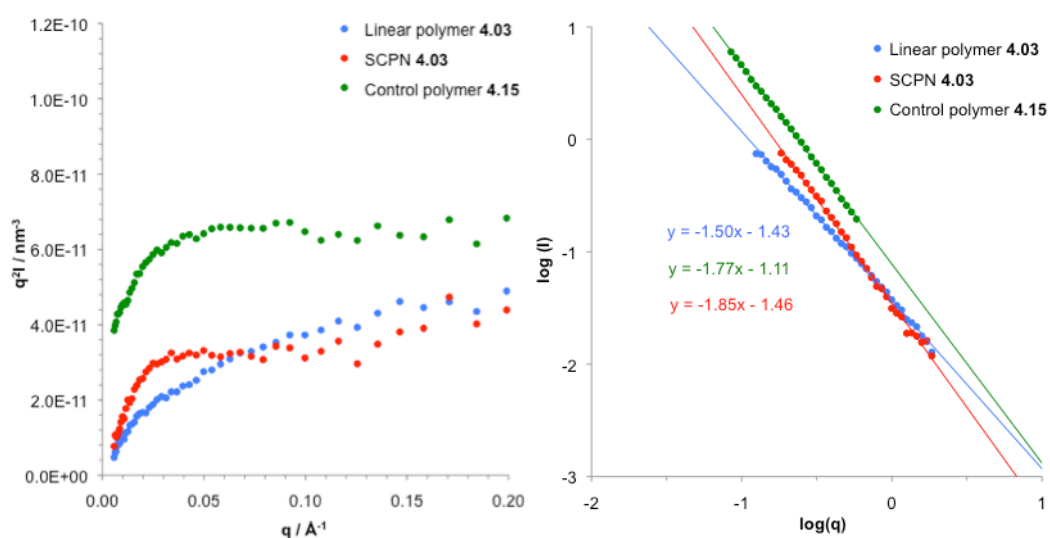
Small Angle Neutron Scattering (SANS) data was collected by Dr Ann Terry at the ISIS facility in Oxford, for the linear polymer and SCPN of **4.03** and the control polymer **4.15**. The predicted scattering length densities (SLD) for the polymers were between  $1.2\text{--}1.5 \times 10^{-6} \text{ \AA}^{-2}$ , so to maximise contrast with the solvent, THF- $d_8$  was chosen as the solvent ( $\text{SLD} = 6.38 \times 10^{-6} \text{ \AA}^{-2}$ ),<sup>44</sup> and the samples were run at a relatively high concentration (10 mg/mL).



**Figure 4.14 SANS data for the linear and SCPN of 4.03**

To gain information about the conformation of the polymer chains, a Kratky plot was derived ( $Iq^2$  vs.  $q$ ), shown in Figure 4.15. For a linear polymer chain, the shape of the graph tends to a horizontal asymptote, and the Kratky plot highlights any deviation from this. For single branched

molecules such as dendrimers, the plot reaches a maximum, then tends to a constant level at high  $q$ .<sup>45</sup> With this in mind, there is clear evidence that the SCPN is a single globular structure rather than a Gaussian chain in a good solvent. Interestingly, the control polymer **4.15** also shows evidence of a deviation from pure Gaussian behaviour, although with a less obvious maximum than SCPN **4.03**, which lends further weight to the thiol-Nb cyclisation hypothesis proposed earlier.



**Figure 4.15** Kratky plot (left) and Porod plot (right) from SANS data

In the higher  $q$  region, the Porod region, information about the local structure can be obtained. The gradient of  $\log(I)$  vs.  $\log(q)$  gives information about the morphology of the structure, for example a  $q$ -dependence of -1 correlates to a rigid rod, -2 to smooth 2D objects, -3–4 to 3D objects with fractal or smooth surfaces. A Gaussian chain in a good solvent (as THF- $d_8$  is for PS) has a  $q$  dependence of -5/3, and this is displayed by the linear

polymer **4.03** (Figure 4.15, gradient -1.50). That the SCPN **4.03** has a gradient of -1.85 indicates that has deviated from Gaussian chain behaviour shown by the linear polymer, perhaps forming more of a 3D object.

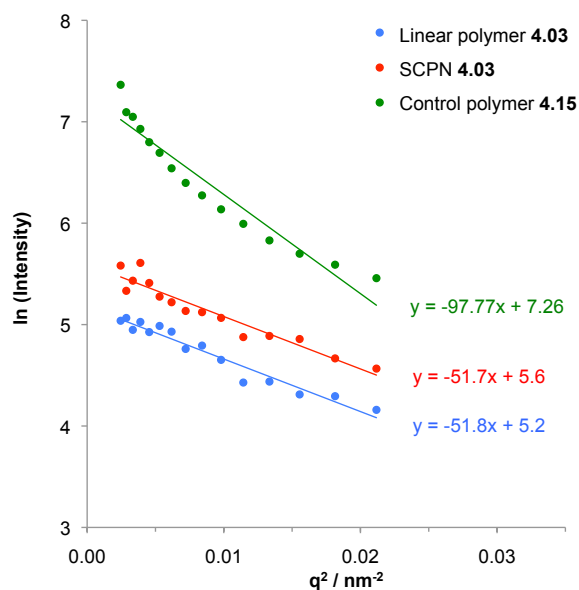
The radius of gyration ( $R_g$ ) of the samples can be obtained in the low  $q$  region (Guinier region), by using the Guinier approximation (Equation 4.4).

#### Equation 4.4 Guinier approximation and Guinier plot derivation

$$I = I_o e^{-\left(\frac{q^2 R_g^2}{3}\right)}$$

$$\ln(I) = \ln(I_o) - \frac{q^2 R_g^2}{3}$$

Equation 4.4 gives the Guinier equation, where  $I$  is the scattering intensity at a given  $q$ ,  $I_o$  is the initial scattering intensity and  $R_g$  is the radius of gyration of the sample. Thus plotting the natural log of the scattered intensity against  $q^2$  (Figure 4.16) gives a gradient equal to  $\frac{1}{3}R_g^2$  for the polymer and SCPN, assuming uniform distribution of mass around the centre of gravity i.e. spherical-like objects. The Guinier approximation is only valid for  $qR_g \ll 1$ , therefore only the low  $q$  values were used for this plot.



**Figure 4.16 Guinier plot for low  $q$  for linear, SCPN 4.03 and control polymer 4.15**

This gave  $R_g$  values of 12.5 nm for both the linear polymer chain **4.03** and the SCPN **4.03**, and 17.1 nm for the control polymer **4.15**, although the lack of linearity in the plot for **4.15** might suggest that the Guinier approximation is not valid in this case and therefore this  $R_g$  value may not be very accurate. These  $R_g$  values are much larger than the  $R_h$  values suggested by the DLS at multiple angles (7.0 nm), and the resulting shape factor ( $R_g/R_h = 1.79$ ) is indicative of a rod-like morphology for the SCPN and linear precursor **4.03**. Given that this directly contradicts the Kratky plot in Figure 4.15, this is perhaps further indication of aggregation of the SCPNs at this concentration and temperature and therefore the  $R_g$  value measured is not for a single SCPN.

#### 4.3.4.4. Static Light Scattering

Light scattering can be used to determine the absolute size (radius of gyration  $R_g$ ) and molecular weight ( $M_w$ ) of macromolecules,<sup>46</sup> using the Debye relationship shown in Equation 4.5.

**Equation 4.5 Debye equation for calculating  $M_w$  and  $R_g$  by light scattering,**

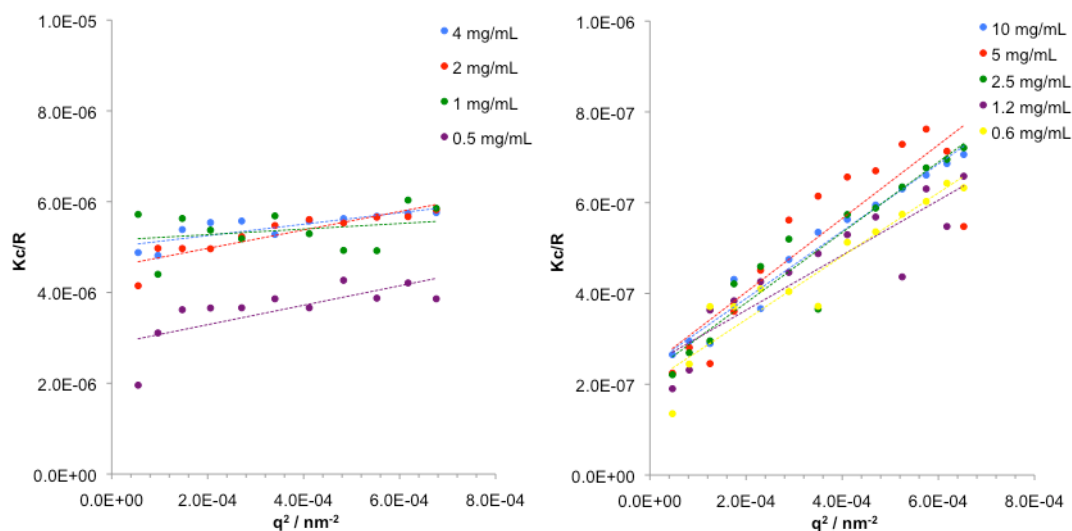
**where K = instrument and sample-dependent optical parameters,**

**c = concentration (mg/mL), R = relative scattering intensity, q = scattering vector,  $A_2$  = second virial coefficient**

$$\frac{Kc}{R} = \frac{1}{M_w} \left( 1 + \frac{R_g^2 q^2}{3} \right) + 2A_2C$$

Control polymer **4.15** and SCPN **4.03** were analysed by SLS at various concentrations in  $\text{CHCl}_3$ , and the scattering corrected for background absorbance. It is not possible to determine the  $R_g$  values by SLS in our case, as shown by the Zimm plots in Figure 4.17; as the figure shows, fitting a linear trend to the data at various concentrations, which would normally result in gradients equal to  $\frac{1}{3}R_g^2$ , does not result in a good fit, nor one that is consistent across the concentration range. This is because the polymers and SCPNs are small enough to have a negligible angular dependence over the q range measurable by SLS.

The  $q$  range of the SLS is limited by the light wavelength used (633 nm), whereas SANS can measure over higher  $q$  values, correlating to smaller length scales, hence why we used that approach to obtain  $R_g$  values. However, the  $M_w$  values for the particles can be calculated using the obtained SLS data, and the results are shown in Table 4.2.



**Figure 4.17 Zimm plots for control polymer 4.15 (left) and SCPN 4.03 (right), showing non-linear dependence of  $Kc/R$  on  $q^2$**

Interestingly, the data suggest that SCPNs are being formed of not one polymer chain, but between 3 and 4. This may explain why the  $R_g$  values calculated by SANS are larger than expected, and give further weight to the aggregation hypothesis proposed earlier in Section 4.3.4.2.

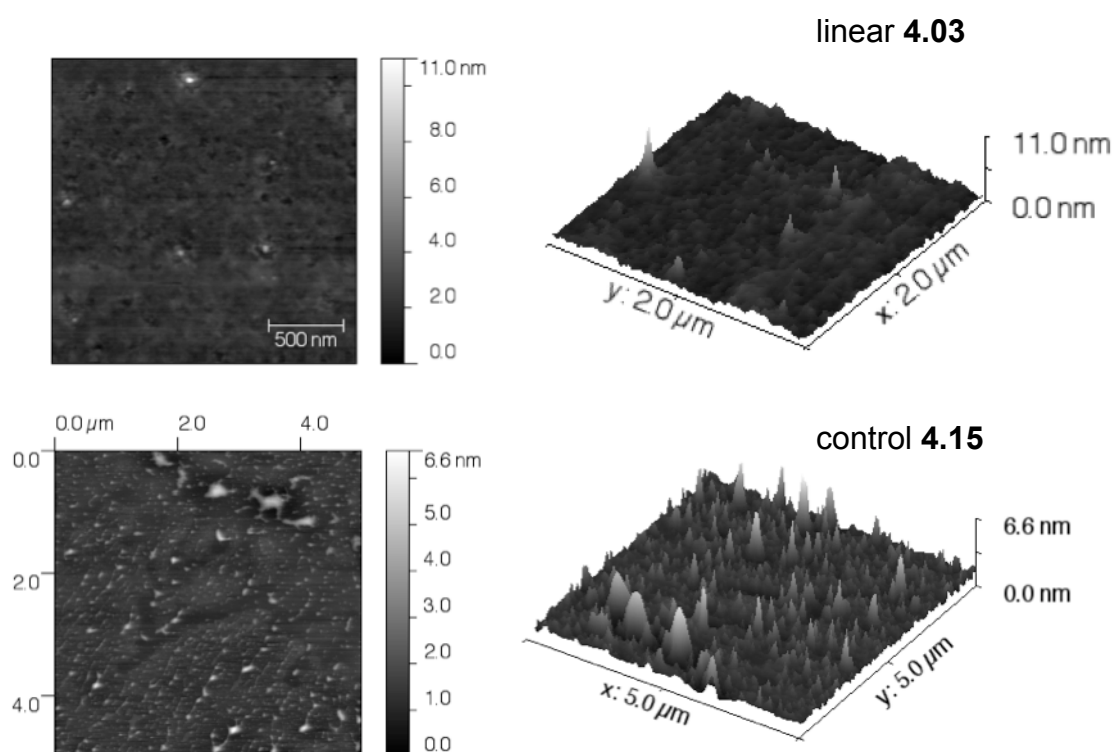


**Table 4.2  $M_w$  values by SLS for SCPN 4.03 and control polymer 4.15 (linear 4.03 by SEC)**

<b>Polymer</b>	<b><math>M_w</math> / Da</b>
Linear <b>4.03</b>	62300
SCPN <b>4.03</b>	227000
Control <b>4.15</b>	79200

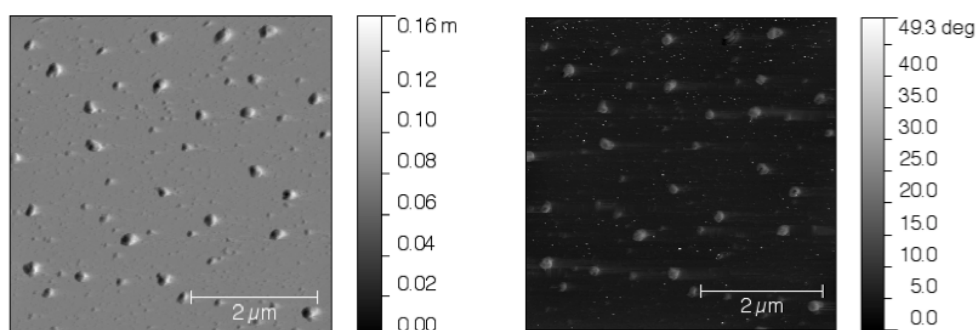
#### **4.3.4.5. Atomic Force Microscopy**

AFM imaging was carried out in tapping mode on dilute solutions of polymer/SCPN **4.03**, and control polymer **4.15** (0.001 mg/mL) drop-cast and air-dried on freshly cleaved mica. The linear polymer **4.03** formed a mainly featureless rough film on the surface (Figure 4.18, top). Control polymer **4.15** displayed some more varied surface topology, with what could be interpreted as SCPNs in evidence, but still was predominantly comprised of a rough polymer film covering the mica surface (Figure 4.18, bottom).

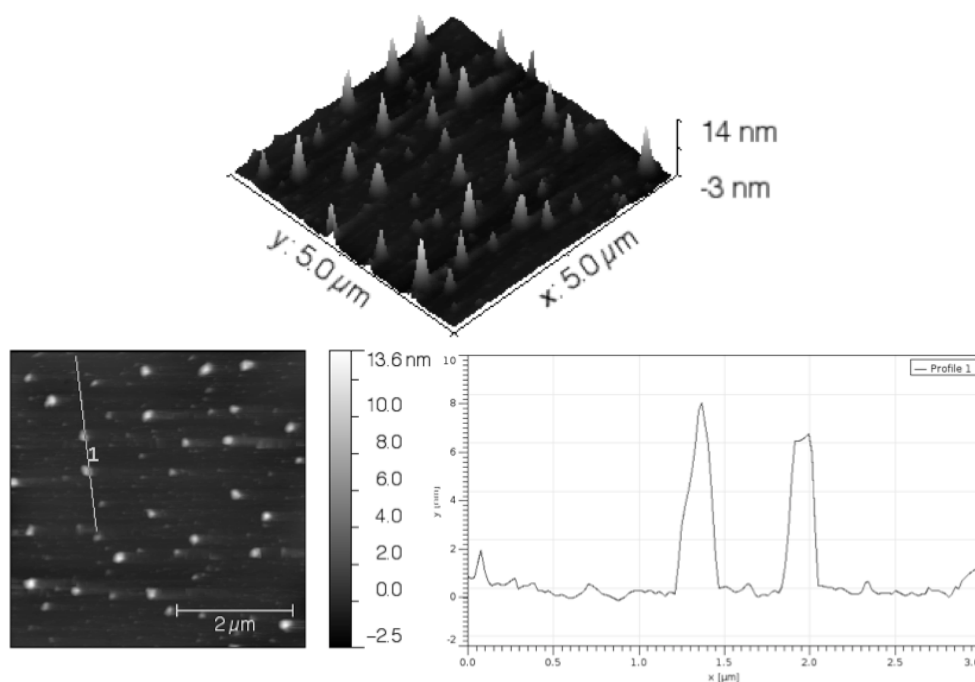


**Figure 4.18 AFM Z height images for linear precursor 4.03 (top) and control polymer 4.15 (bottom)**

A population of discrete particles (height  $5.8 \pm 3.3$  nm, 150 particles measured) was clearly visible in the images (Figure 4.19 and Figure 4.20).



**Figure 4.19 Amplitude (left) and phase (right) AFM images of SCPN 4.03**

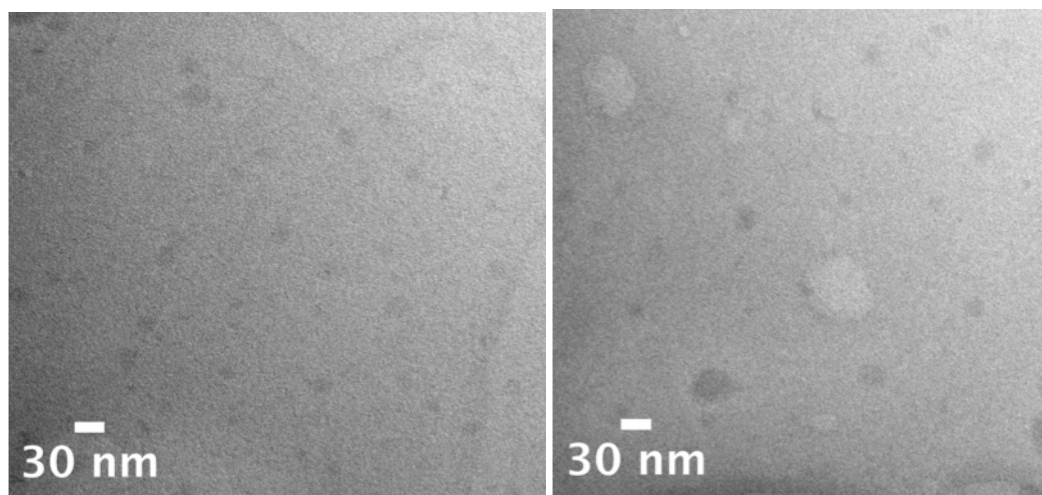


**Figure 4.20 Z height image (top) and line section of two SCPNs (bottom)**

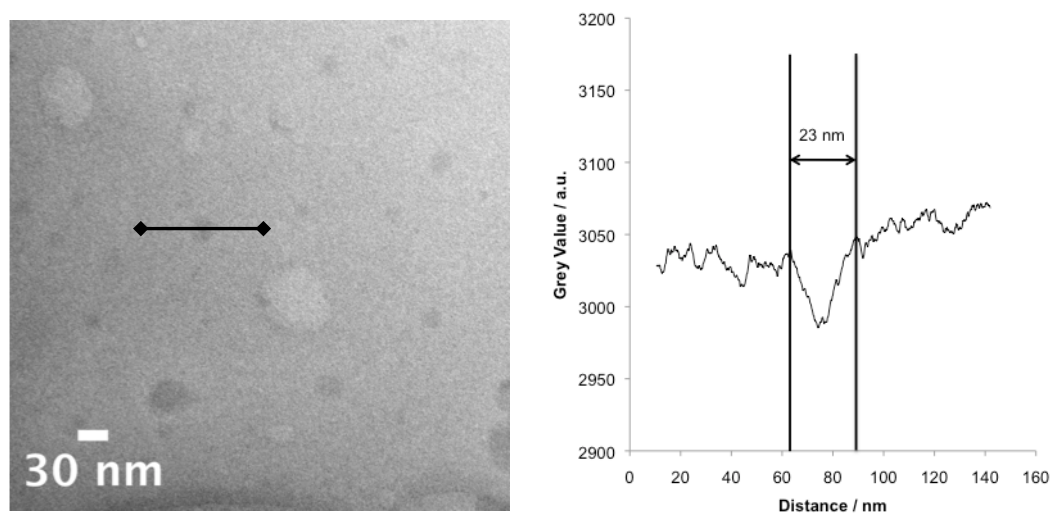
Assuming that the SCPNs dry to the surface in a hemiellipse, and taking the average height of the particles (5.8 nm), and average radius (62 nm), we can solve for the radius of an equivalent sphere.<sup>23</sup> Tip convolution effects mean that the diameter of the particles dried to the AFM grid will be overestimated, and therefore so will the calculated spherical radius, but this method gives a solution particle diameter of 44 nm with no tip correction. Assuming that the AFM tip results in an addition of 7 nm (the width of the silicon tip) to each side of the hemiellipse, resulting in a radius of 55 nm for the collapsed particle, this gives a solution particle diameter of 34 nm; this is still likely to be an overestimate with a large error as it is difficult to assess the consequences of tip effects on the measured radii.

#### 4.3.4.6. *Transmission Electron Microscopy*

TEM images on graphene oxide (GO) of the particles proved difficult to obtain due to their propensity to accumulate not on the GO 'holes', but on the thicker carbon support, reducing the contrast between particles and background significantly — this we attribute to their hydrophobicity.



**Figure 4.21 Representative TEM images on GO of SCPNs 4.03**



**Figure 4.22 Plot profile (right) of one particle in the TEM images, taken from a line scan across the image (left)**

Although the images (Figure 4.21) did not provide us with a good contrast between the particles and background, extracting plot profiles was possible to provide evidence for discrete particulate matter on the grids, as shown in Figure 4.22. The plot of the grey values is a moving average to smooth the profile and enable measurement of the  $D$  values for the particles. In this way we were able to identify 50 particles to measure their diameters, and the results gave  $D_{av} = 15.8 \pm 5.5$  nm, with the histogram of sizes shown in Figure 4.23.

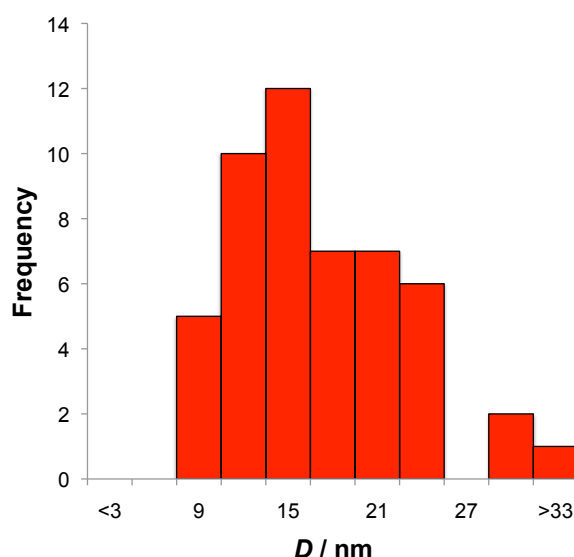


Figure 4.23 Histogram of particle  $D$  for SCPN 4.03 imaged by TEM on GO

#### 4.3.5. Characterisation summary

A summary of the particle size results for SCPN **4.03** are shown below in Table 4.3. There are some discrepancies between the imaging and scattering techniques, which perhaps highlights the difficulty in fully

characterising such small materials, and why in the literature it is predominantly SEC and DLS that are relied upon as primary characterisation methods.

**Table 4.3 SCPN 4.03 sizes by various analytical techniques**

Technique	Property measured	Size / nm
DLS single angle	$R_h$	3.7
DLS multi angle	$R_h$	7.0
AFM	$R_{\text{solid}}$	17.0
TEM	$R_{\text{solid}}$	7.9
SANS	$R_g$	12.5

That the sizes by various techniques do not match up entirely may be due to the proposed aggregation in the scattering experiments, or may also suggest that SCPN formation did not occur with 100% of the polymer chains, and that competing gelation or non-reaction may skew the results of the various techniques and affect them in different ways.

#### **4.4. Conclusions**

SCPN formation was successful to a certain extent, as evidenced by the SEC traces, AFM and TEM imaging. However, the difficulty in carrying out, and the uncertainty in the measurements of size by various scattering techniques suggests that in addition to SCPN formation, there may still be linear polymer present, or multi-chain gel structures might have also been formed. We hypothesise that this could be improved by using a faster rate of reaction to perform the crosslinking. A more reactive DA<sub>inv</sub> pair would most easily be achieved by using a more reactive tetrazine — H-substituted at the terminal position instead of methyl-substituted, and pyridyl- or pyrimidyl-substituted instead of phenyl-substituted. Attempts were made to synthesise these materials, but were unsuccessful due to the need to use anhydrous hydrazine for these more reactive tetrazines, which is not available for sale in Europe.

## 4.5. Experimental

### 4.5.1. Materials and methods

All chemicals and reagents were purchased from Sigma-Aldrich and used without further purification unless otherwise stated. Styrene (St) was distilled over  $\text{CaH}_2$ , 2,2'-Azobis(2-methylpropionitrile) (AIBN) was recrystallised twice from methanol and both were stored at 4 °C in the dark before use.

Nuclear magnetic resonance ( $^1\text{H}$  and  $^{13}\text{C}$  NMR) spectra were recorded at 400 or 500 MHz in  $\text{CDCl}_3$  or  $\text{DMSO}-d_6$  solution at 20 °C on a Bruker DPX-400 or Bruker AM-500 spectrometer. Chemical shifts are reported as  $\delta$  in parts per million (ppm) and referenced to the chemical shift of the residual solvent resonances ( $\text{CDCl}_3$   $^1\text{H}$ :  $\delta$  = 7.26 ppm;  $^{13}\text{C}$   $\delta$  = 77.16 ppm;  $\text{DMSO}-d_6$   $^1\text{H}$ :  $\delta$  = 2.50 ppm;  $^{13}\text{C}$   $\delta$  = 39.52 ppm). Coupling constants ( $J$ ) are given in Hz. The resonance multiplicities are described as s (singlet), d (doublet), app t (apparent triplet), q (quartet) or m (multiplet). For acquired  $^{13}\text{C}$  NMR experiments, multiplicities were distinguished using an ATP pulse sequence whereby methylene and quaternary carbon signals appear 'up' (u) and methyl and methane carbons 'down' (dn). Diffusion ordered spectra were acquired using the standard Bruker 2D sequence for diffusion measurements using stimulated echo and LED, and processed using Bruker Topspin and DOSY Toolbox softwares, assuming a single population of molecules.

Molar mass distributions were measured using size exclusion chromatography (SEC), and all samples were filtered through 0.22  $\mu\text{m}$



PTFE filters before injection. Analyses were performed in HPLC grade THF containing 2 vol% triethyl amine (TEA), dimethylacetamide (DMAc) or  $\text{CHCl}_3$  at 30 °C, at a flow rate of 1.0 mL/min on a set of two PLgel 5  $\mu\text{m}$  Mixed-D columns and one PLgel 5  $\mu\text{m}$  guard column with differential refractive index detection. Polystyrene standards were used for calibration, samples were injected using a PL AS RT autosampler and molecular weight and dispersity indices determined using Cirrus software.

FT-IR spectra were obtained using a Perkin Elmer Spectrum 100 FT-IR. 16 scans from 600 to 4000  $\text{cm}^{-1}$  were taken, and the spectra corrected for background absorbance.

UV/vis measurements were made on a Perkin Elmer Lambda 35 UV/vis spectrometer, far UV quartz cuvettes (Hellma) were used.

Hydrodynamic diameters ( $D_h$ ) and size distributions of SCPNs were determined by DLS on a Malvern Zetasizer Nano ZS operating at 20 °C with a 4 mW He-Ne 633 nm laser module. Samples were filtered through a 0.45  $\mu\text{m}$  PTFE filter prior to measurement and quartz cuvettes were used. Measurements were made at a detection angle of 173° (back scattering), and the data analysed using Malvern DTS 5.02 software, using the multiple narrow modes setting. All measurements were made in triplicate, with 10 runs per measurement. To discount small amounts of aggregates/larger structures in the solutions, which skew the automatically generated results from the Zetasizer, the data were reanalysed by fitting the correlation functions to a stretched exponential function (Kohlrausch-Williams-Watts) from which the relaxation time was derived for the major population, and

from this the  $R_h$  (and therefore  $D_h$ ) was calculated using the Stokes-Einstein equation.

SLS measurements were performed at angles from 30° up to 150° with an ALV CGS3 ( $\lambda = 632$  nm) and at  $25 \pm 1$  °C. The data were collected with 100 s run time in duplicate, calibration was with filtered toluene and the background was measured with filtered  $\text{CHCl}_3$ . The refractive index increment of the polymers in chloroform was assumed to be equal to that of polystyrene (0.15 mL/g).

TEM analyses were performed on a JEOL 2011 ( $\text{LaB}_6$ ) microscope operating at 200 kV, equipped with a GATAN UltraScan 1000 digital camera. Conventional bright field conditions were used to image samples in all cases. TEM grids used were lacey carbon-coated copper grids (Agar Scientific, 400 mesh, S116-4) coated with a thin layer of graphene oxide. SCPN solutions were diluted to 2.5 mg/mL in  $\text{CH}_2\text{Cl}_2$  before 4  $\mu\text{L}$  of each sample was drop-deposited onto the graphene oxide-coated grids, blotted immediately and allowed to air dry. No subsequent staining or treatment of the grids was required prior to imaging the samples.<sup>47</sup> Images were analysed using ImageJ software, and 50 particles were measured to produce a mean and standard deviation for the particle size ( $D_{av}$ ).

AFM images were taken in tapping mode on a Multimode AFM with Nanoscope IIIA controller with Quadrex. Silicon AFM tips were used with nominal spring constant and resonance frequency of  $3.5 \text{ Nm}^{-1}$  and 75 kHz (MikroMasch NSC18). Samples were diluted to 0.001 mg/mL in  $\text{CH}_2\text{Cl}_2$  and 4  $\mu\text{L}$  drop-deposited onto freshly cleaved mica discs (9.9 mm, Agar

Scientific G250-6). Data were processed and analysed using Gwyddion software.

SANS experiments were performed on the ISIS neutron beam facility, sans2d instrument at the Rutherford Appleton Laboratory, Oxford. Samples were measured at 10 mg/mL in THF-d<sub>8</sub> – a good solvent for polystyrene and one that provides a suitably high contrast in scattering length to the polymer.

## **4.5.2. Syntheses**

### **4.5.2.1. General polymer synthesis**

As described in Chapter 3 and a literature precedent,<sup>48</sup> the requisite amounts of styrene and Nb–St (synthesis described in Chapter 3), DDMAT and AIBN (1:0.1 [DDMAT]:[AIBN]) were dissolved in toluene (1:1 <sup>w/v</sup>) and subjected to four freeze-evacuate-thaw cycles. The polymerisation ampoule was warmed to room temperature under nitrogen and then immersed in an oil bath at 70 °C for 23–24 h. Monomer conversions were determined by <sup>1</sup>H NMR spectroscopy, and the polymer was precipitated 3 times from cold methanol and 3 times from cold pentane before being freeze dried from dioxane and recovered as a yellow or white powdery solid.

### **4.5.2.2. [p-(6-Methyl-1,2,4,5-tetrazin-3-yl)phenyl]methanol (Tz–OH)**

Tz–OH was synthesised according to a modified literature procedure.<sup>37</sup> 4-Hydroxymethyl benzonitrile (1.00 g, 7.51 mmol), nickel triflate (1.34 g, 3.76 mmol), acetonitrile (3.92 mL, 75.1 mmol) and hydrazine monohydrate (18.3 mL, 376 mmol) were mixed in a sealed ampoule and stirred at RT for

30 min to ensure complete dissolution of all the reagents. The ampoule was placed in an oil bath at 60 °C for 24 h behind a blast shield, after which it was allowed to cool to room temperature and opened carefully due to the pressure build-up during the reaction. The resulting brown mixture was added to sodium nitrite (5.18 g, 75.1 mmol) in 20 mL water, after which conc. HCl was added extremely slowly, diluting with water as necessary (final volume *ca.* 500 mL) to control the resulting effervescence and being careful of the evolved nitrous gases, until pH 3 was reached. The aqueous phase was extracted with EtOAc (3 x 200 mL), then the organic phase washed with H<sub>2</sub>O and brine and dried over MgSO<sub>4</sub>. The product was isolated by flash column chromatography (2:1 hexanes:EtOAc, R<sub>f</sub> 0.15) as a pink solid (374 mg, 13% yield). <sup>1</sup>H NMR (400 MHz, CDCl<sub>3</sub>) δ (ppm): 8.57 (2H, d, <sup>3</sup>J<sub>H-H</sub> = 8.2 Hz), 7.58 (2H, d, <sup>3</sup>J<sub>H-H</sub> = 8.2 Hz), 4.83 (2H, s), 3.09 (3H, s). <sup>13</sup>C NMR (100 MHz, CDCl<sub>3</sub>) δ (ppm): 167.4 (u), 164.1 (u), 145.8 (u), 131.1 (u), 128.3 (dn), 127.6 (dn), 64.9 (u), 21.3 (dn).

**4.5.2.3. [p-(6-Methyl-1,2,4,5-tetrazine-3-yl)phenyl]acetic acid (Tz-COOH)**

Tz-COOH was synthesised according to a modified literature precedent.<sup>37</sup> 4-Cyanophenylacetic acid (0.90 g, 5.58 mmol), zinc triflate (1.02 g, 2.79 mmol), acetonitrile (2.91 mL, 55.8 mmol) and hydrazine monohydrate (13.6 mL, 279 mmol) were mixed in a sealed ampoule and placed in an oil bath at 60 °C for 24 h behind a blast shield, after which it was allowed to cool to room temperature and opened carefully due to the pressure build-up during the reaction. The resulting orange mixture was added to sodium

nitrite (7.71 g, 112 mmol) in 25 mL water, after which conc. HCl was added extremely slowly, diluting with water as necessary (final volume ca. 500 mL) to control the resulting effervescence and being careful of the evolved nitrous gases, until pH 3 was reached. The aqueous phase was extracted with EtOAc (3 x 200 mL), then the organic phase washed with H<sub>2</sub>O and brine and dried over MgSO<sub>4</sub>. The product was isolated by flash column chromatography (15:1 CH<sub>2</sub>Cl<sub>2</sub>/MeOH, R<sub>f</sub> 0.20) as a pink solid (234 mg, 1.01 mmol, 18% yield). <sup>1</sup>H NMR (400 MHz, CDCl<sub>3</sub>) δ (ppm): 8.49 (2H, d, <sup>3</sup>J<sub>H-H</sub> = 8.3 Hz), 7.48 (2H, d, <sup>3</sup>J<sub>H-H</sub> = 8.3 Hz), 3.74 (2H, s), 3.07 (3H, s). <sup>13</sup>C NMR (100 MHz, CDCl<sub>3</sub>) δ (ppm): 176.0 (u), 167.4 (u), 164.0 (u), 138.1 (u), 131.1 (u), 130.5 (dn), 128.4 (dn), 41.0 (u), 21.3 (dn).

#### **4.5.2.4. Ethyl [p-(6-methyl-1,2,4,5-tetrazin-3-yl)phenyl] acetate (Tz-COOEt) 4.01**

The product was an unexpected product of the attempted synthesis of a Tz-Tz crosslinker by EDCI-mediated coupling of 1,4-butane diol.

Tz-COOH (120 mg, 0.521 mmol), EDCI·HCl (99.9 mg, 0.521 mmol) and DMAP (8.49 mg, 0.0695 mmol) were dissolved in dry CH<sub>2</sub>Cl<sub>2</sub> (20 mL) under a N<sub>2</sub> atmosphere. 1,4-Butanediol (15.4 uL, 0.174 mmol) was added *via* syringe and the mixture stirred at room temperature for 24 h. The mixture was washed with water (2 x 20 mL), brine (20 mL) and saturated NaHCO<sub>3</sub> (20 mL), dried over MgSO<sub>4</sub> and the solvent removed *in vacuo*. The product was isolated by flash column chromatography (CH<sub>2</sub>Cl<sub>2</sub>, R<sub>f</sub> 0.3) as a bright pink solid (86.3 mg, 0.335 mmol, 64% yield). HRMS (ESI, [M+Na]<sup>+</sup>) *m/z*: predicted 281.1014, found 281.1009. <sup>1</sup>H NMR (400 MHz, CDCl<sub>3</sub>) δ (ppm): 8.55 (2H, d, <sup>3</sup>J<sub>H-H</sub> = 8.2 Hz), 7.52 (2H, d, <sup>3</sup>J<sub>H-H</sub> = 8.2 Hz), 4.18 (2H, q,

$^3J_{\text{H-H}} = 7.2$  Hz), 3.73 (2H, s), 3.09 (3H, s), 1.27 (3H, t,  $^3J_{\text{H-H}} = 7.2$  Hz).  $^{13}\text{C}$  NMR (100 MHz,  $\text{CDCl}_3$ )  $\delta$  (ppm): 171.0 (u), 167.4 (u), 164.1 (u), 139.1 (u), 130.8 (u), 130.4 (dn), 128.3 (dn), 61.3 (u), 41.5 (u), 21.3 (dn), 14.3 (dn). IR  $\nu$  ( $\text{cm}^{-1}$ ): 2927, 1723, 1616, 1472, 1402, 1368, 1339, 1223, 1167, 1090, 1017, 889, 800, 755, 689. Elemental analysis: expected C 60.45, H 5.46, N 21.69, O 12.39, found C 60.79, H 5.57, N 20.21.

#### 4.5.2.5. *Di[p-(6-methyl-1,2,4,5-tetrazin-3-yl)phenyl]methyl glutarate (Tz–Tz) 4.02*

Tz–OH (336 mg, 1.66 mmol) was dissolved in dry  $\text{CH}_2\text{Cl}_2$  (15 mL) under a  $\text{N}_2$  atmosphere, and glutaryl chloride (106  $\mu\text{L}$ , 141 mg, 0.831 mmol) added *via* syringe. The mixture was stirred at room temperature for 24 h, the solvent removed *in vacuo* and the product isolated by flash column chromatography (2% MeOH in  $\text{CH}_2\text{Cl}_2$ ,  $R_f$  0.6) as a pink solid (315 mg, 0.629 mmol, 38% yield). HRMS (ESI,  $[\text{M}+\text{H}]^+$ )  $m/z$ : predicted 501.1999, found 501.1997.  $^1\text{H}$  NMR (400 MHz,  $\text{CDCl}_3$ )  $\delta$  (ppm): 8.57 (4H, d,  $^3J_{\text{H-H}} = 8.4$  Hz), 7.55 (4H, d,  $^3J_{\text{H-H}} = 8.4$  Hz), 5.23 (4H, s), 3.10 (6H, s), 2.51 (4H, t,  $^3J_{\text{H-H}} = 7.2$  Hz), 2.06 (2H, quin,  $^3J_{\text{H-H}} = 7.2$  Hz).  $^{13}\text{C}$  NMR (100 MHz,  $\text{CDCl}_3$ )  $\delta$  (ppm): 172.1 (u), 167.5 (u), 163.9 (u), 140.7 (u), 131.8 (u), 128.7 (dn), 128.3 (dn), 65.8 (u), 33.3 (u), 21.3 (dn), 20.2 (u). IR  $\nu$  ( $\text{cm}^{-1}$ ): 2926, 1733, 1612, 1401, 1364, 1285, 1147, 1089, 984, 955, 887, 796, 615. UV/vis ( $\text{CH}_2\text{Cl}_2$ ):  $\lambda_{\text{max}} = 320$  nm,  $\lambda_{\text{secondary peak}} = 545$  nm.

#### 4.5.2.6. *General SPCN synthesis*

PS(Nb) polymer was dissolved in DMF at a concentration of 0.01 M of Nb groups, and added at 1 mL/h to a solution of Tz–Tz **4.02** in DMF (0.5 eq.

relative to Nb groups on the polymer, volume equivalent to the volume of polymer solution added) held at 80 °C. The solution was stirred for 24 h at 80 °C, before being cooled to room temperature and an excess of bicyclo[2.2.1]hept-2-ene (norbornene) added to quench any **4.02**. DMF was removed *in vacuo* and the SCPNs isolated by precipitation once from cold MeOH and once from cold hexanes.

## 4.6. References

- (1) Taranekar, P.; Park, J.-Y.; Patton, D.; Fulghum, T.; Ramon, G. J.; Advincula, R. *Adv. Mater.* **2006**, *18*, 2461-2465.
- (2) Park, K.-s.; Kim, D.-y.; Choi, S.-k.; Suh, D. H. *Jpn. J. Appl. Phys., Part 1* **2003**, *42*, 3877-3880.
- (3) Mecerreyes, D.; Lee, V.; Hawker, C. J.; Hedrick, J. L.; Wursch, A.; Volksen, W.; Magbitang, T.; Huang, E.; Miller, R. D. *Adv. Mater.* **2001**, *13*, 204-208.
- (4) (a) Tuteja, A.; Duxbury, P. M.; Mackay, M. E. *Macromolecules* **2007**, *40*, 9427-9434. (b) Mackay, M. E.; Dao, T. T.; Tuteja, A.; Ho, D. L.; Van, H. B.; Kim, H.-C.; Hawker, C. J. *Nat. Mater.* **2003**, *2*, 762-766. (c) Tuteja, A.; Mackay, M. E.; Hawker, C. J.; Van, H. B. *Macromolecules* **2005**, *38*, 8000-8011. (d) Schmidt, R. G.; Gordon, G. V.; Dreiss, C. A.; Cosgrove, T.; Krukoni, V. J.; Williams, K.; Wetmore, P. M. *Macromolecules* **2010**, *43*, 10143-10151.
- (5) (a) Wulff, G.; Chong, B.-O.; Kolb, U. *Angew. Chem., Int. Ed.* **2006**, *45*, 2955-2958. (b) Liu, J.-Q.; Wulff, G. *J. Am. Chem. Soc.* **2008**, *130*, 8044-8054.
- (6) Ouchi, M.; Badi, N.; Lutz, J.-F.; Sawamoto, M. *Nat. Chem.* **2011**, *3*, 917-924.
- (7) Harth, E.; Horn, B. V.; Lee, V. Y.; Germack, D. S.; Gonzales, C. P.; Miller, R. D.; Hawker, C. J. *J. Am. Chem. Soc.* **2002**, *124*, 8653-8660.



- (8) Jiang, J.; Thayumanavan, S. *Macromolecules* **2005**, *38*, 5886-5891.
- (9) (a) Croce, T. A.; Hamilton, S. K.; Chen, M. L.; Muchalski, H.; Harth, E. *Macromolecules* **2007**, *40*, 6028-6031. (b) Adkins, C. T.; Muchalski, H.; Harth, E. *Macromolecules* **2009**, *42*, 5786-5792.
- (10) Dobish, J. N.; Hamilton, S. K.; Harth, E. *Polym. Chem.* **2012**, *3*, 857-860.
- (11) (a) Ergin, M.; Kiskan, B.; Gacal, B.; Yagci, Y. *Macromolecules* **2007**, *40*, 4724-4727. (b) Wang, P.; Pu, H.; Jin, M. *J. Polym. Sci., Part A: Polym. Chem.* **2011**, *49*, 5133-5141.
- (12) Jiang, X.; Pu, H.; Wang, P. *Polymer* **2011**, *52*, 3597-3602.
- (13) (a) Oria, L.; Aguado, R.; Pomposo, J. A.; Colmenero, J. *Adv. Mater.* **2010**, *22*, 3038-3041. (b) de Luzuriaga, A. R.; Ormategui, N.; Grande, H. J.; Odriozola, I.; Pomposo, J. A.; Loinaz, I. *Macromol. Rapid Comm.* **2008**, *29*, 1156-1160. (c) Perez-Baena, I.; Loinaz, I.; Padro, D.; Garcia, I.; Grande, H. J.; Odriozola, I. *J. Mater. Chem.* **2010**, *20*, 6916-6922.
- (14) Sanchez-Sanchez, A.; Asenjo-Sanz, I.; Buruaga, L.; Pomposo, J. A. *Macromol. Rapid Comm.* **2012**, *33*, 1262-1267.
- (15) He, J.; Tremblay, L.; Lacelle, S.; Zhao, Y. *Soft Matter* **2011**, *7*, 2380-2386.
- (16) Njikang, G.; Liu, G.; Curda, S. A. *Macromolecules* **2008**, *41*, 5697-5702.

(17) (a) Zhu, B.; Sun, S.; Wang, Y.; Deng, S.; Qian, G.; Wang, M.; Hu, A. *J. Mater. Chem., C* **2013**, *1*, 580-586. (b) Zhu, B.; Qian, G.; Xiao, Y.; Deng, S.; Wang, M.; Hu, A. *J. Polym. Sci., Part A: Polym. Chem.* **2011**, *49*, 5330-5338. (c) Zhu, B.; Ma, J.; Li, Z.; Hou, J.; Cheng, X.; Qian, G.; Liu, P.; Hu, A. *J. Mater. Chem.* **2011**, *21*, 2679-2683.

(18) Cherian, A. E.; Sun, F. C.; Sheiko, S. S.; Coates, G. W. *J. Am. Chem. Soc.* **2007**, *129*, 11350-11351.

(19) Beck, J. B.; Killops, K. L.; Kang, T.; Sivanandan, K.; Bayles, A.; Mackay, M. E.; Wooley, K. L.; Hawker, C. J. *Macromolecules* **2009**, *42*, 5629-5635.

(20) Dirlam, P. T.; Kim, H. J.; Arrington, K. J.; Chung, W. J.; Sahoo, R.; Hill, L. J.; Costanzo, P. J.; Theato, P.; Char, K.; Pyun, J. *Polym. Chem.* **2013**, *4*, 3765-3773.

(21) Seo, M.; Beck, B. J.; Paulusse, J. M. J.; Hawker, C. J.; Kim, S. Y. *Macromolecules* **2008**, *41*, 6413-6418.

(22) (a) Foster, E. J.; Berda, E. B.; Meijer, E. W. *J. Am. Chem. Soc.* **2009**, *131*, 6964-6966. (b) Foster, E. J.; Berda, E. B.; Meijer, E. W. *J. Polym. Sci., Part A: Polym. Chem.* **2011**, *49*, 118-126.

(23) Berda, E. B.; Foster, E. J.; Meijer, E. W. *Macromolecules* **2010**, *43*, 1430-1437.

(24) Stals, P. J. M.; Gillissen, M. A. J.; Nicolay, R.; Palmans, A. R. A.; Meijer, E. W. *Polym. Chem.* **2013**, *4*, 2584-2597.

- (25) Mes, T.; van der Weegen, R.; Palmans, A. R. A.; Meijer, E. W. *Angew. Chem., Int. Ed.* **2011**, *50*, 5085-5089.
- (26) (a) Terashima, T.; Mes, T.; De Greef, T. F. A.; Gillissen, M. A. J.; Besenius, P.; Palmans, A. R. A.; Meijer, E. W. *J. Am. Chem. Soc.* **2011**, *133*, 4742-4745. (b) Huerta, E.; Stals, P. J. M.; Meijer, E. W.; Palmans, A. R. A. *Angew. Chem., Int. Ed.* **2013**, *52*, 2906-2910.
- (27) Gillissen, M. A. J.; Voets, I. K.; Meijer, E. W.; Palmans, A. R. A. *Polym. Chem.* **2012**, *3*, 3166-3174.
- (28) Hosono, N.; Gillissen, M. A. J.; Li, Y.; Sheiko, S. S.; Palmans, A. R. A.; Meijer, E. W. *J. Am. Chem. Soc.* **2013**, *135*, 501-510.
- (29) Thibault, R. J.; Hotchkiss, P. J.; Gray, M.; Rotello, V. M. *J. Am. Chem. Soc.* **2003**, *125*, 11249-11252.
- (30) (a) Altintas, O.; Gerstel, P.; Dingenouts, N.; Barner-Kowollik, C. *Chem. Commun.* **2010**, *46*, 6291-6293. (b) Altintas, O.; Rudolph, T.; Barner-Kowollik, C. *J. Polym. Sci., Part A: Polym. Chem.* **2011**, *49*, 2566-2576.
- (31) Altintas, O.; Lejeune, E.; Gerstel, P.; Barner-Kowollik, C. *Polym. Chem.* **2012**, *3*, 640-651.
- (32) Appel, E. A.; Barrio, J. d.; Dyson, J.; Isaacs, L.; Scherman, O. A. *Chem. Sci.* **2012**, *3*, 2278-2281.
- (33) Mavila, S.; Diesendruck, C. E.; Linde, S.; Amir, L.; Shikler, R.; Lemcoff, N. G. *Angew. Chem., Int. Ed.* **2013**, *52*, 5767-5770.

- (34) Jackson, A. W.; Fulton, D. A. *Polym. Chem.* **2013**, *4*, 31-45.
- (35) Murray, B. S.; Fulton, D. A. *Macromolecules* **2011**, *44*, 7242-7252.
- (36) Whitaker, D. E.; Mahon, C. S.; Fulton, D. A. *Angew. Chem., Int. Ed.* **2013**, *52*, 956-959.
- (37) Yang, J.; Karver, M. R.; Li, W.; Sahu, S.; Devaraj, N. K. *Angew. Chem., Int. Ed.* **2012**, *51*, 5222-5225.
- (38) Schmidt, B. V. K. J.; Fechner, N.; Falkenhagen, J.; Lutz, J.-F. *Nat. Chem.* **2011**, *3*, 234-238.
- (39) Liu, J. W.; Mackay, M. E.; Duxbury, P. M. *Macromolecules* **2009**, *42*, 8534-8542.
- (40) Morris, K. F.; Johnson, C. S. *J. Am. Chem. Soc.* **1992**, *114*, 3139-3141.
- (41) Pomposo, J. A.; Perez-Baena, I.; Buruaga, L.; Alegria, A.; Moreno, A. J.; Colmenero, J. *Macromolecules* **2011**, *44*, 8644-8649.
- (42) Wagner, H. L. *J. Phys. Chem. Ref. Data* **1985**, *14*, 1101-1106.
- (43) Chassenieux, C.; Nicolai, T.; Durand, D. *Macromolecules* **1997**, *30*, 4952-4958.
- (44) Sears, V. F. *Neutron News* **1992**, *3*, 26-37.
- (45) Hammouda, B. *J. Polym. Sci., Part B: Polym. Phys.* **1992**, *30*, 1387-1390.
- (46) Wyatt, P. J. *Anal. Chim. Acta* **1993**, *272*, 1-40.

(47) Patterson, J. P.; Sanchez, A. M.; Petzetakis, N.; Smart, T. P.; Epps III, T. H.; Portman, I.; Wilson, N. R.; O'Reilly, R. K. *Soft Matter* **2012**, 8, 3322-3328.

(48) Chen, L.; Hillmyer, M. A. *Macromolecules* **2009**, 42, 4237-4243.

## **Chapter 5. Expanding the scope of tetrazine cycloadditions using alkene polymers**

### **5.1. Abstract**

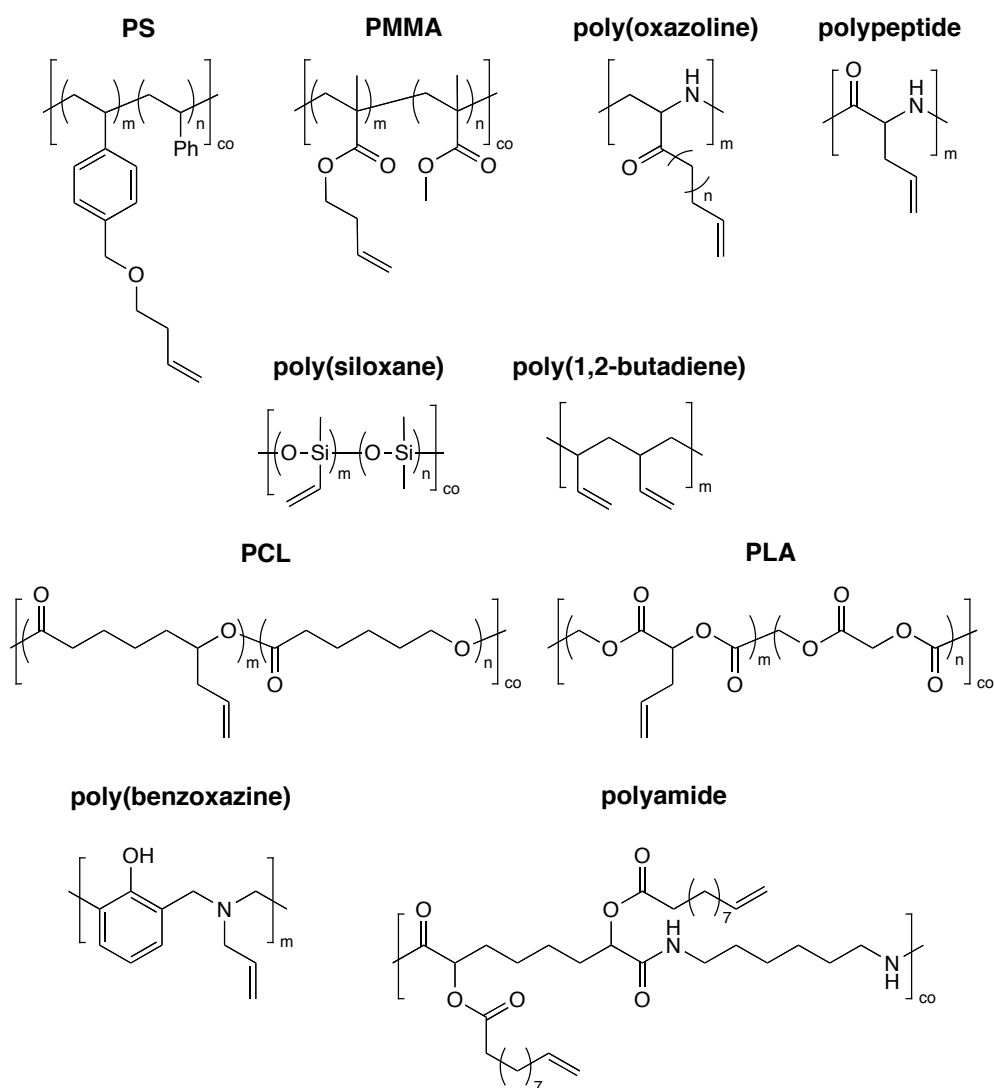
In this Chapter we describe the synthesis of pendent alkene acrylate-based copolymers by RAFT polymerisation methods, with a view to using their reaction with tetrazines for polymer functionalisation, albeit in a non-click type manner by using excess reagents and possibly forcing conditions. We synthesise three tetrazine-functionalised molecules of interest to investigate the possibility of polymer functionalisation without using norbornene as the dienophile, and explore the reaction rate when varying the solvent, temperature and with added catalysts.

## 5.2. Background

In previous chapters we have described the use of norbornene-containing polymers (both end-functional and main chain-functionalised) for synthesis and modification of a variety of macromolecular architectures. However, norbornene as a reactive site does have some disadvantages. In the first instance, its smell is quite pungent, although this effect is significantly diminished when it is incorporated into a polymer. Additionally, it is susceptible to degradation by acid,<sup>1</sup> thus copolymerisation with, and deprotection of, typical acrylic acid precursor *tert*-butyl acrylate (*t*BuA) is not a viable route to forming hydrophilic, norbornene-embedded polymers, as discussed in Chapter 3. When polymerising norbornene by radical methods, it is also necessary to keep the conversions low due to competitive reaction of the norbornene double bond, although this handicap is unlikely to be fully overcome by using a less reactive alkene, as it still is inherently reactive towards the radicals present in a polymerisation.

Polymers containing pendent unstrained alkenes are a prospective alternative to the norbornene-based polymers, and have been primarily used to demonstrate the utility of thiol-ene reactions in the literature thus far. A wide range of polymers have been used for both Michael addition and radical thiol-ene reactions, many of which are shown in Figure 5.1. Some of the earliest examples were the functionalisation of polysiloxanes,<sup>2</sup> polybutadiene<sup>3</sup> and oligomeric polyisobutenes.<sup>4</sup> Controlled radical polymerisation techniques have also been combined with post-polymerisation modification by thiol-ene reactions when synthesising

methacrylic, styrenic<sup>5</sup> and pentafluorostyrenic<sup>6</sup> polymers of defined molecular weights and narrow dispersities.



**Figure 5.1** Pendant alkene-containing polymers found in the literature: PS,<sup>5</sup> PMMA,<sup>5</sup> poly(oxazoline),<sup>7</sup> polypeptide,<sup>8</sup> poly(siloxane),<sup>2</sup> poly(butadiene),<sup>3</sup> PCL,<sup>5</sup> PLA,<sup>9</sup> poly(benzoxazine)<sup>10</sup> and polyamide<sup>11</sup>

Using other (non-radical) controlled polymerisation techniques has also yielded alkene-functional polyoxazolines as peptide mimics,<sup>7</sup> actual



polypeptides,<sup>8</sup> polybenzoxazines<sup>10</sup> and polyamides,<sup>11</sup> although in this case the alkene functionalities were introduced in a post-polymerisation step. ROP techniques have also been used as a route to alkene-functionalised poly(ester)s,<sup>5</sup> and allyl-functionalised polylactides.<sup>9</sup>

There is some precedent for tetrazines reacting with unstrained alkenes<sup>12</sup> and alkynes<sup>13</sup> — for example the reaction of dipyrityl tetrazine with a terminal alkyne reached full conversion after 90 minutes at 150 °C,<sup>13a</sup> and alkenes are more reactive towards tetrazines than alkynes<sup>12c</sup> — and therefore we were motivated to investigate whether it would be possible to combine existing knowledge of alkene-containing polymer preparation with tetrazine functionalisation in order to overcome some of the limitations of the norbornene-functionalised polymers described previously.

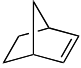
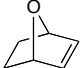

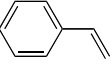
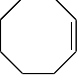
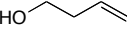
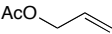
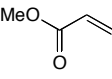
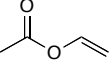
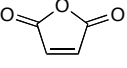
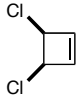
## **5.3. Results and discussion**

### **5.3.1. Preliminary rate screening**

We first wanted to confirm that the reaction with an unstrained alkene would proceed to full conversion, and on what timescale that would occur. In order to do this, we carried out a small molecule model reaction between dipyrityl tetrazine and various double bond-containing small molecules. Using a tenfold excess of alkene relative to tetrazine (0.1 M and 0.01 M respectively) in CDCl<sub>3</sub>, the reaction conversion at room temperature was monitored by <sup>1</sup>H NMR spectroscopy. Conversion was determined using the

relative integrations of the tetrazine pyridine signals at 9.01, 8.77, 8.03 and 7.60 ppm, and the pyradizine product signals from 7.30–8.70 ppm.

**Table 5.1 Relative reaction rates of alkenes with dipyridyl tetrazine, measured by  $^1\text{H}$  NMR spectroscopy**

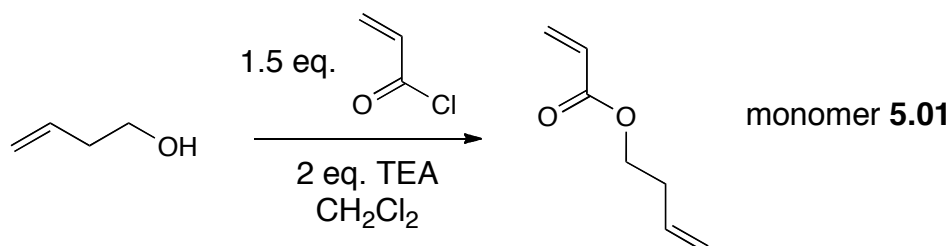
Entry	Alkene	Tetrazine conversion / %				
		2 h	4 h	24 h	5 d	12 d
1		100% at 7 min				
2		87	100	-	-	-
3		76	100	-	-	-
4		51	100	-	-	-
5		25	44	100	-	-
6		14	30	82	100	-
7		2	7	34	87	100
8		0	0	10	51	82
9		0	0	10	40	78
10		0	11	12	22	29
11		0	0	0	-	-

Of the data obtained from a larger study performed by Shirley Ye and summarised in Table 5.1<sup>12b</sup>, we were primarily interested in what type of acyclic alkene-containing monomer would be the most reactive. As such we looked at whether a pendent alkene, allyl or otherwise conjugated monomer would be most suitable to synthesise (entries **6–8** in Table 5.1).

The results of the initial screening suggested that functionalisation of pendent alkene monomers would be possible to 100% conversion (see entry **6**, where 100% conversion was achieved between 1 and 5 days), albeit at a much slower rate than the equivalent norbornene, provided that an unconjugated, rather than allyl (entry **7**) or acrylate (entry **8**), alkene was incorporated into a monomer and used for the reaction.

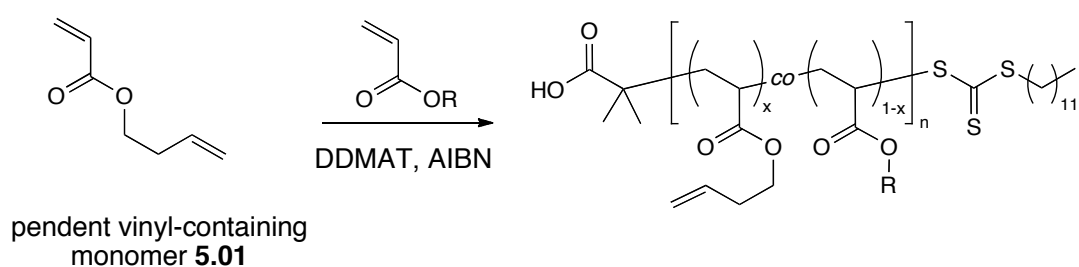
### 5.3.2. Polymer synthesis

Based on the results of the small molecule screen, we selected an acrylate monomer that contained an alkene unconjugated to the polymerisable moiety.



**Scheme 5.1** Synthesis of pendent alkene-containing monomer **5.01**

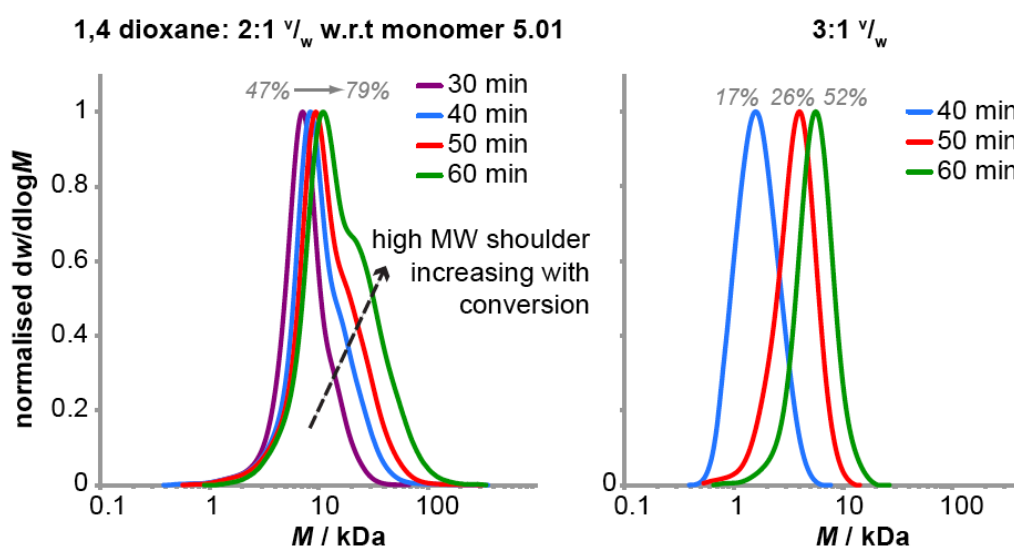
The monomer **5.01** was synthesised according to a reported procedure,<sup>14</sup> purified by column chromatography and isolated in 75% yield (Scheme 5.1) however to the best of our knowledge it has not been polymerised before using radical polymerisation, conventional or controlled, although the methacrylate equivalent has been polymerised by ATRP.<sup>5</sup> The general approach to the RAFT copolymerisation<sup>15</sup> of **5.01** with acrylate comonomers is shown in Scheme 5.2. We opted to first investigate RAFT copolymerisation of 10 mol% **5.01** with *t*BuA, using DDMAT<sup>16</sup> as the chain transfer agent (CTA), a monomer to CTA ratio of 100:1 and [CTA]:[AIBN] = 1:0.1.



**Scheme 5.2 General RAFT copolymerisation of 5.01 and acrylate monomers**

Initial trials using 1,4-dioxane as the solvent (1:1  $v/w$  i.e. 1 mL dioxane for 1 g **5.01**) resulted in insoluble gels or ill-defined polymers, even after very short polymerisation times (30 minutes) and low loadings of **5.01** (10 mol%). Thus we diluted the polymerisation mixtures in an effort to slow the polymerisation down and therefore make it easier to halt the polymerisations at low conversions, before any competing cross-linking reactions could occur.

Figure 5.2 shows the evolution of the SEC traces with time for a *t*BuA copolymerisation with **5.01**, where  $[t\text{BuA}]:[\mathbf{5.01}]:[\text{DDMAT}]:[\text{AIBN}] = 90:10:1:0.1$ . On the left is a solvent:monomer ratio of 2:1  $v/w$ , and on the right 3:1  $v/w$ . The evolution of a high molecular weight shoulder can be clearly seen throughout the 2:1  $v/w$  polymerisation, increasing in definition as the polymerisation proceeds.



**Figure 5.2 Evolution of SEC traces with time for copolymerisation of **5.01** with *t*BuA at different concentrations in 1,4-dioxane (grey numbers are average monomer conversions achieved at each time point)**

In contrast, the higher dilution of the polymerisation mixture at 3:1  $v/w$  dioxane results in lower conversions with time and hence increased control over the polymerisation, as evidenced by the narrow dispersities achieved and the lack of any high molecular weight shoulder in the SEC elugrams. The conversions of *t*BuA and monomer **5.01** were broadly similar over the

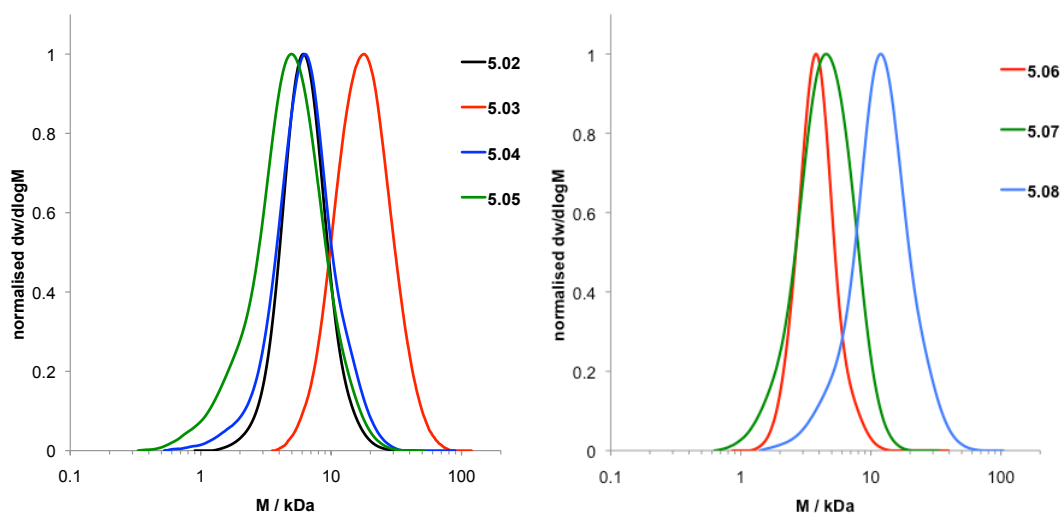
course of the polymerisations, and the conversion reached after 60 minutes was 52%.

Further dilutions slowed the polymerisation more, but also introduced irreproducible and unpredictable induction periods into the polymerisation, thus 3:1  $v_w$  was chosen as the optimum monomer concentration to balance polymerisation times with limiting the conversion to avoid unwanted reaction of the pendent alkene group.

The pendent alkene-bearing monomer **5.01** was copolymerised with several acrylate monomers, the details of which are summarised in Table 5.2. In all cases the polymerisations were quenched when monomer conversions of approximately 30–40% were reached, in a similar manner to the Nb-based polymerisations described in Chapters 2 and 3. It was possible to copolymerise monomer **5.01** with all acrylates that were tested, namely methyl acrylate (MA), *t*BuA, isobornyl acrylate (IBA) and tri(ethylene glycol) acrylate (TEGA), with monomer **5.01** at an incorporation of 10 mol% (polymers **5.02**, **5.06** and **5.08** in Table 5.2). Higher molecular weights were also achievable by increasing the monomer equivalents, but still stopping the polymerisation at 30–40% conversion, as in polymer **5.03**. Upon increasing the proportion of **5.01**, as seen in polymers **5.04** and **5.05**, it was still possible to obtain polymers with reasonably narrow, symmetrical distributions, although control over the polymerisation was reduced relative to the 10 mol% copolymers, as evidenced by the increase in dispersities. However, for all polymers, there were no pronounced high or low molecular weight shoulders evident in the SEC traces produced (Figure 5.3).

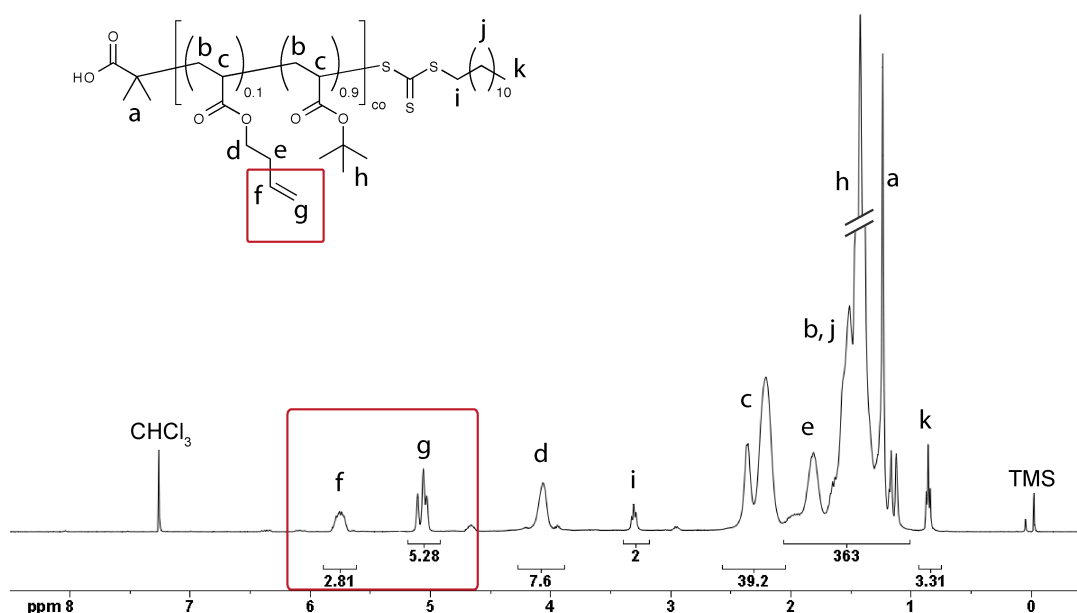
**Table 5.2 Copolymerisations of monomer 5.01 with various acrylate monomers, whereby M is the comonomer type and f is the mole fraction of alkene monomer 5.01**

Polymer	M	f / mol%	$M_n^{\text{NMR}}$ / kDa	$M_n^{\text{SEC}}$ / kDa	$M_w/M_n$
5.02	tBuA	10	5.4	5.7	1.18
5.03	tBuA	10	16.1	15.5	1.26
5.04	tBuA	25	6.2	5.3	1.33
5.05	tBuA	50	4.9	3.7	1.50
5.06	MA	10	3.4	3.6	1.12
5.07	IBA	10	5.5	3.8	1.28
5.08	TEGA	10	9.9	10.1	1.32



**Figure 5.3 SEC traces for polymers 5.02–5.08**

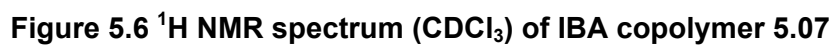
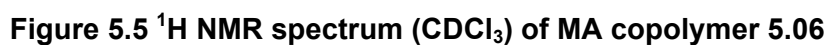
After purification by precipitation from cold solvents, or dialysis against water in the case of the TEGA copolymer,  $^1\text{H}$  NMR spectroscopy was used to confirm the presence of the alkene moieties. As shown in Figure 5.4, clear signals at ca. 5.0 and 5.8 ppm (labelled f and g) are evident in the  $^1\text{H}$  NMR spectrum, showing that the alkene moieties are still present after polymerisation and purification.



**Figure 5.4**  $^1\text{H}$  NMR spectrum ( $\text{CDCl}_3$ ) of *t*BuA copolymer 5.02

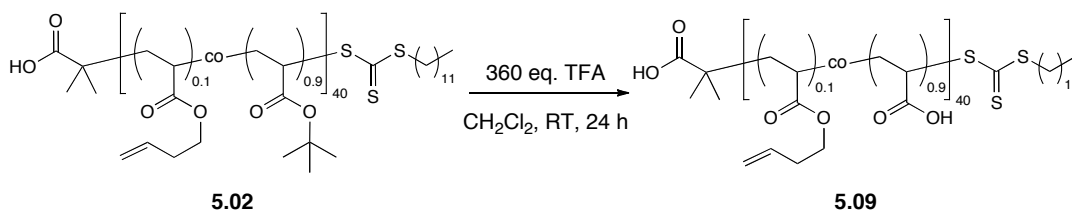
The same signals arising from the alkene functionalities were also observed in copolymers **5.06–5.08**, and are highlighted in the  $^1\text{H}$  NMR spectra of those polymers shown in Figure 5.5, Figure 5.6 and Figure 5.7.





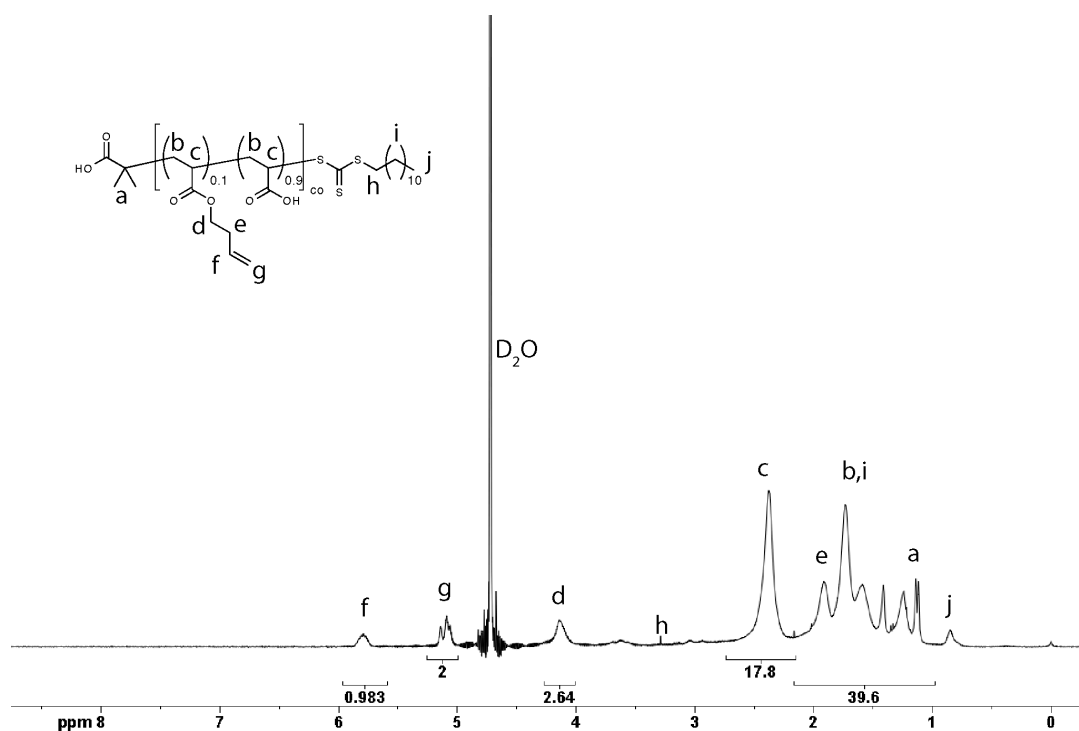


241



**Scheme 5.3** Acid-catalysed deprotection of *t*BuA copolymer **5.02**

Deprotection was carried out by addition of trifluoroacetic acid (10 eq. per *t*BuA unit) to a solution of **5.02** in  $\text{CH}_2\text{Cl}_2$  (10 mg/mL).<sup>17</sup> Alkene-loaded PAA **5.09** was recovered by precipitation from hexanes and dialysis against water, and  $^1\text{H}$  NMR spectroscopy confirmed the retention of alkene signals at 5.1 and 5.9 ppm, as shown in Figure 5.8.



**Figure 5.8**  $^1\text{H}$  NMR spectrum ( $\text{D}_2\text{O}$ ) of AA copolymer **5.09**

### 5.3.3. Functional tetrazine synthesis

Having formulated a library of polymers containing pendent alkene groups, we set about synthesising functional tetrazines for reaction with the alkene groups. We opted for three functional tetrazines: a biotin–Tz conjugate **5.10**, BODIPY–Tz **5.11** and low  $M_w$  PVL–Tz **5.12**. Biotin is a biologically relevant molecule useful for its extremely strong and specific binding with streptavidin, BODIPY exhibits strong fluorescence<sup>18</sup> and is useful in fluorescent labelling experiments; there is also some recent evidence that combining Tz and BODIPY in a single molecule can result in ‘turn-off’ quenching upon the reaction of Tz with a strained alkene.<sup>19</sup> PVL–Tz was synthesised in order to access both hydrophobic and amphiphilic graft copolymers, schematically illustrated in Figure 5.9.

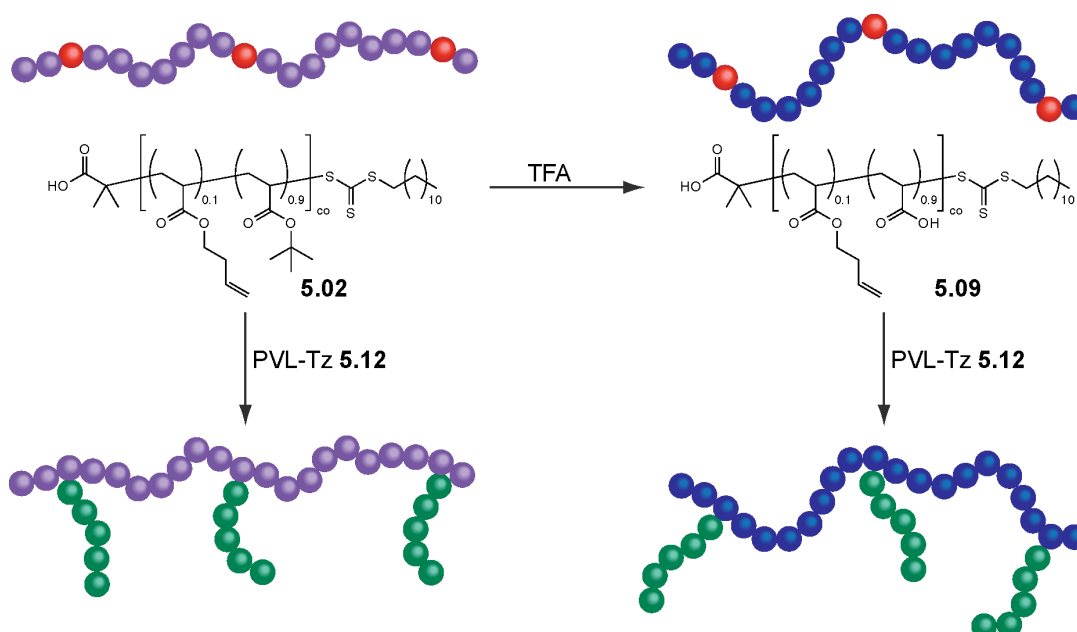
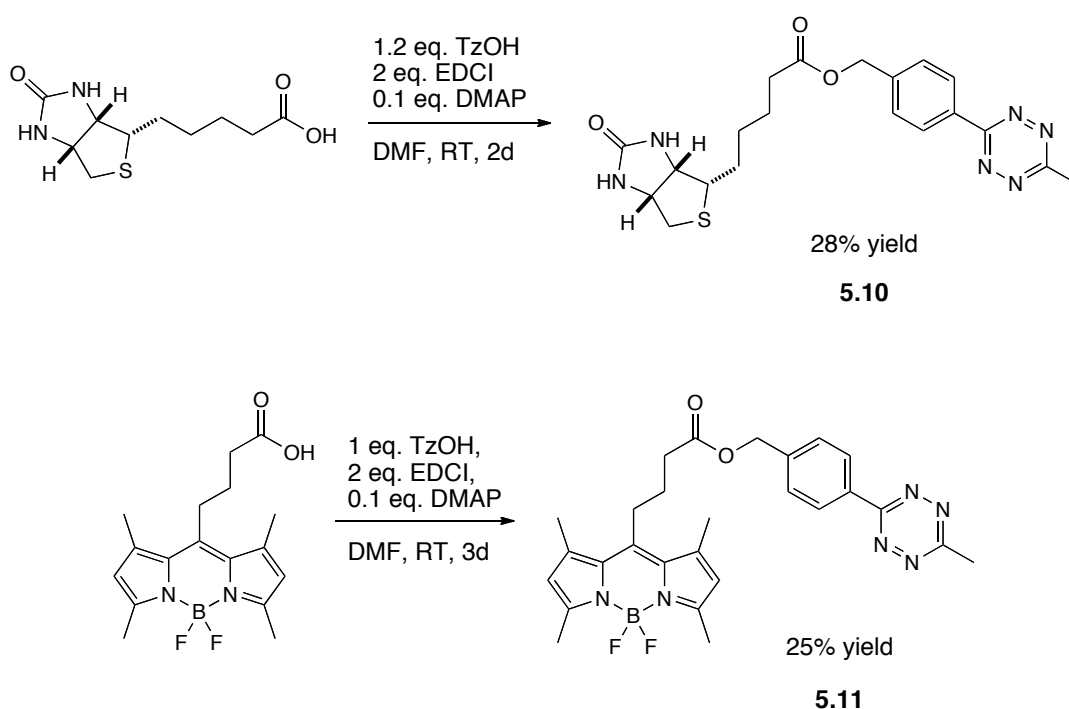


Figure 5.9 Illustration of potential route to fully hydrophobic (left) and amphiphilic (right) graft copolymers

The precursor to **5.10**, **5.11** and **5.12** was an alcohol-functionalised tetrazine (Tz–OH), chosen due to its relative ease of synthesis in comparison to the functional tetrazine described and synthesised in Chapter 2.<sup>20</sup> Biotin–Tz and BODIPY–Tz were both synthesised by EDCI-mediated coupling between Tz–OH and the carboxylic acid functionality inherent to biotin (Scheme 5.4), and present in functional BODIPY–COOH which we synthesised from a literature precedent.<sup>21</sup>



**Scheme 5.4 Synthesis of tetrazine-functionalised biotin **5.10** and fluorescent BODIPY dye **5.11****

Identity and purity were confirmed by  $^1\text{H}$ ,  $^{13}\text{C}$ ,  $^{11}\text{B}$  and  $^{19}\text{F}$  NMR spectroscopies, HRMS, IR and elemental analyses. Yields in both cases were modest, which we attribute to the fact that the tetrazine is susceptible

to degradation upon prolonged contact with silica gel during purification, and even with the aggressive solvent mixtures employed, the  $R_f$  values were still low; thus a combination of degradation and loss on the column probably artificially deflated the yields obtained.

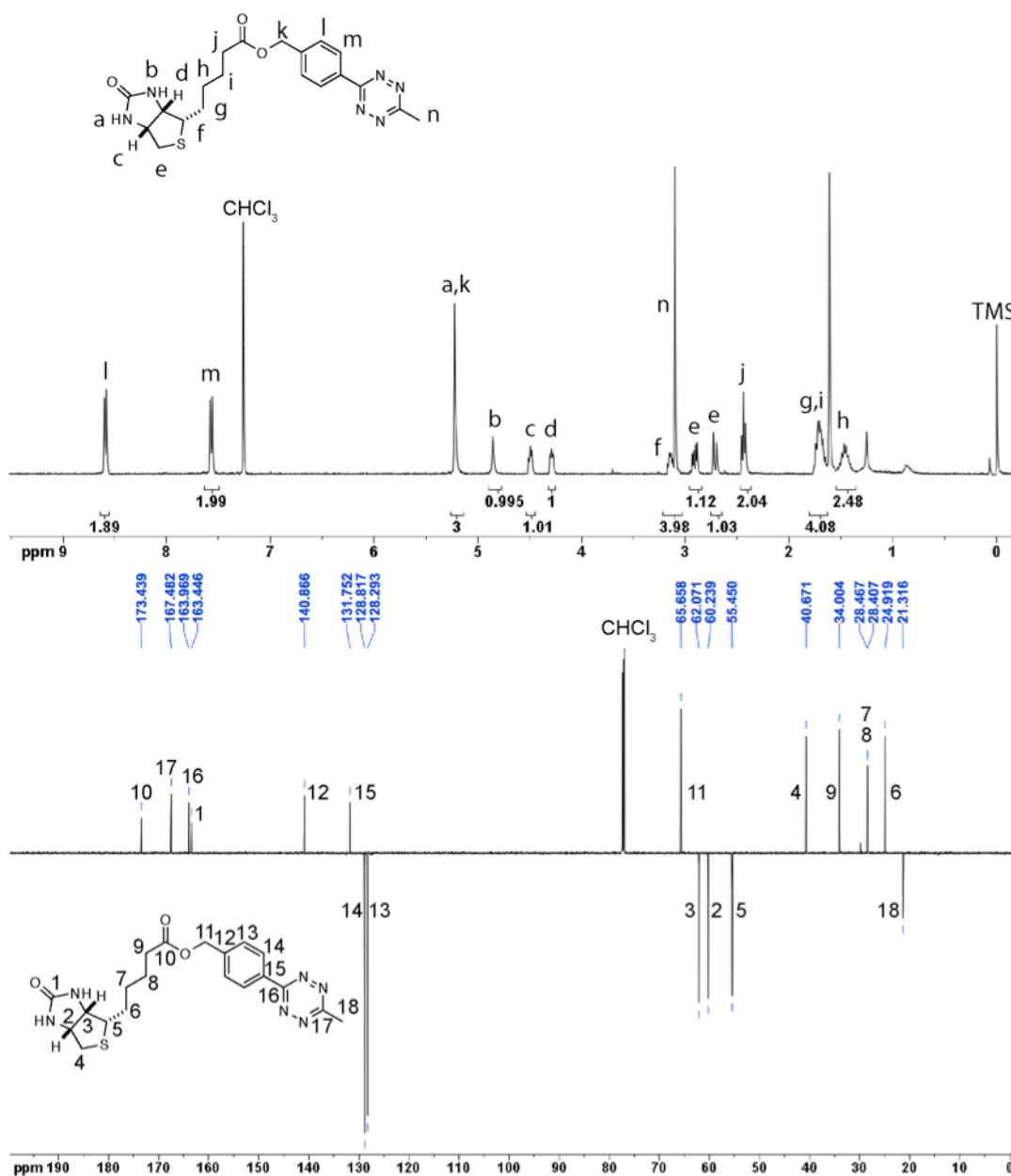


Figure 5.10 <sup>1</sup>H (top) and <sup>13</sup>C (bottom) NMR (CDCl<sub>3</sub>) spectra of biotin-Tz 5.10

The  $^1\text{H}$  NMR spectrum of biotin-Tz **5.10** shows the expected shifts of the methylenes adjacent to the newly-formed ester (2.2 to 2.4 ppm and 4.8 to 5.2 ppm for j and k respectively in Figure 5.10), and both the  $^1\text{H}$  and  $^{13}\text{C}$  NMR spectra were fully assigned *via* COSY, HSQC and HMBC NMR experiments, as shown in Figure 5.10.

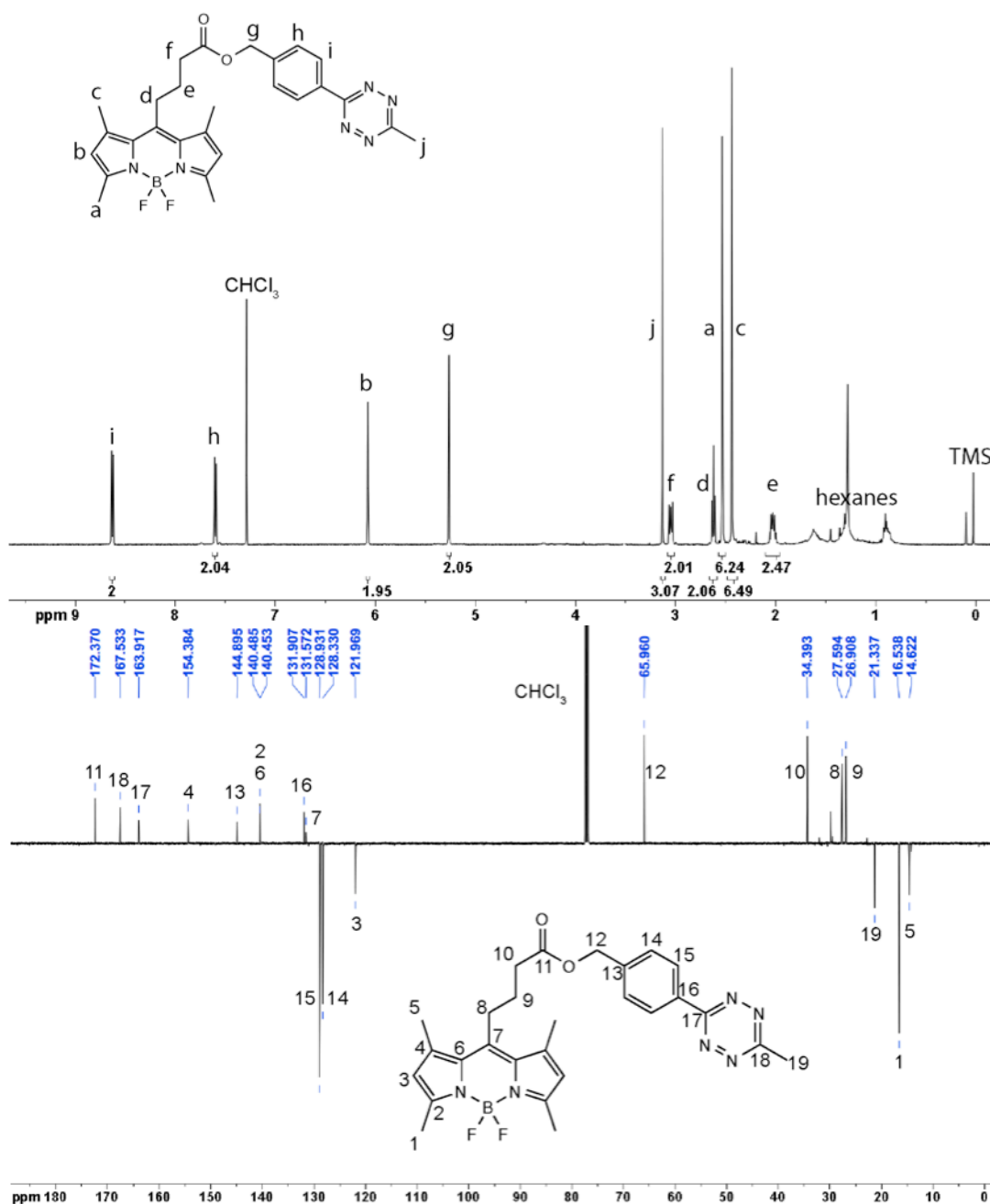
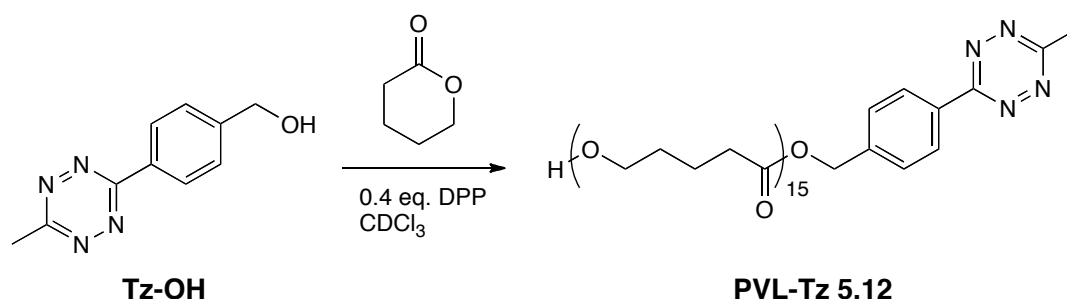


Figure 5.11  $^1\text{H}$  (top) and  $^{13}\text{C}$  (bottom) NMR ( $\text{CDCl}_3$ ) spectra of BODIPY-Tz **5.11**

In a similar vein, the successful synthesis of BODIPY-Tz **5.11** was confirmed by  $^1\text{H}$  and  $^{13}\text{C}$  NMR experiments, shown in Figure 5.11. Additionally, the presence of the boron and fluorine atoms was confirmed by the presence of only one triplet at 0.55 ppm (coupling to two  $^{19}\text{F}$  atoms) signal in the  $^{11}\text{B}$  NMR spectrum, and only one quintet at -147 ppm (coupling to one  $^{11}\text{B}$  atom with  $I = 3/2$ ) signal in the  $^{19}\text{F}$  NMR spectrum, both with a 33 Hz coupling constant.

PVL-Tz was synthesised by acid-catalysed ROP<sup>22</sup> from Tz-OH, similarly to the method described in Chapter 2 (Scheme 5.5).



**Scheme 5.5 Synthesis of PVL-Tz 5.12 by acid-catalysed ROP**

The presence of the tetrazine at the PVL chain end was confirmed by  $^1\text{H}$  NMR spectroscopy (Figure 5.13), and good agreement in the integrations of aromatic protons (f and g) with methyl protons (h) supports no degradation of the tetrazine during synthesis or workup. By integration of the end group proton signals and the main chain signals, the DP was calculated to be 15.



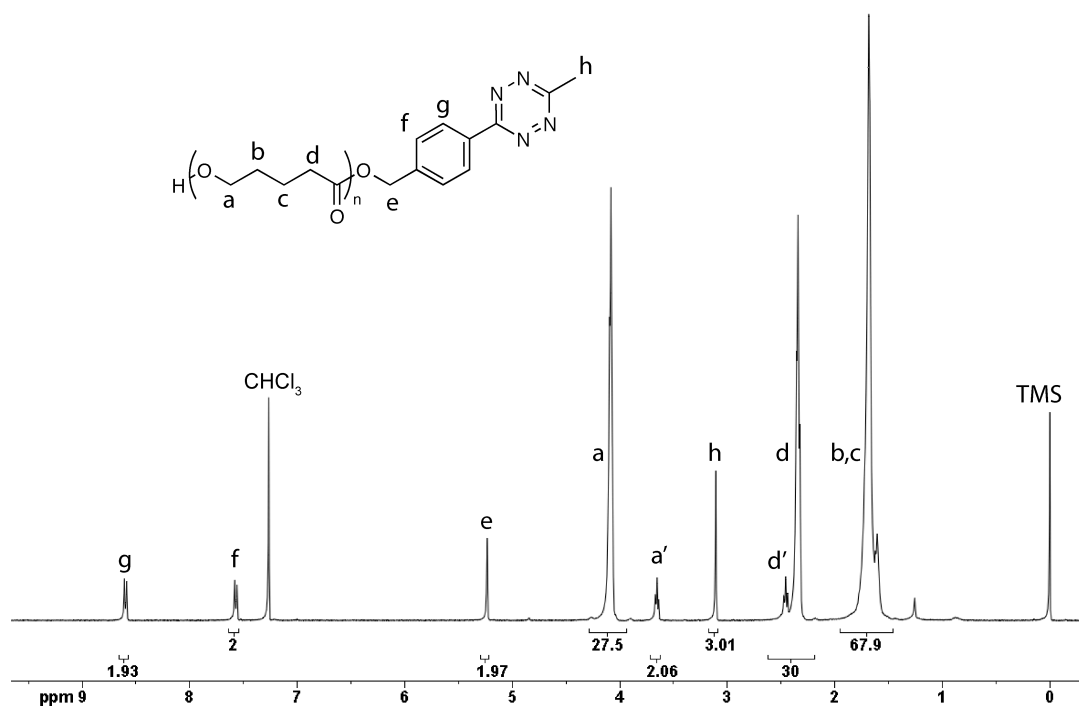


Figure 5.12  $^1\text{H}$  NMR spectrum ( $\text{CDCl}_3$ ) of PVL-Tz 5.12

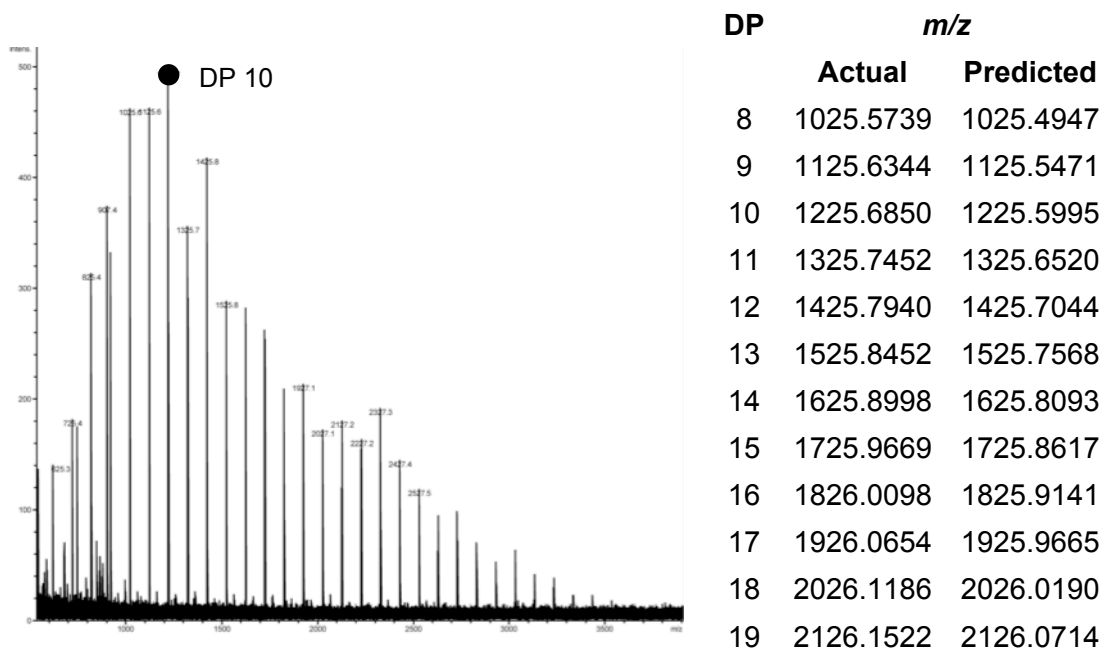
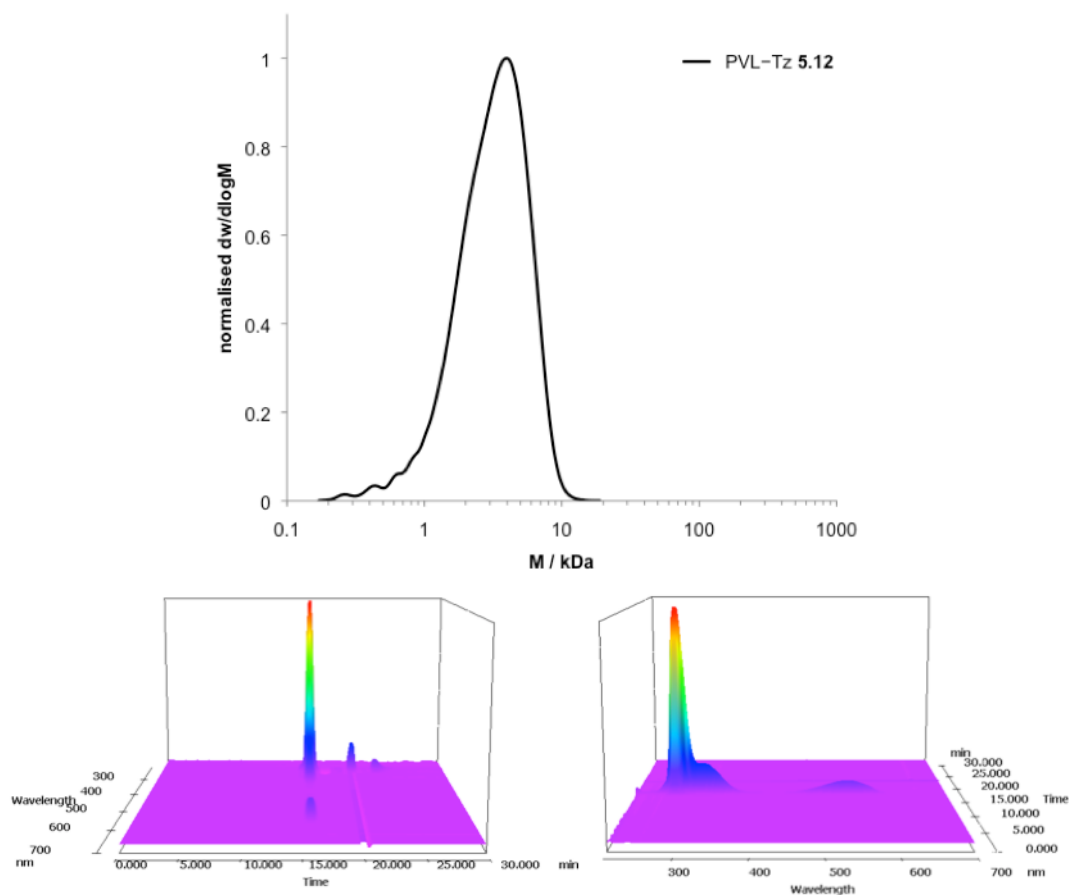


Figure 5.13 MALDI mass spectrum (left, major distribution  $\text{Na}^+$  adduct) of PVL-Tz 5.12, a portion of the predicted and actual mass values thereof (right)

MALDI mass spectrometry corroborated this (Figure 5.13), with the observed  $m/z$  values being consistent with the predicted values for all chains to bear a Tz unit. Additionally, the characteristic UV/vis spectrum arising from the tetrazine can be seen in the SEC-UV/vis spectra shown in Figure 5.14.



**Figure 5.14 SEC trace (top) for PVL–Tz 5.12, and SEC-UV/vis traces, shown in the SEC dimension (left) and UV/vis dimension (right)**

PVL has no characteristic UV/vis absorbance, and since there is only one species present in both the SEC and UV/vis dimensions, it follows that all tetrazine moieties in the sample are attached to the PVL.

### 5.3.4. Polymer functionalisation

We initially used the same conditions as in the small molecule screening (0.01 M alkene functionality, 10-fold excess of tetrazine, room temperature in CH<sub>2</sub>Cl<sub>2</sub>) to react 10 mol% alkene-loaded PtBuA copolymer **5.02** with biotin-Tz **5.10**, BODIPY-Tz **5.11** and PVL-Tz **5.12**. However, after stirring at room temperature for 7 days, the expected characteristic colour change from pink to orange had not occurred, and upon analysis by <sup>1</sup>H NMR spectroscopy, very low conversion of the alkene groups had been achieved (< 15% in all cases). Increasing the temperature to 50 °C in a sealed vessel only increased the conversion to 20%, which is contrary to what we would expect, given the results of the small molecule screening in Section 5.3 and the knowledge that the rate of the reaction is increased with temperature. We postulated that the alkene groups were inaccessible to the functionalised tetrazine and therefore that changing the solvent might be beneficial.

#### 5.3.4.1. Solvent screening

The solvent can have two primary influences on the reaction: the first being the quality of the solvent with respect to the polymer, and thus how available the alkene groups are to react, and the second is the polarity – more polar solvents increase the rate of the DA<sub>inv</sub> reaction.

In order to investigate this, we selected copolymer **5.02** and used a tenfold excess of Tz(pyr)<sub>2</sub>, stirred at room temperature in a variety of solvents (50 mg/mL polymer = 0.009 M) for 24 hours, after which a <sup>1</sup>H NMR spectrum was measured. Deuterated solvents were used where possible;

else the  $^1\text{H}$  NMR spectrum was measured with solvent suppression. The conversion of alkene was measured by comparing the integrations of the vinyl signals at 5.0 and 5.8 ppm with the methylene adjacent to the acrylate group at 4.1 ppm in the  $^1\text{H}$  NMR spectrum.

**Table 5.3 Conversion of alkene in polymer 5.02 after 24 h reaction with  $\text{Tz}(\text{pyr})_2$  in varying solvents (deuterated equivalents used in some cases) with increasing polarity**

Solvent	Polarity	Conversion / %
benzene	0.111	15
1,4-dioxane	0.164	**
THF	0.207	21
$\text{CHCl}_3$	0.259	18
$\text{CH}_2\text{Cl}_2$	0.309	**
acetone	0.355	19
DMF	0.386	30
MeCN	0.46	35
hexafluoroisopropanol	1.068	**

\*\* significant/complete overlap of solvent peak with peaks of interest

The rate of the DA<sub>inv</sub> reaction should correlate with the solvent polarity, with more polar solvents increasing the rate of reaction. Thus any large discrepancies in this generally expected trend we can attribute to solvent quality for polymer **5.02**.

The first thing to note in Table 5.3 is that the conversion achieved in chloroform after 24 h is only a little less than the conversion reached after 7 days in our initial trials. This would seem to suggest a ceiling to the conversions rather than just a very sluggish rate. There does appear to be a broad correlation between solvent polarity and conversion but the conversion of alkene functionalities is still not good. This is especially pertinent given that the Tz(pyr)<sub>2</sub> we used here is more reactive than the Tz–OH precursor to **5.10**, **5.11** and **5.12**, and so might be expected to react a little faster, reach higher conversions or both. From the absence of any dramatic spikes in the correlation between conversion and solvent polarity we can conclude that the solvent quality does not appear to be having an undue influence, and thus it is beneficial to use the most polar solvent that will still solubilise polymer **5.02**.

#### **5.3.4.2.      *Lewis acid catalyst screening***

As organocatalysis<sup>23</sup> has both been shown to accelerate the reaction between tetrazines and ketones, and other hetero-DA<sub>inv</sub> reactions, not necessarily involving tetrazines, have also been shown to be accelerated by Lewis acids,<sup>24</sup> we decided to pursue this as an avenue to increasing the rates and conversions of the reaction. Four Lewis acid catalysts were chosen from ones that have previously been shown to accelerate or enhance conversions of hDA<sub>inv</sub> reactions,<sup>24a,25</sup> and the same reaction

protocol as described in Section 5.3.4.1 carried out. MeCN was used as the solvent as it had produced the highest conversions in the solvent screen. The Lewis acid catalysts (25 or 50 mol% relative to alkene units) were added to a solution of polymer **5.02** (0.01 M alkene) and Tz(pyr)<sub>2</sub> (0.1 M). The reaction was stirred for 24 h at room temperature, after which the solvent was removed *in vacuo* and the polymer analysed using the relative integrals of the alkene and methylene signals in the <sup>1</sup>H NMR spectrum.

**Table 5.4 Conversion of alkene functionalities in the Lewis acid-catalysed reaction of polymer 5.02 with Tz(pyr)<sub>2</sub>**

Catalyst	mol%	Conversion / %
<i>none</i>	-	35
TiCl <sub>4</sub>	25	18
SnCl <sub>4</sub>	25	20
Yb(OTf) <sub>3</sub>	25	16
Sc(OTf) <sub>3</sub>	25	17
TiCl <sub>4</sub>	50	21
SnCl <sub>4</sub>	50	18
Yb(OTf) <sub>3</sub>	50	21
Sc(OTf) <sub>3</sub>	50	19

No demonstrable improvement in conversion was observed in any case; in fact  $\text{TiCl}_4$  formed a precipitate upon addition so it is reasonable to assume it was oxidised and therefore rendered useless immediately ( $\text{SnCl}_4$  is also water sensitive though did not form a precipitate upon addition), and thus did not participate in any catalysis. Thus, given the similarity of the conversions achieved across the board, we can extrapolate that none of the catalysts promoted the reaction in any way. Although  $\text{Yb}(\text{OTf})_3$  and  $\text{Sc}(\text{OTf})_3$  are water tolerant and have been used to accelerate  $\text{DA}_{\text{inv}}$  reactions with diazines, they also did not catalyse the reaction, and worse still, a control reaction with  $\text{Tz}(\text{pyr})_2$  showed partial degradation of the tetrazine functionality by  $\text{Yb}(\text{OTf})_3$ , thus leaving  $\text{Sc}(\text{OTf})_3$  as the only remaining candidate for possible catalysis. Increasing the temperature to  $50\text{ }^\circ\text{C}$  with the addition of  $\text{Sc}(\text{OTf})_3$  resulted in a conversion of 29%, which was no improvement over the uncatalysed experiment.

Thus of the surveyed Lewis acid catalysts, none were found to be suitable or able to catalyse the reaction, and this route was rejected.

## 5.4. Conclusions

We have successfully synthesised a library of pendent alkene acrylate-based copolymers by RAFT polymerisation methods, and three functional tetrazine molecules of interest to investigate the possibility of polymer functionalisation without using norbornene as the dienophile. However, the reduction in reactivity of an unstrained alkene relative to norbornene led to insurmountable retardations in rate and conversions achieved, even in the presence of large excess of small molecules, highly polar solvents, high temperatures and potential catalysts for the reaction. Thus we conclude that pendent alkenes are not reactive enough for any meaningful 'click' reaction with tetrazines to occur, even though some reaction was observed.



## 5.5. Experimental

### 5.5.1. Materials and methods

All chemicals were purchased from Sigma-Aldrich and used as received unless otherwise stated. Solvents were purchased from Fisher and were of at least analytical grade. AIBN was recrystallised twice from methanol and stored in the dark at 4 °C prior to use. *t*BuA and IBA were distilled over CaH<sub>2</sub> prior to use. TEGA was synthesised according to a published procedure. <sup>1</sup>H and <sup>13</sup>C NMR spectra were recorded on a Bruker DPX-400 or Bruker DRX-500 spectrometer at 25 °C in CDCl<sub>3</sub> or D<sub>2</sub>O. Chemical shifts are reported as  $\delta$  in ppm relative to CHCl<sub>3</sub> (<sup>1</sup>H:  $\delta$  = 7.26 ppm; <sup>13</sup>C:  $\delta$  = 77.2 ppm) or D<sub>2</sub>O (<sup>1</sup>H:  $\delta$  = 4.79 ppm) using an internal reference of TMS, and coupling constants are reported in Hz. <sup>13</sup>C NMR peaks are reported as 'up' (u) for methylene and quaternary carbons and 'down' (dn) for methyl and methine carbons. SEC data was obtained in HPLC grade THF containing 2% triethyl amine (TEA) at 30 °C, with a flow rate of 1.0 mL/min, on a set of two PLgel 5  $\mu$ m Mixed-D columns, plus one guard column. SEC data was analysed with Cirrus SEC software calibrated using poly(methyl methacrylate) standards (690 to 271,400 Da). A Shimadzu SPD-M20A prominence diode array (PDA) detector was also coupled to the THF SEC system and used to extract UV/vis spectra for the synthesised polymers. These data were analysed using LC Solution software. Infrared spectroscopy was recorded on a Perkin Elmer Spectrum 100 FT-IR ATR Spectrometer. 16 scans from 600 to 4000 cm<sup>-1</sup> were taken, and the spectra corrected for background absorbance. UV/vis spectra were recorded on a

Perkin Elmer Lambda 35 UV/vis spectrophotometer. Fluorescence spectra were obtained using a single-beam Perkin-Elmer LS55 fluorometer. High resolution mass spectra (HRMS) were collected using a Bruker MaXis UHR-ESI-ToF. MALDI mass spectra were acquired by MALDI-ToF (matrix-assisted laser desorption and ionisation time-of-flight) mass spectrometry using a Bruker Daltonics Ultraflex II MALDI-ToF mass spectrometer, equipped with a nitrogen laser delivering 2 ns laser pulses at 337 nm with positive ion ToF detection performed using an accelerating voltage of 25 kV. Solutions of dithranol as matrix, sodium trifluoroacetate as cationisation agent and analyte were mixed prior to being spotted on the MALDI plate and air-dried. The samples were measured in reflectron ion mode and calibrated by comparison to SpheriCal (Polymer Factory) single molecular weight dendrimer standards.

### **5.5.2. Syntheses**

#### **5.5.2.1. 3-Butenyl acrylate (monomer 5.01)**

**5.01** was synthesised according to a literature report.<sup>14</sup> Buten-1-ol (5.00 mL, 58.1 mmol) and triethylamine (16.2 mL, 116 mmol) were dissolved in CH<sub>2</sub>Cl<sub>2</sub> (300 mL) under a N<sub>2</sub> atmosphere and cooled to 0 °C. Acryloyl chloride (7.08 mL, 87.2 mmol) was added dropwise and the mixture stirred at 0 °C for 2 h, after which it was warmed to room temperature, washed with water (2 x 300 mL), saturated NaHCO<sub>3</sub> (300 mL) and brine (300 mL) and dried over MgSO<sub>4</sub>. The solvent was removed *in vacuo* and the product isolated by flash column chromatography (30:70 Et<sub>2</sub>O/hexanes, R<sub>f</sub> 0.35) as

a colourless oil (5.50 g, 43.6 mmol, 75% yield).  $^1\text{H}$  NMR (400 MHz,  $\text{CDCl}_3$ )  $\delta$  (ppm): 6.40 (1H, dd,  $^3J_{\text{H-H}} = 17.3$  Hz,  $^2J_{\text{H-H}} = 1.4$  Hz), 6.11 (1H, dd,  $^3J_{\text{H-H}} = 17.3$  Hz,  $^3J_{\text{H-H}} = 10.5$  Hz), 5.80 (2H, m), 5.11 (2H, m), 4.21 (2H, t,  $^3J_{\text{H-H}} = 6.8$  Hz), 2.46-2.40 (2H, m).  $^{13}\text{C}$  NMR (100 MHz,  $\text{CDCl}_3$ )  $\delta$  (ppm): 165.9 (u), 133.8 (dn), 130.3 (u), 128.4 (dn), 117.1 (u), 63.4 (u), 32.9 (u).

**5.5.2.2. [p-(6-Methyl-1,2,4,5-tetrazin-3-yl)phenyl]methanol (Tz-OH)**

Tz-OH was synthesised according to a modified literature procedure.<sup>20</sup> 4-Hydroxymethyl benzonitrile (0.500 g, 3.76 mmol), nickel triflate (0.670 g, 1.88 mmol), acetonitrile (1.96 mL, 37.6 mmol) and hydrazine monohydrate (9.13 mL, 188 mmol) were mixed in a sealed ampoule and stirred at room temperature for 30 min to ensure complete dissolution of all the reagents. The ampoule was placed in an oil bath at 60 °C for 24 h behind a blast shield, after which it was allowed to cool to room temperature and opened carefully due to the pressure build-up during the reaction. The resulting brown mixture was added to sodium nitrite (5.18 g, 75.1 mmol) in 20 mL water, after which conc. HCl was added extremely slowly, diluting with water as necessary to control the resulting effervescence and being careful of the evolved nitrous gases, until pH 3 was reached. The aqueous phase was extracted with EtOAc (3 x 200 mL), then the organic phase washed with  $\text{H}_2\text{O}$  and brine and dried over  $\text{MgSO}_4$ . The product was isolated by flash column chromatography (2:1 hexanes/EtOAc,  $R_f$  0.15) as a pink solid (117 mg, 16% yield).  $^1\text{H}$  NMR (400 MHz,  $\text{CDCl}_3$ )  $\delta$  (ppm): 8.57 (2H, d,  $^3J_{\text{H-H}} = 8.2$  Hz), 7.58 (2H, d,  $^3J_{\text{H-H}} = 8.2$  Hz), 4.83 (2H, s), 3.09 (3H, s).  $^{13}\text{C}$

NMR (100 MHz, CDCl<sub>3</sub>)  $\delta$  (ppm): 167.4 (u), 164.1 (u), 145.8 (u), 131.1 (u), 128.3 (dn), 127.6 (dn), 64.9 (u), 21.3 (dn).

**5.5.2.3. [p-(6-Methyl-1,2,4,5-tetrazin-3-yl)phenyl]methyl 5-[(4S)-2-oxo-5-thia-1,3-diazapent-1,3,4,6,7,8-hexahydropentalen-4-yl]valerate (Biotin-Tz) 5.10**

Biotin (50.0 mg, 0.205 mmol), EDCI•HCl (78.5 mg, 0.409 mmol) and DMAP (2.50 mg, 0.0205 mmol) were vacuum dried in a round-bottomed flask equipped with a stirrer bar and septum, anhydrous DMF (4 mL) was added and the solution purged with N<sub>2</sub> for 10 min. Tz-OH (49.7 mg, 0.246 mmol) in anhydrous DMF (1 mL) was added slowly at 0 °C, after which the mixture was warmed to room temperature and stirred for 48 h. DMF was removed and the crude mixture redissolved in DCM (8 mL), washed with 1 M NaOH (5 mL) and water (4 x 5 mL), and dried over MgSO<sub>4</sub>. The product was purified by flash column chromatography eluting with 15:1 CH<sub>2</sub>Cl<sub>2</sub>/MeOH (R<sub>f</sub> 0.08) and isolated as a bright pink solid (24.8 mg, 28% yield). HRMS (ESI, [M+Na]<sup>+</sup>) *m/z*: predicted 451.1523, found 451.1518. <sup>1</sup>H NMR (500 MHz, CDCl<sub>3</sub>)  $\delta$  (ppm): 8.59 (2H, d, <sup>3</sup>J<sub>H-H</sub> = 8.2 Hz), 7.57 (2H, d, <sup>3</sup>J<sub>H-H</sub> = 8.2 Hz), 5.22 (3H, s), 4.85 (3H, s), 4.49 (1H, m), 4.29 (1H, m), 3.14 (1H, m), 3.07 (3H, s), 2.90 (1H, dd, <sup>2</sup>J<sub>H-H</sub> = 12.8 Hz, <sup>3</sup>J<sub>H-H</sub> = 4.8 Hz), 2.72 (1H, d, <sup>2</sup>J<sub>H-H</sub> = 12.8 Hz), 2.44 (2H, t, <sup>3</sup>J<sub>H-H</sub> = 7.2 Hz), 1.76-1.37 (6H, m). <sup>13</sup>C NMR (125 MHz, CDCl<sub>3</sub>)  $\delta$  (ppm): 173.4 (u), 167.5 (u), 164.0 (u), 163.4 (u), 140.9 (u), 131.8 (u), 128.8 (dn), 128.3 (dn), 65.6 (u), 62.1 (dn), 60.2 (dn), 55.5 (dn), 40.7 (u), 34.0 (u), 28.47 (u), 28.41 (u), 24.9 (u), 21.3 (dn). IR  $\nu$

(cm<sup>-1</sup>): 3202 (br), 2931 (br), 2855, 1735, 1670, 1614, 1464, 1404, 1362, 1167, 1090, 890, 795, 729.

**5.5.2.4. 4-(4,4-Difluoro-1,3,5,7-tetramethyl-11,12-diaza-4-bora-s-indacen-8-yl)butyric acid (BODIPY-COOH)**

BODIPY-COOH was synthesised according to a literature procedure.<sup>21</sup> Glutaric anhydride (270 mg, 2.37 mmol) was dissolved in dry THF (40 mL), to which 4 Å molecular sieves had been added. 2,4-dimethyl pyrrole (0.487 mL, 450 mg, 4.73 mmol) and BF<sub>3</sub>•OEt<sub>2</sub> (390 µL, 1.33 mmol) were added and the mixture heated to reflux for 8 h. The mixture was then cooled to room temperature and a further portion of BF<sub>3</sub>•OEt<sub>2</sub> (1.95 mL, 17.6 mmol) and triethylamine (1.65 mL, 11.8 mmol) added, before being stirred at 50 °C under a N<sub>2</sub> atmosphere for 4 h. The solvent was removed *in vacuo* and the crude product redissolved in CH<sub>2</sub>Cl<sub>2</sub> (50 mL), washed with H<sub>2</sub>O (2 x 100 mL) and dried over MgSO<sub>4</sub>. The product was isolated by flash column chromatography (80:40:1 hexanes/EtOAc/AcOH, R<sub>f</sub> 0.15) and isolated as an orange solid (94.0 mg, 0.281 mmol, 12% yield). <sup>1</sup>H NMR (400 MHz, CDCl<sub>3</sub>) δ (ppm): 6.05 (2H, s), 3.02 (2H, m), 2.57-2.45 (4H, m), 2.51 (6H, s), 2.42 (6H, s), 2.05 (2H, m). <sup>13</sup>C NMR (100 MHz, CDCl<sub>3</sub>) δ (ppm): 177.9 (u), 154.2 (u), 144.7 (u), 140.3 (u), 131.5 (u), 121.9 (dn), 35.6 (u), 27.5 (u), 26.7 (u), 16.3 (dn), 14.5 (dn).

**5.5.2.5. [p-(6-Methyl-1,2,4,5-tetrazin-3-yl)phenyl]methyl 5-[(4S)-2-oxo-5-thia-1,3-diaza-1,3,4,6,7,8-hexahydropentalen-4-yl]valerate (BODIPY-Tz) 5.11**

BODIPY-COOH (50.0 mg, 0.150 mmol), EDCI (57.4 mg, 0.299 mmol) and DMAP (1.83 mg, 0.0150 mmol) were dissolved in DMF (0.8 mL) under nitrogen. Tz-OH (30.3 mg, 0.150 mmol) in DMF (0.5 mL) was added slowly and the mixture stirred at room temperature for 2 days. The product was purified by column chromatography, eluting in a gradient of 2:1 hexanes/EtOAc → 1:2 hexanes/EtOAc ( $R_f$  for 2:1 hexanes/EtOAc 0.56), and isolated as a red-orange solid (19.3 mg, 0.0372 mmol, 25% yield). HRMS (ESI,  $[M+Na]^+$  of  $^{10}B$  species)  $m/z$ : predicted 541.2310, found 541.2315.  $^1H$  NMR (500 MHz,  $CDCl_3$ )  $\delta$  (ppm): 8.60 (2H, d,  $^3J_{H-H} = 8.2$  Hz), 7.57 (2H, d,  $^3J_{H-H} = 8.2$  Hz), 6.05 (2H, s), 5.24 (2H, s), 3.10 (3H, s), 3.04-3.00 (2H, m), 2.60 (2H, t,  $^3J_{H-H} = 7.2$  Hz), 2.51 (6H, s), 2.39 (6H, s), 2.04–1.96 (2H, m).  $^{13}C$  NMR (125 MHz,  $CDCl_3$ )  $\delta$  (ppm): 172.4 (u), 167.5 (u), 163.9 (u), 154.4 (u), 144.9 (u), 140.48 (u), 140.45 (u), 131.9 (u), 131.6 (u), 128.9 (dn), 128.3 (dn), 122.0 (dn), 66.0 (u), 29.9 (u), 27.6 (u), 26.9 (u), 21.3 (dn), 16.5 (dn), 14.6 (dn).  $^{19}F$  NMR (375 MHz,  $CDCl_3$ )  $\delta$  (ppm): -146.6 (2F, quin,  $^1J_{F-B} = 33.3$  Hz).  $^{11}B$  NMR (160 MHz,  $CDCl_3$ )  $\delta$  (ppm): 0.55 (1B, t,  $^1J_{B-F} = 32.9$  Hz). IR  $\nu$  ( $cm^{-1}$ ): 3276 (br), 2923 (br), 1736, 1614, 1548, 1505, 1463, 1402, 1354, 1307, 1157, 1072, 972, 796, 716. UV/vis:  $\lambda_{max}$  (in  $CH_2Cl_2$ ) 501 nm. Fluorescence emission  $\lambda_{max}$  512 nm.

#### 5.5.2.6. PVL–Tz 5.12

Tz–OH (8.08 mg, 0.0400 mmol),  $\delta$ -valerolactone (50.0 mg, 0.799 mmol) and diphenyl phosphate (5.00 mg, 0.0200 mmol) were dissolved in  $\text{CDCl}_3$  (0.5 mL) in the glovebox and stirred at room temperature for 2 h.<sup>22</sup> The polymerisation was quenched with the addition of Amberlyst A21, and the polymer isolated by precipitation from cold hexanes three times.  $^1\text{H}$  NMR (400 MHz,  $\text{CDCl}_3$ )  $\delta$  (ppm): 8.59 (2H, d,  $^3J_{\text{H-H}} = 8.2$  Hz), 7.57 (2H, d,  $^3J_{\text{H-H}} = 8.2$  Hz), 5.22 (2H, s), 4.08 (28H, m), 3.65 (2H, t,  $^3J_{\text{H-H}} = 6.3$  Hz), 3.10 (3H, s), 2.45 (2H, t,  $^3J_{\text{H-H}} = 7.1$  Hz), 2.34 (28H, m), 1.66 (68H, m). DP 15,  $M_n^{\text{NMR}}$  1.7 kDa. SEC (eluting in THF with 2% TEA, relative to PMMA standards):  $M_n$  2.5 kDa,  $M_w$  3.6 kDa,  $M_w/M_n$  1.43.

#### 5.5.3. General polymerisation procedure

The requisite amounts of monomer **5.01**, comonomer (*t*BuA, MA, IBA or TEGA), DDMAT and AIBN were dissolved in dioxane, transferred to a polymerisation ampoule and subjected to four freeze-thaw-evacuate cycles. The ampoule was warmed to room temperature and backfilled with nitrogen, before being sealed and immersed in a preheated oil bath (70 °C). The polymerisation was quenched by opening the ampoule to oxygen and cooling quickly to room temperature. The copolymers were isolated by precipitation three times from cold solvents (*t*BuA from MeOH/H<sub>2</sub>O 70:30, MA from hexanes, IBA from MeOH and TEGA from hexanes), with the exception of TEGA, which was precipitated once from hexanes and then

dialysed exhaustively against 18.2 M $\Omega$ cm<sup>-1</sup> Type I water. Analysis by <sup>1</sup>H NMR spectroscopy and SEC was carried out.

#### **5.5.3.1. Deprotection of PtBuA to PAA 5.09**

**5.02** (200 mg, 0.0370 mmol) was dissolved in CH<sub>2</sub>Cl<sub>2</sub> (20 mL), and trifluoroacetic acid (1.02 mL, 13.3 mmol) added dropwise at room temperature.<sup>17</sup> The mixture was stirred for 24 h, after which the solvent was removed *in vacuo*, the polymer precipitated once from cold hexanes and then dissolved in water and dialysed against 18.2 M $\Omega$ cm<sup>-1</sup> Type I water (5 water changes) before being recovered by lyophilisation as a white powder (82.5 mg, 0.0242 mmol, 66% yield).

#### **5.5.4. General polymer functionalisation procedure**

The requisite amount of polymer **5.02** was dissolved in solvent (adjusted such that the alkene functionalities were at a concentration of 0.01 M), and a tenfold excess (relative to alkene functionalities) of functional tetrazine **5.10**, **5.11**, **5.12** or Tz(pyr)<sub>2</sub> added. If Lewis acid catalysts TiCl<sub>4</sub>, SnCl<sub>4</sub>, Yb(OTf)<sub>3</sub> or Sc(OTf)<sub>3</sub> were used, these were added at 25 or 50 mol% relative to the number of alkene units. The mixture was stirred at room temperature for 7 days in a sealed vial to negate any effects of solvent evaporation.



## 5.6. References

- (1) Sasaki, T.; Eguchi, S.; Yamaguchi, M.; Esaki, T. *J. Org. Chem.* **1981**, *46*, 1800-1804.
- (2) Herczynska, L.; Lestel, L.; Boileau, S.; Chojnowski, J.; Polowinski, S. *Eur. Polym. J.* **1999**, *35*, 1115-1122.
- (3) (a) David, R. L. A.; Kornfield, J. A. *Macromolecules* **2008**, *41*, 1151-1161. (b) ten Brummelhuis, N.; Diehl, C.; Schlaad, H. *Macromolecules* **2008**, *41*, 9946-9947. (c) Justynska, J.; Hordyjewicz, Z.; Schlaad, H. *Polymer* **2005**, *46*, 12057-12064.
- (4) Boileau, S.; Mazeaud-Henri, B.; Blackborow, R. *Eur. Polym. J.* **2003**, *39*, 1395-1404.
- (5) Campos, L. M.; Killops, K. L.; Sakai, R.; Paulusse, J. M. J.; Damiron, D.; Drockenmuller, E.; Messmore, B. W.; Hawker, C. J. *Macromolecules* **2008**, *41*, 7063-7070.
- (6) Ma, J.; Cheng, C.; Sun, G.; Wooley, K. L. *Macromolecules* **2008**, *41*, 9080-9089.
- (7) (a) Gress, A.; Voelkel, A.; Schlaad, H. *Macromolecules* **2007**, *40*, 7928-7933. (b) Kempe, K.; Hoogenboom, R.; Jaeger, M.; Schubert, U. S. *Macromolecules* **2011**, *44*, 6424-6432.
- (8) Sun, J.; Schlaad, H. *Macromolecules* **2010**, *43*, 4445-4448.

- (9) Leemhuis, M.; Akeroyd, N.; Kruijtzter, J. A. W.; van Nostrum, C. F.; Hennink, W. E. *Eur. Polym. J.* **2008**, *44*, 308-317.
- (10) Oie, H.; Sudo, A.; Endo, T. *J. Polym. Sci., Part A: Polym. Chem.* **2013**, *51*, 2035-2039.
- (11) Wang, Y.-Z.; Deng, X.-X.; Li, L.; Li, Z.-L.; Du, F.-S.; Li, Z.-C. *Polym. Chem.* **2013**, *4*, 444-448.
- (12) (a) Carboni, R. A.; Lindsey, R. V., Jr. *J. Am. Chem. Soc.* **1959**, *81*, 4342-4346. (b) Thalhammer, F.; Wallfahrer, U.; Sauer, J. *Tet. Lett.* **1990**, *31*, 6851-6854. (c) Sauer, J.; Heldmann, D. K.; Hetzenegger, J.; Krauthan, J.; Sichert, H.; Schuster, J. *Eur. J. Org. Chem.* **1998**, *1998*, 2885-2896.
- (13) (a) Hoogenboom, R.; Moore, B. C.; Schubert, U. S. *Chem. Commun.* **2006**, *42*, 4010-4012. (b) Hoogenboom, R.; Wouters, D.; Schubert, U. S. *Macromolecules* **2003**, *36*, 4743-4749. (c) Hoogenboom, R.; Kickelbick, G.; Schubert, U. S. *Eur. J. Org. Chem.* **2003**, *2003*, 4887-4896.
- (14) D'Annibale, A.; Ciaralli, L.; Bassetti, M.; Pasquini, C. *J. Org. Chem.* **2007**, *72*, 6067-6074.
- (15) Chiefari, J.; Chong, Y. K.; Ercole, F.; Krstina, J.; Jeffery, J.; Le, T. P. T.; Mayadunne, R. T. A.; Meijs, G. F.; Moad, C. L.; Moad, G.; Rizzardo, E.; Thang, S. H. *Macromolecules* **1998**, *31*, 5559-5562.
- (16) Skey, J.; O'Reilly, R. K. *Chem. Commun.* **2008**, *44*, 4183-4185.
- (17) Mori, H.; Seng, D. C.; Lechner, H.; Zhang, M.; Müller, A. H. E. *Macromolecules* **2002**, *35*, 9270-9281.

- (18) Ulrich, G.; Ziesel, R.; Harriman, A. *Angew. Chem., Int. Ed.* **2008**, *47*, 1184-1201.
- (19) (a) Carlson, J. C. T.; Meimetis, L. G.; Hilderbrand, S. A.; Weissleder, R. *Angew. Chem., Int. Ed.* **2013**, *52*, 6917-6920. (b) Dumas-Verdes, C.; Miomandre, F.; Lépicier, E.; Galangau, O.; Vu, T. T.; Clavier, G.; Méallet-Renault, R.; Audebert, P. *Eur. J. Org. Chem.* **2010**, *2010*, 2525-2535.
- (20) Yang, J.; Karver, M. R.; Li, W.; Sahu, S.; Devaraj, N. K. *Angew. Chem., Int. Ed.* **2012**, *51*, 5222-5225.
- (21) Wang, D.; Fan, J.; Gao, X.; Wang, B.; Sun, S.; Peng, X. *J. Org. Chem.* **2009**, *74*, 7675-7683.
- (22) Makiguchi, K.; Satoh, T.; Kakuchi, T. *Macromolecules* **2011**, *44*, 1999-2005.
- (23) Xie, H.; Zu, L.; Oueis, H. R.; Li, H.; Wang, J.; Wang, W. *Org. Lett.* **2008**, *10*, 1923-1926.
- (24) (a) Hanessian, S.; Compain, P. *Tetrahedron* **2002**, *58*, 6521-6529. (b) Kessler, S. N.; Neuburger, M.; Wegner, H. A. *J. Am. Chem. Soc.* **2012**, *134*, 17885-17888.
- (25) Boger, D. L.; Robarge, K. D. *J. Org. Chem.* **1988**, *53*, 5793-5796.

## Conclusions and further work

In this thesis we have demonstrated proof-of-principle for the use of the tetrazine–norbornene reaction in several macromolecular applications: polymer–polymer coupling and functionalisation, polymeric self-assembly functionalisation in tandem with the CuAAC reaction and nanoparticle formation by single chain collapse.

There are many directions this work could take; and with the increasing uptake of the tetrazine–alkene reaction in the literature and recent developments in the synthesis of functional tetrazines it is likely that a greater array of interesting tetrazine-bearing molecules will be available in the future.

The work in Chapter 2 could be extended to form graft or comb copolymers, or functionalisation with fluorescent, biologically-relevant or other modified tetrazines could be carried out on a range of polymer scaffolds. Functionalisation of the micelles in Chapter 3 has perhaps the most potential for avenues of further exploration, with micelle structures showing great promise as drug delivery vehicles. Given that the Tz–Nb reaction has already been shown to function *in vivo*, this opens up opportunities to use similar (non-styrenic) micelles as targeted delivery vehicles, with the simplicity of the dual functionalisation approach meaning that libraries of potential functional micelles could be synthesised easily and screened.

The SCPN work described in Chapter 4 showed the feasibility of forming SCPNs using the Tz–Nb reaction, but could be improved by using a more reactive tetrazine crosslinker, possibly meaning that the SCPNs could be synthesised at room temperature. This would give them advantages, in terms of synthetic accessibility, over most other approaches to non-dynamic SCPNs in the literature. SCPN conjugates where the conjugate is temperature-sensitive, such as DNA, could then be synthesised.

Chapter 5 was an ultimately unsuccessful avenue of exploration, but could possibly be further explored by using microwave irradiation to drive the reaction to completion, or at least higher conversions, as this has been demonstrated in the literature to be a feasible promoter of tetrazine–alkyne cycloadditions.